

## **Distribution Agreement**

In presenting this thesis or dissertation as a partial fulfillment of the requirements for an advanced degree from Emory University, I hereby grant to Emory University and its agents the non-exclusive license to archive, make accessible, and display my thesis or dissertation in whole or in part in all forms of media, now or hereafter known, including display on the world wide web. I understand that I may select some access restrictions as part of the online submission of this thesis or dissertation. I retain all ownership rights to the copyright of the thesis or dissertation. I also retain the right to use in future works (such as articles or books) all or part of this thesis or dissertation.

Signature:

---

**Cameron J. Herting**

---

**Date**

**Preclinical Investigations of the Immune Microenvironment in Glioblastoma**

By

Cameron J. Herting  
Doctor of Philosophy

Graduate Division of Biological and Biomedical Science  
Molecular Systems Pharmacology

---

Dolores Hambardzumyan, Ph.D., M.B.A.  
Advisor

---

Raymond J. Dingleline, Ph.D.  
Committee Member

---

Randy A. Hall, Ph.D.  
Committee Member

---

H. Trent Spencer, Ph.D.  
Committee Member

Accepted:

---

Lisa A. Tedesco, Ph.D.  
Dean of the James T. Laney School of Graduate Studies

---

Date

# **Preclinical Investigations of the Immune Microenvironment in Glioblastoma**

By

Cameron John Herting  
B.S., Emory University, 2015

Advisor: Dolores Hambardzumyan, Ph.D., M.B.A.

An abstract of  
A dissertation submitted to the Faculty of the  
James T. Laney School of Graduate Studies of Emory University  
in partial fulfillment of the requirements for the degree of Doctor of Philosophy  
  
in Graduate Division of Biological and Biomedical Science  
Molecular Systems Pharmacology  
2019

## Abstract

### **Preclinical Investigations of the Immune Microenvironment in Glioblastoma**

By Cameron J. Herting

Glioblastoma is the most common and malignant primary brain tumor with a dismal survival of just over one year following diagnosis even with the most aggressive treatment regimens. Limited advances have been made with respect to development of efficacious anti-neoplastic therapies to treat this deadly disease over the past fifty years. Part of the limited success stems from the models used for preclinical investigation that neglect the molecular characteristics of human glioblastoma as well as the immune microenvironment. Herein, I present novel subtype-specific murine models of glioblastoma that leverage the driver mutations uncovered through molecular analysis of human patient samples. I establish that the murine models display gene expression profiles and microenvironmental compositions that closely mirror what is observed in the human disease. Notably, I show that tumor-associated macrophages are present in these murine tumors at similar levels to what is observed in human tumors. I demonstrate that these models respond differently to anti-neoplastic therapies used to combat glioblastoma and suggest that molecular profiling should be employed clinically to inform on treatment plans. Using these models, I then investigate the role that tumor-associated macrophages play in the development of cerebral edema in glioblastoma with a focus on interleukin-1 signaling. My *in vitro*, *ex vivo*, and *in vivo* results establish interleukin-1 as a downstream target of dexamethasone; the drug currently employed to combat cerebral edema in glioblastoma. Additionally, I provide evidence that bone marrow-derived macrophages and not microglia are the primary producers of interleukin-1 in the tumor microenvironment. I demonstrate that genetic ablation of interleukin-1 signaling is able to phenocopy dexamethasone treatment with respect to inhibition of bone marrow-derived macrophage chemotaxis and inhibition of edema development *in vivo*. Finally, I reveal that genetic or pharmacological inhibition of interleukin-1 signaling *in vivo* does not impair response to radiation therapy that is seen following dexamethasone treatment. In total, these results suggest that specific inhibition of interleukin-1 signaling offers an attractive alternative to dexamethasone treatment.

# **Preclinical Investigations of the Immune Microenvironment in Glioblastoma**

By

Cameron John Herting  
B.S., Emory University, 2015

Advisor: Dolores Hambardzumyan, Ph.D., M.B.A.

A dissertation submitted to the Faculty of the  
James T. Laney School of Graduate Studies of Emory University  
in partial fulfillment of the requirements for the degree of Doctor of Philosophy

in Graduate Division of Biological and Biomedical Science  
Molecular Systems Pharmacology  
2019

## Acknowledgements

No good work is ever performed in complete isolation. Throughout my life, I have had the absolute pleasure of receiving guidance from countless fantastic individuals. If I were to thank all those people to the degree that they deserve, these acknowledgments would overshadow the rest of this dissertation. For the sake of brevity, I will limit this section only to those who have made the greatest impact during the time period that this work was completed. Bear in mind that these select few are only just the tip of the iceberg.

First, I would like to thank my dissertation committee consisting of Drs. Randy Hall, Trent Spencer, and Ray Dingleline for their input and guidance during this process. Your insight and thorough questioning during this work made me a better scientist and prepared me to describe and defend my work in front of any audience. You all showed me how an elite scientist thinks and acts. I hope to one day emulate your scientific prowess.

Next, I would like to thank those who I worked most closely with in lab: James Ross, Dr. Zhihong “Z” Chen, and Dr. Victor Maximov. Completing a Ph.D. takes many long hours and countless experiments. To some, it can be a chore; however, completing it alongside each of you made it a pleasure. To Z and Victor, thank you for teaching me many of the techniques I used to perform these experiments. It truly would not have been possible without you.

To Dr. Dolores Hambarzumyan, I will forever be indebted to you for the opportunity you provided me with in being a member of your lab. Although unconventional, my decision to rotate with and join the lab of my next-door neighbor turned out to be one of the better choices I have made; even if you did try and deter me from it in the beginning. You have continually challenged and pushed me to be a better scientist, mentor, writer, presenter, and thinker. I feel that I have progressed more during the last four and a half years than any other point in my life. Your guidance has been the largest contributor to my development. Thank you.

Finally, to my family and friends, your support, love, and friendship has kept me positive even during the most difficult times during this work. Having a supportive group of individuals to celebrate my successes with and lean on during my defeats was invaluable. I cannot emphasize enough how much you all helped me. In particular, I would like to thank my mother Erin, my sister Claire, and my girlfriend Kelsey. You three have done so much to help me discover and stay focused on what is most important in my life. I love you guys.

## Table of Contents

	<u>Page</u>
<b><u>Chapter 1: Introduction</u></b> .....	1
1.1 Glioblastoma Historical Perspective and Current Status .....	2
1.2 Clinical and Epidemiological Characteristics of Glioblastoma .....	4
1.3 Histological and Molecular Classification .....	9
1.4 The Glioblastoma Tumor Microenvironment .....	11
1.5 Therapeutic Interventions in Glioblastoma .....	22
1.6 Rationale and Goals of this Project .....	31
<b><u>Chapter 2: Subtype-Specific Mouse Modeling of Glioblastoma</u></b> .....	33
2.1 Introduction .....	34
2.2 Materials and Methods .....	39
2.3 Results .....	45
2.4 Discussion .....	79
<b><u>Chapter 3: The Role of Interleukin-1 in the Formation of Glioblastoma-Associated Cerebral Edema</u></b> .....	89
3.1 Introduction .....	90
3.2 Materials and Methods .....	95
3.3 Results .....	105
3.4 Discussion .....	140

<b><u>Chapter 4: Conclusions and Future Directions</u></b> .....	145
<b>4.1 Conclusions</b> .....	146
<b>4.2 Future Directions</b> .....	149
<b><u>References</u></b> .....	158

## List of Figures and Tables

<u>Figures</u>	<u>Page</u>
<b>Figure 1.1.</b> Brain tumor grades, histological, and molecular subtypes.	5
<b>Figure 1.2.</b> Molecular subtypes of glioblastoma are defined by notable alterations in gene expression.	12
<b>Figure 1.3.</b> Characteristics of GSCs in glioblastoma.	14
<b>Figure 1.4.</b> Clonal evolution in cancer.	16
<b>Figure 1.5.</b> The ontogeny and localization of TAMs in glioblastoma.	21
<b>Figure 2.1.</b> PDGFB-overexpression generates grade IV glioblastoma regardless of the location of RCAS injection.	47
<b>Figure 2.2.</b> PDGFB-overexpressing and NF1-silenced murine HGG display significantly different median survivals and tumor initiation times, but similar tumor growth kinetics.	48
<b>Figure 2.3.</b> Kaplan-Meier survival curves of patients with Proneural and Mesenchymal human HGG; and PDGFRA-amplified and NF1-deleted/mutant human HGG.	51
<b>Table 2.1.</b> Prominence of PDGFRA, NF1, and EGFR mutations in Proneural, Mesenchymal, and Classical human HGG.	53
<b>Figure 2.4.</b> Log <sub>2</sub> z-score values of the 18 genes in PDGFB-overexpressing or NF1-silenced murine HGG analyzed with quantitative-PCR.	54
<b>Figure 2.5.</b> Log <sub>2</sub> z-score values of the 18 genes analyzed in PDGFRA-amplified and NF1-deleted/mutant human HGG.	55
<b>Figure 2.6.</b> Log <sub>2</sub> z-score values of the 18 genes analyzed in Proneural and Mesenchymal human HGG.	56
<b>Figure 2.7.</b> Genetic driver mutations determine expression patterns of various markers.	57

<b>Figure 2.8.</b> Inverse correlation of OLIG2 and GFAP expression in PDGFB-overexpressing and NF1-silenced murine HGG.	60
<b>Figure 2.9.</b> Inverse correlation of DCX and CD44 expression in PDGFB-overexpressing and NF1-silenced murine HGG.	61
<b>Figure 2.10.</b> Murine tumor quantitative-PCR analysis.	63
<b>Figure 2.11.</b> Human tumor gene expression analysis.	64
<b>Figure 2.12.</b> Human tumor subtype expression data and the corresponding mouse models cluster similarly based on a 30-gene panel.	66
<b>Figure 2.13.</b> NF1-silenced murine HGG exhibits increased tumor-associated macrophage infiltration and reduced vessel size compared to PDGFB-overexpressing murine HGG.	69
<b>Figure 2.14.</b> Blood vessels in PDGFB-overexpressing murine HGG are larger and more permeable than those in NF1-silenced murine HGG.	71
<b>Figure 2.15.</b> Non-tumor regions of brains from both PDGFB-overexpressing and NF1-silenced murine HGG-bearing mice display normal vasculature.	73
<b>Figure 2.16.</b> Commonly used doses and schedules of TMZ produce no difference in survival of PDGFB-overexpressing murine HGG.	75
<b>Figure 2.17.</b> Radiotherapy provides a survival advantage to mice with either PDGFB-overexpressing or NF1-silenced murine HGG, while temozolomide provides a survival advantage only to mice with PDGFB-overexpressing tumors.	76
<b>Figure 2.18.</b> NF1-silenced murine HGG displays a trend towards increased malignancy upon recurrence.	78
<b>Figure 2.19.</b> Murine PDGFB-overexpressing and NF1-silenced tumors do not respond to PD-L1 neutralizing therapy.	80

<b>Figure 3.1.</b> Dexamethasone blocks LPS/IFN $\gamma$ and IL-1-induced IL-1 expression in primary BMDM and MG.	106
<b>Figure 3.2.</b> Differentiation of primary cells in media supplemented with M-CSF produces pure BMDM and MG cultures.	108
<b>Figure 3.3.</b> IL-1 $\alpha$ and IL-1 $\beta$ dose response experiments in primary BMDM and MG reveal effective doses for downstream analysis.	110
<b>Figure 3.4.</b> Dexamethasone is non-toxic to primary murine BMDM and MG.	112
<b>Figure 3.5.</b> Dexamethasone treatment ablates <i>Il1</i> upregulation by BMDM exposed to organotypic tumor slides and reduces expression of MCP cytokines by tumor tissue.	114
<b>Figure 3.6.</b> Dexamethasone treatment has no effect on tumor angiogenesis, but significantly reduces the number of tumor-associated macrophages.	117
<b>Figure 3.7.</b> Validation of the <i>in vivo</i> administration of dexamethasone by quantitative-PCR analysis of previously-reported markers.	119
<b>Figure 3.8.</b> Dexamethasone treatment significantly impairs the ability of immune cells to infiltrate the tumor from the circulation.	121
<b>Figure 3.9.</b> Administration of dexamethasone to naïve C57BL/6 mice causes a significant reduction in circulating lymphoid cells and a significant increase in circulating myeloid cells.	124
<b>Figure 3.10.</b> Stimulation of <i>Il1r1</i> <sup>-/-</sup> BMDMs with IL-1 $\alpha$ and IL-1 $\beta$ produces no change in the expression of the IL-1 responsive genes <i>Il1a</i> , <i>Il1b</i> , or <i>Ccl5</i> .	125
<b>Figure 3.11.</b> IL-1R1 ablation reduces the influx of circulating myeloid cells in the tumors of mice bearing PDGFB-overexpressing glioblastoma.	126
<b>Figure 3.12.</b> Tumor-bearing <i>Ntv-a</i> and <i>Ntv-a/Il1r1</i> <sup>-/-</sup> mice display no differences in circulating immune cell profile.	129

<b>Figure 3.13.</b> Interleukin-1 ligand-ablated mice display a reduction in tumor tissue levels of MCP-family cytokines.	130
<b>Figure 3.14.</b> Ablation of IL-1 signaling reduces blood-brain barrier permeability in mice bearing PDGFB-overexpressing tumors.	132
<b>Figure 3.15.</b> IL-1 ligand ablation reduces edema formation in tumor-bearing mice.	134
<b>Figure 3.16.</b> Dexamethasone reduces edema formation as assessed by a wet/dry tissue weight assay.	136
<b>Figure 3.17.</b> Genetic and pharmacological inhibition of IL-1 signaling have no impact on radiotherapy efficacy.	137
<b>Figure 3.18.</b> Gallium nitrate inhibits the synthesis and secretion of IL-1 $\beta$ protein from primary BMDM.	139
<b>Figure 4.1.</b> An illustrative summary of the results obtained in Chapter 2.	147
<b>Figure 4.2.</b> A graphical summary of the results presented in Chapter 3.	150

## List of Abbreviations

- 5-ALA:** 5-aminolevulinic acid
- ALV:** avian leukosis virus
- ANOVA:** analysis of variance
- AP:** anterior posterior
- ASV:** avian sarcoma virus
- ATCC:** American Type Culture Collection
- ATP:** adenosine triphosphate
- BBB:** blood-brain barrier
- BMDM:** bone marrow-derived macrophage
- BSA:** bovine serum albumin
- CCL12:** C-C motif chemokine ligand 12
- CCL2:** C-C motif chemokine ligand 2
- CCL7:** C-C motif chemokine ligand 7
- CCL8:** C-C motif chemokine ligand 8
- CCR2:** C-C motif chemokine receptor 2
- CD133:** prominin-1
- cDNA:** complimentary deoxyribonucleic acid
- CL:** Classical
- CNS:** central nervous system
- CSF-1R:** colony-stimulating factor-1 receptor
- CT:** computed tomography
- CX3CR1:** C-X3-C motif chemokine receptor 1
- CXCL12:** C-X-C motif chemokine ligand 12

**CXCR4:** C-X-C motif chemokine receptor 4

**CyTOF:** cytometry by time of flight

**DCX:** doublecortin

**DEX:** dexamethasone

**DG:** dentate gyrus

**DMEM:** Dulbecco's modified eagle medium

**DMSO:** dimethyl sulfoxide

**DNA:** deoxyribonucleic acid

**DPBS:** Dulbecco's phosphate-buffered saline

**DT:** diphtheria toxin

**DTR:** diphtheria toxin receptor

**EDTA:** ethylenediaminetetraacetic acid

**EGFR:** epidermal growth factor receptor

**EGFRvIII:** epidermal growth factor receptor variant III

**ELISA:** enzyme-linked immunosorbent assay

**FBS:** fetal bovine serum

**FFPE:** formalin-fixed paraffin-embedded

**FGFR:** fibroblast growth factor receptor

**FLAIR:** fluid-attenuated inversion recovery

**FOV:** field of view

**GBW:** Gehan Breslow Wilcoxon

**G-CIMP:** glioma CpG island methylator phenotype

**GFAP:** glial fibrillary acidic protein

**GFP:** green fluorescent protein

**GN:** gallium nitrate

**GSC:** glioblastoma stem cell

**Gy:** Gray

**H&E:** hematoxylin and eosin

**HA:** hyaluronic acid

**HBSS:** Hank's balanced salt solution

**HGFR:** hepatocyte growth factor receptor

**HGG:** high-grade glioma

**hHGG:** human high-grade glioma

**HSC:** hematopoietic stem cell

**IBA1:** ionizing calcium-binding adaptor molecule 1

**IFN $\gamma$ :** interferon gamma

**IL-1:** interleukin-1

**IL-1R1:** interleukin-1 receptor 1

**IL-1 $\alpha$ :** interleukin-1 alpha

**IL-1 $\beta$ :** interleukin-1 beta

**IP:** intraperitoneal

**LPS:** lipopolysaccharide

**MC:** Mantel Cox

**MCP:** monocyte-chemoattractant protein

**MCP-1:** monocyte-chemoattractant protein-1

**MCP-2:** monocyte-chemoattractant protein-2

**MCP-3:** monocyte-chemoattractant protein-3

**MCP-4:** monocyte-chemoattractant protein-4

**M-CSF:** macrophage-colony stimulating factor

**MDSC:** myeloid-derived suppressor cell

**MES:** mesenchymal

**MG:** microglia

**MGMT:** O<sup>6</sup>-methylguanine-DNA methyltransferase

**MHC II:** major histocompatibility complex class II

**mHGG:** murine high-grade glioma

**MRI:** magnetic resonance imaging

**mRNA:** messenger RNA

**MS:** median survival

**NANOG:** homeobox protein NANOG

**NCI:** National Cancer Institute

**NESTIN:** neuroepithelial stem cell protein

**NF1:** neurofibromin 1

**ns:** not significant

**N*tv-a*:** Nestin *tv-a*

**OLIG2:** oligodendrocyte transcription factor 2

**PBS:** phosphate-buffered saline

**PCA:** principle component analysis

**PCR:** polymerase chain reaction

**PD-1:** programmed cell death protein-1

**PDGF:** platelet-derived growth factor

**PDGFB:** platelet-derived growth factor B

**PDGFR:** platelet-derived growth factor receptor

**PDGFRA:** platelet-derived growth factor receptor alpha

**PD-L1:** programmed cell death protein-ligand 1

**PDX:** patient-derived xenograft

**PFA:** paraformaldehyde

**pH3:** phosphohistone H3

**PN:** Proneural

**RARE:** rapid acquisition with relaxation enhancement

**Rb:** retinoblastoma

**RBC:** red blood cell

**RCAS/*tv-a*:** replication competent avian sarcoma leukosis virus long terminal repeat with splice acceptor/ tumor virus-A

**RFP:** red fluorescent protein

**RNA:** ribonucleic acid

**RT:** radiation therapy

**RTK:** receptor tyrosine kinase

**SD:** standard deviation

**SEM:** standard error of the mean

**SOX2:** sex determining Y-box 2

**SVZ:** subventricular zone

**TAM:** tumor-associated macrophage

**TCGA:** The Cancer Genome Atlas

**TCR:** T cell receptor

**TE:** time of excitement

**TF:** tumor formation

**TMZ:** temozolomide

**TR:** time of relaxation

**VEGF:** vascular endothelial growth factor

**VEGFR:** vascular endothelial growth factor receptor

**WHO:** World Health Organization

**Chapter 1: Introduction**

## 1.1 Glioblastoma Historical Perspective and Current Status

Gliomas as a disease were first described as “medullary sarcoma” by the English medical community and “fungus medullare” by the German’s during the early 1800s<sup>1</sup>. Researchers in this era were limited by macroscopic descriptions of the tumor tissue and were only able to determine that these tumors resembled brain tissue in substance and structure. Glioblastoma was first described microscopically in the late 1800’s by the German scientist Rudolf Virchow<sup>2</sup>. He pioneered the utilization of microscopic techniques to describe the cellular nature of neoplastic tissues and established much of the early knowledge in the field. Using these methods, he was able to establish that gliomas likely arise from glial cells; a fact evident by the tumor’s modern name. He also defined the infiltrative nature of the tumors evidenced by the lack of clear boundaries with non-neoplastic tissue. Both discoveries have held true even as technological advancement has allowed for further characterization of the disease.

The next major discoveries in the field were made by Bailey and Cushing in the mid-1920s, the scientists who first began to subclassify brain tumors<sup>3</sup>. These studies illustrated the first attempts at defining different types of gliomas; a characteristic that would be proven molecularly nearly 100 years later. They put forth a description regarding the “histogenetic cellular types” observed in glioma tissue and established the idea that these tumors consist of a mixture of different cell types.

Following Bailey and Cushing, the next scientist to provide a significant advance to the field was Hans-Joachim Scherer in the late 1930s and early 1940s prior to his untimely death as a civilian during the late stages of World War II. Scherer was a strong proponent of combining microscopic and macroscopic descriptions of the disease while considering the totality of the tumor instead of drawing broad conclusions from small pieces of biopsy tissue or stained tumor slices<sup>1</sup>. Using these methods, Scherer described numerous ultracellular structures within gliomas and further hypothesized the angiogenic nature of tumors long before the concept was put forth by Judah

Folkman in the 1970s<sup>4</sup>. He was the first to characterize pseudopalisading necrosis as well as the glomerular neovascular structures within glioblastomas<sup>5</sup>. The latter were deemed Scherer structures in homage to his scholarly contributions. Scherer was also the first to distinguish between primary and secondary glioblastomas. He hypothesized that the former arose *de novo* while the later progressed from previously existing astrocytomas and that each disease would share histological characteristics, but differ in their biological behaviors<sup>5</sup>.

The later portion of the 20<sup>th</sup> century was devoid of major advances regarding the biological characteristics of glioblastoma. Apart from technological improvements in the histological characterization of the disease, and small advances in therapeutic intervention, limited discoveries were made. With the advent of molecular biology during the late 1990s, however, this changed, and a modern era of discovery commenced. The crowning achievement of this modern era was likely the confirmation of Bailey and Cushing's description of different subclasses of glioblastoma with the molecular classifications put forth in the 2000s and 2010s<sup>6,7</sup>. These classifications have now been integrated into the official description of the disease by the World Health Organization (WHO) and are beginning to inform about the clinical behavior and outcomes of the disease<sup>8</sup>.

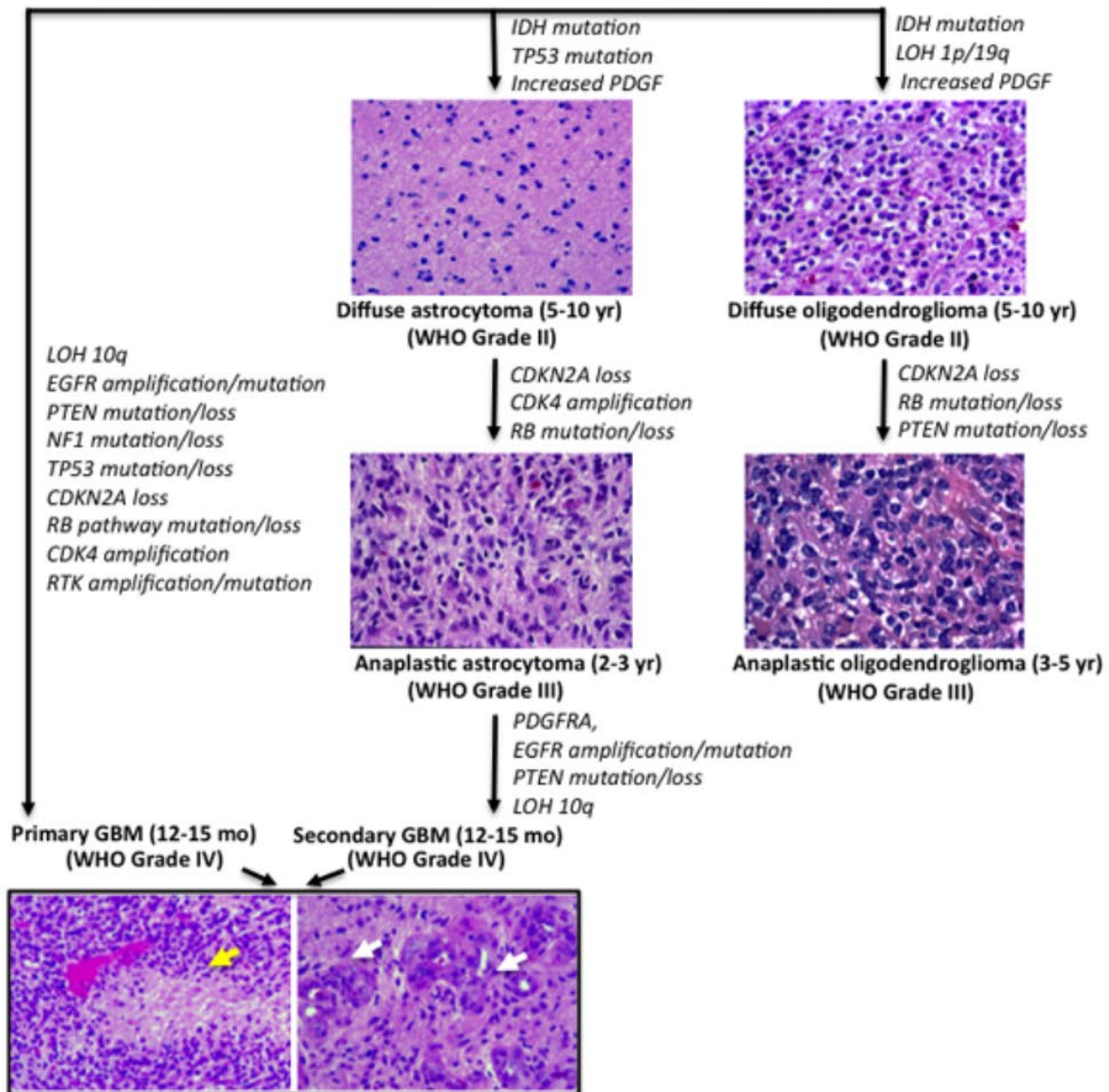
Current research in glioblastoma is focused not only on subclassification of the disease into subtypes that inform on biological behavior and treatment response, but also on the heterogeneous cellular nature of the disease. It is now appreciated that many neoplastic and non-neoplastic cell types interact within the tumor microenvironment present in glioblastoma and other cancers<sup>9,10</sup>. It is hypothesized that the different genetic subtypes display differential immune cell compositions and that the interaction of the immune cells with the tumor cells may be leveraged to produce a positive therapeutic effect<sup>11,12</sup>. The actions of both the innate and adaptive immune system in glioblastoma remain relatively undefined and offer an attractive avenue for preclinical and clinical therapeutic investigation.

## 1.2 Clinical and Epidemiological Characteristics of Glioblastoma

Primary brain tumor classification spans four grades (I-IV) based on histological characteristics and clinical traits with the highest grade (IV) being referred to as glioblastoma<sup>8</sup>. Within grades, tumors can be further subdivided based on the glial cells that give rise to the tumors with astrocytes, oligodendrocytes, and ependymal cells producing astrocytomas, oligodendrogliomas, mixed oligo-astrocytomas and ependymomas respectively<sup>13</sup>. Of these grades, grade I tumors are the least malignant and display none of the characteristics that define higher grade tumors (atypical cells, mitoses, endothelial proliferation, and necrosis). The tumors that reside in this class include pilocytic astrocytomas, dysembryoplastic neuroepithelial tumors, and pleomorphic xanthoastrocytomas<sup>13</sup>. Gliomas that possess one of the aforementioned features fall into grade II and are further subdivided based on the cell types that make up the tumor as well as the mutations present (**Figure 1.1**)<sup>14</sup>. Tumors with two or more features fall into grades III and IV with the latter distinguished from the former based on the presence of pseudopalisading necrosis and microvascular proliferation.

Glioblastomas are the most common and aggressive primary brain tumors and account for ~50% of all malignant brain tumors with ~17,000 new diagnoses annually<sup>15,16</sup>. The annual incidence is 7.15 cases per 100,00 people and men are affected more frequently than women (incidence of 1.6:1)<sup>17,18</sup>. Glioblastoma is typically considered a disease of old age with a median age of ~64 years at diagnosis; however, individuals of any age can be afflicted<sup>19</sup>. The incidence in adolescents and children is about half that of adults<sup>17</sup>. Age remains the most significant prognostic factor in glioblastoma with the most elderly patients having the worst prognosis<sup>20</sup>. Due to the association with age and the increase in the overall age of the global population, the incidence of glioblastoma is predicted to increase over the coming decades and the development of improved therapies is of utmost importance.

A



B

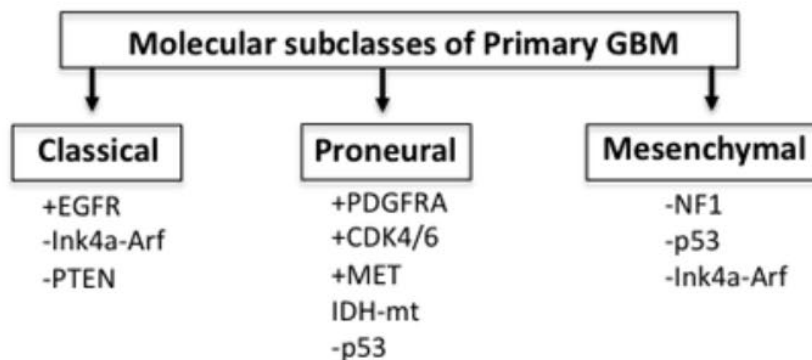


**Figure 1.1. Brain tumor grades, histological, and molecular subtypes.** (A) Brain tumor grading, and histological subtypes based on the primary cell type present in the tumor mass. (B) Molecular subclassification of glioblastoma based on the mutations present in the tumor. Figure adapted from Neuroglia Chapter 59<sup>14</sup>.

There are limited environmental and genetic risk factors that have been identified for the development of glioblastoma. The only environmental risk factor known to induce a significant risk for glioblastoma development is exposure to ionizing radiation<sup>18</sup>. Other risk factors such as exposure to industrial chemicals and smoking have been loosely associated with an increased risk of glioblastoma development; however, no conclusive correlations have been established<sup>15</sup>. There are a variety of genetic risk factors that predispose individuals to glioblastoma. These include neurofibromatosis type 1 and 2, Li-Fraumeni syndrome, tuberous sclerosis, retinoblastoma, and Turcot syndrome among others; but, the increase in risk of glioblastoma development amongst these groups is less than 1%<sup>18,21</sup>.

The anatomic location of tumor development depends on the age of incidence, as well as the molecular characteristics of the disease<sup>22,23</sup>. Adult glioblastomas occur throughout the brain and display minimal preference for specific anatomical locations<sup>22</sup>. Regardless of the location of tumor development, molecular characteristics of the disease, or the age of diagnosis, the prognosis for patients diagnosed with glioblastoma is dismal. Glioblastomas are recognized as tumors with diffuse growth; meaning they have a tendency to spread into adjacent tissue and lack a clearly defined tumor border<sup>24</sup>. Glioma cells tend to invade the brain along myelinated fibers in white matter tracts<sup>25</sup>. This invasion pattern guarantees that complete surgical resection is impossible and the infiltrative tumor cells that remain following surgery will cause tumor recurrence. It has been established that extent of resection is associated with survival following surgery with a higher percent of resection displaying longer median survival<sup>26,27</sup>. These studies additionally established that maximal surgical resection is around 98% and even these patients eventually suffered from tumor recurrence.

Glioblastomas display significant treatment resistance to both chemotherapeutic compounds as well as radiation therapy. It has been proposed that resistance to chemotherapy in glioblastoma stems from a subset of tumor cells called glioblastoma stem cells (GSCs) that are inherently resistant

to both treatment modalities<sup>28,29</sup>. The precise mechanisms underlying this phenomenon will be enumerated in chapter 1.4. Moreover, the tumor-supportive immune microenvironment has been suggested to contribute to treatment resistance through a variety of mechanisms<sup>10</sup>. A subset of tumors has been shown to express the protein O<sup>6</sup>-methylguanine-DNA methyltransferase (MGMT), a protein capable of removing the toxic DNA alkylation stimulated by standard of care temozolomide treatment<sup>30</sup>. This effect renders the treatment ineffective and neutralizes any survival benefit.

Glioblastoma is usually identified by patient presentation with continually developing neurological deficits over an extended period or by seizure onset in otherwise healthy individuals<sup>31</sup>. Symptoms associated with glioblastoma include severe headache, papilledema, cognitive difficulties, personality changes, gait imbalance, and significant sensory alterations<sup>15</sup>. Many of these symptoms are dependent upon the location of tumor development and what brain structures are impacted or displaced by tumor growth. Considering the median age of diagnosis in glioblastoma, many of these symptoms are initially attributed to other psychiatric and neurological disorders such as dementia and stroke<sup>15</sup>. Seizures are a common occurrence in glioblastoma patients with 40-60% of patients experiencing them at some point during disease progression<sup>32</sup>. In fact, up to 40% of glioblastoma patients will present with epilepsy<sup>32,33</sup>. Typically, seizures are managed with anti-epileptic drugs or by corticosteroids that reduce intracranial pressure through edema reduction<sup>34-36</sup>.

Upon presentation with glioblastoma-associated symptoms, patients will immediately undergo either magnetic resonance imaging (MRI) or computed tomography (CT) scan<sup>37</sup>. Typically, MRI is favored, however, CT scans are utilized in patients in which MRI would be prohibited (eg. patients with pacemakers or metal implants). Most-frequently, T1-weighted MRI and T2-weighted MRI with gadolinium enhancement are used to initially characterize and diagnose glioblastoma<sup>38</sup>. Due to a disrupted blood-brain barrier (BBB), glioblastomas will display significant enhancement

with gadolinium administration. In addition to initial diagnosis, specialized MRI scans such as fluid-attenuated inversion recovery (FLAIR) can be used to assess edema development, more accurately represent tumor burden, and evaluate extent of resection following surgery<sup>39</sup>. Investigation of the association of these techniques with survival has demonstrated that MRI manifestations are associated with survival of glioblastoma patients<sup>40</sup>. In particular, patients with apparent edema as assessed by MRI have a worse prognosis than those with no edema (median survival of 120.9 weeks vs. 237.2 weeks)<sup>40</sup>. It should be noted that non-neoplastic neurological diseases are capable of mimicking brain tumors on neuroimaging as well as histological examination<sup>41</sup>. These include, but are not limited to, multiple sclerosis, stroke, brain abscess, and venous thrombosis. As technology has advanced in the immunohistochemical and molecular classification of glioblastoma, these techniques have been advised to confirm diagnoses made via imaging and histology<sup>41</sup>.

### **1.3 Histological and Molecular Classification**

To confirm the identity of tumors observed with neuroimaging, clinicians will resort to histological analysis of biopsy material<sup>42</sup>. Historically, brain tumors have been classified based on histological concepts stemming from microscopic analysis of hematoxylin and eosin (H&E)-stained sections, immunohistochemical analysis of lineage associated proteins such as oligodendrocyte transcription factor 2 (OLIG2) and glial fibrillary acidic protein (GFAP), and analysis of ultracellular structures<sup>5,8</sup>. OLIG2 and GFAP are the typical markers used to identify oligodendrogliomas and astrocytomas respectively. Tumors that express both markers are referred to as mixed oligo-astrocytomas. The classical analyses based on OLIG2 and GFAP defined glioblastomas as oligodendroglial and/or astrocytic in nature based on gross histological appearance<sup>5,43,44</sup>. The most recent WHO guidelines emphasize that glioblastomas can be distinguished from lower grade gliomas via histology based on the appearance of hypercellularity, nuclear atypia, mitotic figures, and

evidence of necrosis and angiogenesis<sup>8,45</sup>. A combination of neuroimaging and histological analysis of biopsy tissue is necessary to conclusively diagnose glioblastoma.

Over the past two decades, attention has shifted from histological classification of tumors to molecular characterization with burgeoning molecular biology techniques such as gene expression microarrays and RNA-sequencing. Initial investigations of chromosomal and gene expression alterations in glioblastoma revealed significantly enriched events but were limited in scope due to small sample size<sup>46-48</sup>. They were successful in laying a framework for future analyses though. These investigators established that glioblastomas that present similarly with neuroimaging and histological techniques are caused by a variety of genetic alterations. This established the concept that with a sufficient sample size, it may be possible to categorize glioblastomas into molecularly defined subtypes with different druggable targets, response to therapy, and overall prognosis. This framework was thought to offer a path towards development of personalized medicine in glioblastoma<sup>49,50</sup>.

The establishment of The Cancer Genome Atlas (TCGA) in 2008 provided researchers with an exceptional opportunity to study the functional genomics of these tumors and provided a database with enough samples to perform the first robust subclassifications based on gene expression<sup>51</sup>. The initial analysis identified that key alterations in p53, retinoblastoma (Rb), and receptor tyrosine kinase (RTK) pathways were key drivers of glioblastoma formation<sup>51</sup>. Further analysis and unsupervised clustering identified four major subtypes: Proneural, Neural, Classical, and Mesenchymal named after the cell lineages that the tumor expression data most closely matched<sup>7,52</sup>. The Proneural and Mesenchymal subtypes had been previously described and associated with clinical tumor behavior<sup>53</sup>.

For three of these subtypes, clear driver mutations were identified that were enriched when compared to the others. For Proneural, platelet-derived growth factor receptor (PDGFR)

amplification, p53 loss, and isocitrate dehydrogenase 1 (IDH1) mutations were common. Classical tumors showed an enrichment in activating mutations in the epidermal growth factor receptor (EGFR) signaling pathway. Finally, Mesenchymal tumors demonstrated inactivating mutations in neurofibromin 1 (NF1).

Over time, TCGA adopted next-generation sequencing techniques that allowed for more robust classification of glioblastoma subtypes<sup>54</sup>. Analysis of this improved dataset initially confirmed all the previously established subtypes<sup>6</sup>. More vigorous classification has resulted in the deletion of the Neural subtype<sup>12</sup>. The currently accepted subtypes include Proneural, Mesenchymal, and Classical, with the Proneural subtype split into glioma CpG island methylator phenotype (G-CIMP) positive and negative tumors (**Figures 1.1 and 1.2**)<sup>12</sup>. This change was reasonable considering the lack of a defining mutation in the Neural group. It should be noted, that these analyses consider the predominant expression pattern of the bulk tumor. It is therefore possible for multiple subtypes to exist in the same tumor at the cellular level and single cells display varying functional characteristics and response to therapy co-exist within single tumors<sup>55-57</sup>. These studies overall highlight the heterogeneity of glioblastoma not only at the transcriptomic level, but also the cellular level.

#### **1.4 The Glioblastoma Tumor Microenvironment**

Glioblastomas are a complex cellular microenvironment consisting of both neoplastic and non-neoplastic cells<sup>9</sup>. Within each of these categories lie subcategories of cells, each displaying different transcription profiles, surface markers, and actions within the tumor. The major categories of cells within the microenvironment include: cancer cells, endothelial cells, pericytes, and a variety of immune cells<sup>58</sup>. These subsets of cells are known to interact with each other extensively, and these interactions drive many of the phenomena observed at the tumor level including angiogenesis, tumor invasion, immune evasion, treatment resistance, and more. The link between inflammation and cancer and primitive explanations of the idea of a tumor microenvironment were postulated by

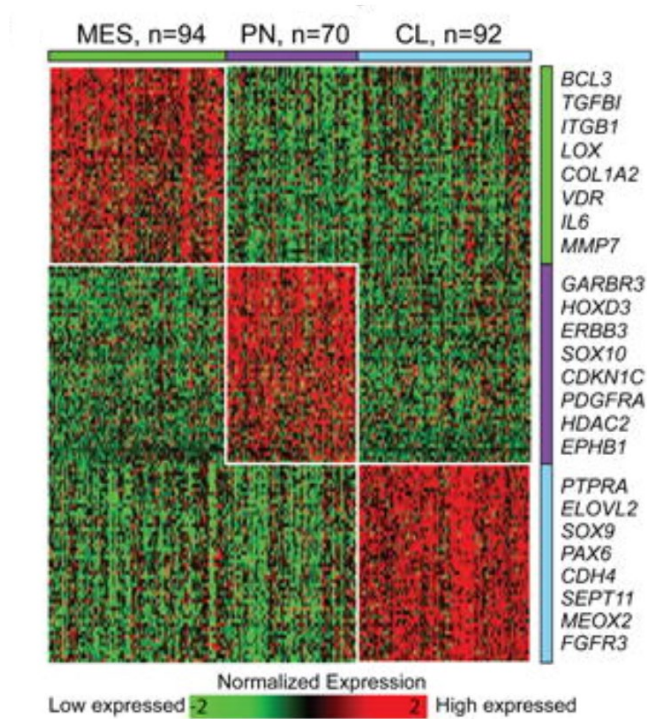


**Figure 1.2. Molecular subtypes of glioblastoma are defined by notable alterations in gene expression.** Representative genes and their expression in human Mesenchymal (MES), Proneural (PN), and Classical (CL) tumor samples. Figure adapted from Wang et al. 2017<sup>12</sup>.

Rudolf Virchow over 150 years ago<sup>59</sup>.

Of these cell types, perhaps the most widely studied are the cancer cells themselves. As mentioned in chapter 1.2, glioblastomas are typically thought to be oligodendroglial, astrocytic, or mixed oligodendroglial and astrocytic. This nature arises from the fact that most glioblastoma tumor cells display glial cell or astrocyte characteristics, likely due to the tumors originating in precursors of these cell types<sup>8</sup>. It has been proposed and validated in animal models that glioblastomas can arise when mutations occur in neural stem cells, multipotent progenitors, bipotential progenitors, and unipotent progenitors<sup>60,61</sup>. These stem-like cell types typically reside in the vascular neurogenic regions of the brain, such as the subventricular zone, and are the cells responsible for generation of new neurons, glial cells, and astrocytes throughout life<sup>62,63</sup>. The growth characteristics of cancer cells in glioblastoma can be described by two hypotheses: the cancer stem cell hypothesis and clonal evolution<sup>64</sup>. Although distinct and competing, these hypotheses likely coexist in their descriptions of tumor growth and can be applied to describe different aspects of tumor behavior.

The cancer stem cell hypothesis states that there is a population within tumors that displays traits of stem cells and behaves differently from the tumor bulk<sup>65</sup>. Furthermore, it suggests that these cancer stem cells give rise to the tumor bulk, which display a differentiated phenotype. The functional characteristics of cancer stem cells in glioblastoma include sustained self-renewal and persistent proliferation, low frequency within the tumor, and the ability to differentiate into different lineages of cells (**Figure 1.3**)<sup>66</sup>. In the early 2000s, several groups in parallel demonstrated that a subset of glioblastoma cells displayed stem cell properties; thereby giving rise to the application and maturation of the stem cell hypothesis of cancer in the context of brain tumors<sup>67-69</sup>. GSCs are the only cells capable of true self-renewal and multipotent differentiation properties<sup>70</sup>. These cells have the propensity to express markers such as prominin-1 (CD133), sex determining region Y-box 2 (SOX2), homeobox protein NANOG (NANOG), OLIG2, and neuroepithelial stem cell protein

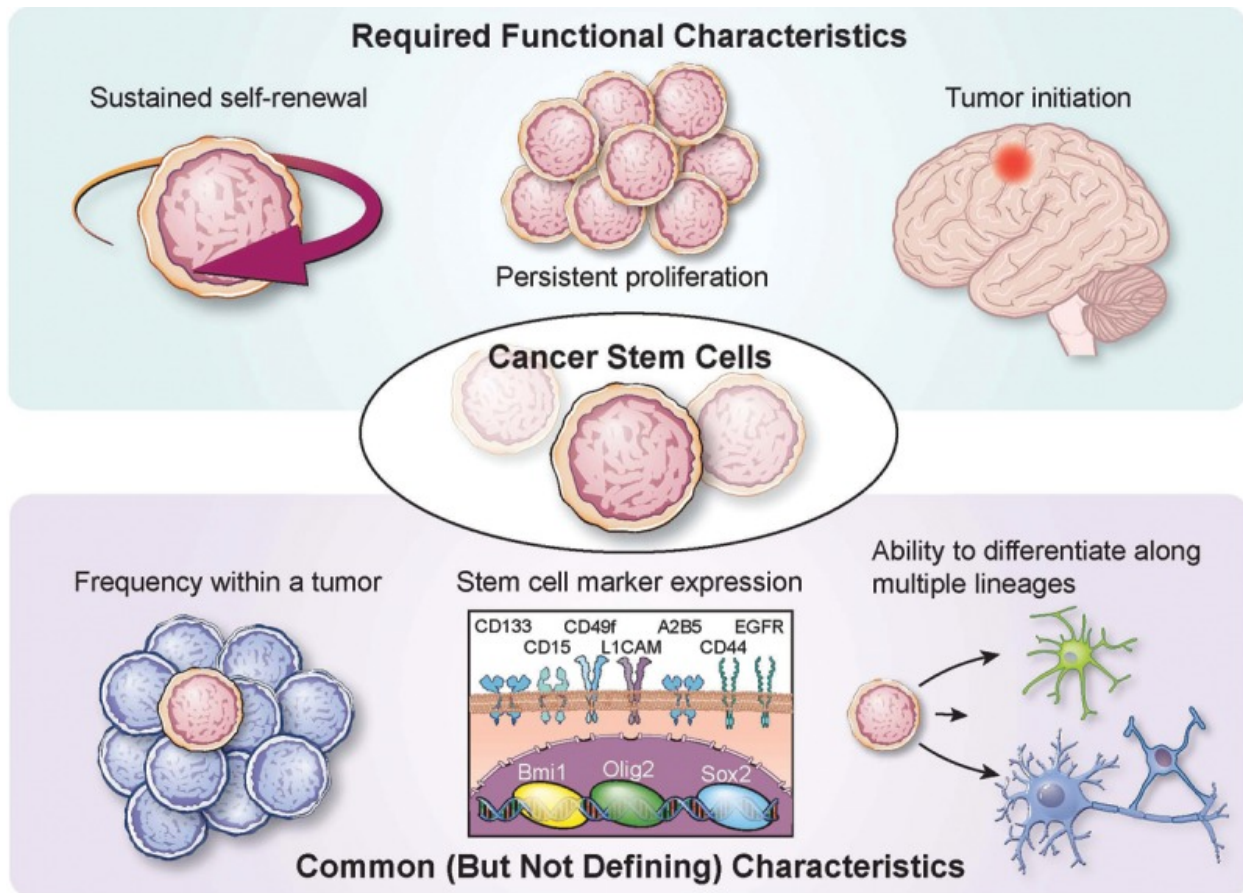


**Figure 1.3. Characteristics of GSCs in glioblastoma.** The characteristics of GSCs in glioblastoma are listed as well as the transcription factors and surface markers that are thought to drive the stem cell phenotype. Adapted from Lathia et al. 2015<sup>71</sup>.

(NESTIN); but no marker or combination of markers are ubiquitously expressed by these cells nor are they exclusively markers of this subset<sup>68,72-74</sup>. The lack of ability to specifically identify this subset *in vivo* makes characterization and therapeutic targeting of these cells difficult. It should be noted that isolation of cells expressing CD133 from tumors generates cultures of cells able to self-renew and form neurospheres, two of the *in vitro* characteristics of GSCs<sup>75</sup>. The maintenance of GSCs *in vivo* is thought to arise from a multitude of factors related to the tumor microenvironment including niche factors, tumor metabolism, epigenetics, genetics, and immune cell interactions. Furthermore, these factors drive the functional characteristics of GSCs *in vivo* including invasion, immune evasion, promotion of angiogenesis, and localization to specific niches within the tumor (eg. the perivascular niche)<sup>66</sup>. These cells as a whole are thought to be minimally proliferative and instead give rise to the rapidly multiplying cells of the tumor bulk<sup>76</sup>.

An alternative explanation to the cancer stem cell hypothesis for the growth characteristics of tumors has been put forth and is called clonal evolution. This model postulates that a tumor arises when any cell type incurs the mutations necessary to turn it into a cancer cell<sup>77</sup>. These cells are genetically unstable and have the propensity to incur additional mutations throughout their life cycle, thereby generating distinct “clones” within the tumor (**Figure 1.4**)<sup>78</sup>. The progeny of these cells are what form the bulk tumor and undergo clonal evolution throughout tumor development<sup>79</sup>. This hypothesis is supported by studies of the cancer genome illustrating the abnormal genetic profiles within tumors as well as their heterogeneity and apparent clonality on the single cell level<sup>55,80</sup>. It is likely that the actual nature of glioblastoma is most accurately described by combining concepts from both the cancer stem cell and clonal evolution models. Perhaps the cancer stem cell hypothesis better describes the ability of these tumors to recur as well as the treatment resistance of certain cells

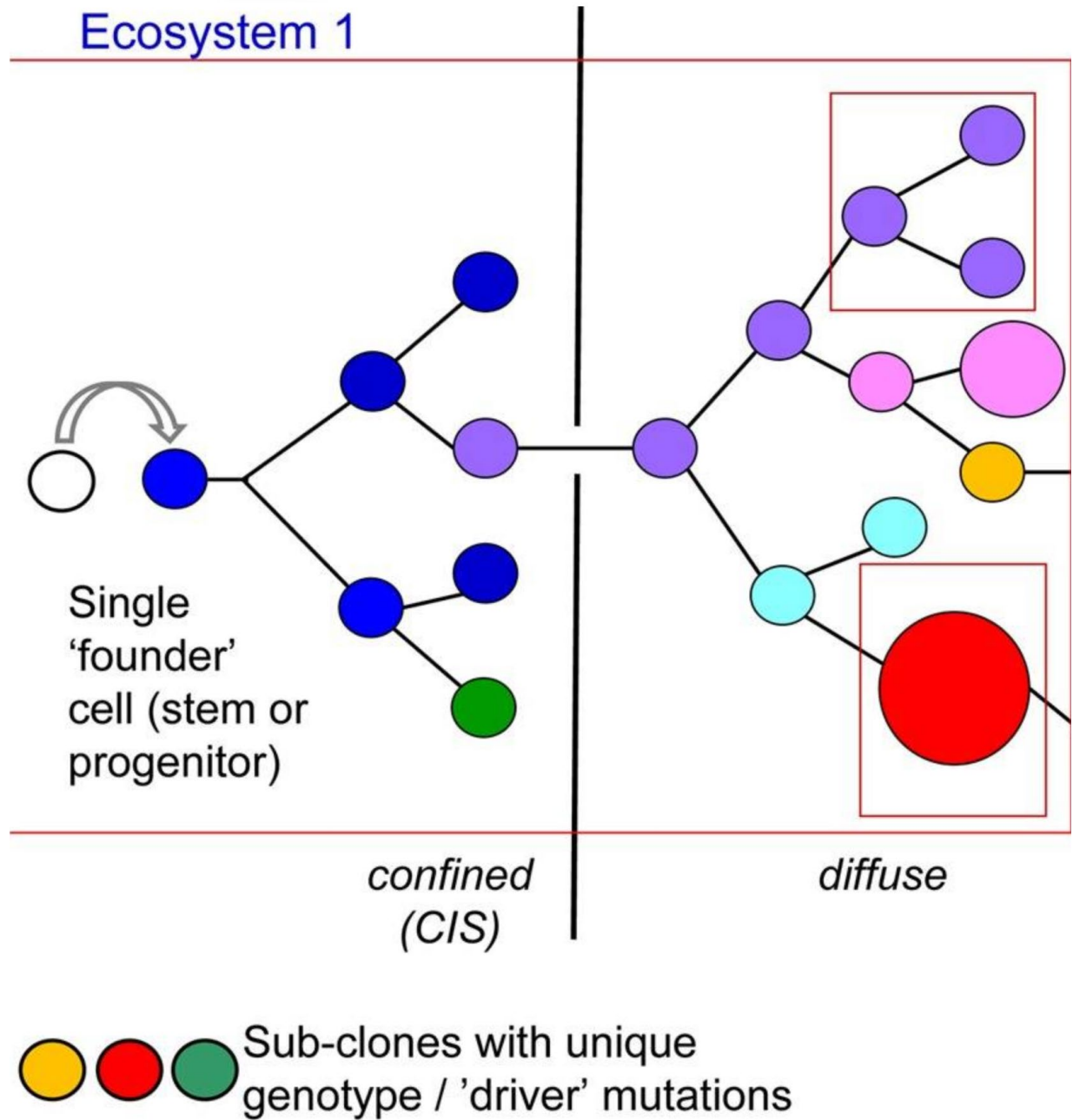


**Figure 1.4. Clonal evolution in cancer.** A depiction of the process of clonal evolution in cancer. A founder cell incurs sufficient mutations for transformation into a cancerous cell. Additional mutations drive the formation of distinct “clones” within the tumor. Adapted from Greaves et al. 2012<sup>77</sup>.

within the tumor. The clonal evolution model, on the other hand, may better describe the growth characteristics of the bulk tumor cells.

Glioblastoma bulk tumor cells are highly proliferative and invasive<sup>81</sup>. Although they display a marked ability to invade the adjacent tissue, glioblastoma cells almost never metastasize to sites outside of the brain<sup>82</sup>. They typically grow near to and ensheath blood vessels in the brain; relying on them to supply the nutrients and oxygen necessary for rapid proliferation<sup>83</sup>. The invasive nature of the cells is thought to arise from the demands they place on the local environment. As glioblastoma cells grow around blood vessels, they cause them to collapse, resulting in a cessation of nutrient and oxygen delivery and starving the cells; thereby generating necrotic regions within the tumor<sup>84,85</sup>. The result of this process is a buildup of acidic metabolic byproducts and local hypoxia that drive the tumor cells to invade adjacent tissue in search of nutrients and oxygen<sup>86,87</sup>. Additionally, in response to hypoxia, glioblastoma cells upregulate expression of pro-angiogenic factors such as vascular endothelial growth factor (VEGF) that leads to the proliferation of endothelial cells and generation of new blood vessels<sup>88,89</sup>.

Glioblastoma has long been regarded as among the most vascular tumors and therefore endothelial cells play a prominent role in the tumor microenvironment<sup>90</sup>. In fact, a direct link between glioblastoma cells and endothelial cells has been established by the demonstration that GSCs can differentiate into endothelial cells or pericytes and integrate into vessels in a process termed vascular mimicry<sup>71,91,92</sup>. In addition to this direct link, tumor cells in glioblastoma are known to secrete pro-mitotic factors such as VEGF and platelet-derived growth factor (PDGF) that act on endothelial cells within and adjacent to the tumor<sup>93</sup>. These pro-angiogenic factors drive the formation of irregular and tortuous blood vessels within the tumor and lead to the disruption of the BBB; allowing for leakage of serum and blood cells into the tumor and driving the formation of

glioblastoma-associated cerebral edema<sup>94</sup>. It should be noted that the BBB is not universally disrupted in glioblastoma and there are areas of the tumor in which it remains intact<sup>95</sup>.

Additional disruption of the BBB in glioblastoma arises from the effects on pericytes within the tumor. Pericytes line the blood vessels in the brain and are known to regulate the functions of the BBB<sup>96</sup>. In glioblastoma, crosstalk between the tumor cells and pericytes disrupts the usual function of these cells. The glioma cells hijack pericytes as a method to obtain new tumor vasculature via vessel co-option<sup>97</sup>. This interaction lifts the pericytes from the vessels, thereby disturbing their ability to modulate vessel permeability. An additional immunosuppressive role of pericytes in glioblastoma has been illustrated<sup>98</sup>.

The immune microenvironment in glioblastoma is perhaps the most pertinent subset related to current studies in the field and certainly the most relevant to this work. Recently it has been shown that the composition of the immune microenvironment is subtype-dependent and that the largest non-neoplastic cell type in glioblastoma are tumor-associated macrophages (TAMs); a cell population that encompasses both brain resident microglia (MG) as well as bone marrow-derived macrophages (BMDM) that are derived from circulating monocytes<sup>10,12,99</sup>. It has been shown experimentally that over 30% of the cells in a glioblastoma tumor are TAMs and that the two subsets, MG and BMDM, have different expression profiles<sup>99,100</sup>. The exact roles of these cell types in glioblastoma initiation and progression remain unclear and an active area of investigation.

MG initially infiltrate the brain during embryogenesis and persist throughout life<sup>101</sup>. The cells derive from a primitive macrophage precursor cell and are dependent on colony-stimulating factor-1 receptor (CSF-1R) signaling for survival<sup>102</sup>. MG were initially discovered in the early 1900s and have long been linked to neuroinflammatory conditions<sup>103,104</sup>. In the non-diseased central nervous system (CNS) MG are the only macrophage cell type present. BMDM only infiltrate during conditions of significant neuroinflammation and MG repopulate through local proliferation when ablated, not by

re-establishment from circulating cells<sup>10</sup>. Resting MG are distributed throughout the brain and constantly surveil their environment for pathogens or inflammatory stimuli<sup>105,106</sup>. When activated, MG express major histocompatibility complex class II (MHC II) molecules and may serve as antigen-presenting cells; thereby serving as a link between the innate and adaptive immune system<sup>107,108</sup>. MG are known to display a dynamic activation pattern and will produce varying inflammatory stimuli depending on the input signal they receive<sup>109</sup>. The diversity in MG activation produces a variety of downstream results with a pro-inflammatory, pathogen killing phenotype lying at one end of the spectrum (M1) and a tissue repair phenotype (M2) at the other<sup>110</sup>. It must be emphasized that the polarization states of MG are extremely diverse and dependent upon the chemokine stimuli present in their immediate environment<sup>111</sup>. This fact is further complicated when moving from *in vitro* to *in vivo* analyses and amplified when considering the regional chemokine expression present in tumors<sup>112,113</sup>.

The presence of macrophages in glioblastoma was first described in 1925 using silver carbonate to stain the cells in human tissue samples<sup>114</sup>. This description classified the cells as amoeboid in shape, an observation that they attributed to the phagocytic activity of the cells. Initially, and for nearly 100 years after, MG were thought to be the only population that existed in glioblastoma as it had not yet been shown that peripheral monocytes were able to infiltrate into the tumor and become macrophages<sup>115</sup>. Early in the 2000s, it was shown that in relevant murine tumor models, MG could be distinguished from BMDM by CD45-positivity<sup>116</sup>. This fact, along with genetically engineered reporter mice, was utilized to demonstrate that in tumors induced by platelet-derived growth factor-B (PDGFB) overexpression, the majority of the TAM population are BMDM<sup>99</sup>.

BMDM originate from stem cells of the hematopoietic compartment and travel throughout the circulatory system as monocytes surveying for sites of inflammation<sup>117</sup>. They are characterized as

two different cellular populations in the circulation by Gr1 expression; Gr1<sup>+</sup> inflammatory monocytes and Gr1<sup>-</sup> circulating monocytes<sup>118</sup>. The former actively search for sites of inflammation while the later are known to enter non-inflamed tissues as their names would suggest. Upon encountering an inflammatory stimulus, monocytes are drawn into the tissue via a variety of chemokine-dependent mechanisms particularly relating to the monocyte-chemoattractant protein (MCP) family of chemokines<sup>119</sup>. These infiltrating BMDM have been shown to be distinct in expression profile, lifespan, and activity when compared to their tissue-resident counterparts<sup>120,121</sup>. This would suggest that the two cell types additionally have different roles in glioblastoma.

On the expression level, it has been shown that tumor-associated MG and BMDM in glioblastoma display a variety of differentially expressed genes relative to naïve cells as well as relative to each other<sup>99,122,123</sup>. It has further been demonstrated that MG and BMDM express M1 and M2 markers within these tumors, suggesting either that both M1 and M2 cells exist in the tumor, or that the cells co-express markers from the two categories<sup>124,125</sup>. Recent single-cell RNA-sequencing results suggest that single TAM cells are capable of expressing both M1 and M2 markers and that cellular ontogeny drives the differences in gene expression seen between the cell types<sup>126</sup>. An additional layer of complexity is introduced when considering the localization of MG and BMDM within the tumor. On top of their different expression profiles, the cells tend to reside in different niches within the tumor (**Figure 1.5**). MG tend to accumulate on the peritumoral edge, while BMDM localize primarily in perivascular and perinecrotic regions within the tumor<sup>99,127</sup>.

In addition to the aforementioned innate immune cells, T cells of the adaptive immune system are known to exist in glioblastoma tumors albeit in limited numbers. Current estimations with flow cytometry place their percentage at around 0.25% of the total cells within the tumor<sup>128</sup>. T cells can be recognized by expression of the marker CD3 with further subdivision into CD4<sup>+</sup> regulatory T cells and CD8<sup>+</sup> cytotoxic T cells<sup>129</sup>. Within glioblastoma tumor samples, only a quarter

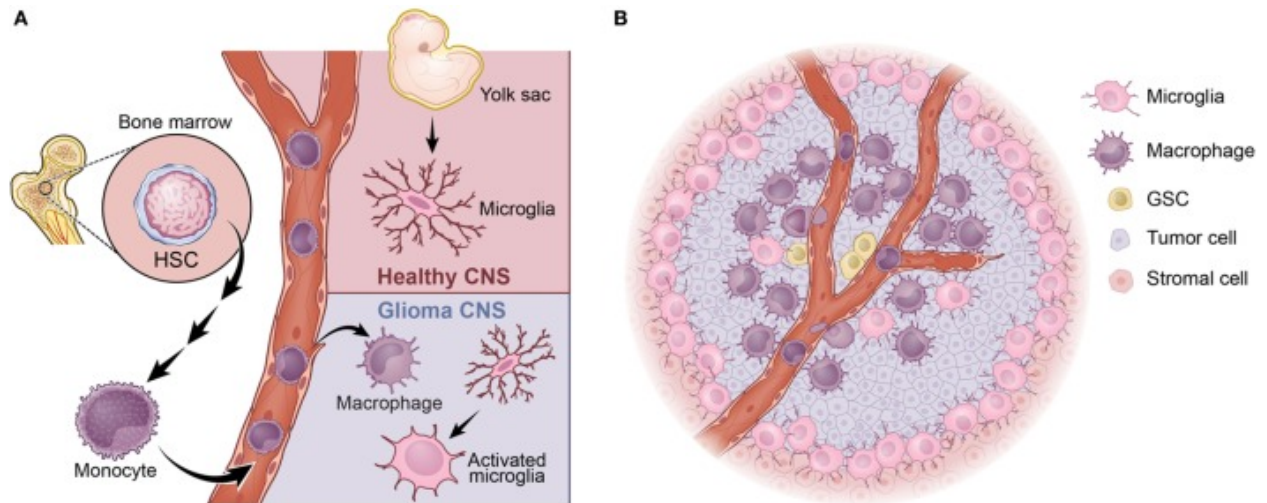


**Figure 1.5. The ontogeny and localization of TAMs in glioblastoma.** (A) A depiction of the ontogeny of the two subsets of TAMs in glioblastoma. (B) A depiction of the localization of MG to the peritumoral space and BMDM to the perivascular space in the tumor microenvironment.

Adapted from Chen et al. 2018<sup>11</sup>.

of the total T cells have been shown to fall in the CD8<sup>+</sup> subset, meaning that the majority of the few T cells within the tumor are not capable of cell killing<sup>128</sup>. The limited presence of these cytotoxic T cells is further diminished by the variety of immunosuppressive mechanisms present within the tumors that quench any activity they may have. The regulatory T cells that are present are thought to exert a strong immunosuppressive effect, an activity that has been demonstrated in other tumor types<sup>130</sup>. T cells isolated from glioblastoma tumor tissue and stimulated also display a reduced response compared to naïve T cells, suggesting an immunosuppressed or anergic state<sup>128</sup>.

In addition to immunosuppression by regulatory T cells, the programmed cell death protein-1 (PD-1)/programmed cell death protein-ligand 1 (PD-L1) signaling axis has been demonstrated to be present in glioblastoma<sup>131</sup>. PD-1 was initially discovered as a pro-death signal in T cells and further demonstrated to be involved in the control of immune activation<sup>132,133</sup>. Its ligand, PD-L1 is highly inducible on antigen-presenting cells as well as macrophages and serves as a way for the innate immune system to “check” the activity of the adaptive immune system, hence the name of the PD-1/PD-L1 axis as an immune checkpoint<sup>134</sup>. PD-L1 expression has been demonstrated on both glioblastoma tumor cells as well as macrophages in glioblastoma<sup>135</sup>. This axis presents another mechanism through which the tumor microenvironment suppresses T cells *in vivo*.

## 1.5 Therapeutic Interventions in Glioblastoma

Treatment for glioblastoma has evolved tremendously over the past 100 years; however, options are still limited and far from perfect. Due to its incredibly fast progression and dismal median survival of 3-4 months without treatment, many extreme treatment modalities have been investigated throughout history<sup>15</sup>. Prior to the advent of radiotherapy, investigators performed extreme surgical procedures such as complete resection of the afflicted cerebral hemisphere in patients with glioblastoma<sup>136</sup>. Others attempted to extend survival by repeatedly infusing patients with bacteria to induce an immune response<sup>137</sup>. Unfortunately, none of these treatments proved to

be particularly effective and patients inevitably succumbed after experiencing brutal attempts at curing the disease.

The classical treatment regimen for patients with glioblastoma, established in the mid-1900s, is maximal surgical resection followed by radiation therapy; which extends median survival to around one year following diagnosis<sup>138,139</sup>. The most significant improvement in median survival following the establishment of surgery and radiation as standard of care was the introduction of the alkylating agent temozolomide (TMZ) to this protocol in the early 2000s which extended the median survival to 14.6 months following diagnosis vs 12.1 months without TMZ treatment<sup>140</sup>. Although somewhat efficacious, this regimen is hampered by the fact that some patients express an enzyme (MGMT) that renders them refractory to this treatment<sup>30</sup>. Furthermore, a median survival that still sits at around one year is far from a cure. Most of the advancements that have been made in the past 50 years have been incremental improvements to existing protocols; however, promising results hint at future breakthroughs in the treatment of glioblastoma.

Surgical resection remains the most effective and longest standing therapy for the treatment of glioblastoma<sup>141</sup>. Not only is surgery ideal for its ability to debulk tumors, but it is essential to obtain tumor tissue to insure proper diagnosis and inform on the proper treatment pathway<sup>141</sup>. There is minimal evidence from prospective clinical trials indicating the relationship between extent of surgical excision and prognosis; however, multiple retrospective studies have shown a strong correlation between extent of resection and median survival<sup>26,27,142-144</sup>. Complete resection of a glioblastoma remains impossible due to the extremely infiltrative nature of the disease and lack of a clear border with adjacent tissue. Imaging techniques involving intraoperative tumor imaging and fluorescent reporter molecules such as 5-aminolevulinic acid (5-ALA) have provided tools to increase the average resected area following surgery<sup>145-147</sup>. Even so, complete resection of enhancing tumor has been shown to occur only in about 68% of patients<sup>148</sup>. Additional hurdles facing

neurosurgeons when performing surgical resections are posed by the location of the tumors within the brain as well as the age of the patients. Due to either factor, surgery may not be an option as tumors in certain brain locations (eg. the brainstem) do not allow for surgical resection and elderly patients are often unfit to undergo surgical debulking<sup>149</sup>. It should be noted, that in patients over 80 years of age, surgical debulking is still associated with a prolongation of median survival when possible<sup>150</sup>.

In addition to maximal safe surgical resection, nearly all glioblastoma patients also receive radiation therapy. Radiation therapy was initially conceptualized in the 1930s, introduced for the treatment of glioblastoma in the 1960s, and extended median survival from 3-6 months with surgery alone to around 12 months<sup>151,152</sup>. Initial regimens consisted of whole brain radiation due to the inability to distinguish the extent of disease with the neuroradiological tools of the era<sup>153</sup>.

Technological advances over the past 50 years have allowed for focal irradiation of tumors and minimization of damage to critical non-tumoral structures adjacent to cancerous tissue<sup>152</sup>. The current standard of care for glioblastoma radiotherapy consists of postoperative radiation with total doses in the range of 50-60 Gy<sup>154</sup>. This radiation is typically delivered as fractionated focal irradiation at a dose of 2 Gy per day 5 days a week for up to 6 weeks<sup>140</sup>. With respect to radiation therapy, there remain hurdles that must be overcome regarding ideal treatment schemes. For example, elderly patients are often excluded from large clinical trials and therefore there are still no standardized protocols regarding their treatment<sup>155</sup>. Currently, researchers are investigating the ideal fractionated radiation therapy regimen in elderly patients<sup>156</sup>.

There have been many clinical trials of traditional chemotherapeutic agents for the treatment of glioblastoma with extremely limited positive results. These agents are often alkylating agents that cause DNA damage to induce apoptosis in replicating cells<sup>157</sup>. Drugs such as carmustine and cisplatin have demonstrated minimal improvement in median survival and are associated with

significant toxicity<sup>158,159</sup>. The current standard of care is the alkylating agent TMZ that is administered as concomitant and adjuvant therapy with radiation in glioblastoma<sup>140</sup>. It was previously established that MGMT expression reduces the efficacy of TMZ to induce apoptosis in cells and shown in glioblastoma patients that epigenetic silencing of MGMT via promoter methylation can predict response to TMZ<sup>30,160</sup>.

In addition to broadly toxic chemotherapeutic agents, significant work has gone into the development of targeted therapies aimed at inhibiting known oncogenic pathways within glioblastoma<sup>161</sup>. For example, many RTKs have signaling that is dysregulated in glioblastoma. Therefore, targeted therapies that normalize these signaling pathways offer logical routes of investigation for management of the disease. For example, EGFR amplification or mutation (eg. EGFRvIII) is present in roughly half of glioblastoma cases<sup>162,163</sup>. Therefore, many groups have implemented trials to test the efficacy of EGFR signaling inhibitors for the treatment of glioblastoma. Erlotinib, a small molecule EGFR inhibitor has been shown to be safe when combined with TMZ and capable of increasing median survival<sup>164</sup>. Treatment with erlotinib alone, however, has no effect on survival<sup>165</sup>. Another EGFR inhibitor, gefitinib, was shown to sensitize glioblastoma cells to radiation *in vitro*, however it too failed to produce an increase in median survival in clinical trials<sup>166,167</sup>.

In addition to aberrant EGFR signaling, glioblastomas are known to demonstrate PDGFR amplification as well as expression of all PDGF ligands<sup>6,168</sup>. Additionally, alterations in hepatocyte growth factor receptor (HGFR), fibroblast growth factor receptor (FGFR), and vascular-endothelial growth factor receptor (VEGFR) signaling pathways are common in glioblastoma and linked to tumor progression and angiogenesis<sup>6,169-171</sup>. Multiple VEGFR inhibitors including sorafenib and tivozanib have been tested in the context of recurrent glioblastoma. The drugs were shown to exert a significant anti-angiogenic effect but were not capable of extending median survival<sup>172,173</sup>. The pan-

VEGFR inhibitor cediranib was also shown to be ineffective at extending median survival in a phase III clinical trial, however, it has been proposed to be a suitable anti-edema therapy in glioblastoma<sup>174,175</sup>

It has been hypothesized that inhibition of a single RTK pathway may not be sufficient to produce a beneficial effect in glioblastoma as compensation can occur through other pathways. Therefore, RTK inhibitors targeting multiple pathways have also been tested in glioblastoma<sup>176</sup>. An initial clinical trial for the dual RTK inhibitor AEE788 was performed on the basis that it inhibited both EGFR and VEGFR, two pathways known to contribute to the pathogenesis of glioblastoma. The phase I clinical trial demonstrated significant toxicity with little efficacy for the treatment of recurrent glioblastoma<sup>177</sup>. The first RTK inhibitor to hit the market, imatinib, is a PDGFR and c-Kit inhibitor<sup>178</sup>. It also has been shown to be ineffective at extending median survival in glioblastoma in a phase I/II clinical trial<sup>179</sup>. Small molecule RTK inhibitors have shown essentially zero efficacy in extending median survival of glioblastoma patients in clinical trials.

In addition to small molecule RTK inhibitors, antibody-based therapies have been employed to target the extracellular domain of these proteins as well as to capture the ligands responsible for activating the receptors. This methodology presents challenges since only 0.1-0.2% of circulating antibodies have been shown to cross the BBB<sup>180</sup>. The BBB is a collection of cells that form and line vasculature in the CNS<sup>181</sup>. The brain has evolved vasculature that is enveloped in smooth muscle cells, pericytes, and astrocytes that prevent the passage of large molecules and charged molecules from the circulation into the brain. The endothelial cells in the BBB are held together by tight junction molecules that establish its size selectivity.<sup>182,183</sup> Apart from physical exclusion, the endothelial cells of the BBB are also known to express multi-drug resistance pumps<sup>184</sup>. These proteins actively recognize and excrete drugs and xenobiotics from the endothelial cells lining the BBB, thereby preventing their entrance into the brain tissue<sup>185,186</sup>. Via the aforementioned

mechanisms, the BBB has been reported to exclude up to 98% of all small molecules from entering the brain<sup>28</sup>. Although the BBB is frequently disrupted in glioblastoma, it is not uniformly disrupted, and these processes can contribute to drug delivery challenges in regions where this barrier is intact.

It is possible that antibody can leak through areas where the BBB is disrupted. The anti-EGFR antibody cetuximab was tested as a salvage therapy on relapsed patients and demonstrated little efficacy<sup>187</sup>. Monotherapy on newly diagnosed patients was also examined in a phase II clinical trial with disappointing results<sup>188</sup>. The lack of efficacy here has not been explained mechanistically, but it is plausible to hypothesize that lack of drug distribution throughout the tumor plays a role.

Some of the receptors targeted by these therapies are present at the cell surface of blood vessels and antibodies have also been engineered to target circulating molecules that agonize the receptors. In these cases, the antibody may not need to cross the BBB to exert its action. For example, bevacizumab is a monoclonal antibody that binds to circulating VEGF and prevents it from activating its receptor, thereby producing a potent anti-angiogenic effect<sup>189</sup>. Initial randomized trials for bevacizumab in the context of newly diagnosed glioblastoma demonstrated no significant improvement in overall survival, but a slight increase in progression free survival albeit less than the stated goal of the study<sup>190</sup>. As analyzed in the AVAglio trial, combination of bevacizumab with standard of care radiation and temozolomide therapy produced a similar benefit with respect to progression free survival and patients receiving bevacizumab required less glucocorticoid treatment to manage edema<sup>191</sup>. It should be noted that patients receiving bevacizumab in this trial demonstrated a higher incidence of adverse events than those receiving placebo. The results of this study also suggested that bevacizumab may serve as an attractive anti-edema therapy in glioblastoma, a result that was confirmed in murine studies<sup>192</sup>. Further stratification of the AVAglio data into molecular subtypes additionally illustrated that patients with Proneural glioblastoma may derive a survival benefit from the addition of bevacizumab to standard of care<sup>193</sup>. This result suggests that the

different molecular subtypes respond differently to therapy and should be treated as separate diseases in some respects. It dictates that all patients should receive genomic tumor profiling at diagnosis and that this information should be used to guide treatment decisions. Furthermore, it suggests that additional information can be gleaned from clinical trials when patients are stratified based on subtype.

In addition to targeting oncogenic signaling pathways in glioblastoma, significant attention over the past decade has focused on how the non-neoplastic cells in the tumor microenvironment can be targeted therapeutically<sup>194</sup>. In a sense, targeting VEGF signaling therapeutically impacts the microenvironment since it interrupts pro-angiogenic signaling between the neoplastic cells and endothelial cells within the tumor. Perhaps the most compelling microenvironment-focused therapies now are fixated on modulating the activity of immune cells within the tumor with the goal of stimulating their ability to kill. Two main methodologies employed to accomplish this goal focus on distinct but related immune cell types: macrophages and T cells.

Targeting macrophages can be accomplished through a variety of mechanisms including re-educating or repolarizing the cells towards an anti-tumor phenotype or simply inhibiting the infiltration of BMDM into the tumor. With respect to the former, it was shown in mice that repolarization of macrophages with an CSF-1R inhibitor could increase survival and decrease tumor volume in a murine model of Proneural glioblastoma<sup>195</sup>. This effect was attributed to a re-education of the cells towards an M1-like phenotype. When the orally bioavailable CSF-1R inhibitor PLX3397 was tested in glioblastoma in a phase II clinical trial, the drug was shown to be well tolerated and BBB penetrant, but no positive effects on survival were demonstrated<sup>196</sup>. Additional clinical trials of CSF-1R inhibitors have demonstrated their tolerability, but no clear efficacy in the treatment of solid tumors has been established<sup>197</sup>. Preclinical analysis of the compounds amphotericin B as well as the toll-like receptor 3 agonist poly I:C has demonstrated the ability of these compounds to polarize

macrophages towards an anti-tumor phenotype and stimulate their ability to inhibit glioblastoma growth<sup>198,199</sup>. In particular, poly I:C has shown some promise in phase II clinical trials as an immune adjuvant therapy<sup>200</sup>.

CSF-1R inhibition has been investigated in combination with anti-angiogenic therapy for its ability to reduce the chemotaxis of peripherally-derived BMDM into tumors<sup>201</sup>. This touches on the idea that instead of re-educating these cells, perhaps it would be more beneficial to block their infiltration in the first place. It is widely accepted that the recruitment of TAMs in glioblastoma mainly provides a pro-tumoral environment<sup>10,202</sup>. Therefore, blocking their infiltration is a logical step towards improving patient outcomes through direct inhibition of a pro-tumoral pathway. BMDM are known to be recruited to sites of inflammation through a wide array of chemotactic pathways<sup>203</sup>. Of these pathways, the C-C motif chemokine ligand 2 (CCL2)/C-C motif chemokine receptor 2 (CCR2) and C-X-C motif chemokine ligand 12 (CXCL12)/C-X-C motif chemokine receptor 4 (CXCR4) pathways have been shown to be intimately related to the chemotaxis of macrophages in glioblastoma<sup>204,205</sup>. Stratification of human glioblastoma patients based on CCL2 expression demonstrates an inverse relationship between CCL2 expression and survival time<sup>99</sup>. Furthermore, heterozygous loss of CCL2 in a murine model of glioblastoma results in an increase in median survival<sup>99</sup>. No clear demonstration of CCL2 ablation resulting in reduced BMDM infiltration has been shown, but this likely stems from the redundant activities of the MCP family members (MCP-1, MCP-2, MCP-3, and MCP-4). Inhibition of CXCR4 signaling when combined with anti-angiogenic therapy in a preclinical model of glioblastoma has been shown to reduce tumor growth and increase overall survival<sup>206</sup>. The precise actions on macrophage chemotaxis were not analyzed, but it is plausible to hypothesize that the mechanism involved these cells. Initial clinical trials validated the tolerability of CXCR4 blockade in glioblastoma and future trials will interrogate the efficacy in extending median survival.

In addition to directly targeting macrophages, a significant body of work has gone into elucidating the interaction between macrophages and T cells and developing therapies that leverage this interaction to produce a positive effect<sup>11</sup>. Perhaps the most prescient interaction between these cell types as of late has involved the PD-1/PD-L1 signaling axis<sup>135</sup>. Due to the resonant successes in treating melanoma with immune checkpoint blockade, the prospect of treating other tumor types, including glioblastoma, has received significant attention<sup>207,208</sup>. The expression of PD-L1 by glioblastoma cells has been demonstrated but called into question due to the antibodies and methodologies employed<sup>135,209</sup>. The more prominent theory is that PD-L1 is expressed by macrophage cell types, termed myeloid-derived suppressor cells (MDSCs) in glioblastoma, and contributes to their immunosuppressive phenotype<sup>210,211</sup>. Regardless of the cell types expressing PD-L1, its expression has been confirmed in glioblastoma tissue and is likely to interact with PD-1 on the T cells that do infiltrate the tumor.

A variety of PD-1 and PD-L1 neutralizing therapies are currently under investigation either as monotherapies or multimodal therapies for the treatment of glioblastoma. Of these, the PD-L1 neutralizing antibodies avelumab and atezolizumab have been demonstrated as safe for use in glioblastoma patients and initial biomarkers of responders have been illuminated, but not yet rigorously analyzed<sup>212,213</sup>. PD-1 neutralizing therapies appear to be slightly more mature in the context of glioblastoma treatment. Neoadjuvant nivolumab treatment has been shown in a phase II clinical trial to boost immune cell infiltration and T cell receptor (TCR) clonal diversity in treated tumors with two of three patients demonstrating a long-term response<sup>214</sup>. A larger clinical trial of the PD-1 neutralizing therapy pembrolizumab with a similar neoadjuvant treatment regimen demonstrated a significant extension in median survival that was attributed to an enhancement of the local and systemic immune response<sup>215</sup>. Considering these results, modulation of T cell actions in

the tumor microenvironment provides a novel and promising therapeutic strategy for the treatment of glioblastoma.

## 1.6 Rationale and Goals for this Project

The lack of progress towards the cure for glioblastoma is likely multimodal and rooted in perceptions about the disease that are incompatible with the recent knowledge generated in the field. The model systems that have been employed for the past 50 years have significant limitations in their ability to emulate the molecular and cellular heterogeneity of glioblastoma and likely have contributed to the limited success in managing this devastating disease. The focus on tumor cell-targeted therapies neglects the now abundant knowledge regarding the tumor microenvironment. Furthermore, the *in vivo* studies performed in immunocompromised mice fail to consider the intricate relationship between the immune system and the tumor in glioblastoma and are limited by the species incompatibility between human and murine signaling molecules and receptors.

With these concepts in mind, I set out to improve the tools available to the glioblastoma research field and utilize these tools to answer disease relevant questions. The overarching goal of this project was to integrate contemporary concepts regarding the molecule underpinnings of glioblastoma as well as the cellular microenvironment to develop novel, subtype-specific, immunocompetent murine models of adult glioblastoma that are driven by disease-relevant genetic driver mutations. I then sought to use these models to investigate the relationship between the innate immune system and the tumors of differing genetic backgrounds. To this end, the enclosed work can be split into two major stages: (1) the development and validation of disease relevant model systems and (2) the utilization of a disease relevant model system to investigate tumor microenvironment signaling as a therapeutic target in glioblastoma.

Chapter 2 will discuss the generation of subtype-specific murine models of glioblastoma based on the driver mutations outlined in chapter 1.3. Utilizing a somatic, cell type-specific gene

transfer system, I display the ability to induce disease relevant oncogenic transformations in the cell type thought to be the cell of origin for glioblastoma. Furthermore, I illustrate that with respect to gene expression profile and histological characteristics, the murine tumors that I generate closely cluster with the human subtypes they are meant to emulate. Investigation of the response of these models to standard of care illustrates that they respond differently based on subtype, a manifestation that should be considered when discussing the validity of stratifying human patients based on subtype. Finally, I demonstrate the significant disruption of the BBB in PDGFB-overexpressing tumors and propose their utilization for the study of glioblastoma-associated cerebral edema.

Chapter 3 will present the results obtained in my effort to find an alternative therapy to dexamethasone for the management of glioblastoma-associated cerebral edema. I illustrate a connection between dexamethasone and interleukin-1 (IL-1) signaling *in vitro*, *ex vivo*, and *in vivo*. Both dexamethasone treatment and IL-1 signaling are shown to inhibit the chemotaxis of BMDM into murine glioblastoma tumors. Furthermore, both strategies are proven to be efficacious at reducing edema in glioblastoma; however, IL-1 signaling inhibition is demonstrated to be superior in the sense that it does not impair the response to radiation in tumor-bearing mice. In total, this chapter suggests that specific IL-1 inhibition may be an attractive alternative to dexamethasone for the management of cerebral edema and demonstrates that IL-1 signaling controls BMDM recruitment through an MCP family dependent signaling axis.

Chapter 4 provides the overarching conclusions of this work and speculates on the logical future directions pertaining directly to this project. Both immediate goals and long-term future directions are laid out.

## Chapter 2: Subtype-Specific Mouse Modeling of Glioblastoma<sup>1</sup>

<sup>1</sup>Portions of this chapter were adapted from the published manuscript: Herting CJ, Chen Z, Pitter KL, Szulzewsky F, Kaffes I, Kaluzova M, Park JC, Cimino PJ, Brennan C, Wang B, Hambarzumyan D. Genetic driver mutations define the expression signature and microenvironmental composition of high-grade gliomas. *Glia*. 2017;65(12):1914-26. Epub 2017/08/25. doi: 10.1002/glia.23203. PubMed PMID: 28836293.

## 2.1 Introduction

Modeling anything, be it mathematical, computational, biological, or any other permutation, is limited in utility and validity. As famously put by the statistician George E. P. Box, “all models are wrong, but some are useful”<sup>216</sup>. When generating models, it is important to consider the questions the model will be used to address and to design them to be well suited for that purpose. When starting this portion of the project, I strove to design, generate, and validate immunocompetent and subtype-specific mouse models of glioblastoma via *in situ* generation of primary tumors. Specifically, I wanted to generate the premier model for interrogation of questions relating to the immune microenvironment in glioblastoma while providing the ability to assess differences between each genetically defined subtype. This chapter will cover the variety of model systems available for studying glioblastoma, highlight the drawbacks that precluded their utilization for assessment of my questions, and finally the design, generation, and validation of the model system.

Glioblastoma modeling can be separated into *in vitro* and *in vivo* categories with various sub-categories present within. One of the first, and perhaps most widely utilized, models of glioblastoma resides in the *in vitro* category and has been the topic of significant discussion in the field as of late. During the late 1960’s, researchers at Uppsala University in Sweden strove to provide a standardized resource for the glioblastoma field and isolated, validated, and distributed a series of patient-derived cell lines for preclinical research<sup>217</sup>. These cell lines, including U87 and U251 cells, have been employed in thousands of papers since with the former garnering over 1900 citations in PubMed and the latter over 1100 citations<sup>218</sup>. Particularly in the early years, these lines provided researchers with an invaluable resource to study human glioblastoma cells, their growth characteristics, and signaling cascades in a tissue culture dish without needing the tools and expertise to derive them independently. Furthermore, the establishment of these lines as a resource for the field allowed for direct comparison and validation of research coming out of different labs.

Although useful, the cell lines were initially an imperfect tool and have since been plagued by additional problems. First, any analysis of cancer cells in a petri dish neglects the complexity of organismal biology and must be taken with a grain of salt. Without considering the activity of cancer cells within an organism, their interaction with non-neoplastic cells within the tissues in which they reside, and the distribution as well as metabolism of compounds meant to target them therapeutically, results become challenging to interpret. Additionally, following their deposition in an American Type Culture Collection (ATCC) database in the 1970's, the handling of these cells as well as their current validity has been questioned<sup>219,220</sup>.

To address the issues raised with simple *in vitro* studies, it is commonplace to utilize *in vivo* vertebrate models of glioblastoma with mice serving as the most common host animal. Frequently, *in vivo* models are employed to answer questions that cannot be addressed with simple *in vitro* systems, or to confirm results seen with *in vitro* studies. Murine models of glioblastoma will be the focus of this chapter. They can be split into three primary categories, each with their own strengths and weaknesses: (1) xenograft models, (2) syngeneic mouse models, and (3) genetically engineered mouse models<sup>221</sup>.

A xenograft is the implantation of cells, tissue, or organs from a donor of a different species from the recipient. With respect to xenograft models of glioblastoma, there are two main flavors that are frequently employed. First, the aforementioned cell lines can be implanted into the flanks or brains of immunocompromised mice. The main attraction of this methodology is it allows for the interrogation of the same cells between *in vitro* and *in vivo* experiments, thereby increasing the probability that results generated with the former will be confirmed by the latter. It is also easy to grow and expand these cell lines *in vitro*, making generation of sufficient cells for an experiment all but guaranteed<sup>222</sup>. Significant limitations with this methodology arise when the histological characteristics of these tumors are considered. Tumors generated with this methodology frequently

lack the histological hallmarks of glioblastoma including microvascular proliferation, pseudopalisading necrosis, and tumor cell invasion into adjacent tissue<sup>223,224</sup>. The lack of a functional immune system in these mice also prohibits their utilization for immune microenvironment or immunotherapy studies, significantly limiting the scope of what can be accomplished with this tool<sup>225</sup>. Considering the recent concerns regarding the identity of the cell lines used in this approach, for the purposes of accurate modeling of human glioblastoma there are certainly better tactics.

The second xenograft model that is frequently employed is called a patient-derived xenograft (PDX). As the name would suggest, this model involves the xenotransplantation of a human glioblastoma sample either as dissociated cells or a tissue chunk into the flank or brain of immunocompromised mice. Since the same mice are employed in this approach as the previous xenograft methodology, the same limitations regarding the immune system apply. The improvement with this model over the previously described xenograft model comes from the cells used for transplantation. This method allows for transplantation of tumor spheroids that retain some of the structure and microenvironmental cells present in the parent tumor<sup>226</sup>. Furthermore, when implanted orthotopically, tumor cells demonstrate the propensity to infiltrate adjacent tissues, recapitulating phenotypes of the human disease<sup>227</sup>. PDXs additionally display more of the histological hallmarks of glioblastoma, thereby offering an improvement over the injection of established cell lines<sup>228</sup>. Finally, the major advantage of this model is that the cells injected come directly from the patient, quelling any fears over the identity of the cells and if they accurately model what is seen in humans.

The utilization of cells directly from human patients raises the possibility of using this model for personalized medicine or co-clinical trials where patient tumors are tested preclinically alongside their analysis in the clinic<sup>228</sup>. Due to the latency of tumor development, in some cases up to 11 months following injection, as well as the variability in establishment of PDXs the feasibility of this approach is questionable, but the theory remains attractive. Overall, PDXs offer improvements over

the other xenograft model, and display noted utility and widespread acceptance; however, the lack of a functional immune system and incompatibility of cellular signaling between human ligands and murine receptors highlight the drawbacks of this technique.

Syngeneic mouse models of glioblastoma are similar to xenografts in that they involve the transplantation of exogenous tumor cells into mice, but are different in that they involve the engraftment of murine tumor cells in immunocompetent mice<sup>229</sup>. The cell lines used in this methodology were originally isolated from spontaneous tumors (SMA-560) or from chemically induced tumors (CT-2A and GL-261)<sup>230-232</sup>. The obvious advantages of this methodology are that since the cells are murine cells, there are no concerns regarding incompatibility of signaling pathways and they can be implanted in immunocompetent mice; allowing for direct interrogation of the involvement of the immune microenvironment on the tumor. The clear drawback, however, also stems from their identity as murine tumor cells. For most researchers, the goal of their work is to cure human tumors. Some argue that progress towards this goal is hampered by studying murine tumors specifically and that utilization of human tumor cells will provide more rapid progress towards this goal. Regardless, the utilization of immunocompetent mice allows for studies that are impossible using either xenograft methodology.

The final technique frequently employed to model glioblastoma involves the utilization of genetically engineered mice to generate tumors. In fact, the first mouse model of brain tumors was developed by delivering oncogenes to the eggs of transgenic mice<sup>233</sup>. Further development of molecular biology techniques allowed for the tissue-specific and conditional expression of oncogenes for cancer modeling<sup>234</sup>. In total, most genetically engineered mouse models utilize either viral delivery of oncogenes, or Cre-lox mediated activation of oncogenes in transgenic mice. These methods allow for generation of primary tumors in immunocompetent mice. This allows for the analysis of immune interactions with the tumor as well as immunotherapies. Furthermore, since

tumor cells are not injected directly into the mice, it allows for tumor development *in situ*, more accurately mimicking the process that occurs in human patients. The final advantage of genetically engineered mouse models stems from their tunability. These methods allow for the delivery of precise oncogenes or combinations of oncogenes to specific cell types at specific times, thereby allowing for more accurate genetic and temporal modeling of what is seen in humans.

The goal of this portion of the project was to generate the premier model for interrogation of questions relating to the immune microenvironment in glioblastoma with the ability to assess differences between each subtype. Considering the inability to perform immunological studies in xenograft models, and limitations regarding the tunability of syngeneic models with respect to the tumor subtype, I chose to investigate genetically engineered mouse models to achieve my goal.

In the early 1990's, a group at the National Cancer Institute (NCI) hypothesized that avian viruses and their associated receptors could provide a tool to specifically transfer genetic information to predetermined mammalian cell types. They noted that avian leukosis viruses (ALVs) had been previously utilized to transfer genetic information to avian cells, but the tool lacked utility in the mammalian space due to its inability to infect mammalian cells. In 1993, however, they isolated and published a chicken gene, *tv-a*, that conferred susceptibility to infection by ALV and avian sarcoma viruses (ASV)<sup>235</sup>. With this information in hand, they designed a transgenic mouse that expressed this gene under the sk-actin promoter, making it specific for skeletal muscle cells and demonstrated the ability of these cells to be infected by ALV<sup>236</sup>. Here they noted that the promoter under which *tv-a* was expressed could be changed, theoretically providing the ability to target any cell within an animal that expressed a cell type-specific promoter. They highlighted that this discovery offered promise of an attractive promise for the cancer research and gene therapy fields.

The first paper that described the utilization of this tool for the modeling of brain tumors termed the system replication competent avian sarcoma leukosis virus long terminal repeat with

splice acceptor/tumor virus-A (RCAS/*tv-a*) and displayed the ability of this system to induce EGFR expression in Nestin- or GFAP-positive cells, thereby creating glioma-like lesions in mice<sup>237</sup>. Over the following decade, this tool was honed and the number of mutations that could be delivered increased<sup>238-240</sup>. In 2009, it was demonstrated that PDGFB could be used as an oncogenic driver to induce glioma-like lesions in adult mice that displayed the histological characteristics of human tumors<sup>241</sup>.

As I set out on this project, my initial goal was to characterize how alike the PDGFB-overexpressing tumors were to human Proneural tumors that are known to have amplifications in PDGF signaling. Furthermore, I wanted to establish models of adult Mesenchymal and Classical glioblastoma in mice driven by NF1-silencing and induced expression of the mutant, constitutively active EGFR, EGFRvIII respectively. Enclosed in this chapter are descriptions of the techniques utilized to generate these models as well as the results of the experiments performed to validate their similarities to human tumors. Finally, I addressed the response of these tumors to standard of care radiation and temozolomide as well as investigative immunotherapies to determine differences in response between the subtypes.

## 2.2 Materials and Methods

### *Mice*

*Ntv-a/Cdkn2a<sup>-/-</sup>/Pten<sup>fl/fl</sup>*, *Ntv-a/Pten<sup>fl/fl</sup>*, and *Ntv-a/Cdkn2a<sup>-/-</sup>/EGFRvIII<sup>fl/fl</sup>/Pten<sup>fl/fl</sup>* mice in the age range of 4-16 weeks were used for all experiments. *Ntv-a/Cdkn2a<sup>-/-</sup>/Pten<sup>fl/fl</sup>* are in a mixed genetic background as previously described<sup>240,242</sup>. *Ntv-a/Pten<sup>fl/fl</sup>* are in a C57BL/6 background and were generated via 10 generations of back crosses. *Ntv-a/Cdkn2a<sup>-/-</sup>/EGFRvIII<sup>fl/fl</sup>/Pten<sup>fl/fl</sup>* are also C57BL/6 background and were generated by crossing the previously described *Cdkn2a<sup>-/-</sup>/EGFRvIII<sup>fl/fl</sup>/Pten<sup>fl/fl</sup>* mice with *Ntv-a/Pten<sup>fl/fl</sup>* mice. All animals were housed in a climate controlled,

pathogen-free facility with *ad libitum* food and water under a 12-hour light/dark cycle. All experiments were performed with equal distribution of gender and age between different groups.

#### *DF-1 Cell Culture and Transfection*

DF-1 cells were purchased from ATCC (ATCC, CRL-12203) and grown in high-glucose DMEM (ATCC, 30-2002) with 10% FBS (ATCC, 30-2020) and 1x Penicillin/Streptomycin (Gibco, 15140122) at 39°C with 5% CO<sub>2</sub> as specified by the manufacturer. Cells were always transfected in early passages (p1-p3) and were discarded following 25 passages. Transfection was performed for RCAS PDGFB-HA, RCAS Cre, RCAS sh*Nf1*, RCAS sh*p53*-RFP, and RCAS sh*Pten*-RFP using the Fugene 6 transfection kit (Roche, 11814443001) according to the manufacturer's instructions. Plasmid concentrations and quality were measured on a Nanodrop 2000 (Thermo Scientific) prior to utilization and were stored at 4°C. Cells were detached with 0.05% trypsin-EDTA (Thermo Fisher, 25300054) every 2-3 days and were split at a 1:6 or 1:8 dilution.

#### *Tumor Generation*

Injections were performed on a stereotactic fixation device (Stoetling). Mice were anaesthetized with intraperitoneal (IP) injections of ketamine (0.1 mg/g) (McKesson, 494158) and xylazine (0.01 mg/g) (Akorn) prior to shaving the head with battery-powered clippers. A local injection of 50 µl of marcaine (McKesson, 57199) was delivered subcutaneously in the scalp for pre-surgical analgesia. Mice were then loaded onto the stereotactic fixation device and a small caudal incision was made on the scalp to the right of the midline with a surgical scalpel. The skull was then blotted dry with sterile cotton tipped applicators and a burr hole was made in the skull with a surgical drill in the appropriate location for tumor generation. DF-1 cells ( $4 \times 10^4$ ) were stereotactically delivered with a Hamilton syringe equipped with a 30-gauge needle. For PDGFB-overexpressing tumors, RCAS PDGFB was injected alone in *Ntv-a/Cdkn2a<sup>-/-</sup>/Pten<sup>fl/fl</sup>* mice and co-injected with RCAS sh*p53*-RFP at a 1:1 ratio for tumors generated in *Ntv-a/Pten<sup>fl/fl</sup>* mice. PDGFB-

overexpressing tumors were generated in the right-frontal striatum with injection locations at AP-1.7 mm and right-0.5 mm from bregma; depth-2 mm from the dural surface<sup>243</sup>. For NF1-silenced tumors, RCAS sh*Nf1*, RCAS sh*p53*-RFP, and RCAS Cre were co-injected at a 1:1:1 ratio in the subventricular zone at AP-0.0mm and right-0.5mm from bregma; depth-1.5mm from the dural surface<sup>243</sup>. EGFRvIII tumors were generated via injection of RCAS Cre, RCAS sh*p53*-RFP, and RCAS sh*Pten*-RFP at a 1:1:1 ratio also in the subventricular zone. The scalp was sealed with GLUture (WPI, 503763) and sterilized with iodine before placing the mice on a heating pad until cessation of anesthesia. Mice were then treated with 50 µl of buprenorphine (McKesson, 1013922) subcutaneously at the site of incision prior to returning to their cage as well as once more within 24 hours of the surgery. Mice were continually monitored for signs of tumor burden and were sacrificed upon observation of endpoint symptoms including head tilt, lethargy, seizures, and excessive weight loss.

#### *Tissue Isolation*

At endpoint, mice were sacrificed via ketamine overdose and perfused with sterile Ringer's solution (Sigma-Aldrich, 96724-100TAB). The brain was extracted, and a piece of tumor was immediately snap-frozen in liquid nitrogen for storage at -80°C. The remainder of the brain was transferred to 10% neutral-buffered formalin (Sigma-Aldrich, HT501128) for 72 hours. Fixed tissues were embedded in paraffin and 5 µm formalin-fixed paraffin embedded (FFPE) sections were cut on a microtome (Leica). The sections were deparaffinized in histo-clear (Fisher Scientific, 50-899-90147) and were passed through graded alcohols prior to H&E staining for tumor verification and grading by a certified neuropathologist.

#### *Radiation and Drug Treatment of Tumor-Bearing Mice*

Prior to irradiation, mice were sedated with ketamine and xylazine at the dose utilized for surgery. Irradiation of the head was performed with the X-RAD 320 irradiator (Precision X-Ray)

with the mice loaded into a lead shield apparatus with only the head exposed to the radiation beam. Radiation was administered at 115 cGy/min for a total daily dose of 2 Gy. Mice received radiation for five consecutive days followed by two days off for two total cycles. TMZ (Sigma-Aldrich, T2577) treatment was administered as a monotherapy at a dose of 25 mg/kg/day in 10% DMSO in saline via oral gavage on the same dosing schedule as the radiation. Vehicle was delivered to control mice following the same schedule. For anti-PD-L1 therapy, mice were administered either a PD-L1 neutralizing antibody (Bio X Cell, BE0101) or its isotype control, Rat IgG2b (Bio X Cell, BE0090) via intraperitoneal injection at a dose of 10  $\mu$ g/kg on the indicated days. Mice were continually monitored and sacrificed upon display of endpoint symptoms.

#### *Immunohistochemistry*

5  $\mu$ m FFPE sections were stained using the DISCOVERY XT automated staining platform (Ventana Medical Systems). Anti-CD31 (BD Pharmingen, 558736, 1:50), anti-CD44 (BD Pharmingen, 550538, 1:1000), anti-pH3 (Ser10) (Millipore, 06-570, 1:400), anti-GFAP (Dako, Z0334, 1:8000), anti-OLIG2 (Millipore, AB9610, 1:400), and anti-IBA1 (Wako, 019-19741, 1:250) were utilized for stainings at the indicated dilutions. Phosphate-buffered saline (PBS) with 2% bovine serum albumin (BSA) was used as a buffer for the antibodies. Coverslips were mounted with Permount (Fisher Scientific, SP15).

#### *Magnetic Resonance Imaging (MRI)*

All MRI data were acquired with a 9.4 T/20 cm horizontal bore Bruker magnet, interfaced to an Avance console (Bruker) and equipped with an actively shielded gradient set (inner diameter, 11.0 cm; maximum gradient strength, 400 mT/m; rise time, 110 ms) with modifications of a previously established protocol<sup>244</sup>. A two-coil actively decoupled imaging set-up was used (a 2 cm diameter surface coil for reception and a 7.2 cm diameter volume coil for transmission) to achieve maximal signal-to-noise ratio over the cortical and subcortical areas of interest. All animals were

imaged with a custom-made ID 32 mm quadrature birdcage body resonator (Stark Contrast MRI Research) while anesthetized using 1.5-2.2% isoflurane (Terrell™, MINRAD Inc.). All images were acquired on a Bruker USR 9.4T scanner (Bruker Biospin MRI Inc.). The mouse head was imaged in the coronal orientation using a T2-weighted rapid acquisition with relaxation enhancement (RARE) sequence with TR= 3.5 s, TE= 60 ms, RARE factor of 8, NE= 4, FOV= 40 x 40 mm<sup>2</sup>, slice thickness = 0.7 mm, with an in-plane resolution of 0.156 x 0.156 mm<sup>2</sup>. Animal breathing was monitored using an animal physiological monitor system (SA instruments). Tumor volumes were determined by outlining the tumor region apparent in each MRI section and multiplying it by the slice thickness. The sum of the tumor volume from each slice was used as the total tumor volume. The growth curves generated with this analysis were fitted with an exponential growth equation of the form  $y = y_0 + e^{k_g * t}$ . The mean value for the growth rate constant ( $k_g$ ) was compared between PDGFB-overexpressing and NF1-silenced tumors.

#### *Image Acquisition and Analysis of Cell Populations*

The Nanozoomer 2.0HT (Hamamatsu Photonics) whole slide scanner was utilized to convert the stained tissue sections into digital files. Subsequent image analysis was carried out using Fiji<sup>245</sup>. For each tumor and staining, the total tumor area was calculated, and several representative images were selected per tumor area. To account for heterogeneity within individual samples, each tissue section was subdivided into different regions. Each region was subsequently attributed a percentage of the total number of images per section based on its relative size. For IBA1, CD44, CD31, and GFAP, the percentage of stained area per 2560 x 1417-pixel area (pixel width: 454 nm) field at 20x magnification was analyzed, whereas positive nuclei per field were quantified for pH3. Additionally, for CD31, average vessel size was calculated by dividing the CD31-positive area by the number of vessels. OLIG2-positive nuclei number was estimated using Aperio's Image Analysis Toolbox (Leica Biosystems). The investigators were blinded as to the tumor type of the samples

during the quantification process. Necrotic and peri-tumoral areas were not included. Final values were standardized to an area of one mm<sup>2</sup>.

#### *RNA Extraction and Quantitative-PCR*

Snap-frozen tumor pieces were utilized for RNA extraction using the RNeasy Lipid Tissue Mini-Kit (Qiagen, 74804) according to manufacturer's instructions. RNA concentrations were measured with a NanoDrop 2000 (Thermo Scientific) and RNA quality was assessed by electrophoresing the samples through a 1% agarose (Sigma-Aldrich, A9539), 1% bleach (Sigma-Aldrich, 425044) gel spiked with ethidium bromide (Sigma-Aldrich, E1510) according to established protocol<sup>246</sup>. A cDNA library was synthesized for each sample using the First Strand Superscript III cDNA synthesis kit (ThermoFisher, 18080051) according to the manufacturer's instructions and with equal amounts of starting RNA. Quantitative-PCR was performed with the validated BioRad PCR primers for murine *Abcg2*, *Aif1*, *Akt2*, *Ascl1*, *Casp1*, *Cebpb*, *Chi3l1*, *Dll3*, *Egfr*, *Elk1*, *Fgfr3*, *Jun*, *Met*, *Mgmt*, *Mmp9*, *Myc*, *Ncam1*, *Nes*, *Olig2*, *Pdgfa*, *Serpine1*, *Snai2*, *Sox2*, *Sp1*, *Src*, *Stat3*, *Taz*, *Tgfb1*, *Tlr4*, *Yap1*, and  $\beta$ -*Actin* using SsoAdvanced Universal green Supermix (BioRad, 1725271). Fold change in gene expression was determined relative to the PDGFB-overexpressing tumors using the  $2^{-\Delta\Delta Ct}$  method with  $\beta$ -Actin as a housekeeping gene. Gene expression results were converted to log<sub>2</sub> z-scores prior to analysis.

#### *TCGA Analysis*

Patient survival data, mRNA expression, gene mutation and copy number values for each gene of interest were obtained from the MSKCC computational biology cancer genomics data server using the R package *cgdsr* (<https://github.com/cBioPortal/cgdsr>)<sup>247,248</sup>. Expression subclasses were assigned based on annotation as previously described and G-CIMP-positive tumors were excluded<sup>6</sup>. EGFR- and PDGFRA-altered tumors were defined by gene amplification (GISTIC score = 2).

NF1-altered tumors were identified as the union of cases with gene loss (GISTIC score = -1) and silencing mutations (nonsense or frameshift). Analysis was performed on two datasets; 1) a dataset where patients with two or more hits (co-amplifications of EGFR, PDGFRA and deletions of NF1) are included and 2) a dataset where patients with two or more hits are excluded. Data for the same genes analyzed with quantitative-PCR in murine tumors were downloaded.

### *Clustering Analysis*

A distance matrix was calculated, and hierarchical clustering was performed on the murine quantitative-PCR data using the factoextra package in R. Principal component analysis on murine tumor and human tumor expression data were also performed using this package. A gene expression heatmap for both sets of data was generated using the pheatmap package.

### *Histopathological Analysis*

Hematoxylin and eosin-stained tumor samples were analyzed in a blinded fashion by a certified neuropathologist (PJC). Grading was performed according to the guidelines presented in the 2016 WHO Classification of Tumors of the CNS<sup>8</sup>.

### *Statistical Analysis*

GraphPad Prism (GraphPad Software) versions 6-8 were used for statistical analysis as well as R version 3.5. The details of specific statistical tests are included in the legends of each figure. Data are presented as mean $\pm$ SD. Significant values were those with  $P\leq 0.05$ .

## **2.3 Results**

*The RCAS/tv-a system produces adult NF1-silenced murine HGG from cells in the subventricular zone*

The RCAS/*tw-a* system has been established as a useful tool to study PDGFB-overexpressing high-grade glioma (HGG) *in vivo*<sup>241</sup>. I demonstrated that RCAS PDGFB injection into the right and left hemispheres as well as the subventricular zone of *Ntw-a/Cdkn2a<sup>-/-</sup>/Pten<sup>fl/fl</sup>* mice results in 100% formation of grade IV glioblastoma (**Figure 2.1**). These tumors displayed microvascular proliferation and pseudopalisading necrosis, which are hallmark histological characteristics of human HGG (hHGG)<sup>241,249</sup>. The expression profile of PDGFB-overexpressing murine HGG (mHGG) has been shown to be similar to the human Proneural subtype when generated with various model systems, including RCAS/*tw-a*<sup>250,251</sup>. To model Mesenchymal hHGG using the RCAS/*tw-a* system, I used both mixed strain *Ntw-a/Cdkn2a<sup>-/-</sup>/Pten<sup>fl/fl</sup>* mice as well as C57BL/6-background *Ntw-a/Pten<sup>fl/fl</sup>* mice and co-injected RCAS *shNf1*, RCAS *shp53*, and RCAS Cre into the striatum as well as the subventricular zone. NF1-silenced tumors only formed when injected into the subventricular zone of adult mice (**Figure 2.2A/B**), in contrast to what was previously published regarding PDGFB-overexpressing tumors<sup>241</sup>. These results suggest that cells at various locations can serve as the cell of origin for transformation by PDGFB-overexpression, but only cells in the subventricular zone can be the cell of origin for NF1-silenced mHGG. This conclusion supports previous publications suggesting that the cell of origin for NF1-silenced HGG is either subventricular zone stem and progenitor cells or subventricular zone progenitor cells alone<sup>60,252</sup>. The unique, stem cell-promoting environment of the subventricular zone may also contribute to the ability of NF1-silenced tumors to form only in this location<sup>253</sup>.

Although both the PDGFB-overexpressing and NF1-silenced mHGG models demonstrated reliable tumor formation, there was a significant difference in their median survivals (**Figure 2.2A**). Since median survival can be affected by tumor initiation and/or growth kinetics, I sought to determine to what extent the median survival difference was driven by altered growth kinetics between the two tumor types. To accomplish this task, I used T2-weighted MRI to assess the

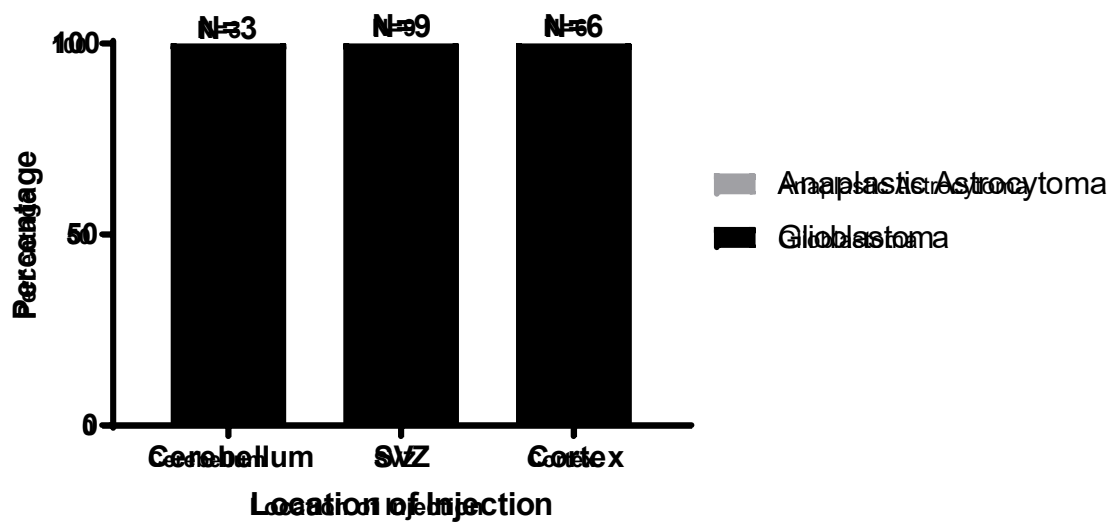
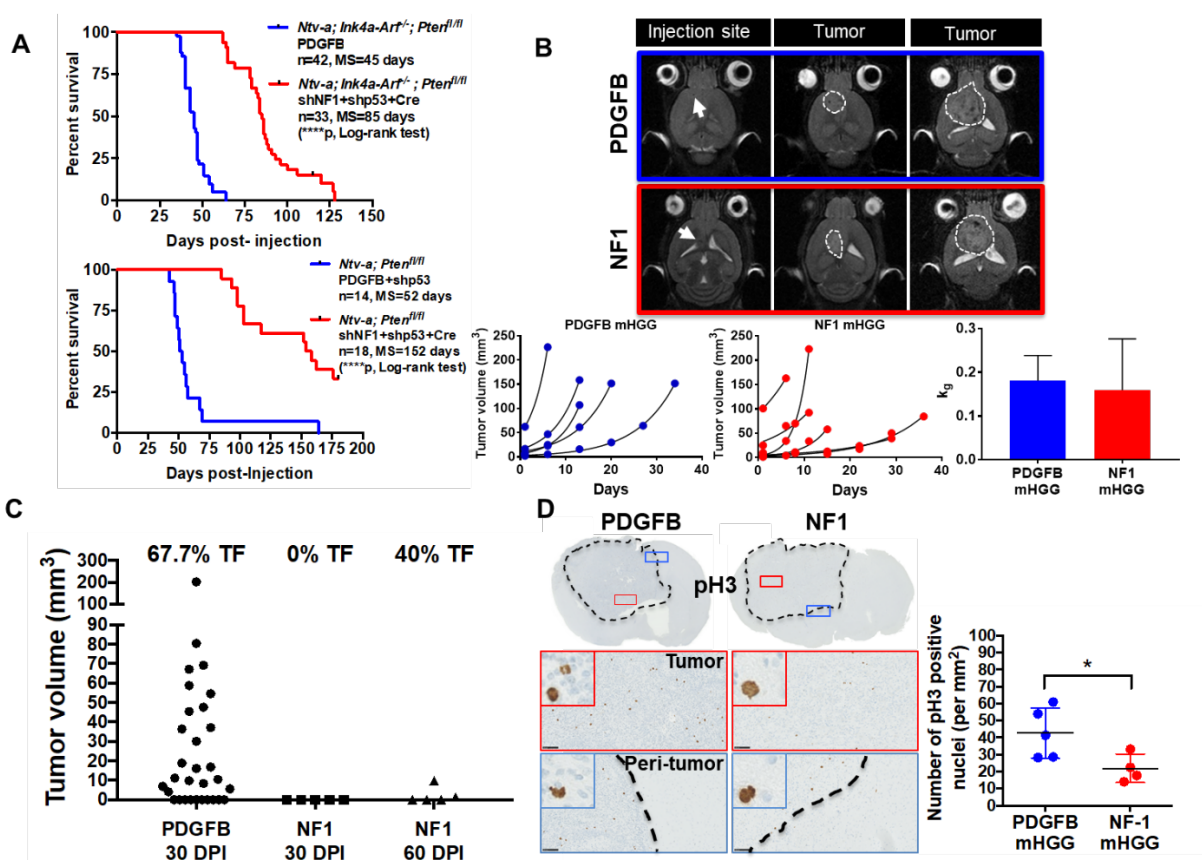


Figure 2.1. PDGFB-overexpression generates grade IV glioblastoma regardless of the location of RCAS injection. PDGFB-overexpressing tumors were generated via RCAS injection in the cerebellum (N=3), SVZ (N=9), and cortex (N=6). H&E-stained tissue samples were analyzed post-sacrifice. No significant difference in malignancy was observed between the groups. Fisher's exact test used for analysis.



**Figure 2.2** PDGF $\beta$ -overexpressing and NF1-silenced murine HGG display significantly different median survivals and tumor initiation times, but similar tumor growth kinetics. (A) Kaplan-Meier survival curve showing overall survival of PDGF $\beta$ -overexpressing and NF1-silenced mHGG in mixed strain *Ntv-a; Cdkn2a<sup>-/-</sup>; Pten<sup>fl/fl</sup>* mice and C57BL/6 background *Ntv-a; Pten<sup>fl/fl</sup>* mice. NF1-silenced mHGG was generated by SVZ RCAS injection, while PDGF $\beta$ -overexpressing mHGG was generated by injections in the frontal striatum. *P*-values were calculated using a log-rank (Mantel-Cox) test. (B) Representative magnetic resonance images of PDGF $\beta$ -overexpressing and NF1-silenced mHGG showing the injection site as well as small and large tumors. Tumor growth curves were fitted with an exponential regression. Comparison of the mean growth rate constant ( $k_g$ ) for each group indicated no significant differences in growth kinetics. The x-axis (days) indicates the number of days after the initial MRI when the scan was taken. (C) Tumor volumes as measured by

T2-weighted MRI scans taken 30 days following RCAS injection for both PDGFB-overexpressing (N=31) and NF1-silenced (N=5) mHGG as well as 60 days following RCAS injection for the NF1-silenced (N=5) model. Percent tumor formation (TF) is indicated above each group. (D) Representative images of immunohistochemistry for pH3 staining of PDGFB-overexpressing (N=5) and NF1-silenced (N=4) mHGG in *Ntr-a/Cdkn2a<sup>-/-</sup>/Pten<sup>β/β</sup>* mice. pH3 quantification shows a significantly increased number of cells in the M-phase of the cell cycle in PDGFB-driven tumors compared to NF1-silenced tumors. Analysis was performed with unpaired, two-tailed Student's t-tests. Scale bars= 100 μm. \* $P < 0.05$ , \*\*\*\* $P < 0.0001$ .

tumor volume once per week following tumor initiation, thereby allowing for determination of the rate of tumor growth over time. This experiment (**Figure 2.2B**) showed that the two tumor types have similar growth kinetics and, therefore, the differences in survival between the two cannot be attributed to this factor. Moreover, MRI scans at 30 days post-RCAS injection in both models, and at 60 days post-injection in the NF1-silenced model, demonstrated that PDGFB-overexpressing tumors form within 30 days of injection, while NF1-silenced tumors take around 60 days to initiate (**Figure 2.2C**). To support the conclusion that PDGFB-overexpressing and NF1-silenced tumors grow at a similar rate, I assessed proliferation in both models using immunohistochemistry for phosphohistone-H3 (pH3), which labels replicating cells in the M-phase of the cell cycle. The quantification of pH3-positive nuclei showed a significantly higher number of positive cells in PDGFB-overexpressing mHGG compared to NF1-silenced mHGG despite apparent heterogeneity in both groups (**Figure 2.2D**). This difference is likely insufficient to completely explain the differences in median survival. These results in total suggest that the main difference seen between survival curves of PDGFB-overexpressing and NF1-silenced mHGG stem from altered latency of the two tumor types following RCAS injection. To corroborate this phenomenon in humans, I evaluated whether there is a difference in the survival of Proneural and Mesenchymal tumors as well as PDGFRA-amplified and NF1-deleted/mutant hHGG using TCGA data and observed no significant difference (**Figure 2.3**).

*Genetic driver mutations determine tumor expression profile and histological characteristics*

Since it was previously demonstrated that enrichment of EGFR, PDGFRA, and NF1 genomic alterations associate with overall transcriptome patterns, I asked whether genetic alterations can directly influence the transcription of factors that are known to be associated with the defined HGG subtypes<sup>6,7</sup>. Through TCGA analysis, it was demonstrated that amplifications in

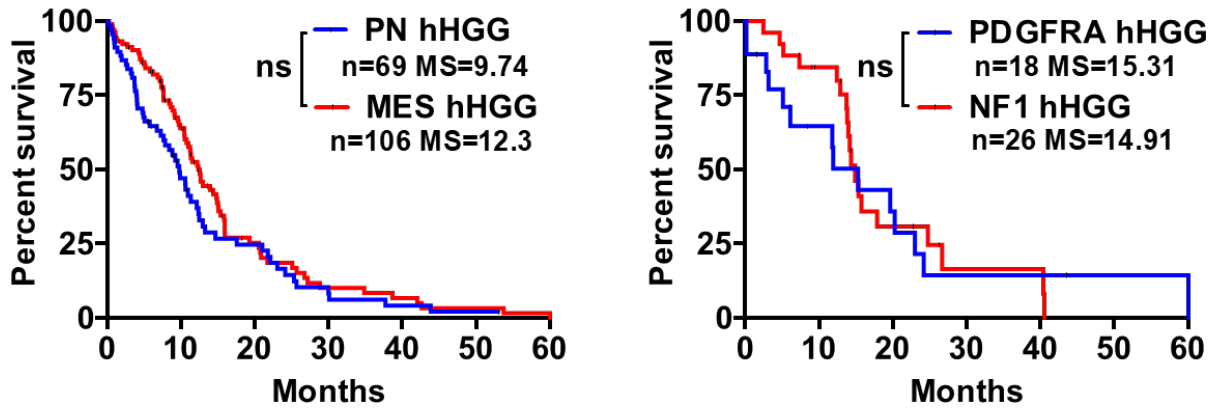


Figure 2.3. Kaplan-Meier survival curves of patients with Proneural and Mesenchymal human HGG; and PDGFRA-amplified and NF1-deleted/mutant human HGG. Analysis performed with a log-rank (Mantel-Cox) test, ns=not significant.

PDGFRA are most prevalent in Proneural hHGG, NF1 loss is most frequently seen in Mesenchymal hHGG, and activating EGFR alterations are enriched in Classical hHGG (**Table 2.1**). Moreover, the fact that PDGFB-overexpression in murine models can drive a transcriptome pattern similar to the human Proneural subtype is direct evidence that genetic mutations can drive defined transcriptome patterns<sup>250,251</sup>. Lending further support to this hypothesis, the loss of NF1 was shown to drive a Mesenchymal expression profile in tumors generated via RCAS/*tw-a*-mediated silencing of NF1 in newborn mice<sup>254</sup>. Here, I initially compared the differences between PDGFB-overexpressing and NF1-silenced mHGG by mining TCGA data to determine genes that are differentially expressed between the corresponding human subtypes. I identified a panel of 18 differentially expressed genes and analyzed their expression in the murine tumors with quantitative-PCR (**Figure 2.4**). Additionally, I analyzed expression of these genes in hHGG comparing either PDGFRA-amplified and NF1-deleted/mutated tumors (**Figure 2.5**) or human Proneural and Mesenchymal tumors (**Figure 2.6**). To simplify the visual comparison of expression profiles between these sets of data I generated a heatmap and performed principal component analysis to cluster the centroids of each dataset (**Figure 2.7A/B**). This analysis demonstrated the tendency of PDGFB-overexpressing mHGG to cluster with PDGFRA-amplified hHGG as well as Proneural hHGG (**Figure 2.7B**). Moreover, NF1-silenced mHGG was shown to cluster with NF1-deleted/mutant hHGG as well as Mesenchymal hHGG (**Figure 2.7B**). Histologically, PDGFB-overexpressing tumors were almost exclusively grade IV glioblastoma, while NF1-silenced tumors displayed a mixture of grade III anaplastic astrocytoma and grade IV glioblastoma in both *Ntw-a/Cdkn2a<sup>-/-</sup>/Pten<sup>β/β</sup>* mice as well as *Ntw-a/Pten<sup>β/β</sup>* mice (**Figure 2.7C/D**).

To further validate these two models histologically, I employed a panel of four markers that have been shown to exhibit polarized expression in human Proneural and Mesenchymal hHGG. These included the Proneural markers OLIG2 and DCX as well as the Mesenchymal markers GFAP

<b>A</b>				<b>B</b>			
Genetic Alteration	CL (n=144)	MES (n=152)	PN (n=95)	Genetic Alteration	CL (n=144)	MES (n=152)	PN (n=95)
NF1 del/mut	9	37	6	NF1 del/mut	3	29	3
PDGFRA amplification	11	10	33	PDGFRA amplification	2	7	28
EGFR amplification	113	49	19	EGFR amplification	99	40	15

**Table 2.1. Prominence of PDGFRA, NF1, and EGFR mutations in Proneural, Mesenchymal, and Classical human HGG.** Copy number alteration data from TCGA was mined to determine the presence of PDGFRA-amplification, NF1-loss/mutation, and EGFR-amplification in hHGG samples. (A) A demonstration of the distribution of the alterations when co-incidence is allowed. (B) A demonstration of the distribution of the alterations when co-incidence is not allowed. These tables illustrate that NF1-loss/mutation, PDGFRA-amplification, and EGFR-amplification tend to occur most frequently in Mesenchymal, Proneural, and Classical hHGG respectively.

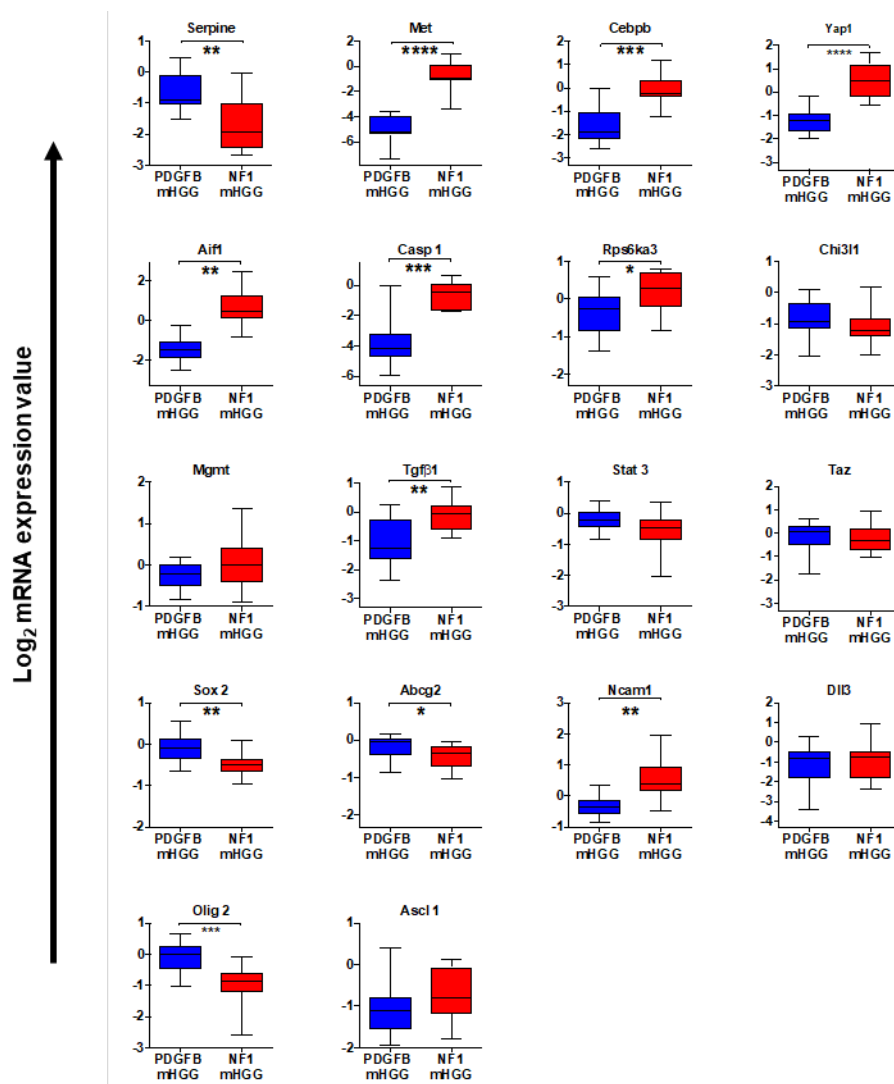


**Figure 2.4.** Log<sub>2</sub> z-score values of the 18 genes in PDGFβ-overexpressing or NF1-silenced murine HGG analyzed with quantitative-PCR (N=13 for both groups). Analysis performed with unpaired, two-tailed Student's t-tests. Welch's correction performed for samples with unequal variance as determined by an F-test. \* $P < 0.05$ , \*\* $P < 0.01$ , \*\*\* $P < 0.001$ , \*\*\*\* $P < 0.0001$ .

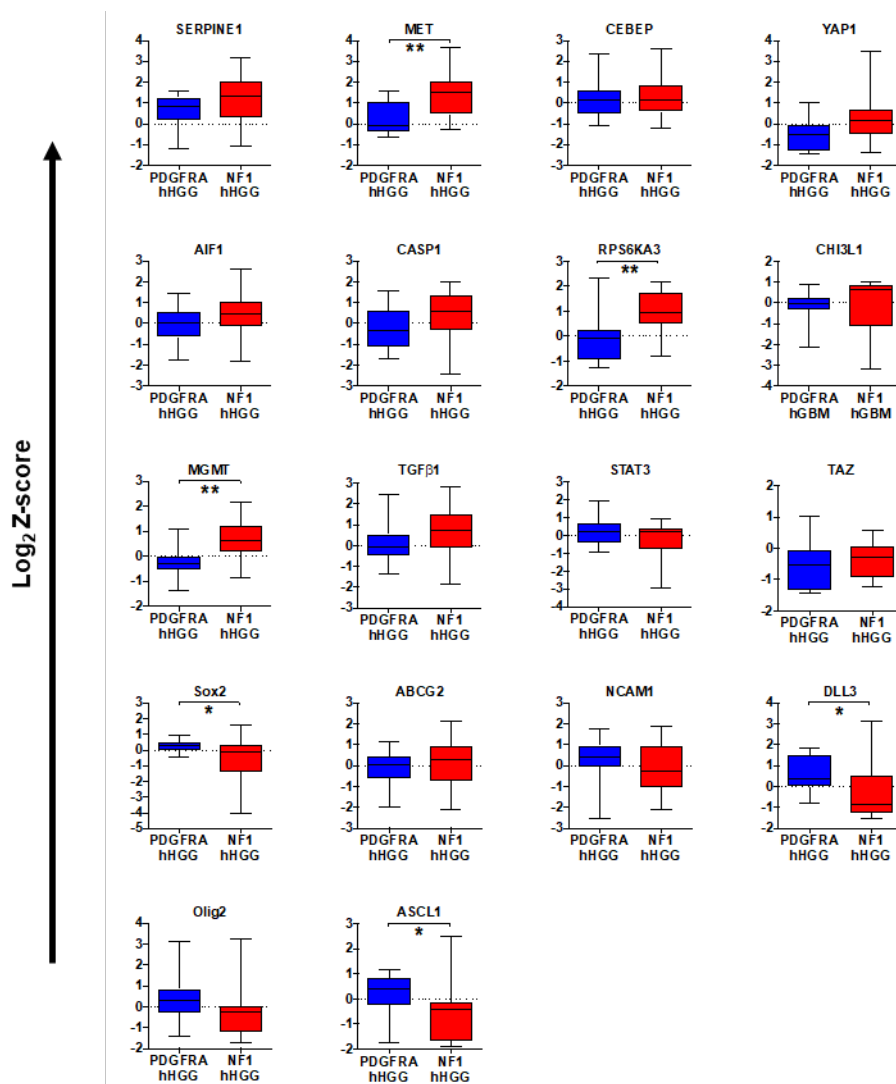


**Figure 2.5.** Log<sub>2</sub> z-score values of the 18 genes analyzed in PDGFRA-amplified and NF1-deleted/mutant human HGG. Data were queried from the TCGA database (N=18 for PDGFRA-amplified and N=26 for NF1-deleted/mutant tumors). Analysis performed with unpaired, two-tailed Student's t-tests. Welch's correction performed for samples with unequal variance as determined by an F-test. \* $P < 0.05$ , \*\* $P < 0.01$ .

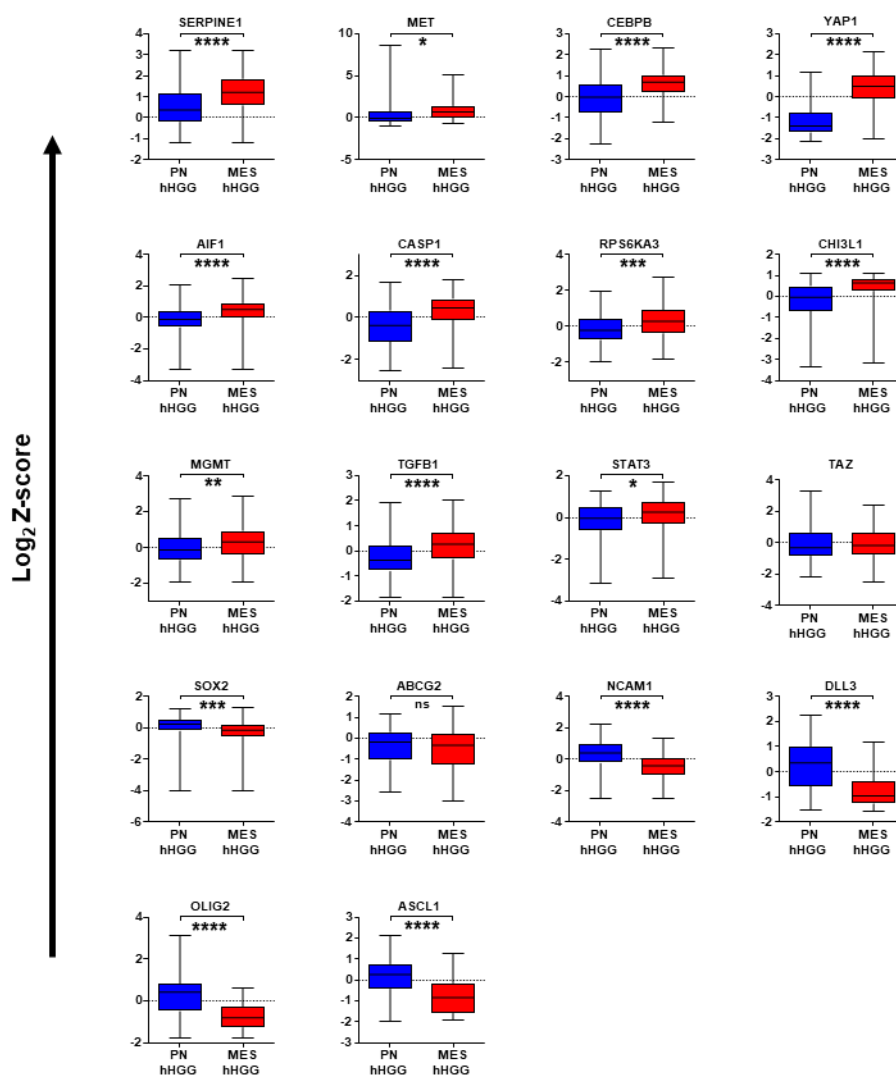


**Figure 2.6.  $\text{Log}_2$  z-score values of the 18 genes analyzed in Proneural and Mesenchymal human HGG.** Data was queried from the TCGA database and cBioPortal at MSKCC (N=69 for PN and N=106 for MES tumors). Analysis performed with unpaired, two-tailed Student's t-tests. Welch's correction performed for samples with unequal variance as determined by an F-test.

\* $P < 0.05$ , \*\* $P < 0.01$ , \*\*\* $P < 0.001$ , \*\*\*\* $P < 0.0001$ .

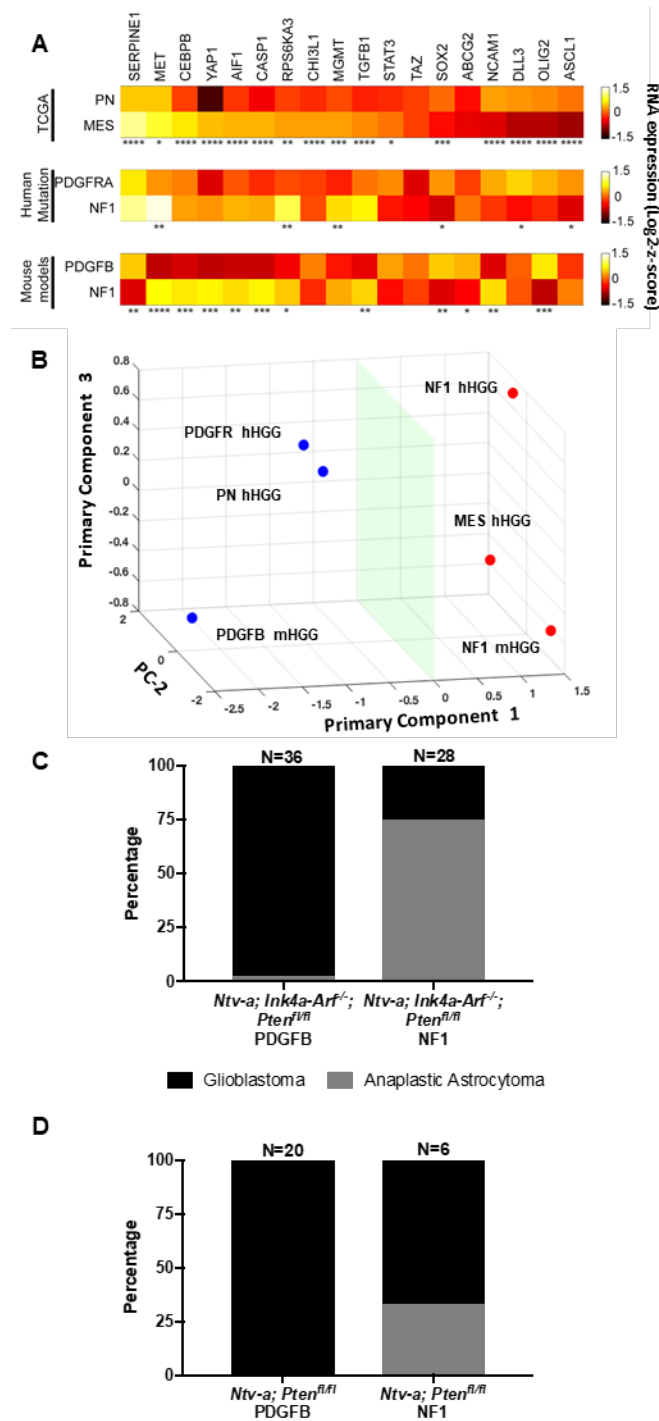


**Figure 2.7. Genetic driver mutations determine expression patterns of various markers.** (A) Heat maps demonstrating 18 selected genes that are differentially expressed in Proneural (N=69) and Mesenchymal (N=106) hHGG, PDGFRA-amplified (N=18) and NF1-deleted/mutant (N=26) hHGG, and PDGFB-overexpressing (N=13) and NF1-silenced (N=13) mHGG. (B) Principal

component analysis showing that Proneural hHGG, PDGFRA-amplified hHGG, and PDGFB-overexpressing mHGG cluster, as do Mesenchymal hHGG, NF1-deleted/mutant hHGG, and NF1-silenced mHGG. (C) Histological grading of PDGFB-overexpressing (N=36) and NF1-silenced (N=28) mHGG in *Ntv-a/Cdkn2a<sup>-/-</sup>/Pten<sup>β/β</sup>* mice. (D) Histological grading of PDGFB-overexpressing (N=20) and NF1-silenced (N=6) mHGG in *Ntv-a/Pten<sup>β/β</sup>* mice. Analysis was performed with unpaired, two-tailed Student's t-tests. Welch's correction was performed for samples with unequal variance as determined by an F-test. \* $P < 0.05$ , \*\* $P < 0.01$ , \*\*\* $P < 0.001$ , \*\*\*\* $P < 0.0001$ .

and CD44<sup>254-256</sup>. As expected, I illustrated increased expression of OLIG2 in the Proneural tumor model and increased expression of GFAP in the Mesenchymal tumor model (**Figure 2.8**). These results hinted at an oligodendroglial phenotype of PDGFB-overexpressing tumors and an astrocytoma phenotype of NF1-silenced tumors. My analysis of DCX and CD44 demonstrated an enrichment in the PDGFB-overexpressing and NF1-silenced tumors respectively (**Figure 2.9**). Overall, these immunohistochemical analyses further establish the similarity of these murine models to their human counterparts.

Following the establishment of models for Proneural and Mesenchymal glioblastoma, I next focused my attention on the development of a mouse model of the Classical subtype. Delivery of the full length EGFRvIII receptor is prohibited with the RCAS system due to the size of the receptor (>100kb) and the insert size limitation of RCAS (~2.5kb)<sup>257,258</sup>. Therefore, I had to develop an alternative method for modeling this subtype in lieu of direct delivery of the mutant receptor. Previously, *Cdkn2a*<sup>-/-</sup>/*EGFRvIII*<sup>fl/fl</sup>/*Pten*<sup>fl/fl</sup> mice had been used in association with a Cre adenovirus to study the role of EGFR in gliomagenesis<sup>259</sup>. I therefore hypothesized that by crossing these mice into the *Ntv-a*/*Pten*<sup>fl/fl</sup> mice, I could model EGFRvIII tumors by inducing expression of the receptor, along with additional co-mutations, specifically in Nestin-positive cells. Once I crossed *Ntv-a*/*Cdkn2a*<sup>-/-</sup>/*EGFRvIII*<sup>fl/fl</sup>/*Pten*<sup>fl/fl</sup> mice, I generated tumors via co-injection of RCAS Cre, RCAS sh*p53*-RFP, and RCAS sh*Pten*-RFP at a 1:1:1 ratio in the subventricular zone. I collected tumors for analysis with a similar quantitative-PCR panel to what I had previously used to analyze PDGFB-overexpressing and NF1-silenced tumors. Here, I expanded the panel to 30 total genes to include those that are enriched in Classical hHGG. Direct comparisons of quantitative-PCR results for these genes between PDGFB-overexpressing, NF1-silenced, and EGFRvIII mHGG displayed expected gene enrichments (**Figure 2.10**). These data additionally were comparable to the corresponding human subtype data accessed through TCGA (**Figure 2.11**).

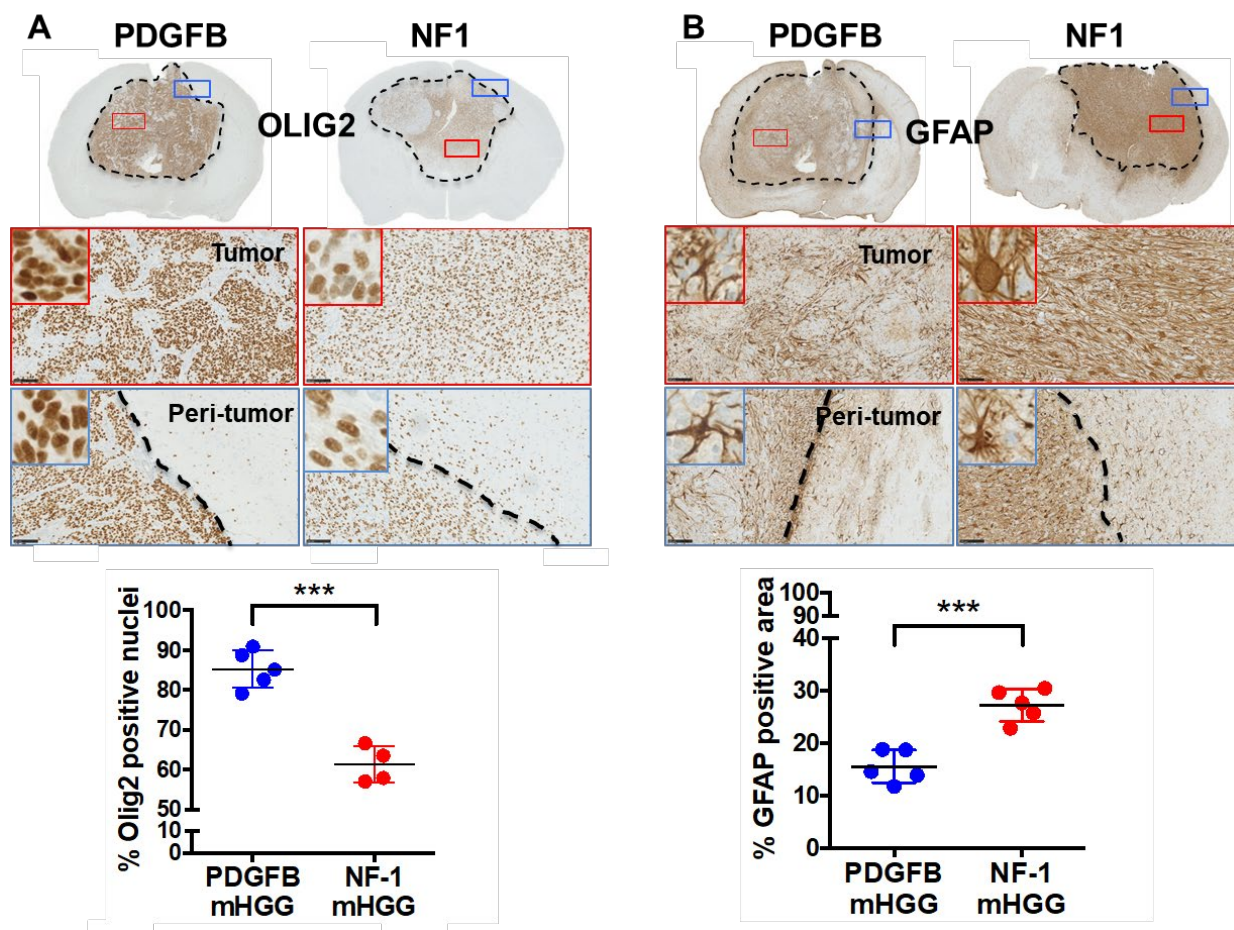


**Figure 2.8. Inverse correlation of OLIG2 and GFAP expression in PDGFB-overexpressing and NF1-silenced murine HGG.** Representative images of immunohistochemistry for (A) OLIG2 (N=5 for PDGFB-overexpressing and N=4 for NF1-silenced) and (B) GFAP (N=5 for both groups) staining of PDGFB-overexpressing and NF1-silenced mHGG. Sections were counterstained with hematoxylin. (A) Quantification of OLIG2 showed significantly increased OLIG2-positive nuclei in PDGFB-overexpressing mHGG. (B) In contrast, NF1-silenced mHGG showed a higher percentage of GFAP-positive area. This suggests more oligodendrogloma character in PDGFB-overexpressing mHGG and more astrocytoma character in NF1-silenced mHGG. Analysis was performed with unpaired, two-tailed Student's t-tests. Scale bars = 100  $\mu$ m. \*\*\* $P$ <0.001.

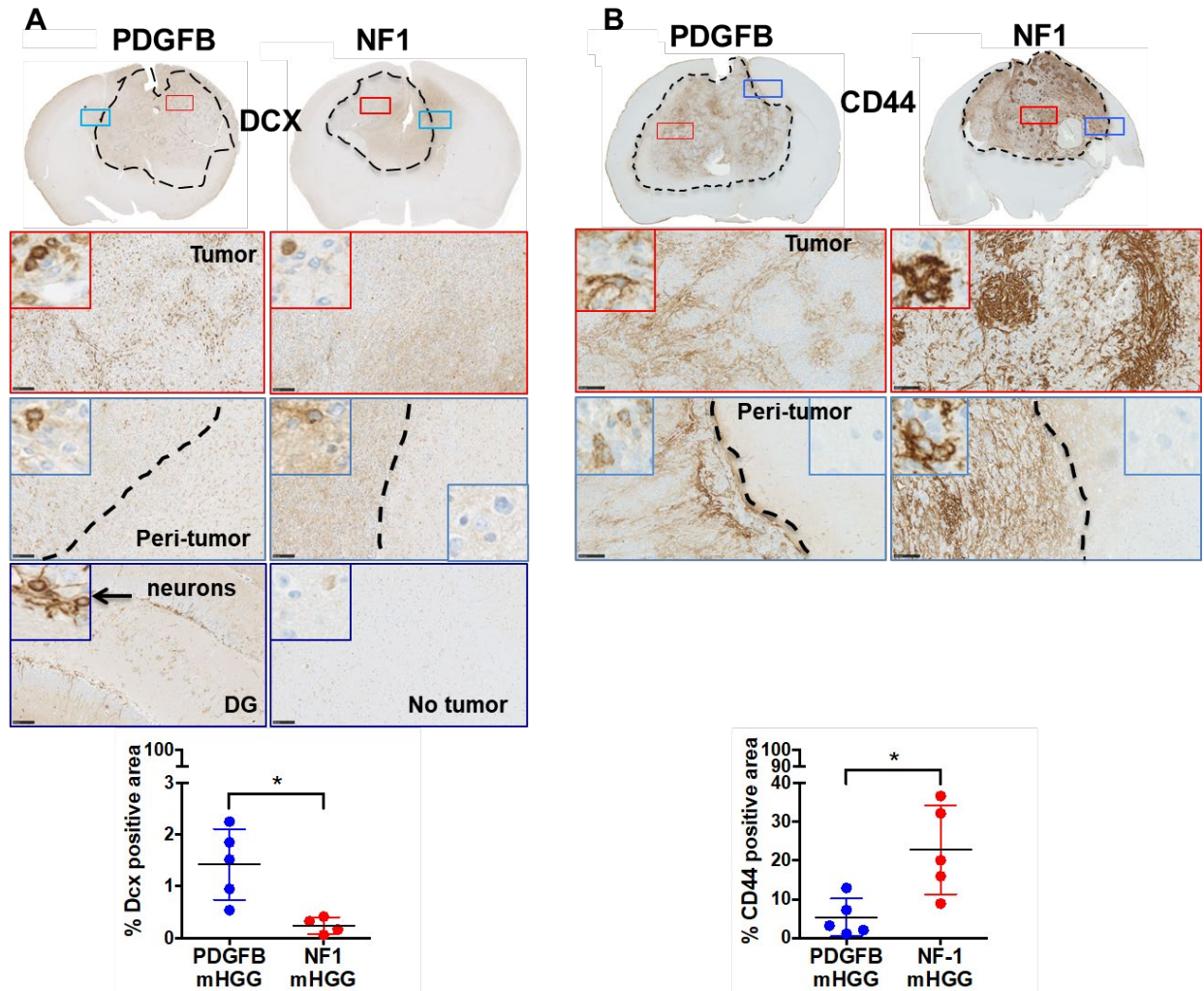


**Figure 2.9. Inverse correlation of DCX and CD44 expression in PDGFB-overexpressing and NF1-silenced murine HGG.** Representative images of immunohistochemistry for (A) DCX (N=5 for PDGFB-overexpressing and N=4 for NF1-silenced) and (B) CD44 (N=5 for both groups) staining of PDGFB-overexpressing and NF1-silenced mHGG. Sections were counterstained with hematoxylin. (A) Quantification of DCX showed a significant increase in positive nuclei in PDGFB-overexpressing compared to NF1-silenced mHGG. (B) Quantification of CD44, showed a significant increase in positive area in NF1-silenced mHGG. In the dentate gyrus (DG), new neurons showed positive staining for DCX and were used as a positive control for staining. Analysis

was performed with unpaired, two-tailed Student's t-tests. Welch's correction was performed for samples with unequal variance as determined by an F-test. Scale bars = 100  $\mu\text{m}$ . \* $P < 0.05$ .

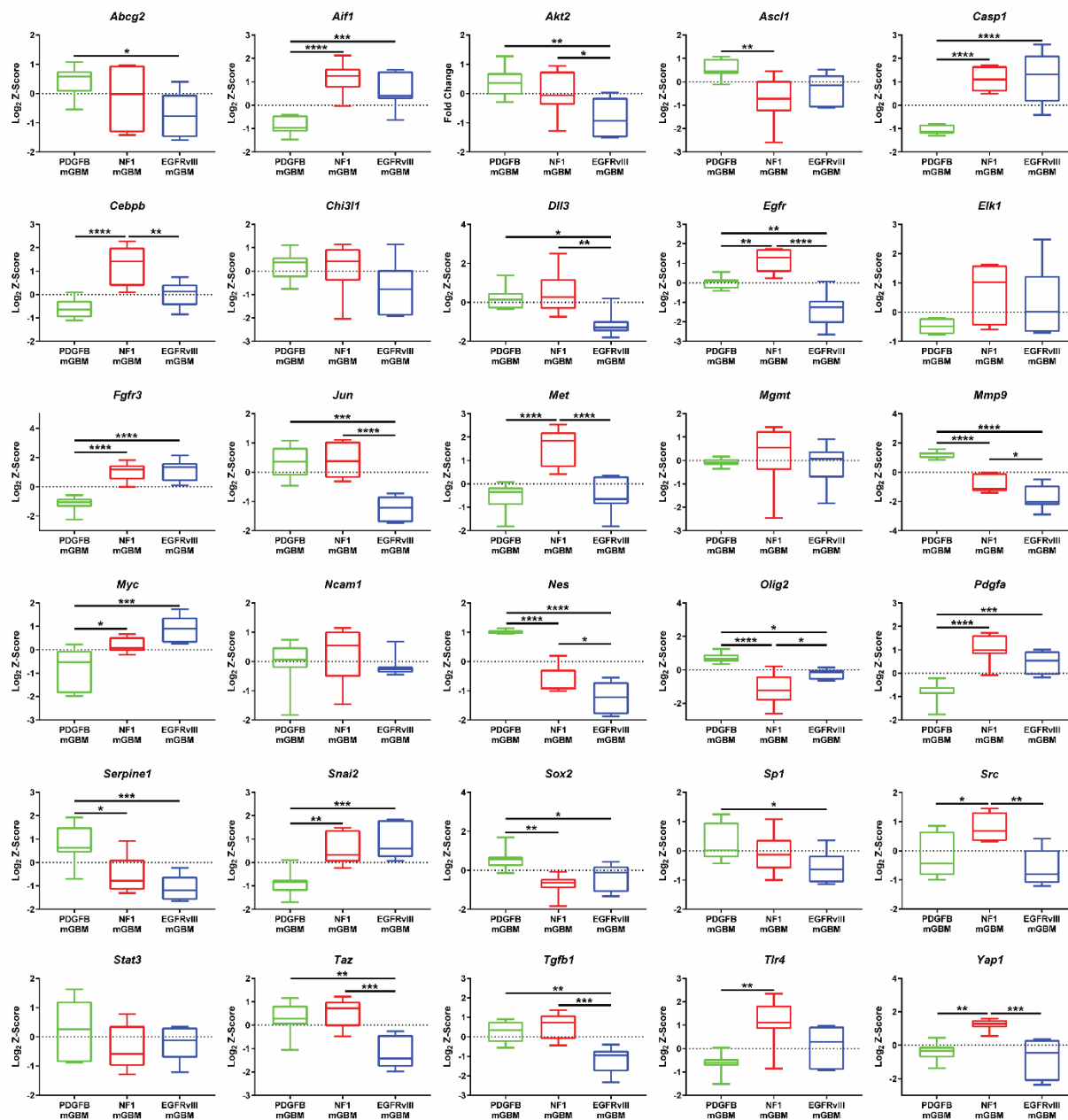


**Figure 2.10. Murine tumor quantitative-PCR analysis.** Illustrations of quantitative-PCR comparison of gene expression in PDGFB-overexpressing, NF1-silenced, and EGFRvIII mHGG (N=7 per group). One-way ANOVA, \* $P < 0.05$ , \*\* $P < 0.01$ , \*\*\* $P < 0.001$ , \*\*\*\* $P < 0.0001$ .

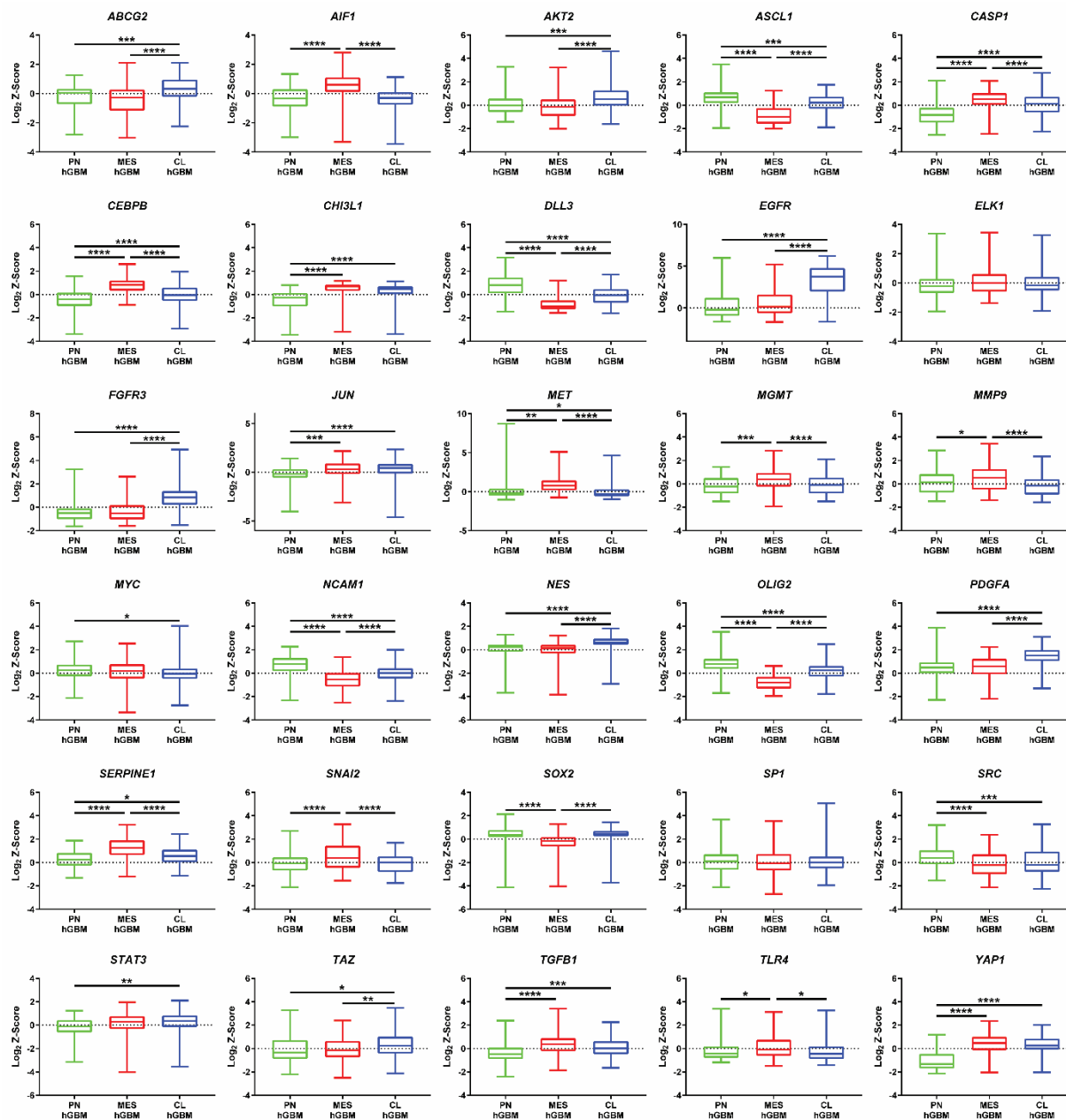


**Figure 2.11. Human tumor gene expression analysis.** Illustrations of the U133 Microarray data for genes differentially expressed between human glioblastoma subtypes (PN: N=87, MES: N=137, and CL: N=128). One-way ANOVA, \* $P < 0.05$ , \*\* $P < 0.01$ , \*\*\* $P < 0.001$ , \*\*\*\* $P < 0.0001$ .

To analyze the clustering tendencies of the murine tumors, I first calculated a distance matrix and visualized the result (**Figure 2.12A**). This analysis revealed that the murine tumor samples displayed greatest similarity with other tumors generated with the same driver mutations as expected. Hierarchical clustering (**Figure 2.12B**) further confirmed these results by displaying that murine tumors with the same driver mutations cluster together with unsupervised hierarchical clustering based on their expression of the 30-gene quantitative-PCR panel that I employed. To validate that this panel is capable of clustering not only the murine tumors, but also the corresponding human subtypes, I accessed U133 Microarray data from TCGA for all 30 genes for samples of each human subtype with all G-CIMP positive samples excluded. Principal component analysis on both the murine quantitative-PCR data (**Figure 2.12C**) and human U133 Microarray data (**Figure 2.12D**) demonstrated the ability of this panel to cluster the tumors. To more effectively visualize the data presented in Figures 2.10 and 2.11, I generated a heatmap for the gene expression results and showed that the murine tumors and their corresponding human subtypes display similar expression of the 30 genes analyzed in this panel (**Figure 2.12E/F**).

#### *Genetic driver mutations determine the microenvironmental composition of murine HGG*

Considering the differences in expression profile between the murine models and their human counterparts, particularly with respect to *Aif1* expression, I was next interested in how different tumor driver mutations would affect the composition of the tumor microenvironment. Non-neoplastic cells in the tumor form the tumor microenvironment and can consist of various infiltrating and resident immune cells, the cells that comprise the vasculature, and other glial cell types<sup>260</sup>. *Aif1*, a gene I found in my analysis to be differentially regulated amongst the murine models and human glioblastoma subtypes, encodes for the protein IBA1 which is a marker of macrophages<sup>261</sup>. TAMs are known to be the most abundant non-neoplastic cell type in

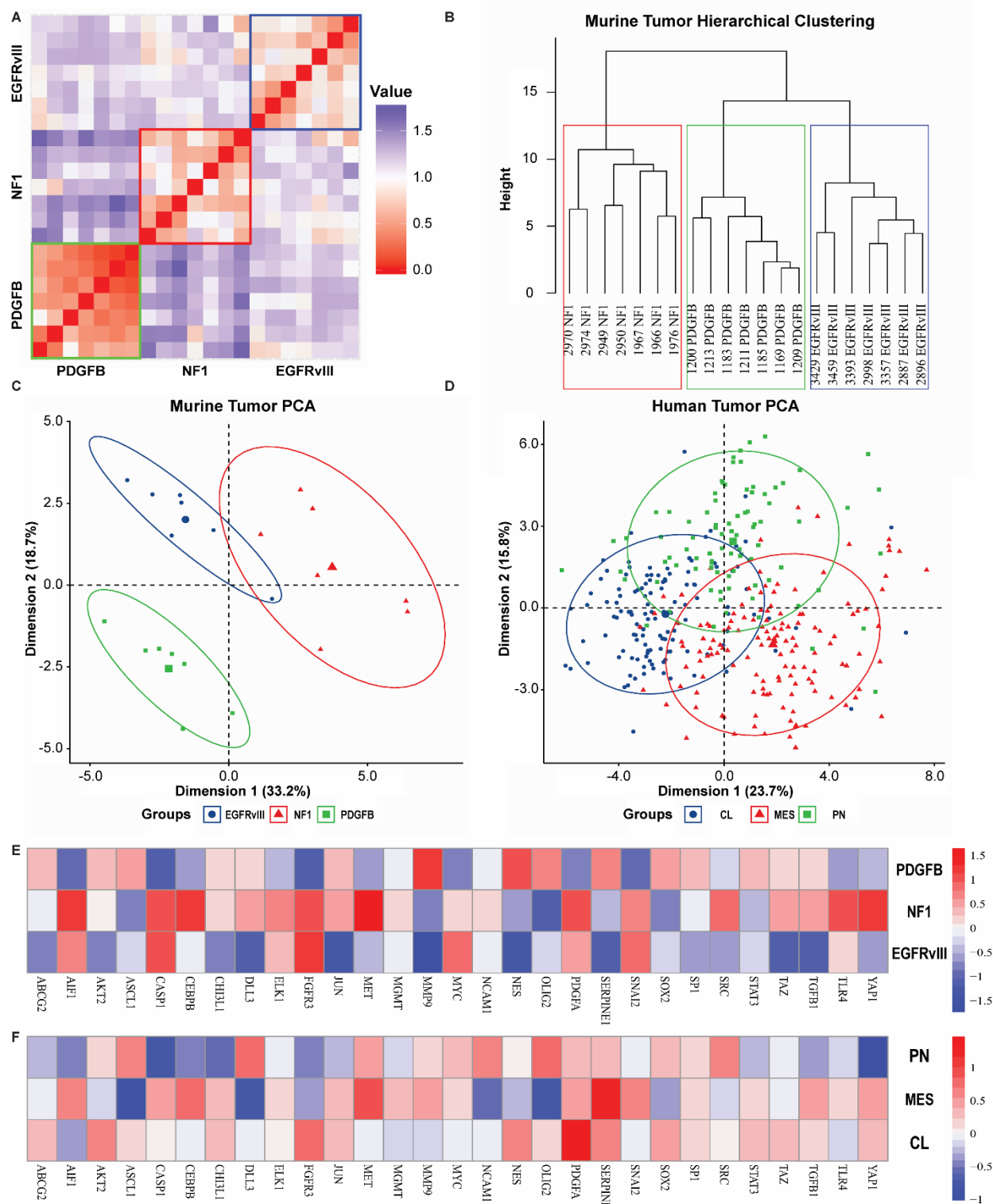


**Figure 2.12. Human tumor subtype expression data and the corresponding mouse models**

**cluster similarly based on a 30-gene panel.** (A) A distance matrix of murine tumor expression data (N=7 per group). (B) Hierarchical clustering of murine tumor expression data (N=7 per group). (C) PCA clustering of murine tumor expression data (N=7 per group) and (D) human tumor expression data (PN: N=87, MES: N=137, and CL: N=128). (E) A heatmap of gene expression data for murine tumors (N=7 per group) and (F) human tumors (PN: N=87, MES: N=137, and CL: N=128).

glioblastoma and can make up more than 30% of the tumor mass<sup>10,260</sup>. I demonstrated that TAMs in glioblastoma come in two flavors, brain resident MG as well as BMDM<sup>99</sup>. To assess macrophages using immunohistochemistry, I probed for the marker IBA1 in tissue samples from PDGFB-overexpressing and NF1-silenced mHGG and determined IBA1-positive area. The NF1-silenced tumors were demonstrated to have a significantly higher IBA1-positive area than their PDGFB-overexpressing counterparts (**Figure 2.13A**). These results are in line with correlative data from TCGA and the Gene Expression Omnibus databases, which have displayed an enrichment in TAM-associated genes in the Mesenchymal subtype<sup>262</sup>. Furthermore, I recently published similar subtype-specific expression of IBA1 in human tumors<sup>263</sup>. In total, these results suggest that TAMs may play a subtype-specific role in glioblastoma. Furthermore, my murine data suggest that genetic alterations in tumor cells can alter the immune cell composition of the tumor.

I next turned my attention towards the differences in the vasculature between the PDGFB-overexpressing and NF1-silenced models. Tumors were stained for the endothelial cell-specific marker CD31 and average vessel size was quantified. This analysis displayed significantly larger vessels in the PDGFB-overexpressing tumors (**Figure 2.13B**). The vessels in NF1-silenced mHGG were shown to be more evenly distributed and smaller. These data suggest that major genetic drivers can also impact the architecture of the tumor vasculature. Since I observed larger vessels in the PDGFB-overexpressing tumors, I wondered if the functionality of the vessels was altered. Therefore, I assessed blood vessel permeability with a Hoechst dye leakage assay and identified functional vessels by labeling with intravenously-administered FITC-lectin (**Figure 2.14**). Consistent with the CD31 staining (**Figure 2.13B**), vasculature in PDGFB-overexpressing tumors was shown to be disorganized and enlarged with this assay. There was no statistically significant difference in total vessel area observed with this assay; however, the area occupied by Hoechst dye,

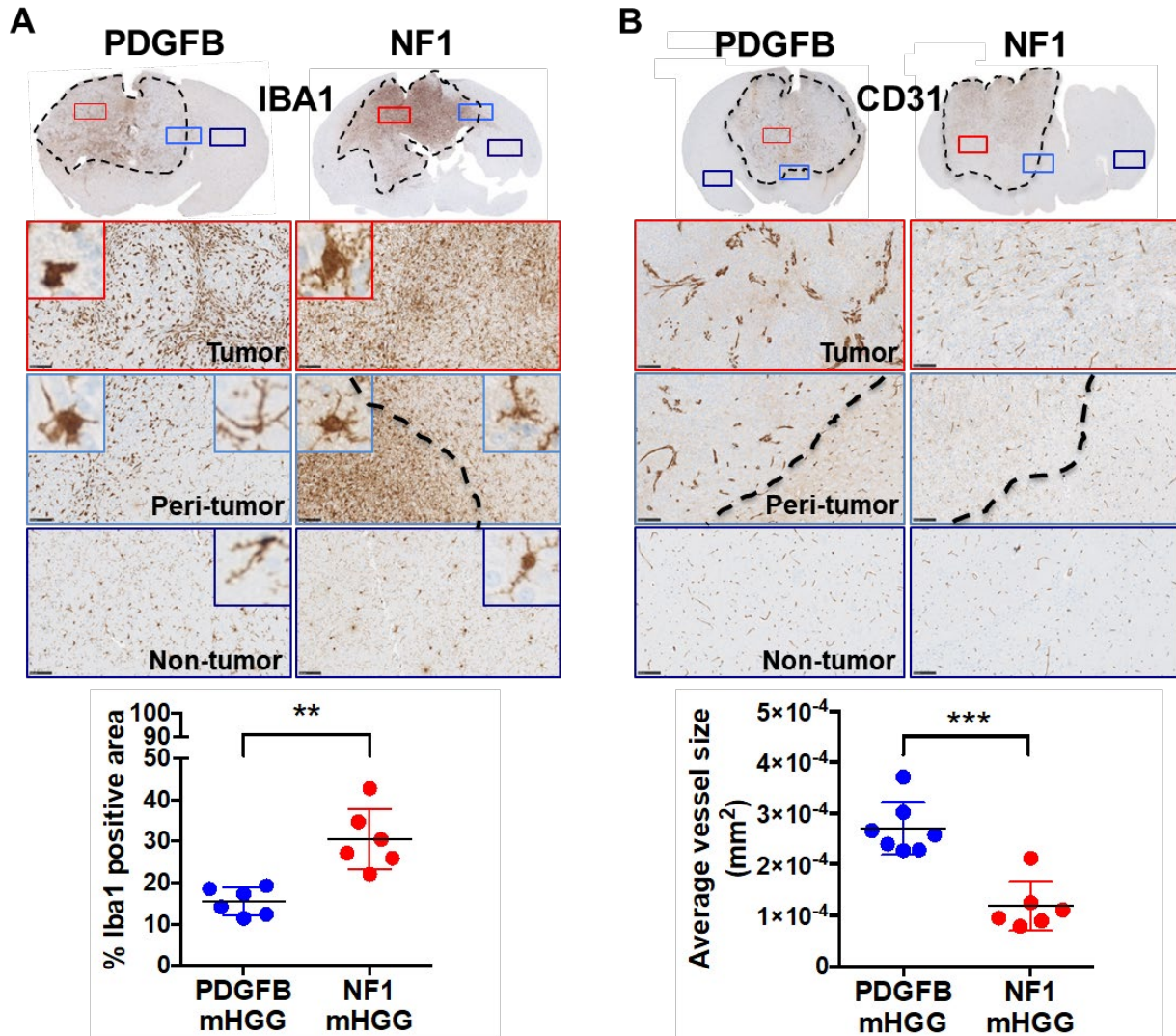


**Figure 2.13. NF1-silenced murine HGG exhibits increased tumor-associated macrophage infiltration and reduced vessel size compared to PDGFB-overexpressing murine HGG.**

Representative images of immunohistochemistry for (A) IBA1 (N=6 for both groups) and (B) CD31 (N=7 for PDGFB-overexpressing and N=6 for NF1-silenced) staining of PDGFB-overexpressing and NF1-silenced mHGG. Sections were counterstained with hematoxylin. (A) Quantification of IBA1 showed significantly increased positive area in NF1-silenced mHGG. (B) CD31 staining showed smaller vessels in NF1-silenced mHGG compared to PDGFB-driven mHGG. Analysis was

performed with unpaired, two-tailed Student's t-tests. Welch's correction was performed for samples with unequal variance as determined by an F-test. Scale bars = 100  $\mu\text{m}$ . \*\* $P < 0.01$ , \*\*\* $P < 0.001$ .

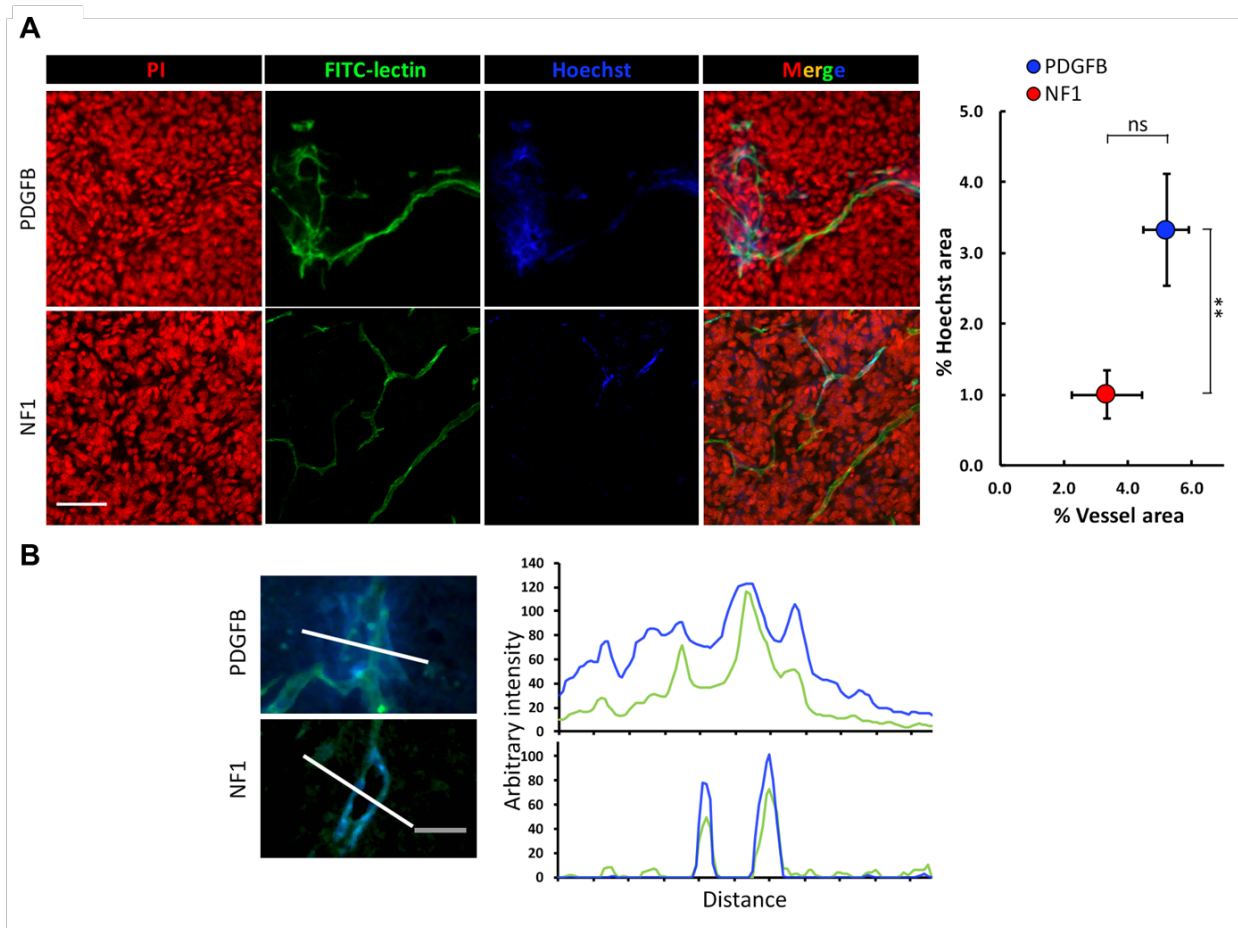


**Fig 2.14. Blood vessels in PDGFB-overexpressing murine HGG are larger and more permeable than those in NF1-silenced murine HGG.** (A) Representative images of vessel functionality and permeability assessments with FITC-conjugated lectin and Hoechst dye injections in PDGFB-overexpressing and NF1-silenced mHGG. The corresponding quantification of vessel area and Hoechst-positive area are shown. Scale bar = 50  $\mu\text{m}$ . (B) Arbitrary fluorescent intensities of either Hoechst or FITC-lectin were measured along defined lines and plotted against the length of the lines. Scale bar = 25  $\mu\text{m}$ . Analysis was performed with unpaired, two-tailed Student's t-tests.  $**P < 0.01$ .

which is indicative of vessel leakage, was significantly higher in PDGFB-overexpressing mHGG. This indicates that the BBB is disrupted in PDGFB-overexpressing mHGG, but not significantly NF1-silenced mHGG. The line profile (**Figure 2.14B**) clearly illustrates this phenomenon with the analysis of Hoechst dye intensity. In NF1-silenced tumors, the Hoechst dye is shown to be confined to the vessel walls whereas it freely diffuses around the vessels and into the tumor parenchyma in PDGFB-overexpressing tumors. In non-tumor tissue from the same brains analyzed in this assay, the vessels were demonstrated to be normal with respect to their functionality, size, and distribution (**Figure 2.15**). Additionally, no Hoechst dye leakage was observed in the non-tumor regions of brains from mice bearing either tumor type.

#### *Subtype-specific preclinical therapeutic analysis*

Once these model systems were validated as similar to their human counterparts with respect to expression profile and microenvironmental composition, I chose to use them to assess the efficacy of various drug treatment regimens preclinically. First, I chose to analyze the sensitivity of PDGFB-overexpressing and NF1-silenced mHGG to radiation therapy (RT) as well as TMZ treatment as these are currently the standard of care for human glioblastoma patients<sup>140</sup>. Using a calculation for dose translation from human to mouse, I determined that the standard human dose of 75 mg/m<sup>2</sup> of TMZ corresponds to 25 mg/kg in mice. For RT, I determined that the standard 60 Gy of radiation in humans corresponds to 20 Gy in mice. To match the RT administration scheme, I chose to administer as 2 Gy per day in a five day on, two day off cycle as performed with human patients. Since various doses of TMZ have been used in the literature preclinically, I first assessed whether escalating the dose of TMZ would increase the effect on median survival of PDGFB-overexpressing mHGG. I utilized T2-weighted MRI to distribute size-matched tumors into 25 mg/kg and 100 mg/kg treatment groups with endpoint survival time as the experimental

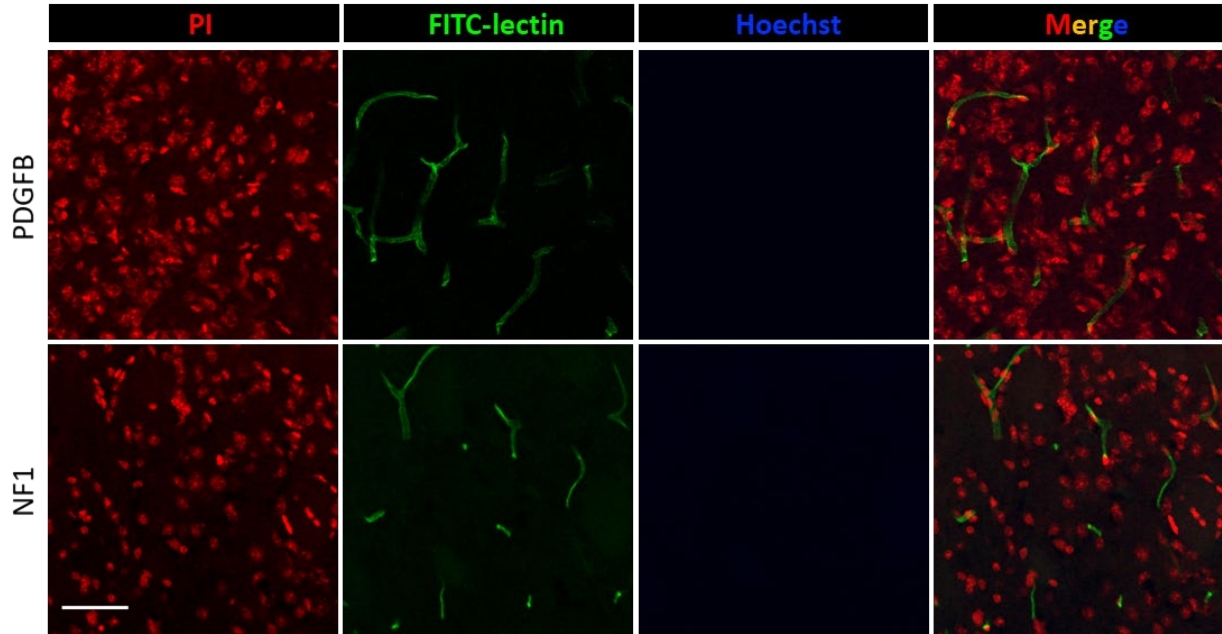


**Figure 2.15. Non-tumor regions of brains from both PDGFB-overexpressing and NF1-silenced murine HGG-bearing mice display normal vasculature.** The non-tumor areas of brains from both models indicate normal, non-permeable blood vessels as assessed by Hoechst dye and FITC- lectin injections. Scale bar = 50  $\mu\text{m}$ .

readout (**Figure 2.16**). This experiment demonstrated no difference in median survival time between the two treatment regimens.

Since the PDGFB-overexpressing tumors occur mainly within a defined time period, and T2-weighted MRI was demonstrated as efficacious in sorting mice into treatment groups, I again employed this methodology to sort mice into vehicle, TMZ, and RT treatment groups (**Figure 2.17B**). NF1-silenced tumor-bearing mice were randomly assigned treatment groups, but age and sex were matched. Mice were treated with the indicated regimens of vehicle, TMZ, and RT (**Figure 2.17A**) and survival time post-treatment was documented. This analysis illustrated that PDGFB-overexpressing tumors display sensitivity to both TMZ and RT treatment (**Figure 2.17C**). Between the two therapies, RT extends median survival more than TMZ. NF1-silenced tumors also displayed marked sensitivity to RT; however, these tumors were demonstrated to have no response to TMZ at the dose and schedule tested (**Figure 2.17D**). NF1-silenced tumors were also demonstrated to exhibit an increase in grade IV malignancy following TMZ or RT treatment (**Figure 2.18**).

Previous literature has demonstrated that expression of MGMT is associated with resistance to TMZ treatment<sup>30</sup>. Therefore, I assessed the expression levels of MGMT in PDGFB-overexpressing and NF1-silenced mHGG with quantitative-PCR (**Figure 2.4**). Additionally, I queried TCGA database and compared MGMT expression between Proneural and Mesenchymal hHGG as well as PDGFRA-amplified and NF1-deleted/mutant hHGG (**Figure 2.5 and 2.6**). Analysis of the murine quantitative-PCR data demonstrated no significant difference between the two groups. The human data demonstrated significantly higher expression of MGMT in MES and NF1-deleted/mutant hHGG compared to PN and PDGFRA-amplified hHGG, respectively. Considering the lack of a significant change in the murine samples I analyzed, this pathway likely does not confer the TMZ-resistance seen in NF1-silenced mHGG.

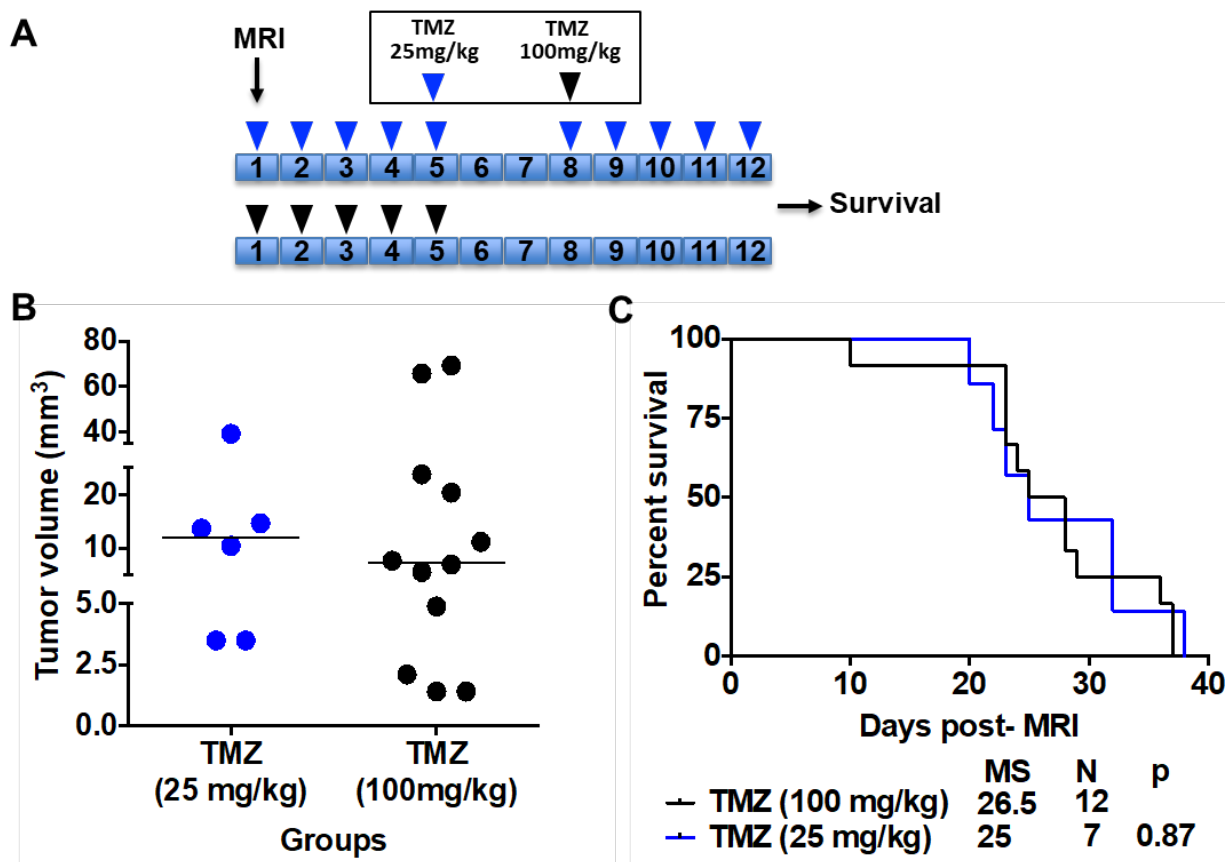


**Figure 2.16. Commonly used doses and schedules of TMZ produce no difference in survival of PDGFB-overexpressing murine HGG.** (A) Treatment schedule for the 25 mg/kg and 100 mg/kg doses of TMZ. (B) 4 weeks post-injection, mice with PDGFB-overexpressing mHGG were separated into 25mg/kg and 100mg/kg TMZ treatment groups with matched sex, age, and average tumor size as measured by T2-weighted MRI. (C) Kaplan-Meier survival curves for the treatment groups showing no difference in survival time when treated with 25mg/kg and 100mg/kg doses. Analysis performed with a log-rank (Mantel-Cox) test.

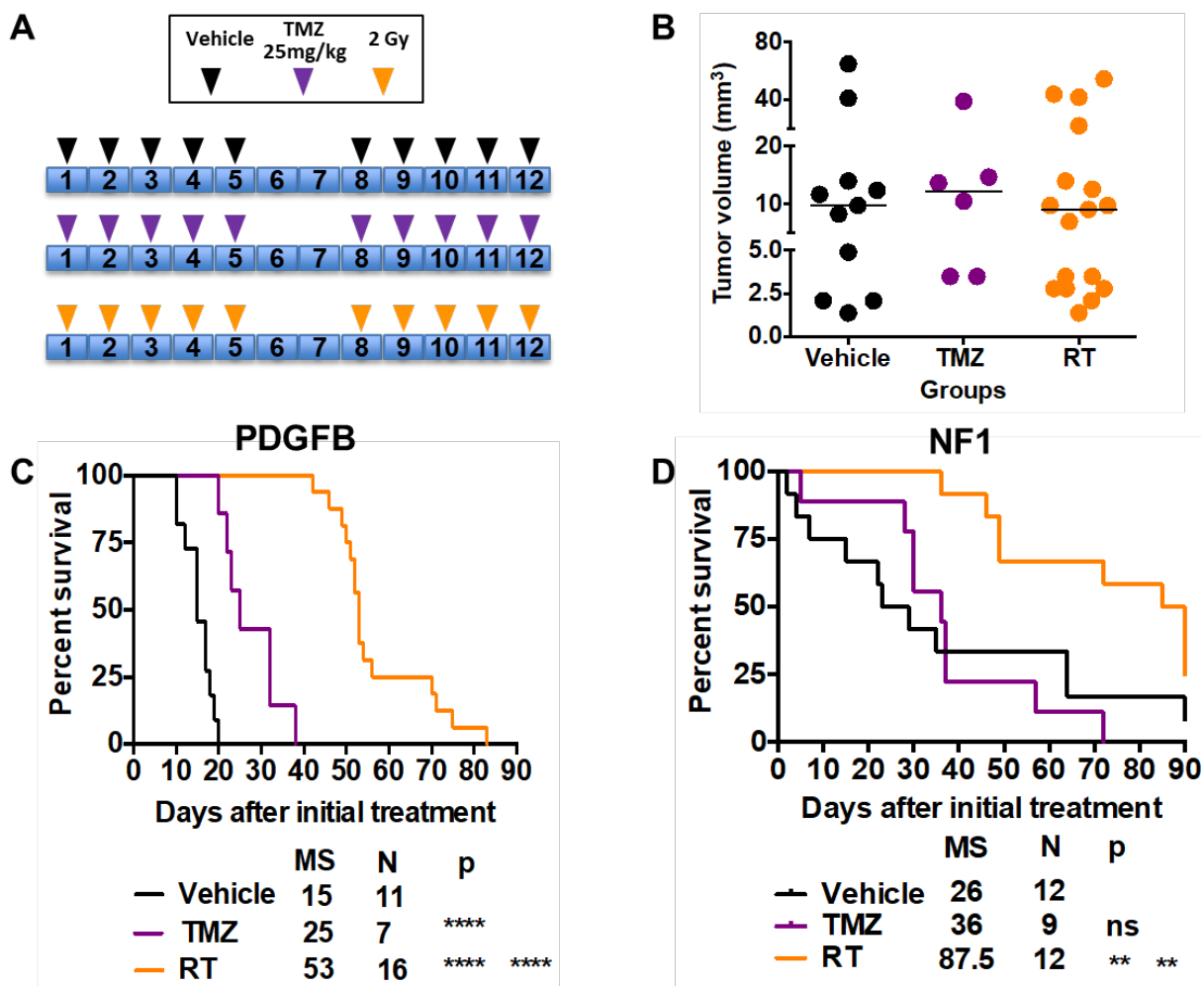


**Figure 2.17.** Radiotherapy provides a survival advantage to mice with either PDGFB-overexpressing or NF1-silenced murine HGG, while temozolomide provides a survival advantage only to mice with PDGFB-overexpressing tumors. (A) Schematic illustrations of treatment paradigms and groups. (B) Four weeks post-injection, mice with PDGFB-overexpressing tumors were separated into treatment groups with matched sex, age, and average tumor size as measured by T2-weighted MRI. Similarly, mice with NF1-silenced tumors were randomized into vehicle, TMZ, and RT treatment cohorts 8 weeks post-injection with age and sex equally distributed. (C) Kaplan-Meier survival curves for the different treatment groups for PDGFB-overexpressing

mHGG. (D) Kaplan-Meier survival curves for the different treatment groups for NF1-silenced mHGG. Analysis was performed with a log-rank (Mantel-Cox) test. \*\* $P < 0.01$ , \*\*\*\* $P < 0.0001$ .

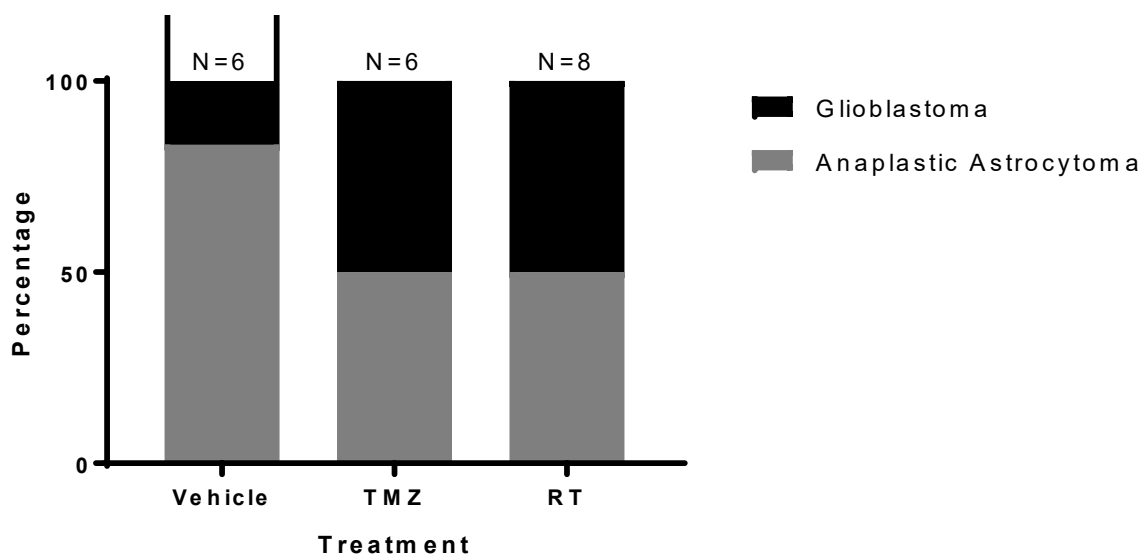


**Figure 2.18. NF1-silenced murine HGG displays a trend towards increased malignancy upon recurrence.** Mice bearing NF1-silenced tumors were treated with either vehicle (N=6), TMZ (N=6), or RT (N=8). Hematoxylin and eosin stained tissue samples were analyzed post-treatment. A trend towards increased malignancy was observed ( $P=0.3782$ ). Fisher's exact test used for analysis.

Considering the advent of immunotherapy in glioblastoma, I decided to test the sensitivity of the models to PD-L1 neutralizing therapy with and without concomitant RT according to the indicated treatment regimens (**Figure 2.19A**)<sup>215</sup>. I first treated mice bearing PDGFB-overexpressing tumors with isotype control or PD-L1 neutralizing antibody with or without concomitant RT (**Figure 2.19B**). This experiment confirmed the previous results that RT extends median survival. Moreover, it demonstrated that PD-L1 neutralization does not extend median survival with or without concomitant RT (**Figure 2.19B**). For NF1-silenced tumors, I assessed the ability of PD-L1 neutralization to extend median survival only in combination with RT. Similar to the results with PDGFB-overexpressing tumors, no increase in median survival following PD-L1 neutralization was observed compared to isotype control (**Figure 2.19C**). These results are in line with the response to PD-L1 neutralization observed in glioblastoma patients clinically<sup>212</sup>.

## 2.4 Discussion

The arrival of genomic level molecular biology and its applications to the study of brain tumors has established that multiple different subcategories reside under the umbrella term glioblastoma. Initial investigations subcategorized these tumors into four groups based on expression profiling, but recent analysis has trimmed the number to three robust groups; each of which displays a unique expression profile and presence of tumor-defining mutations<sup>6,7,12</sup>. Further studies employing single-cell RNA sequencing as well as studies analyzing the expression profiles of tumors before and after treatment have established that individual cells harboring expression profiles of each subtype can coexist within the same tumor and that glioblastoma can switch from one subtype to another under the selection pressure of certain therapies<sup>55,264</sup>. To investigate these phenomena preclinically, it is vital that subtype specific models are generated, validated, and openly provided to the field. In order to address the generation and validation of subtype-specific

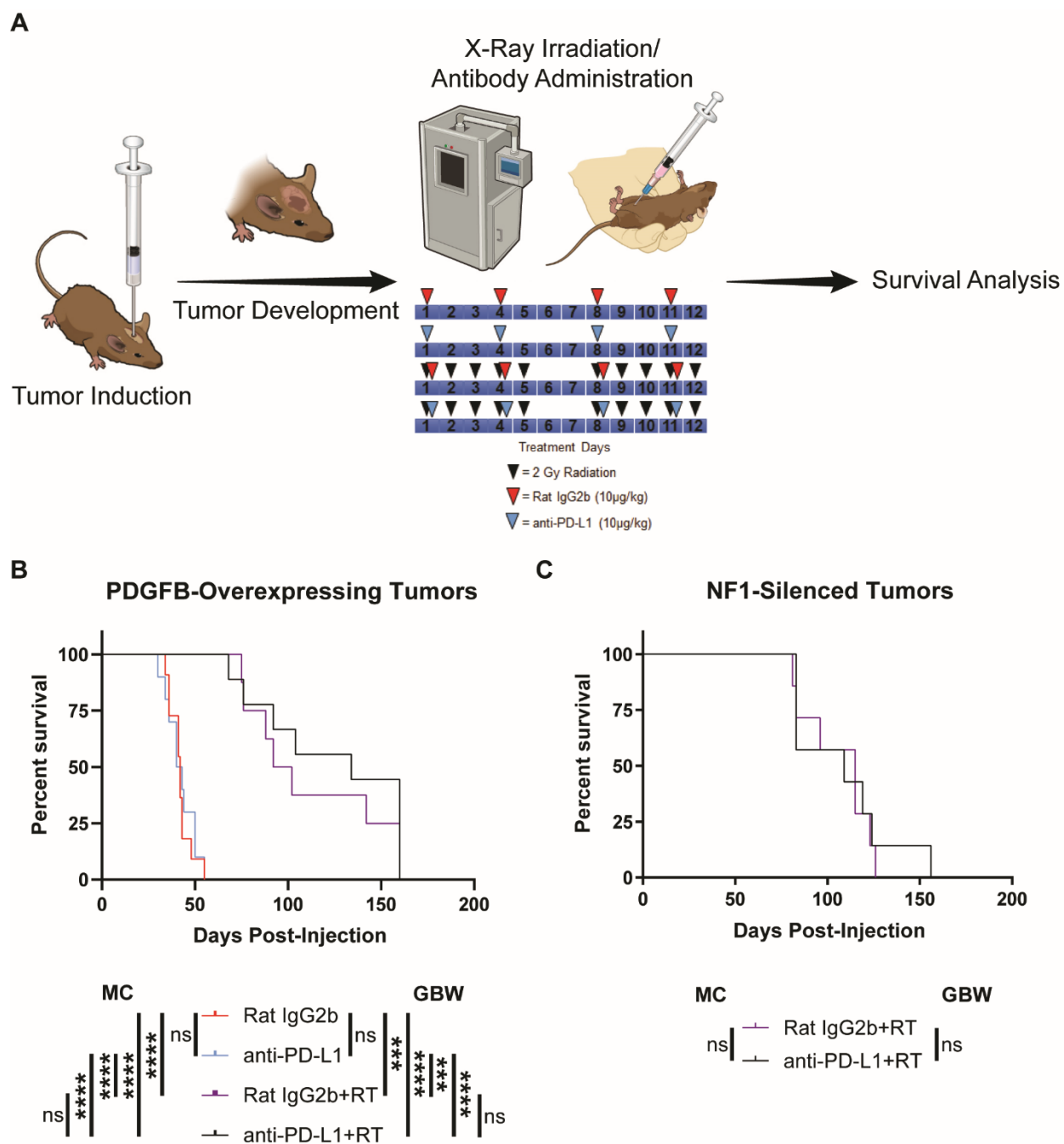


**Figure 2.19. Murine PDGFB-overexpressing and NF1-silenced tumors do not respond to PD-L1 neutralizing therapy.** (A) A schematic illustration of the experimental protocol. (B) Survival curves comparing mice bearing PDGFB-overexpressing tumors treated with isotype control antibody (N=11), PD-L1 neutralizing antibody (N=10), isotype control antibody plus x-ray

irradiation (N=8), and PD-L1 neutralizing antibody plus x-ray irradiation (N=9). (C) Survival curves comparing mice bearing NF1-silenced tumors treated with isotype control antibody plus x-ray irradiation (N=7) and PD-L1 neutralizing antibody plus x-ray irradiation (N=6). Mantel-Cox (MC) and Gehan-Breslow-Wilcoxon (GBW) tests, ns=not significant, \*\*\* $P<0.001$ , \*\*\*\* $P<0.0001$ .

preclinical models of glioblastoma I utilized the previously established RCAS/*tv-a* system to deliver precise oncogenic driver mutations to Nestin-positive cells of adult mice. To properly model each subtype with specific driver mutations, I queried TCGA database and elucidated that Proneural, Mesenchymal, and Classical hHGG are defined by alterations in the PDGF, NF1, and EGFR pathways respectively. Therefore, I designed murine models based on PDGFB-overexpression, NF1-silencing, and induced expression of the constitutively active mutant EGFRvIII. I then utilized a series of RNA and protein expression assays to compare the murine tumors to one another as well as to their human counterparts to validate their similarities with respect to baseline expression profile. Finally, I assessed the response of these tumors to therapy to elucidate if the models could detect differences between the different subtype models and determine if these alterations provide information that could inform clinical practice. Overall, the PDGFB-overexpressing, NF1-silenced, and EGFRvIII murine models will allow investigators to scrutinize the role that these mutations play in determining the response to therapy, thereby improving the ability to develop and utilize precision therapeutics.

Single-cell RNA sequencing has suggested that the clinical outcome of Proneural glioblastoma is influenced by the presence of cancer cells of alternate subtypes within the tumor<sup>55</sup>. Clinically, the transition of tumors from the Proneural to Mesenchymal subtype has been observed in response to both radiation and anti-angiogenic therapy<sup>250,265</sup>. It is yet unclear what the precise mechanism of this process entails, and multiple hypotheses have been presented. One mechanism involves the elimination of sensitive Proneural cells and the presence of resistant Mesenchymal cells within the tumor. In this case, therapies that exert a selective pressure on Proneural cells will change the overall subtype of the tumor by eliminating this population and allowing the Mesenchymal population to take over. Alternatively, it is possible that the expression profile of individual cells is altered by tumor treatment. Analysis of single-cell expression profiles before and after treatment

would provide an avenue for assessing the mechanism directly. Furthermore, this would elucidate whether Proneural glioblastoma is able and likely to acquire NF1 mutations during the transition to Mesenchymal glioblastoma. Utilization of the PDGFB-overexpressing and NF1-silenced models presented here in conjunction with preclinical therapeutic administration and single-cell or whole tumor RNA sequencing will allow for these questions to be addressed directly. Furthermore, analysis of these models in future experiments will display what role genetic driver mutations play in determining the overall phenotype of the tumor as well as the expression of tumor- and stroma-specific markers.

In this work, I also determined the influence of location of injection on the tumorigenic potential of the genetic driver mutations. I showed that delivery of RCAS PDGFB can generate tumors when injected in either striatum, the subventricular zone, or the cerebellum. Typically, these tumors spread throughout the frontal lobe and into the olfactory bulb, likely following the rostral migratory stream as demonstrated in human gliomas<sup>22</sup>. Previously, I demonstrated that PDGFB-overexpressing tumors do not display different incidence, latency, or mortality when generated in different locations<sup>241</sup>. By contrast, both NF1-silenced and EGFRvIII tumors only formed when RCAS viruses were injected into the subventricular zone. These tumors occurred with similar incidence and progression to the PDGFB-overexpressing tumors, but with significantly increased latency following injection. In total, these data imply that the cell of origin may differ between the PDGFB-overexpressing tumors and the other two models. In particular, the subventricular zone may provide either a cellular niche or cell type that is a necessity for NF1-silenced and EGFRvIII tumor generation.

The subventricular zone is a region of the brain known to house neuroblasts, precursor cells, astrocytes, and ependymal cells<sup>266</sup>. The typical cells known to express Nestin in the subventricular

zone are neural stem and progenitor cells<sup>267</sup>. Therefore, it is plausible to propose that these cells may be the cell of origin for NF1-silenced and EGFRvIII tumors since *w-a*, the prerequisite gene for RCAS infection, is under control of the Nestin promoter. In addition to neural precursor cells, reactive astrocytes have demonstrated the ability to upregulate Nestin in response to injury<sup>268</sup>. Since these models employ stereotactic injection of RCAS, producing injury at the site of tumor generation is unavoidable and likely capable of generating reactive astrocytes. Upon upregulation of Nestin, these cells gain the ability to be transformed by the RCAS virus. It is possible that any injections outside of the subventricular zone generate these reactive astrocytes that are consequently transformed by the RCAS viruses. The ability of only RCAS PDGFB to generate tumors in these cells likely stems from the fact that expression of PDGFB by these cells won't only alter the cells themselves, but also the surrounding cells through paracrine actions of the growth factor. NF1-silencing and induction of EGFRvIII by RCAS injection only alter the growth characteristics of the infected cells and may not be as powerful in inducing tumor growth in otherwise non-proliferative cells. Overall, these results are intriguing considering that it has been demonstrated that a different cell of origin, even when the same genetic driver mutation is employed, changes the expression profile and drug sensitivity of the resulting tumor<sup>269</sup>. This factor may partially explain differences in drug sensitivity that I observed in my experiments.

Direct comparison of PDGFB-overexpressing and NF1-silenced murine tumors with quantitative-PCR and evaluation of the similarities with their human counterparts demonstrated that these models accurately recapitulate the overall tumor expression profile observed in subtype-stratified human patients. Addition of the EGFRvIII model to this analysis further confirmed my conclusions and displayed that all three of the subtype specific murine models cluster most closely with the other tumors with the same driver mutation. This clustering tendency closely mirrored what was observed when analyzing human tumors annotated with subtype. Overall, these experiments

validated that on the gene expression level, the subtype-specific murine models closely recapitulate what is observed in human tumors.

I additionally used histology to validate the PDGFB-overexpressing and NF1-silenced tumors. The markers OLIG2 and DCX were previously demonstrated to be upregulated in Proneural hHGG<sup>255</sup>. I recapitulated this phenotype in the murine models by demonstrating an enrichment in these markers in PDGFB-overexpressing tumors when compared to NF1-silenced tumors. The markers GFAP and CD44 have been shown to be expressed most highly in Mesenchymal hHGG<sup>254,256</sup>. When I compared the expression of these markers between PDGFB-overexpressing and NF1-silenced mHGG with immunohistochemistry, I saw the highest expression in the NF1-silenced tumors as expected. Finally, my immunohistochemical analyses of the stromal cell markers CD31 and IBA1 demonstrated the ability of driver mutations to influence the composition of the tumor microenvironment. Direct comparison of PDGFB-overexpressing and NF1-silenced tumors showed significantly higher levels of IBA1-positive cells in NF1-silenced tumors. PDGFB-overexpressing tumors were shown to have more irregular vasculature than NF1-silenced tumors based on CD31 staining. Functional assessment of the vasculature with a Hoechst dye and FITC-lectin assay confirmed that the vessels are not only irregular in appearance, but also in function. The PDGFB-overexpressing tumors have increased vascular permeability when compared to NF1-silenced tumors. Together, these results suggest that genetic driver mutations and cell of origin are significant contributors to the inter- and intra-tumoral heterogeneity observed in glioblastoma.

Finally, I turned my investigation towards the utilization of these models for the assessment of preclinical therapies. First, I aimed to establish the response of each model to standard of care TMZ and RT therapy. TMZ in combination with RT has been shown to provide survival benefit in

human glioblastoma patients and now comprises the standard of care<sup>140</sup>. Further analysis has demonstrated that roughly half of glioblastoma patients do not respond to TMZ. In fact, about half of patients display expression of the DNA damage repair enzyme MGMT and these patients have been shown not to respond to TMZ treatment<sup>30</sup>. High MGMT expression has also been shown to confer TMZ resistance in patient-derived cell lines and xenografts<sup>270</sup>. In PDGFB-overexpressing tumors generated with RCAS, it has also been demonstrated that a subset of stem-like cells expresses higher levels of MGMT and are more resistant than non-stem-like cells to TMZ therapy<sup>271</sup>. Here, I demonstrated that TMZ is only capable of extending median survival in PDGFB-overexpressing tumors but not NF1-silenced tumors. Both tumor types were shown to be sensitive to RT. No significant differences in MGMT expression between the two murine models was observed. Significantly higher expression of MGMT was shown in Mesenchymal and NF1-deleted/mutant tumors when compared to Proneural and PDGFRA-amplified tumors respectively. It should be noted that other DNA repair enzymes can alter response to TMZ, including MSH6<sup>272</sup>. Expression of these enzymes was not analyzed in this work but offers an interesting avenue for future investigation.

Apart from MGMT expression, there are two other explanations that could account for the differences in sensitivity to TMZ observed between the PDGFB-overexpressing and NF1-silenced tumors. First, I demonstrated noted alterations in both the vasculature and immune microenvironment between the two tumors. Although TMZ is highly bioavailable and able to pass freely through the BBB, it is possible that the significant disruption of the BBB in PDGFB-overexpressing tumors allowed for locally higher concentrations of TMZ around disrupted vasculature<sup>273</sup>. This increased accumulation of the drug could partially explain the increased efficacy observed in this model. Additionally, the PDGFB-overexpressing tumors were shown to have significantly lower amounts of TAMs. The relationship between TAMs and treatment resistance has

been established and it is plausible to believe that the increased amount of these cells in NF1-silenced tumors contributes to their resistance to TMZ<sup>10</sup>. The second explanation for the TMZ resistance observed in NF1-silenced tumors results from the intrinsic characteristics of the tumor cells. It has been shown that oligodendroglioma cells are more sensitive to TMZ than astrocytoma-like glioma cells<sup>274</sup>. Since the OLIG2 staining presented here illustrated an oligodendroglial phenotype in the PDGFB-overexpressing tumors, and the GFAP staining and tumor grading illustrated an astrocytoma character in the NF1-silenced tumors, this point may account for some of the difference observed in TMZ response in the models.

The immunocompetent background of the mice used to generate these models provides the opportunity to preclinically analyze immunotherapeutic strategies. Of late, immunotherapy has come to the forefront of glioblastoma clinical trials with numerous immune checkpoint blockade therapies currently under investigation<sup>212,214,215</sup>. Of these, only PD-1 neutralization has shown significant benefit with respect to extension of median survival. To further validate the models and demonstrate their utility in analysis of immunotherapy, I chose to assess the response to PD-L1 neutralizing therapy either alone or in combination with radiation in the PDGFB-overexpressing murine tumors. Additionally, I interrogated the efficacy of combined PD-L1 neutralization and radiation in the NF1-silenced model. In both experiments, PD-L1 neutralization was not shown to confer a significant survival advantage when compared to isotype control antibody administration. The mechanism of this resistance is still unclear, but there are explanations that deserve future investigation.

It is possible that PD-L1 neutralization is ineffective at extending median survival in glioblastoma. Crossing the *Ntv-a* mice with *Pd11*<sup>-/-</sup> mice and comparing the difference in survival between tumor-bearing *Ntv-a/Pd11*<sup>+/+</sup> and *Ntv-a/Pd11*<sup>-/-</sup> mice would demonstrate if PD-L1

neutralization is efficacious in extending median survival. Perhaps the distribution of the PD-L1 neutralizing antibody is insufficient to effectively inhibit the interaction of PD-1 and PD-L1 in the tumor. Additionally, I chose to use the recommended dose of PD-L1 neutralizing antibody suggested by the manufacturer. It is possible that this dose is too low to observe an effect in this model. Observation of an extension in median survival in mice with PD-L1 genetically ablated would suggest that either or both factors contribute to the lack of response to PD-L1 neutralizing therapy.

In total, PDGFB-overexpressing, NF1-silenced, and EGFRvIII murine HGG models offer exceptional tools for the evaluation of subtype-specific phenomena as well as preclinical pharmaceutical analysis and development. MRI techniques further complement these models, allowing for non-invasive monitoring of therapeutic response, tumor initiation, and tumor progression in a clinically relevant manner. These models allow for the assessment of the effects of tumor location, genetic driver mutations, stromal composition, and the mechanism of the Proneural to Mesenchymal switch. Furthermore, the tunability of the genetic mutations utilized for tumor generation, as well as the ability to extract, dissociate, and culture tumor cells generated with these models, will allow for the generation of a library of mouse tumor cell lines that can be employed for syngeneic studies. Due to the immunocompetent background of these mice, these models provide perhaps the most useful tool for the assessment and development of immunotherapy in glioblastoma. In the future, I hope that these models will provide a method for the development of individualized, targeted therapies and will accelerate their progression into clinical trials.

**Chapter 3: The Role of Interleukin-1 in the Formation of Glioblastoma-Associated Cerebral Edema<sup>1</sup>**

<sup>1</sup>Portions of this chapter were adapted from the published manuscript: Herting CJ, Chen Z, Maximov V, Duffy A, Szulzewsky F, Shayakhmetov DM, Hambardzumyan D. Tumour-associated macrophage-derived interleukin-1 mediates glioblastoma-associated cerebral oedema. *Brain*. 2019. Epub 2019/10/31. doi: 10.1093/brain/awz331. PubMed PMID: 31665239.

### 3.1 Introduction

Pharmacological interventions in glioblastoma are multi-faceted and must consider not only how to most effectively combat the tumor, but also how to manage detrimental symptoms associated with progression of the disease. In Chapter 1, it was discussed that many patients afflicted with glioblastoma are susceptible to development of epilepsy and that this condition is frequently managed with anti-convulsant compounds or drugs that manage extra-tumoral mass effect in the form of cerebral edema<sup>15</sup>. In this portion of the project, I strove to identify and validate a novel therapeutic target for the management of glioblastoma-associated cerebral edema. The major driving force behind this work was the recent discovery that glioblastoma patients who receive the corticosteroid dexamethasone to manage their cerebral edema have reduced response to the anti-neoplastic therapies employed to combat the tumor and have a worse overall prognosis<sup>192</sup>. These results, among others, emphasized that a novel therapeutic approach is needed, and I hypothesized that using the validated mouse models from Chapter 2, I possessed a prime tool to address this problem.

In patients afflicted with glioblastoma, the development of glioblastoma-associated cerebral edema is almost universal and most frequently is managed with the corticosteroid dexamethasone<sup>275</sup>. Dexamethasone has been the gold standard for treatment of cerebral edema since its introduction by researchers at the University of Minnesota in the early 1960's<sup>36</sup>. During these initial trials, corticosteroids were a relatively novel class of drugs and their potent anti-inflammatory effects were only just being defined. Additionally, MRI had not yet been established as a technique, so researchers resorted to x-ray angiography to define the effects of anti-inflammatory compounds in the context of brain tumors. During these initial studies, patients who were displaying clear signs of tumor burden, including hemiplegia, stupor, and severe headaches were treated with a bolus dose of

10-40mg of dexamethasone intramuscularly followed by oral maintenance of 4mg every 6 hours. Remarkably, 13 out of 14 patients enrolled in this study displayed a positive response to dexamethasone treatment. Their symptoms resolved within 24 hours of starting the treatment and the position of their midline cerebral artery returned to normal, indicating a reduction in the mass effect of their tumors. Within a few days, the patients returned to a relatively normal life until the tumor progressed to a point that the symptoms returned, and the patients succumbed to the disease. All-in-all, the results of this study were a groundbreaking achievement for the management of cerebral edema, and dexamethasone administration became standard practice. In fact, this discovery was recently hailed as one of the greatest contributions to the history of neurosurgery<sup>276,277</sup>. Although particularly efficacious for acute management of cerebral edema, time has uncovered a variety of significant drawbacks associated with prolonged use of dexamethasone and particularly alarming interactions in the context of glioblastoma.

Since their introduction, side-effects of glucocorticoid therapy, including abnormal fat deposition, amenorrhea, myopathy, mental excitement, and hyperglycemia have been well documented<sup>278</sup>. Initial trials of dexamethasone therapy for the management of cerebral edema additionally encountered the difficulties in weaning patients off of the drug due to suppression of the production of endogenous glucocorticoids cause by prolonged administration<sup>279</sup>. Uncertainties surrounding the proper dosing schedule were also uncovered during these trials, a caveat of dexamethasone therapy that has yet to be conclusively resolved<sup>36,276</sup>. In fact, the recent sentiment in the field appears to be that less is more in the utilization of corticosteroids for the management of edema in glioblastoma and prominent names in the field are stressing that the use should be restricted as much as possible<sup>280</sup>. This opinion stems from the recent work that has elucidated the severe impact of dexamethasone on anti-neoplastic therapies and patient outcomes in the context of glioblastoma.

It has been demonstrated through retrospective analysis of human patient data in glioblastoma that even when stratified for confounding variables such as Karnofsky performance score, age, and treatment, patients that receive dexamethasone have decreased median survival when compared to those that do not receive it<sup>192</sup>. These results were replicated in an RCAS PDGFB-overexpressing murine model where it was shown that dexamethasone directly interferes with the efficacy of radiotherapy that is employed to combat tumor growth<sup>192</sup>. Further human studies have demonstrated that a dexamethasone-associated gene signature predicts poor prognosis in human patients<sup>281</sup>. The detrimental effects of dexamethasone have been shown to be dose-responsive with maximal treatment interference and worse prognosis occurring in patients receiving the highest daily doses of dexamethasone<sup>282</sup>. With respect to the burgeoning field of immunotherapy in glioblastoma, dexamethasone has been shown to exert profound immunosuppressive effects and must be considered as these therapies are developed and deployed<sup>282,283</sup>. Considering the noted quality of life benefit afforded by dexamethasone therapy and the significant drawbacks associated with its use, I strove to identify a therapeutic target that could phenocopy the beneficial effects of dexamethasone while eliminating the off-target and detrimental effects.

The underpinnings of cerebral edema were initially uncovered and described in the late 1700's and early 1800's. During this time, researchers correctly hypothesized that cerebral edema results from extravasation of fluids from leaky vasculature into the brain<sup>284,285</sup>. In the early 1920's it was established that cerebral edema and brain swelling are distinct entities with the former producing a wet brain and the latter a dry brain<sup>286</sup>. A connection between edema and brain swelling was never conclusively established. In the 1960's, it was determined that the mechanistic pathophysiology of edema was a result of exudation of plasma from the circulation into the tissue as a result of damaged vasculature<sup>287</sup>. This process was hence termed "vasogenic edema" and further research established that dexamethasone specifically reduces the formation of cerebral edema in

glioblastoma by decreasing the permeability of the vessels that comprise the BBB<sup>288-291</sup>. The exact cellular and molecular mechanism of action that underlies this effect has remained elusive and is yet undefined.

In the context of brain tumors, it has been suggested that the mechanism of action of dexamethasone stems from its suppression of the production of VEGF – also known as vascular permeability factor – by the tumor<sup>292</sup>. Analysis of human tumor samples with microarray has disputed this hypothesis and illustrated no relationship between dexamethasone use and VEGF expression in malignant gliomas<sup>293</sup>. The relationship between dexamethasone and VEGF has been further obscured by results indicating that specific inhibition of VEGF signaling with small molecule or antibody therapy is capable of mimicking the anti-edema effect observed following dexamethasone treatment<sup>175,192</sup>. With these results in mind, I strove to provide clarity regarding the relationship between VEGF production and dexamethasone treatment using the murine models. Moreover, I aimed to identify a specific downstream target of dexamethasone that could be specifically inhibited to provide the anti-edema effects of the drug without the inhibition of anti-neoplastic therapy observed with dexamethasone treatment. Ultimately, these investigations lead me to the IL-1 family of cytokines, and I chose to interrogate specific inhibition of IL-1 as an alternative to dexamethasone for the management of edema in the PDGFB-overexpressing mouse model.

The IL-1 family of cytokines were originally discovered by researchers interested in areas ranging from physiology and metabolism to immunology and cancer; each of whom ascribed the cytokines with unique names such as endogenous pyrogen, lymphocyte activating factor, and mononuclear cell factor<sup>294</sup>. It wasn't until the 1980's that the founding members of this family, IL-1 $\alpha$  and IL-1 $\beta$ , were cloned, named, and their molecular structures and characteristics were established<sup>295</sup>. It is now known that IL-1 $\alpha$  and IL-1 $\beta$  both signal through the same receptor (IL-1R1)

although with different potencies<sup>296</sup>. The two cytokines are also now known to be produced by different cell types and in response to different cellular events. IL-1 $\alpha$  is produced in its active form in nearly all cells and is secreted as an alarmin following extensive cell damage or cell death<sup>297</sup>. IL-1 $\beta$  is synthesized in a pro-form and must be cleaved by the NLRP3 inflammasome, that is specific to macrophages, prior to secretion<sup>298</sup>. IL-1 $\beta$  is frequently cleaved and secreted when macrophages encounter pathogens or damage-associated alarmins<sup>299</sup>. In glioblastoma, TAMs are the largest non-neoplastic cell type, constituting over 30% of the tumor bulk, and contributing significantly to tumor progression and treatment resistance<sup>10</sup>. In the PDGFB-overexpressing murine model, the tumor-associated macrophage population has been shown to encompass both MG as well as BMDM from the circulation<sup>99</sup>. RNA-sequencing from these tumors suggests that BMDM in the tumor produce significant amounts of IL-1 $\beta$ , but this has not been validated experimentally. Considering the prevalence of tumor-associated macrophages in glioblastoma as well as their purported propensity to produce IL-1 $\beta$ , I considered investigation of IL-1 signaling in glioblastoma as a promising avenue of investigation.

Dexamethasone has been shown to have significant effects on cytokine production in the context of glioblastoma<sup>300</sup>. Research on the role of IL-1 signaling in neuroinflammatory conditions such as multiple sclerosis, Alzheimer's, and Parkinson's has linked IL-1 signaling to disruption of the BBB<sup>301,302</sup>. In the context of traumatic brain injury, specific IL-1 $\beta$  inhibition has shown the ability to reduce edema formation<sup>303</sup>. These studies, coupled with my early data linking IL-1 signaling inhibition and dexamethasone in BMDM, kindled my interest in macrophage-derived IL-1 acting as a driver of edema formation in glioblastoma. My overarching hypothesis was that dexamethasone inhibits the production of IL-1 cytokines in the context of TAMs in glioblastoma and that this effect partially drives the beneficial results observed with dexamethasone-based management of edema in glioblastoma.

The data presented herein illustrate that dexamethasone inhibits the production of IL-1 cytokines in the context of tumor-associated macrophages in glioblastoma and they further suggest that specific inhibition of IL-1 signaling would provide a therapeutic effect similar to dexamethasone. I found that dexamethasone prevents IL-1 production and dampens IL-1 signaling in primary murine BMDM and MG. Similar results were observed in an *ex vivo* system where organotypic tumor slices and BMDM or MG were co-cultured. A reduction in *Il1a* and *Il1b* mRNA was observed in tumor tissue from dexamethasone-treated tumor-bearing mice. Infiltration of myeloid and lymphoid cells from the blood was impaired in murine tumors following dexamethasone administration. A similar reduction of myeloid cell chemotaxis was also observed in *Nw-a/Il1r1<sup>-/-</sup>* mice with flow cytometry and immunohistochemistry. Ablation of IL-1R1 *in vivo* resulted in decrease vessel leakage as measured by a Hoechst dye-based assay. Genetic loss of IL-1 ligands resulted in decreased edema as measured by MRI, serial histology, and a methodology analyzing wet/dry tissue weight. The results presented here demonstrate that dexamethasone broadly impairs the function of the immune system, a phenomenon that warrants further investigation in the light of recent advances in glioblastoma immunotherapy. The complete impacts of IL-1 inhibition on immune function remain largely undefined outside of myeloid cell chemotaxis and also merit further examination. Finally, by using genetic and pharmacological approaches, I demonstrate that targeting IL-1 signaling does not compromise efficacy of radiation therapy in tumor-bearing mice. These results suggest that specific IL-1 signaling inhibition may be a preferred alternative to dexamethasone for the management of glioblastoma-associated cerebral edema.

### **3.2 Materials and Methods**

#### *Bone marrow-derived macrophage isolation and culture*

BMDM were isolated from 4-12-week-old C57BL/6 mice using modified established protocol<sup>304</sup>. The mice were euthanized via CO<sub>2</sub> asphyxiation. The whole, intact femur and tibia were stripped of muscle with sterile forceps and collected in sterile Dulbecco's phosphate-buffered saline (DPBS). Both ends of the bone were cut and the marrow was flushed into a clean petri dish using DPBS supplemented with 4% BSA (ThermoFisher, 15260037), heparin (STEMCELL, #07980), DNase I (Sigma-Aldrich, 11284932001), and penicillin/streptomycin (Fisher, SV30010). The resulting mixture was briefly triturated and passed through a 70 µm cell strainer. The cells were plated in a 15 cm non-cell culture-treated plate for a six-day differentiation in 15 ml of DMEM (ThermoFisher, 10569010) with 10% FBS (HyClone, SH30396.03) and 40 ng/ml of macrophage-colony stimulating factor (M-CSF) (Peprotech, 315-02). An additional 15 ml of media with M-CSF was added after day three. The cells were harvested for experimentation via 10-minute incubation in DPBS with 5 mM EDTA on ice. Cells were plated in 6-well plates in 2 ml of culturing media with M-CSF at a concentration of 20 ng/ml for experimentation.

#### *Microglia isolation and culture*

MG were isolated from p0-p3 pups using a modified established protocol<sup>305</sup>. Whole brains were extracted from p0-p3 C57BL/6 pups using sterile instruments, followed by three consecutive washes in sterile DPBS. Brains were then digested in 0.5% trypsin (ThermoFisher, 15400054) and DNaseI (Sigma-Aldrich, 11284932001) followed by mechanical dissociation and filtration through a 70 µm cell strainer. The filtrate was spun at low speed for two consecutive rounds in a centrifuge to eliminate cellular debris and was then plated in flasks pre-coated with poly-D-lysine (Sigma-Aldrich, P6407). The cells were plated in DMEM (ThermoFisher, 10569010) with 10% FBS (HyClone, SH30396.03) and M-CSF (Peprotech, 315-02) at a concentration of 40 ng/ml. The cells grew until astrocytes reached confluence on the bottom of the flask and MG were observed ballooning off the

surface. During this time, additional M-CSF was periodically added. MG were collected by gently rinsing the back of the flask with culturing media and were plated in 6-well plates in 2 ml of the culturing media with M-CSF at a concentration of 40 ng/ml for experimentation.

*Bone marrow-derived macrophage and microglia immunofluorescent validation*

BMDM and MG were plated in 24-well plates on sterile coverslips and allowed to adhere overnight. The cells were then briefly fixed in 4% paraformaldehyde (PFA), washed, and blocked. The cells were stained for IBA1 (Wako) and visualized with donkey anti-rabbit Alexa Fluor 647nm (Abcam, ab150075). Imaging was performed with Fluoview FV1000 confocal microscope (Olympus).

*Bone marrow-derived macrophage and microglia flow validation*

BMDM and MG were isolated from  $Cx3cr1^{+/GFP}/Ccr2^{+/RFP}$  mice as described. Following isolation, an aliquot of cells was taken, and red blood cells were lysed in red blood cell (RBC) lysis buffer (BioLegend, 420301). The remainder of the cells were differentiated as described. The aliquot of cells was then washed, blocked, and stained with CD11b PerCP-Cy5.5 (BioLegend, 101227). Cells were analyzed on an LSRII flow cytometer and CD11b, CCR2, and CX3CR1 positivity were quantified. This procedure was repeated with the remainder of the cells after culturing and differentiation.

*Bone marrow-derived macrophage and microglia stimulation*

A three-hour starvation in FBS-deficient media was performed prior to stimulation with 100ng/ml lipopolysaccharide (LPS) (Sigma Aldrich, L5293), 40ng/ml interferon gamma (IFN $\gamma$ ) (Peprotech, 315-05), 75 pM or 400 pM IL-1 $\alpha$  (R&D, 400-ML-005/CF), or 200 pM or 1 nM IL-1 $\beta$  (R&D, 401-ML-005/CF). Six-hour incubations with the indicated stimulants were performed.

Dexamethasone (Sigma-Aldrich, D4902) was included as a two-hour pretreatment at a dose of 5  $\mu$ M where indicated. Gallium nitrate (Sigma-Aldrich, 289892-5G) was included as a two-hour pretreatment at a dose of 500  $\mu$ M where indicated. Cells were treated with 5 mM ATP (Sigma, A2383) for thirty minutes following the six-hour simulation to induce cytokine release as previously described<sup>306</sup>.

#### *Bone marrow-derived macrophage and microglia apoptosis assay*

BMDM and MG were isolated and cultured as described. Cells were treated with vehicle solution, dexamethasone (Sigma-Aldrich, D4902), or LPS (Sigma Aldrich, L5293) to induce apoptosis. Following a six-hour incubation, cells were collected via trypsinization and allowed to rest in culturing media for thirty minutes. The cells were then assessed with a propidium iodide and annexin V apoptosis assay (ThermoFisher, V13242) according to the manufacturer's protocol.

#### *Quantitative-PCR analysis*

RNA was isolated from cell cultures or snap-frozen tumor pieces using a RNeasy Lipid Tissue Mini Kit (Qiagen, 74804) according to the manufacturer's instructions. RNA quantity was assessed with a NanoDrop 2000 spectrometer, while quality was confirmed via electrophoresis of samples in a 1% bleach gel as previously described<sup>246</sup>. Following RNA validation, cDNA synthesis was performed with a First Strand Superscript III cDNA synthesis kit (ThermoFisher, 18080051) according to the manufacturer's instructions and with equal amounts of starting RNA. Quantitative-PCR was performed with the validated BioRad PCR primers for murine *Il1a*, *Il1b*, *Vegfa*, *Aurka*, *Cdc20*, *Plk1*, *Cenpa*, *Ccnb1*, *Kif2c*, *Ccl2*, *Ccl5*, *Ccl7*, *Ccl8*, *Ccl12*, *Aif1*, and  $\beta$ -*Actin* using a SsoAdvanced Universal SYBR green Supermix (BioRad, 1725271). Fold change in gene expression was determined relative to a defined control group using the  $2^{-\Delta\Delta C_t}$  method with  $\beta$ -Actin as a housekeeping gene.

### *Enzyme-linked immunosorbent assay*

Cell lysates for enzyme-linked immunosorbent assay were collected via sonication of cells in lysis buffer supplemented with protease and phosphatase inhibitors. Tissue lysates were collected via mechanical homogenization in lysis buffer followed by sonication. Protein concentration was determined using a Bradford protein assay (BioRad, 5000001) according to the manufacturer's instructions. Enzyme-linked immunosorbent assays were performed for murine IL-1 $\alpha$  (R&D, MLA00) IL-1 $\beta$  (R&D, DY401), CCL2 (R&D, DY-479), CCL7 (Boster, EKO683), CCL8 (R&D, DY790), CCL12 (R&D, MCC120), IL-6 (R&D, M6000B), and VEGFA (R&D, MMV00) according to the manufacturer's instructions.

### *Mice*

*Ntv-a/Cdken2a*<sup>-/-</sup> and *Ntv-a* mice in the age range of 8-16 weeks were used for experiments as previously described<sup>241,307</sup>. The former is a mixed genetic background, while the latter is a C57BL/6 background. All animals were housed in a climate controlled, pathogen-free facility with *ad libitum* food and water under a 12-hour light/dark cycle. Additionally, the previously-described and validated *Il1r1*<sup>-/-</sup>, *Il1b*<sup>-/-</sup>, and *Il1a/b*<sup>-/-</sup> mice were crossed with the *Ntv-a* mice to generate *Ntv-a/Il1r1*<sup>-/-</sup> mice, *Ntv-a/Il1b*<sup>-/-</sup> mice, and *Ntv-a/Il1a/b*<sup>-/-</sup> mice<sup>308,309</sup>. For validation of BMDM and MG cultures, *Cx3cr1*<sup>+ /GFP</sup> / *Ccr2*<sup>+ /RFP</sup> mice were utilized as previously described<sup>99</sup>. Genotypes were confirmed by Transnetyx.

### *Virus production and tumor generation*

DF-1 cells (ATCC, CRL-12203) were purchased and grown at 39°C according to supplier instructions. Cells were transfected with RCAS PDGFB-HA or RCAS *shp53*-RFP using a Fugene 6 transfection kit (Roche, 11814443001) according to the manufacturer's instructions. DF-1 cells (4x10<sup>4</sup>) were stereotactically delivered with a Hamilton syringe equipped with a 30-gauge needle for

tumor generation. For the *Ntv-a/Cdkn2a*<sup>-/-</sup> background mice, RCAS PDGFB-HA was delivered alone. RCAS PDGFB-HA and RCAS *shp53*-RFP were co-injected at a 1:1 mixture for tumor generation in *Ntv-a* background mice. The target coordinates were in the right-frontal striatum at AP-1.7mm and right-0.5mm from bregma; depth-2mm from the dural surface<sup>243</sup>. Prior to surgery, mice were anaesthetized with intraperitoneal injections of ketamine (McKesson, 494158) (0.1 mg/g) and xylazine (Akorn) (0.01 mg/g). A local injection of marcaine (McKesson, 57199) was delivered for pre-surgical analgesia followed by two post-operative administrations of buprenorphine (McKesson, 1013922) within 24 hours of completion. Mice were continually monitored for signs of tumor burden and were sacrificed upon observation of endpoint symptoms.

#### *Organotypic tumor slice culture*

At endpoint, *Ntv-a/Cdkn2a*<sup>-/-</sup> mice harboring PDGFB-overexpressing tumors were euthanized via CO<sub>2</sub> asphyxiation. Without perfusion, the brain was rapidly extracted and embedded in 4% low-melt agarose in PBS. The embedded brain was then mounted on a vibratome (Leica) and submerged in ice cold Hank's balanced salt solution (HBSS). The brain was cut into 300 μm-thick sections and the slices were transferred to inserts in a 6-well plate. Slices were cultured in Neurobasal media (STEMCELL, 05700) supplemented with B27 supplement (ThermoFisher, 17504044), sodium pyruvate (ThermoFisher, 11360070), and glutamine (ThermoFisher, 35050061). M-CSF at a concentration of 40 ng/ml was included in the media during co-culture experiments with BMDM and MG. Dexamethasone (Sigma-Aldrich, D4902) was included at a dose of 5 μM where administration is indicated.

#### *In vivo dexamethasone administration*

Mice were given intraperitoneal injections of either dexamethasone (West-ward, 462-329-02) at a dose of 10 mg/kg or a corresponding volume of 0.9% saline solution (McKesson, 2718344) for

five days prior to sacrifice. Treatment was initiated when mice began to show neurological signs of tumor burden. Mice were sacrificed on day six after treatment initiation and tumor tissue was collected for analysis as described.

### *Immunohistochemistry*

Prior to staining, 5  $\mu$ m-thick sections were cut on a microtome (Leica). Sections were deparaffinized and antigen unmasking was performed with a citrate solution (Vector, H-3300) according to the manufacturer's instructions. CD31 (Dianova, DIA-310) was stained by hand, while IBA1 (Wako) was stained using an automated system (Ventana). Quantification of percent positive area and average vessel size was performed blinded to treatment condition using Fiji as previously described<sup>307</sup>.

### *Flow cytometry*

At endpoint, mice were sacrificed with an overdose of ketamine. Blood was collected via cardiac puncture and de-coagulated with EDTA. Mice were then perfused with cold Ringers solution (Sigma-Aldrich, 96724-100TAB) and the brains were extracted and placed in dishes with sterile HBSS. Tumor dissociation was performed with a neural tissue dissociation kit (Milltenyi, 130-092-628) using 1 mg/ml collagenase D (Sigma-Aldrich, 11088882001) in water as a digestive enzyme. The resulting cell suspension was cleaned of debris via Percoll density gradient centrifugation and was blocked with Fc-block (BD Biosciences, 553141), FBS (HyClone, SH30396.03), normal rat serum (ThermoFisher, 10710C), normal mouse serum (ThermoFisher, 10410), and normal rabbit serum (ThermoFisher, 31883) on ice. Staining was performed in the blocking solution with the following antibodies: CD45-APC (BioLegend, 103111), CD11b-PerCP-Cy5.5 (BD Biosciences, 550993), Ly6C-PE-Cy7 (BD Biosciences, 560593), and Ly6G-V450 (BD

Biosciences, 560603). Cells were washed and resuspended in a buffer consisting of PBS, BSA, EDTA, and sodium azide prior to analysis on a LSRII cytometer (BD).

#### *Tumor tissue isolation*

At endpoint, mice were euthanized with an overdose of ketamine and xylazine and perfused with cold Ringer's solution (Sigma-Aldrich, 96724-100TAB). The brain was extracted, and a piece of tumor was immediately snap-frozen in liquid nitrogen for storage at -80°C. The rest of the brain was fixed in 10% formalin for 72 hours for histology.

#### *Hoechst dye leakage assay*

Mice were anaesthetized with ketamine and xylazine prior to this procedure. Five minutes prior to euthanasia 50 µl of Hoechst 33342 (Sigma, #H6024) was injected intravenously through the retroorbital sinus. Animals were then perfused with 4% PFA in PBS and the brains were extracted. The brains were embedded in O.C.T. (VWR, 25608-930) and cut into 30 µm sections on a cryostat (Leica). Sections were permeabilized with 0.3% Triton X-100 in PBS and stained with propidium iodide (ThermoFisher, P1304MP) for 30 min at 37 °C. Sections were then washed with PBS before mounting with 70% glycerol. Whole-slice images were obtained using the multi-area time lapse function on the Fluoview FV1000 microscope (Olympus). Four z-planes were acquired at a spacing of 5 µm for each channel analyzed. The grid/collection stitching plugin in Fiji was used to combine the individual tiles from the multi-area time lapse into a complete image of the brain slice<sup>310</sup>. Z-projection was employed to reduce the separate z-planes into one image. The percent positive Hoechst area was determined and divided by the total tumor area, as judged by propidium iodide staining, to generate a readout of tumor vessel leakage. All image analysis and quantification were performed blinded to treatment condition.

#### *B20-4.1.1 treatment*

Treatment with B20-4.1.1 (Genentech) commenced 30 days following tumor induction via RCAS injection. Mice were administered B20-4.1.1 at 5 mg/kg via intraperitoneal injection every 4 days until endpoint symptoms developed.

#### *MRI tumor volume reconstruction*

I employed a 9.4 T, 20 cm horizontal bore Bruker magnet interfaced to an Avance console (Bruker) and equipped with an actively shielded gradient set. This set up has an inner diameter of 11 cm, a maximum gradient strength of 100 mT/m, and a rise time of 110 ms. A two-coil actively decoupled imaging set-up was employed with a 3 cm surface coil used to receive the signal generated by a 7.2 cm diameter volume transmission coil. The receiving coil was positioned over the cortical and subcortical areas of interest to maximize the signal-to-noise ratio. Mice were imaged while anaesthetized with 1.5-2% isoflurane (Baxter, 1001936060) and held in a custom-made cradle. Body temperature and respiration rate were continually monitored throughout the experiment with an animal physiological monitoring system (SA Instruments). The mouse head was imaged in the axial orientation using a T2-weighted fast spin-echo RARE sequence with a TR of 3.5 seconds, a TE of 50 ms, a RARE factor of 8, a NEX value of 24, a field of view of 3 x 2 cm, and a slice thickness of 0.7 mm generating an in-plane resolution of 117x156  $\mu$ m. During the procedure, 14 slices were obtained. To reconstruct tumor volume, the tumor area in each slice was outlined in the Bruker software and multiplied by the thickness of the slice. The total volume for all slices within each tumor was summed to generate the total tumor volume. All tumors were analyzed in a blinded fashion.

#### *Hematoxylin and eosin tumor volume reconstruction*

At endpoint, mice were sacrificed with an overdose of ketamine and xylazine and perfused with 4% PFA in PBS. The brain was carefully extracted and incubated in 4% PFA in PBS for 24

hours following a 72-hour incubation in 30% sucrose in PBS. The brain was then embedded in O.C.T. compound (VWR, 25608-930) and frozen on dry ice. The entire brain was then serially sectioned on a cryostat (Leica) set to cut 30  $\mu$ m sections. Every tenth section was collected and mounted on a slide for automated hematoxylin and eosin staining. The slides were scanned at 20x magnification with a whole slide scanner (Hamamatsu). Tumor area in each section was determined in a blinded fashion in NDP.view2 and multiplied by the thickness of ten slices. The resulting volumes for the slides of each tumor were then summed, producing an estimation of the total volume.

#### *Wet/dry tissue weight edema measurement*

At endpoint, whole brains were extracted without perfusion and immediately weighed. Tissue was then placed in a vacuum oven (Across International) and dried at complete vacuum and 95°C for 24 hours. Dry tissue was then re-weighed, and the percent brain water was calculated as previously described<sup>311</sup>.

#### *Mouse irradiation and gallium nitrate administration*

Irradiation of tumor-bearing mice was performed as previously described<sup>307</sup>. Gallium nitrate (Sigma-Aldrich, 289892-5G) was administered via intraperitoneal injection in saline at a dose of 50mg/kg as indicated. Mice were followed until endpoint criteria were met and overall survival was recorded.

#### *Statistical Analysis*

Statistical analysis and figure generation were performed in GraphPad Prism version 8 and Adobe Illustrator, respectively. Significant effects were considered at  $P < 0.05$ . Specific statistical

analyses utilized for each experiment are indicated in the figure legends. All data are presented as mean  $\pm$  SEM.

### 3.3 Results

#### *Dexamethasone blocks the production of IL-1 cytokines in primary murine BMDM and MG in vitro*

For *in vitro* analysis of the effects of dexamethasone on IL-1 production by macrophages, primary murine BMDM and MG culturing protocols (**Figure 3.1A and B**) were established by modification of existing methods<sup>304,305</sup>. To validate the purity of cells isolated with these methodologies, immunofluorescent staining for IBA1 and flow cytometric analysis of CCR2 and CX3CR1 were employed (**Figure 3.2**).

Macrophages are known to upregulate IL-1 cytokines following stimulation with LPS and IFN $\gamma$ , and they secrete IL-1 $\beta$  following activation of the P2X<sub>7</sub> purinergic receptor by ATP<sup>306,312</sup>. Therefore, I employed a scheme consisting of LPS and IFN $\gamma$  stimulation, followed by ATP treatment, to functionally validate my primary BMDM and MG cultures (**Figure 3.1C-F**). Dexamethasone pre-treatment suppressed LPS and IFN $\gamma$ -induced *Il1a* and *Il1b* RNA expression in both BMDM (**Figure 3.1C**) and MG (**Figure 3.1D**). Intracellular and secreted IL-1 $\beta$  protein levels were also suppressed by dexamethasone in both cell types (**Figure 3.1E and F**).

IL-1 stimulation has been shown to upregulate IL-1 cytokines in multiple different cell types and I next investigated this phenomenon in my primary murine BMDM and MG<sup>313-315</sup>. First, I performed dose-response experiments in BMDM and MG to determine the optimal doses of IL-1 $\alpha$  and IL-1 $\beta$  to use for further experiments (**Figure 3.3**). I chose to use doses of 75 pM IL-1 $\alpha$  and 200 pM IL-1 $\beta$  in primary BMDM (**Figure 3.3A and C**). Doses of 400 pM IL-1 $\alpha$  and 1 nM IL-1 $\beta$  were used in experiments with primary MG (**Figure 3.3B and D**).

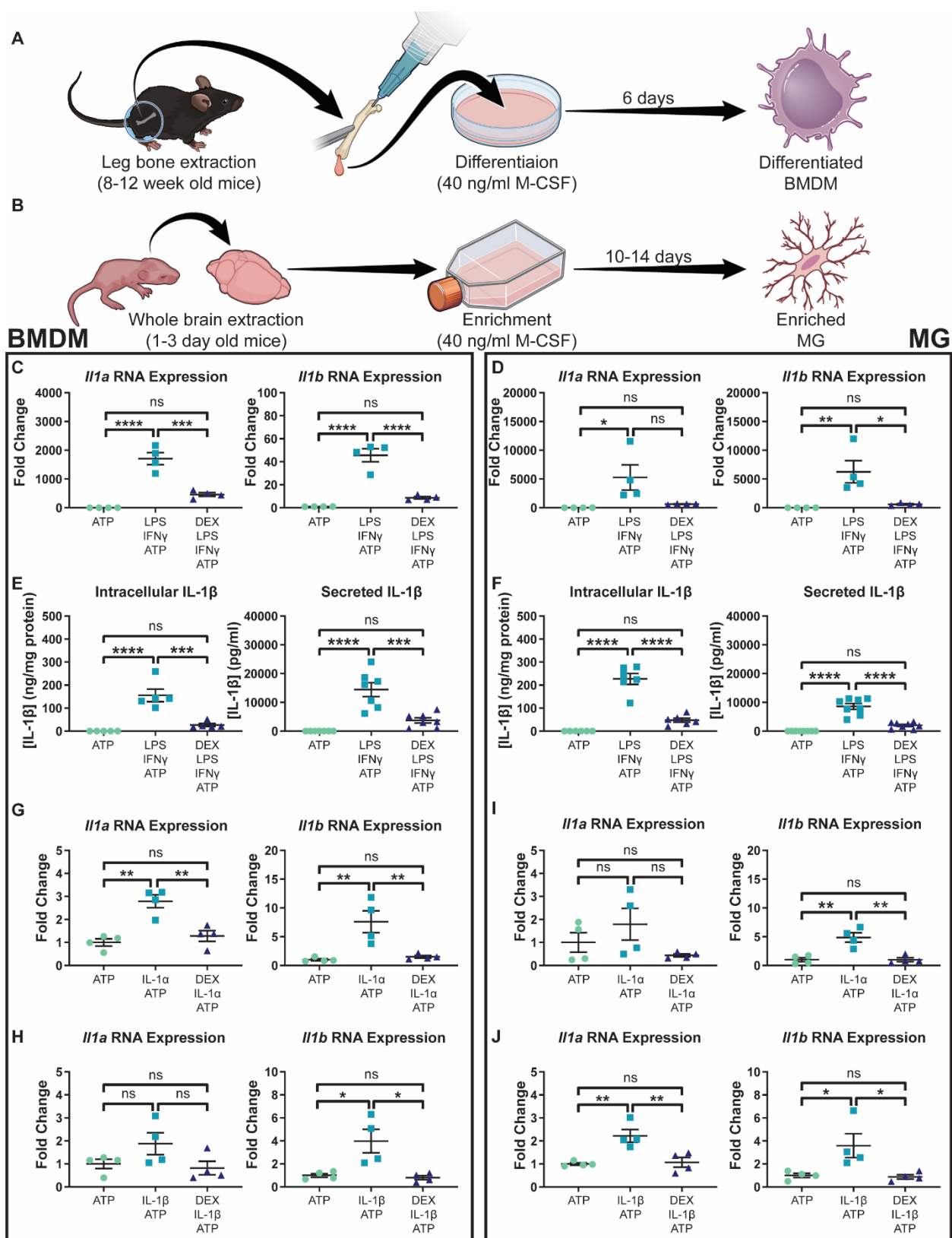


**Figure 3.1. Dexamethasone blocks LPS/IFN $\gamma$  and IL-1-induced IL-1 expression in primary BMDM and MG.** Primary murine BMDM (A) and MG (B) were cultured using modifications of previously established protocols. *Ili* expression in BMDM (N=4) (C) and MG (N=4) (D) following stimulation with LPS and IFN $\gamma$ . Intracellular (N=5) and secreted (N=7) IL-1 $\beta$  protein levels in BMDM (E) as well as intracellular (N=6) and secreted (N=8) IL-1 $\beta$  protein levels in MG (F) following stimulation with LPS and IFN $\gamma$ . IL-1 $\alpha$  (G) and IL-1 $\beta$  (H) stimulation of BMDM (N=4). IL-1 $\alpha$  (I) and IL-1 $\beta$  (J) stimulation of MG (N=4). One-way ANOVA, ns=not significant, \* $P$ <0.05, \*\* $P$ <0.01, \*\*\* $P$ <0.001, \*\*\*\* $P$ <0.0001.

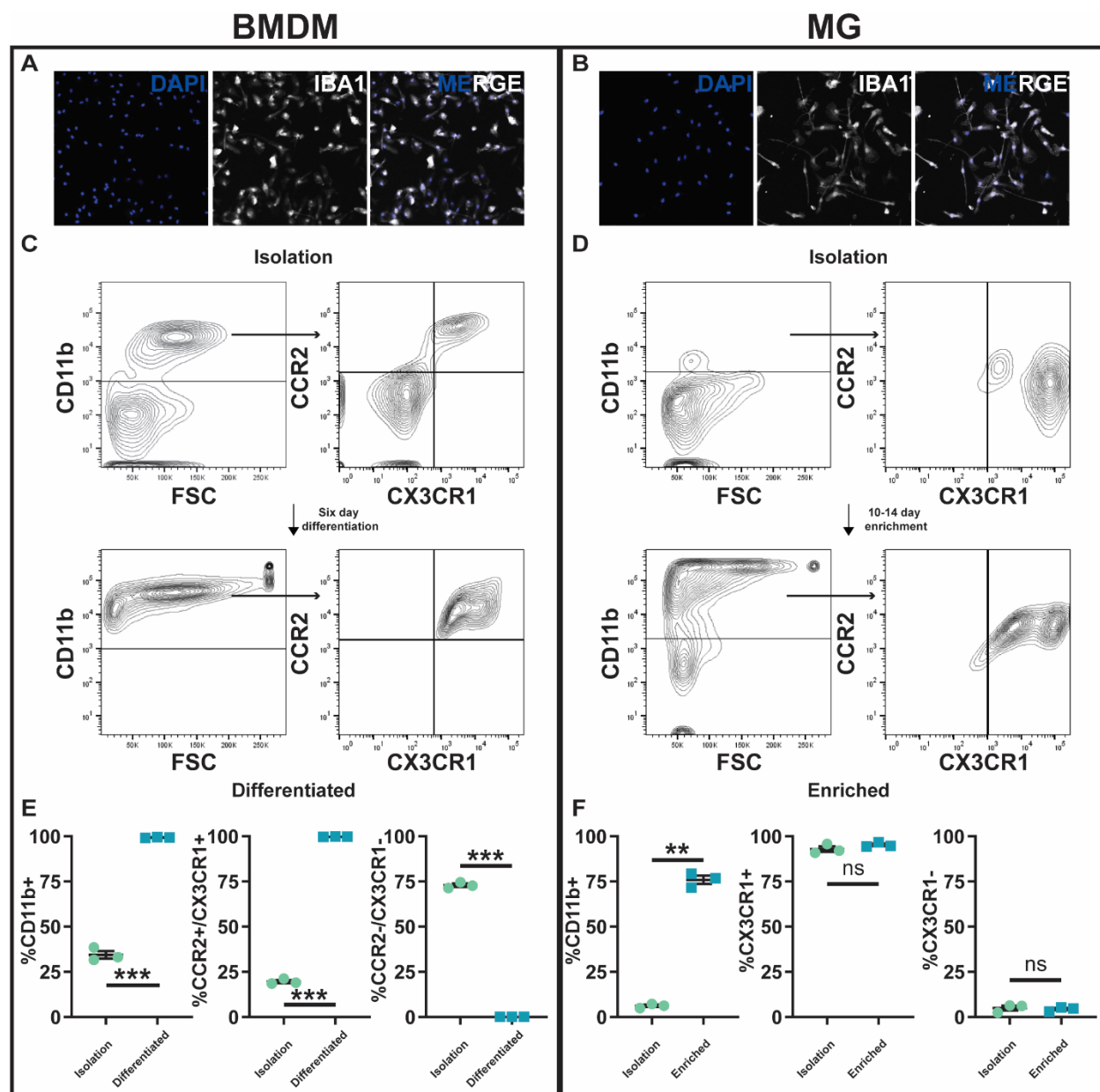


**Figure 3.2. Differentiation of primary cells in media supplemented with M-CSF produces pure BMDM and MG cultures.** (A) Representative immunofluorescent staining of differentiated BMDM for the pan-macrophage marker IBA1. (B) Representative immunofluorescent staining of enriched MG for the pan-macrophage marker IBA1. (C) Representative flow cytometry plots of BMDM cultures from *Cx3cr1*<sup>+/GFP</sup>/*Ccr2*<sup>+/RFP</sup> mice on the day of isolation (top) and terminal differentiation (bottom). (D) Representative flow cytometry plots of MG cultures from

*Cx3cr1<sup>+/GFP</sup>/Ccr2<sup>+/RFP</sup>* mice on the day of isolation (top) and following enrichment (bottom). (E)

Quantification of the BMDM flow data (N=3). (F) Quantification of the MG flow data (N=3).

Two-tailed Student's t-test, ns=not significant, \*\* $P < 0.01$ , \*\*\* $P < 0.001$ .

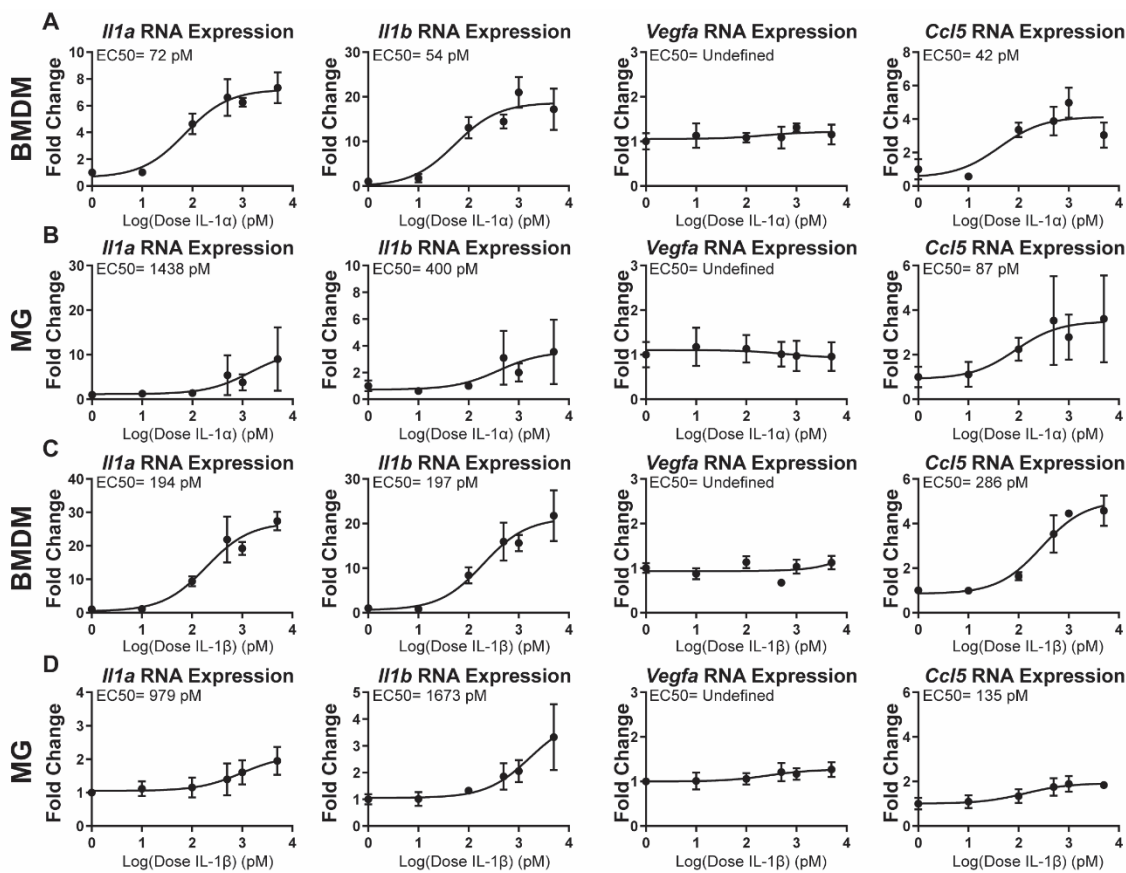


**Figure 3.3.** IL-1 $\alpha$  and IL-1 $\beta$  dose response experiments in primary BMDM and MG reveal effective doses for downstream analysis. Quantitative-PCR analysis of *I11a*, *I11b*, *Vegfa*, and *Ccl5* in BMDM stimulated with varying doses of IL-1 $\alpha$  (A) or IL-1 $\beta$  (C) (N=3). Quantitative-PCR analysis of *I11a*, *I11b*, *Vegfa*, and *Ccl5* in MG stimulated with varying doses of IL-1 $\alpha$  (B) or IL-1 $\beta$  (D) (N=3). EC<sub>50</sub> values were determined via three parameter non-linear regression and resulting trendlines are illustrated.

I next assessed the effects of dexamethasone on IL-1-induced IL-1 production. In both BMDM (**Figure 3.1G and H**) and MG (**Figure 3.1I and J**), dexamethasone was shown to inhibit *Il1a* and *Il1b* RNA expression following stimulation with either IL-1 cytokine. These *in vitro* results confirm that dexamethasone is capable of blocking IL-1 $\alpha$  and IL-1 $\beta$  production following multiple different stimulation schemes. A propidium iodide and annexin V-based apoptosis assay confirmed that these results were not due to dexamethasone toxicity in BMDM or MG (**Figure 3.4**).

*Dexamethasone blocks IL-1 cytokine and MCP chemokine production in myeloid cells and organotypic tumor slices co-cultured ex vivo*

Based on the inhibitory effect of dexamethasone on IL-1 signaling in BMDM and MG *in vitro*, I next designed an *ex vivo* system to interrogate questions more specific to the glioblastoma tumor microenvironment. Previously, by using RNA-sequencing, I showed that BMDM, and not MG, primarily express *Il1b* in glioblastoma and that BMDM are recruited to the tumor through a MCP family chemokine-dependent mechanism<sup>99</sup>. To evaluate whether BMDM or MG upregulate IL-1 family cytokines in the tumor microenvironment, and what effects dexamethasone has on this process, I developed a system for co-culturing BMDM and MG with organotypic tumor slices (**Figure 3.5A**).

The results of this experiment demonstrated that BMDM exposed to organotypic tumor slices upregulate both *Il1a* and *Il1b* (**Figure 3.5B**). This effect was shown to be abrogated by dexamethasone treatment. Tumor slices co-cultured with BMDM and treated with dexamethasone were shown to downregulate *Il1a* and *Il1b*, as well as *Ccl2*, *Ccl7*, and *Ccl12*; three of the four MCP family members (MCP-1/CCL2, MCP-2/CCL7, MCP-3/CCL8, and MCP-4/CCL12) (**Figure 3.5C**). Contrary to the results in BMDM, MG did not upregulate *Il1a* or *Il1b* following co-culture

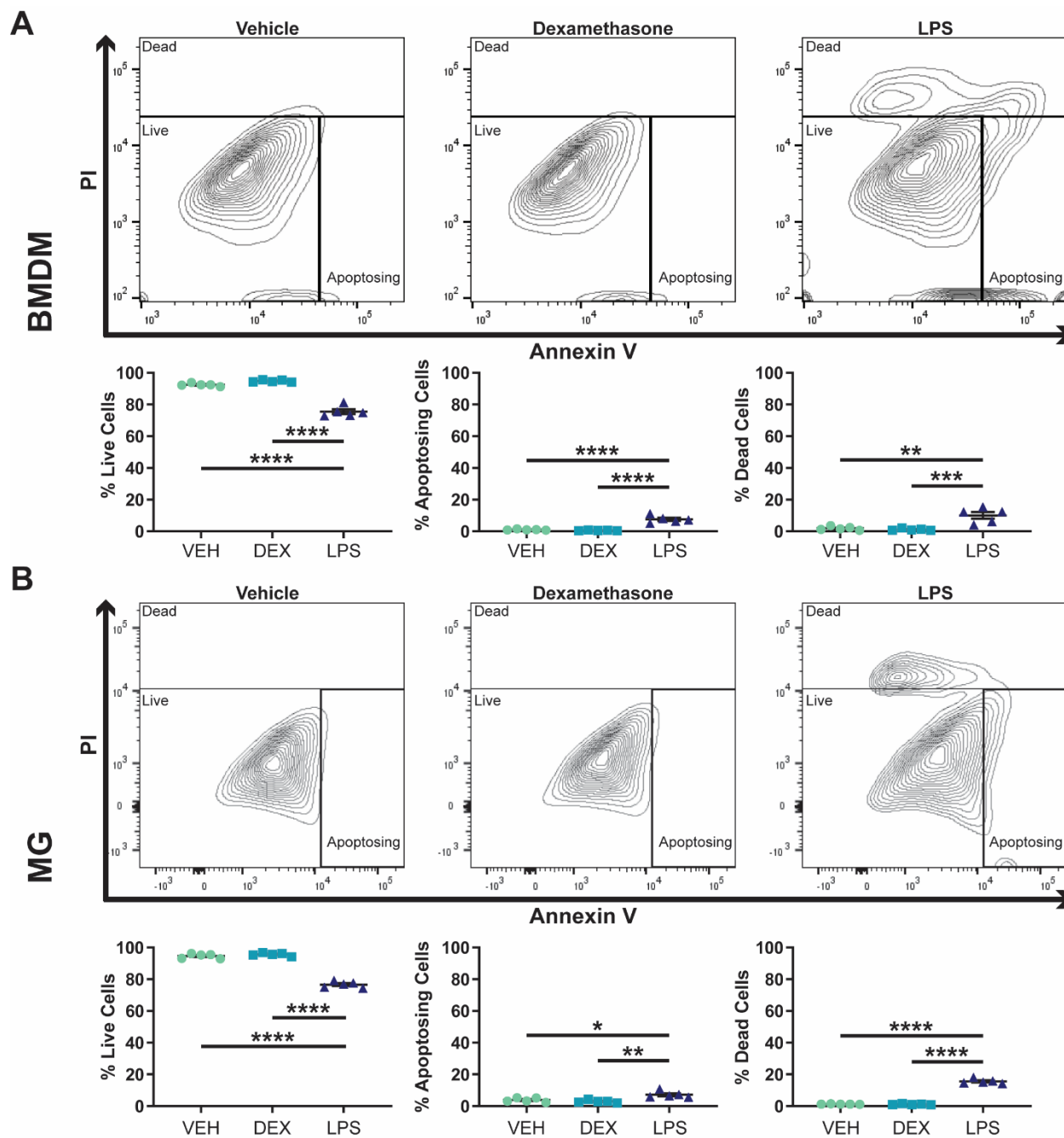


**Figure 3.4. Dexamethasone is non-toxic to primary murine BMDM and MG. (A)**

Representative flow cytometry plots and quantification for BMDM stimulated with vehicle, dexamethasone, or LPS and assessed with an annexin V and propidium iodide-based apoptosis assay (N=5). (B) Representative flow cytometry plots and quantification for MG stimulated with vehicle,

dexamethasone, or LPS and assessed with an annexin V and propidium iodide-based apoptosis assay (N=5). One-way ANOVA, \* $P < 0.05$ , \*\* $P < 0.01$ , \*\*\* $P < 0.001$ , \*\*\*\* $P < 0.0001$ .

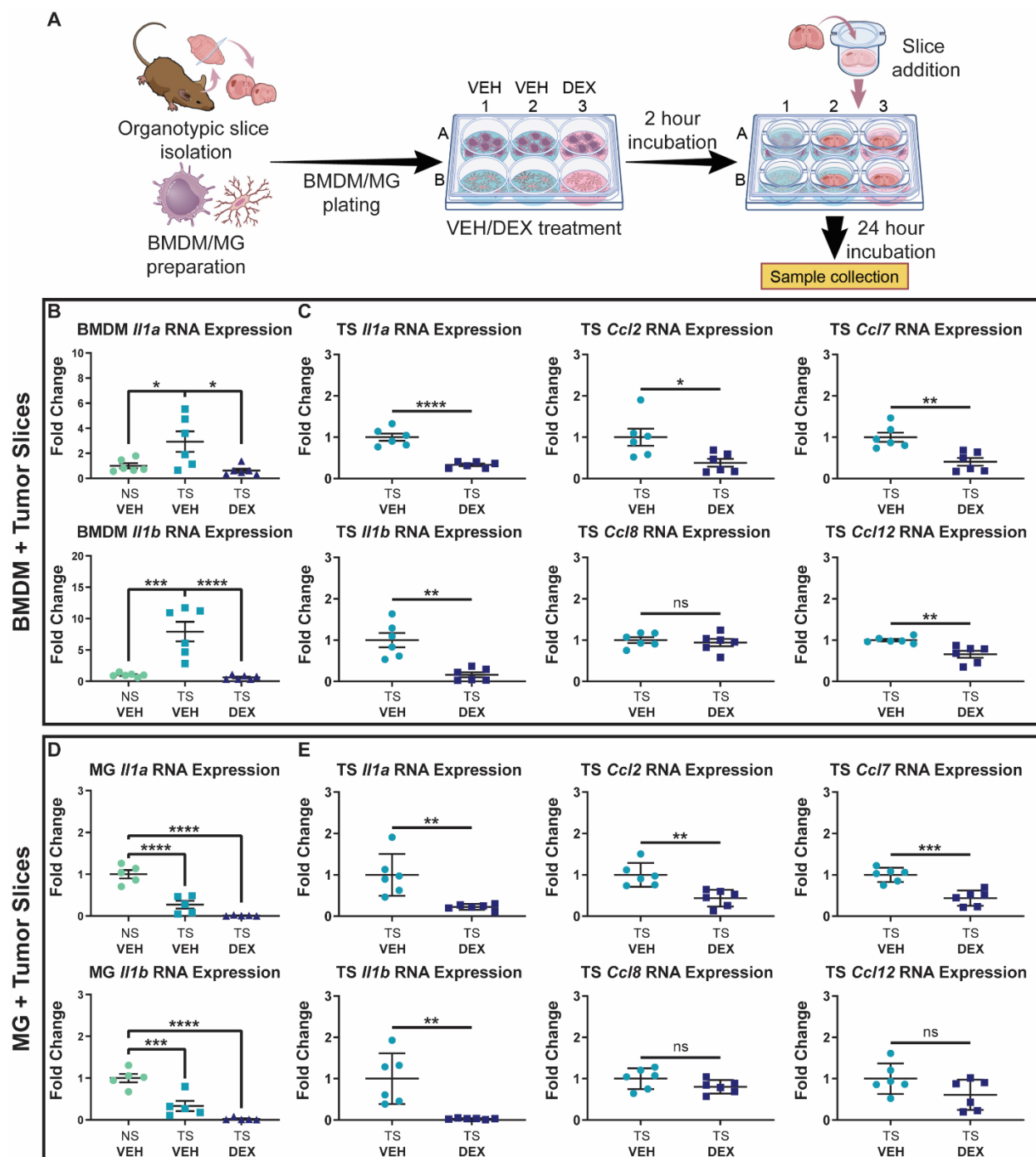


**Figure 3.5. Dexamethasone treatment ablates *Il1* upregulation by BMDM exposed to organotypic tumor slices and reduces expression of MCP cytokines by tumor tissue. (A) An experimental outline of the co-culture of BMDM and MG with organotypic tumor slices (TS). (B) Expression of *Il1a* and *Il1b* in BMDM co-cultured with tumor slices (N=6). (C) *Il1a*, *Il1b*, *Ccl2*, *Ccl7*,**

*Ccl8*, and *Ccl12* expression in tumor slices co-cultured with BMDM (N=6). (D) Expression of *Il1a* and *Il1b* in MG co-cultured with tumor slices (N=5). (E) *Il1a*, *Il1b*, *Ccl2*, *Ccl7*, *Ccl8*, and *Ccl12* expression in tumor slices co-cultured with MG (N=6). In all experiments, dexamethasone was added at a dose of 5  $\mu$ M where indicated. One-way ANOVA and two-tailed Student's t-test, ns=not significant, \* $P$ <0.05, \*\* $P$ <0.01, \*\*\* $P$ <0.001, \*\*\*\* $P$ <0.0001.

with tumor slices (**Figure 3.5D**). In fact, MG were surprisingly shown to downregulate *Il1a* and *Il1b* in this context. Both *Il1a* and *Il1b* expression were still downregulated by dexamethasone treatment relative to the control MG. Tumor slices co-cultured with MG and treated with dexamethasone were shown to downregulate *Il1a* and *Il1b*, as well as *Ccl2* and *Ccl7*, similar to what was seen in tumor slices co-cultured with BMDM (**Figure 3.5E**). The downregulation of MCP chemokine family members suggested the dexamethasone may alter BMDM chemotaxis.

*Dexamethasone significantly reduces the number of tumor-associated macrophages without altering blood vessel morphology*

To assess the effects of dexamethasone on tumor-associated macrophages and angiogenesis *in vivo*, PDGFB-overexpressing tumors were generated in *Ntv-a/Cdkn2a<sup>-/-</sup>* mice as previously described<sup>307</sup>. The treatment schematic for this experiment (**Figure 3.6A**) involved dosing tumor-bearing mice with vehicle solution (saline) or dexamethasone (10 mg/kg) for five days prior to sacrifice, with mice displaying endpoint symptoms. The efficacy of this dexamethasone treatment scheme was verified by assessing the expression levels of *Aurka*, *Cdc20*, *Plk1*, *Cenpa*, *Ccnb1*, and *Kif2c* genes in tumor tissue with quantitative-PCR (**Figure 3.7**). These genes were previously demonstrated to be downregulated by dexamethasone treatment<sup>192</sup>. Quantitative-PCR analysis of the isolated tumors indicated a decrease in total *Il1a* and *Il1b* post-dexamethasone treatment (**Figure 3.6B**). Contrary to prior reports that dexamethasone alters the expression of *Vegfa*, I observed no difference in *Vegfa* expression in tumors isolated from vehicle- or dexamethasone-treated mice (**Figure 3.6B**). *Aif1*, a pan-macrophage marker, was shown to be significantly downregulated by dexamethasone (**Figure 3.6B**).

Based on these results, I questioned whether vehicle- and dexamethasone-treated mice would display differences in angiogenesis or tumor-associated macrophage accumulation. Therefore,

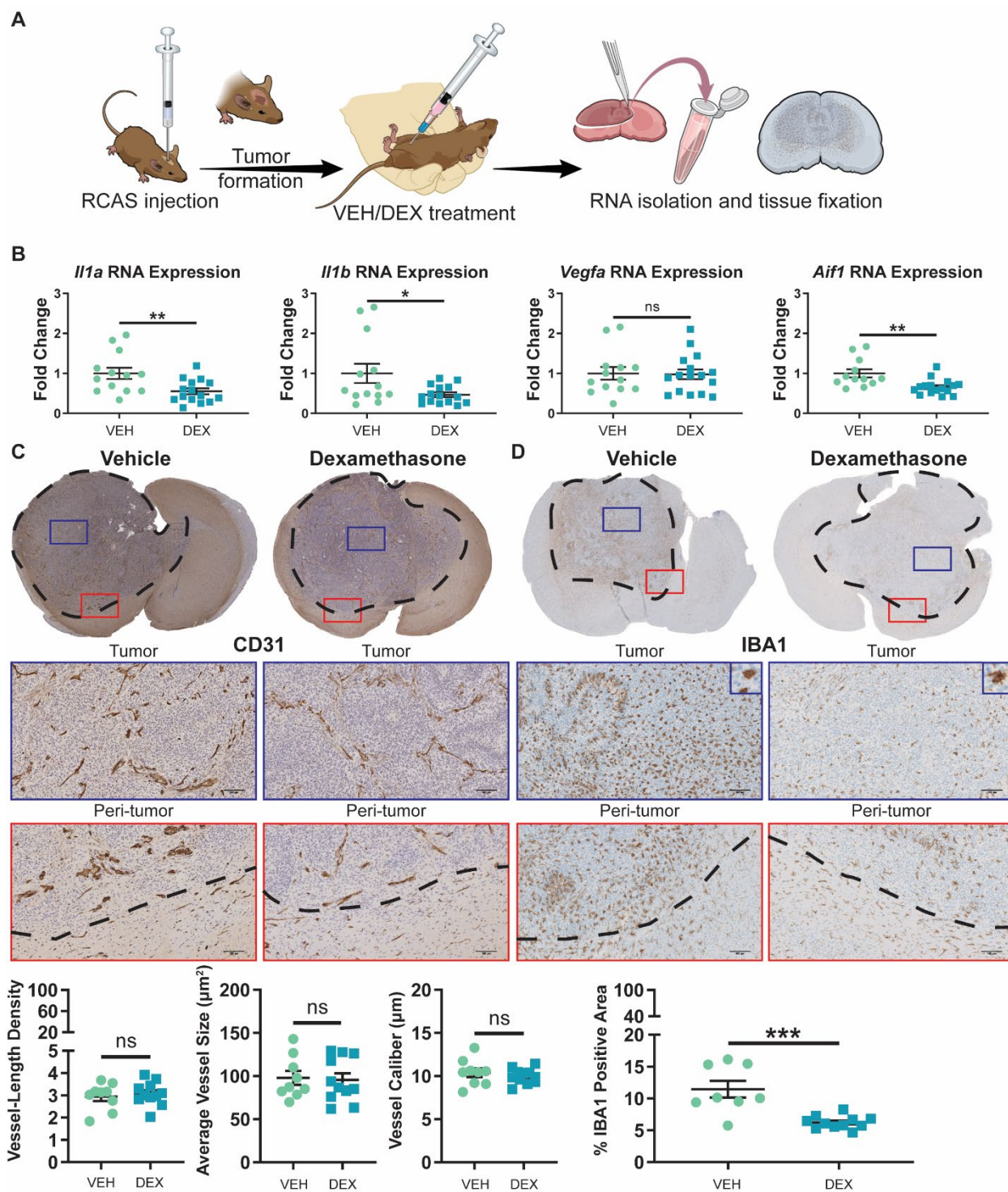


**Figure 3.6. Dexamethasone treatment has no effect on tumor angiogenesis, but significantly reduces the number of tumor-associated macrophages.** (A) An experimental outline of the generation and treatment of PDGFB-overexpressing tumors. (B) Quantitative-PCR of tumor

samples and interrogation of *Il1a*, *Il1b*, *Vegfa*, and *Aif1* expression from vehicle- (N=13) and dexamethasone-treated mice (N=15). Immunohistochemical analysis of CD31 (C) and IBA1 (D) expression in formalin-fixed, paraffin-embedded tumor slices from vehicle- (N=9) and dexamethasone-treated mice (N=11). Scale bars are 100  $\mu$ m. Two-tailed Student's t-test, ns=not significant, \* $P$ <0.05, \*\* $P$ <0.01, \*\*\* $P$ <0.001.

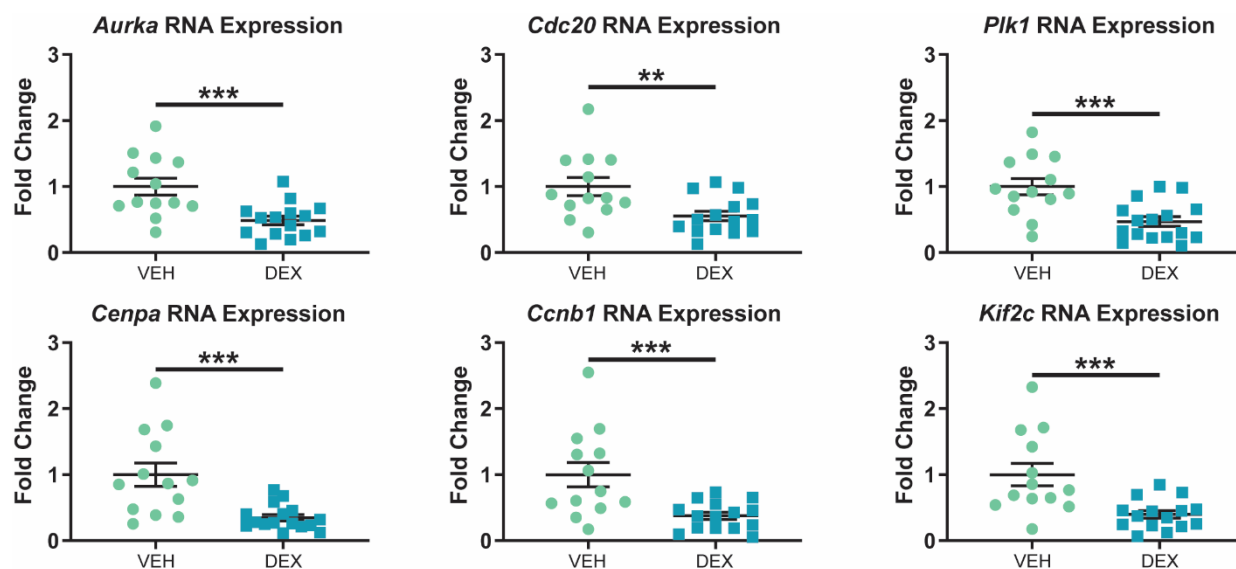


**Figure 3.7. Validation of the *in vivo* administration of dexamethasone by quantitative-PCR analysis of previously-reported markers.** Quantitative-PCR for the markers *Aurka*, *Cdc20*, *Plk1*, *Cenpa*, *Ccnb1*, and *Kif2c* in tumor samples from mice following vehicle (N=13) or dexamethasone (N=15) treatment. Two-tailed Student's t-test, \*\* $P < 0.01$ , \*\*\* $P < 0.001$ .

I stained my tumor specimens for the endothelial cell marker CD31 and the pan-macrophage marker IBA1 (the protein product of the *Aif1* gene)<sup>261,316</sup>. Quantification of vessel-length density, average vessel size, and vessel caliber based on CD31 positive staining revealed no differences between vehicle- or dexamethasone-treatment (**Figure 3.6C**). There was a reduction in IBA1-positive area in tumor samples from mice treated with dexamethasone compared to vehicle-treated mice (**Figure 3.6D**). These results suggested that while having no effect on angiogenesis, dexamethasone decreases the number of tumor-associated macrophages.

*Dexamethasone impairs the influx of circulating myeloid and lymphoid cells into glioblastomas in vivo*

Since IBA1 is a shared marker between BMDM and MG it is unable to distinguish between the two lineages by immunohistochemistry. To specifically determine whether dexamethasone decreases tumor-associated macrophages through alterations in BMDM or MG, I next chose to employ flow cytometry to analyze tumor samples from vehicle- and dexamethasone-treated mice. I previously demonstrated the ability to distinguish between BMDM and MG based on CD45-protein expression levels by flow cytometry<sup>99</sup>. PDGFB-overexpressing tumors were generated in *Ntv-a* mice and treated with vehicle or dexamethasone following the same treatment schematic previously employed (**Figure 3.8A**). As expected, I observed a reduction in total myeloid cells (CD45<sup>+</sup>CD11b<sup>+</sup>) in tumors of dexamethasone-treated mice (**Figure 3.8B**). When the myeloid cells were divided into BMDM (CD45<sup>high</sup>) and MG (CD45<sup>low</sup>) by CD45-positivity, the reduction in total myeloid cells could be completely attributed to a reduction in the infiltration of BMDM from the circulation (**Figure 3.8B**). Additionally, I demonstrated that dexamethasone significantly impairs the ability of lymphoid cells (CD45<sup>+</sup>CD11b<sup>-</sup>) to infiltrate the tumors (**Figure 3.8B**).

These results indicated that dexamethasone has an inhibitory effect on immune cell infiltration into the tumor. Next, I evaluated whether this decreased infiltration stemmed from

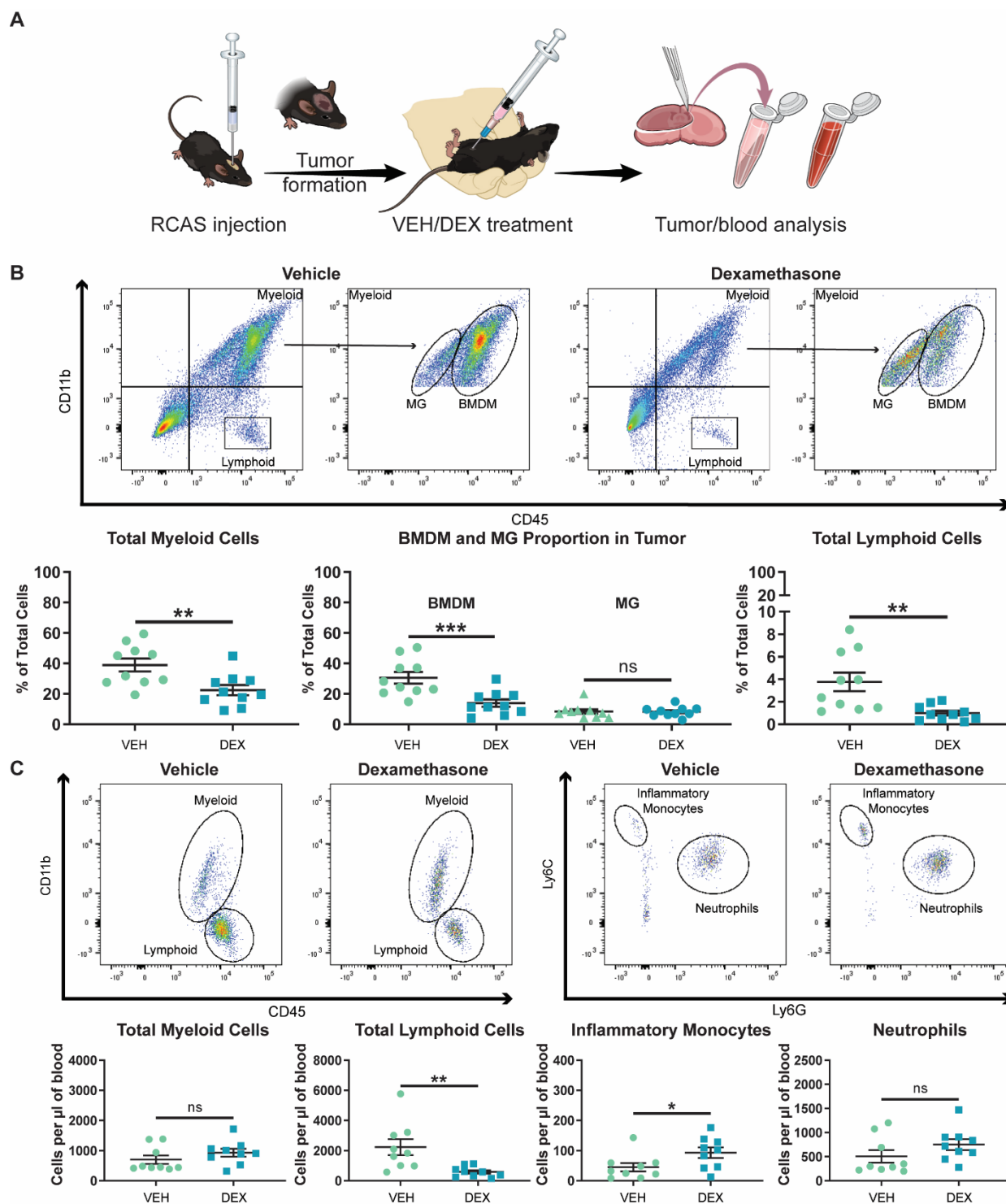


**Figure 3.8. Dexamethasone treatment significantly impairs the ability of immune cells to infiltrate the tumor from the circulation.** (A) An experimental outline of the treatment of mice bearing PDGFB-overexpressing tumors with vehicle or dexamethasone. (B) Representative flow

cytometry plots and quantification of total myeloid cells, BMDM, MG, and lymphoid cells in PDGFB-overexpressing tumors from mice treated with vehicle (N=10) or dexamethasone (N=10).

(C) Representative flow cytometry plots and quantification of circulating myeloid cells, lymphoid cells, inflammatory monocytes, and neutrophils in the blood of tumor-bearing mice treated with vehicle (N=9) or dexamethasone (N=9) at endpoint. Two-tailed Student's t-test, ns=not significant, \* $P < 0.05$ , \*\* $P < 0.01$ , \*\*\* $P < 0.001$ .

effects on immune cell extravasation from the bone marrow or circulation. To accomplish this task, I determined circulating immune cell levels in tumor-bearing mice treated with vehicle or dexamethasone. My results indicated that dexamethasone has different effects on cells of the myeloid and lymphoid compartments. No significant effect was observed on the circulating levels of total myeloid cells (CD45<sup>+</sup>CD11b<sup>+</sup>) or neutrophils (CD45<sup>+</sup>CD11b<sup>+</sup>Ly6G<sup>high</sup>Ly6C<sup>mid</sup>) (**Figure 3.8C**). I did, however, observe an increase in circulating inflammatory monocytes (CD45<sup>+</sup>CD11b<sup>+</sup>Ly6G<sup>low</sup>Ly6C<sup>high</sup>) (**Figure 3.8C**). Circulating lymphoid cell (CD45<sup>+</sup>CD11b) levels were strongly depressed by dexamethasone administration (**Figure 3.8C**). These effects were confirmed via administration of dexamethasone to tumor-naïve C57BL/6 mice. In fact, in this experiment, significant increases in circulating total myeloid cells (CD45<sup>+</sup>CD11b<sup>+</sup>), inflammatory monocytes (CD45<sup>+</sup>CD11b<sup>+</sup>Ly6G<sup>low</sup>Ly6C<sup>high</sup>), and neutrophils (CD45<sup>+</sup>CD11b<sup>+</sup>Ly6G<sup>high</sup>Ly6C<sup>mid</sup>) were observed (**Figure 3.9**). The significant reduction in circulating lymphoid cells (CD45<sup>+</sup>CD11b) observed in tumor-bearing mice was also recapitulated in naïve mice (**Figure 3.9**). These experiments illustrated that dexamethasone likely impacts lymphoid cell release from the bone marrow and myeloid cell extravasation from the circulation into inflammatory sites.

*IL-1R1 ablation has no effect on angiogenesis but reduces the influx of BMDM in PDGFB-overexpressing tumors*

Since dexamethasone was shown to exert such a profound effect on IL-1 signaling *in vitro* (**Figure 3.1**), *ex vivo* (**Figure 3.5**), and *in vivo* (**Figure 3.6**), I questioned if I could recapitulate phenotypes observed following dexamethasone administration by specifically ablating IL-1 signaling. To investigate this hypothesis, PDGFB-overexpressing tumors were generated in *Ntv-a* and *Ntv-a/Il1r1<sup>-/-</sup>* mice. Ablation of IL-1R1 activity was confirmed by stimulating *Il1r1<sup>-/-</sup>* BMDM with IL-1 $\alpha$  and IL-1 $\beta$  *in vitro* (**Figure 3.10**). Immunohistochemical analysis of CD31 (**Figure 3.11A**) and IBA1 (**Figure 3.11B**) demonstrated no significant effect on angiogenesis, but a significant reduction in

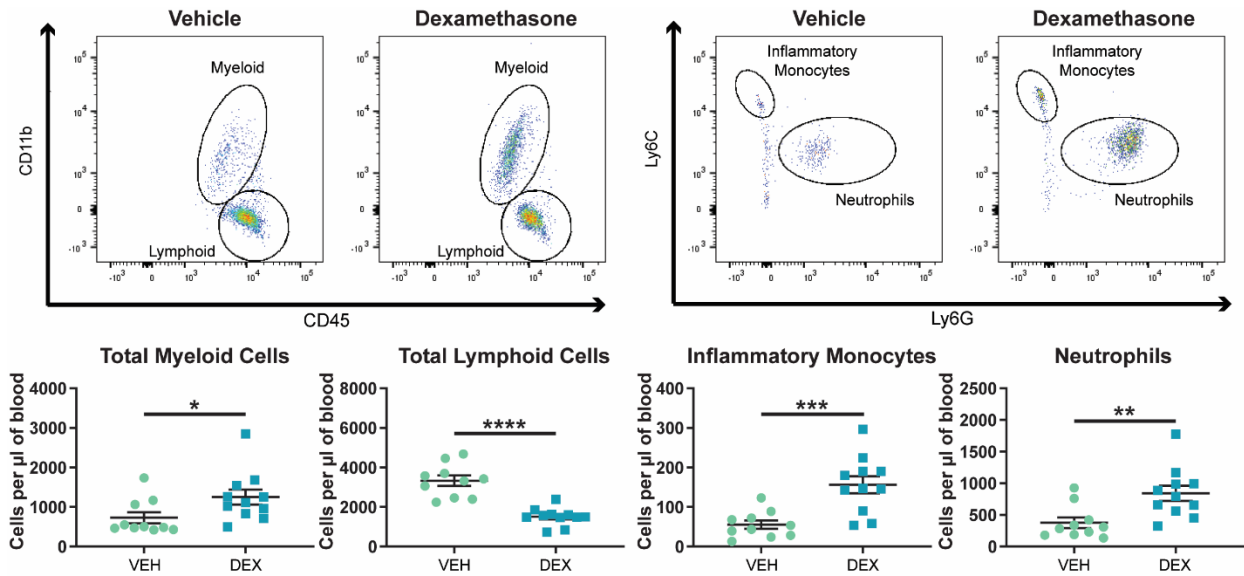


**Figure 3.9. Administration of dexamethasone to naïve C57BL/6 mice causes a significant reduction in circulating lymphoid cells and a significant increase in circulating myeloid cells.** Representative flow cytometry plots for total circulating myeloid cells, lymphoid cells, inflammatory monocytes, and neutrophils in naïve C57BL/6 mice treated with vehicle (N=10) or dexamethasone (N=11). Two-tailed Student's t-test, \* $P < 0.05$ , \*\* $P < 0.01$ , \*\*\* $P < 0.001$ , \*\*\*\* $P < 0.0001$ .

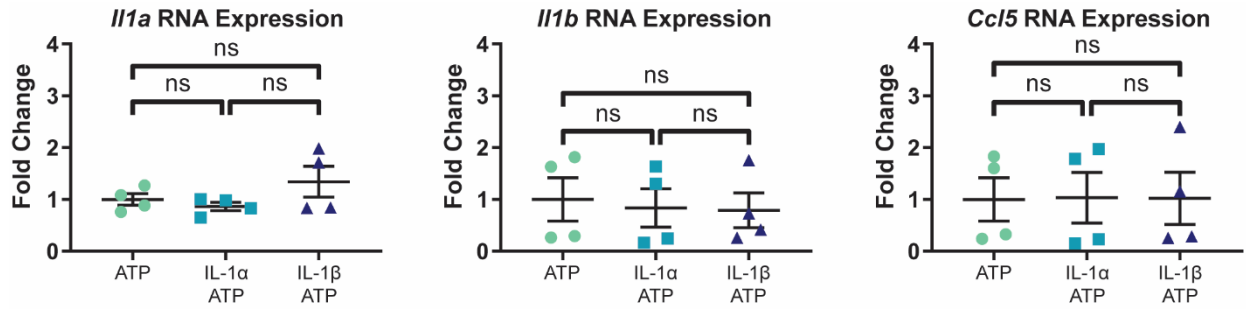


**Figure 3.10.** Stimulation of *Il1r1*<sup>-/-</sup> BMDMs with IL-1 $\alpha$  and IL-1 $\beta$  produces no change in the expression of the IL-1 responsive genes *Il1a*, *Il1b*, or *Ccl5*. BMDM were isolated from *Il1r1*<sup>-/-</sup> mice and stimulated with IL-1 $\alpha$  and IL-1 $\beta$  (N=4). Quantitative-PCR was performed to assess the expression levels of the IL-1 responsive genes *Il1a*, *Il1b*, and *Ccl5*. One-way ANOVA, ns=not significant.

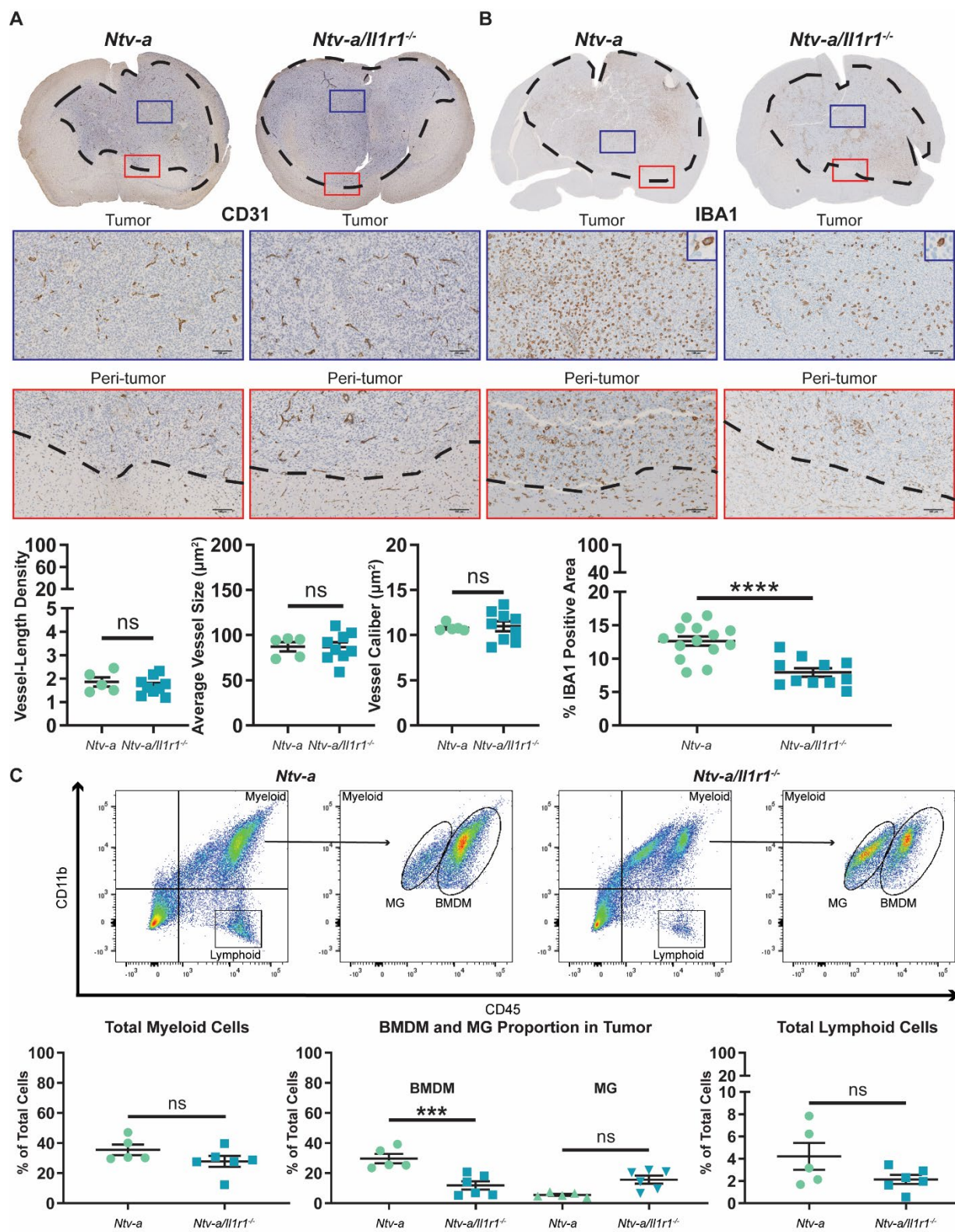


**Figure 3.11. IL-1R1 ablation reduces the influx of circulating myeloid cells in the tumors of mice bearing PDGFB-overexpressing glioblastoma.** Immunohistochemical analysis of CD31 (A) in *Ntv-a* (N=5) and *Ntv-a/Il1r1<sup>-/-</sup>* (N=9) mice. Immunohistochemical analysis of IBA1 (B) in *Ntv-a* (N=14) and *Ntv-a/Il1r1<sup>-/-</sup>* (N=11) mice. (C) Representative flow cytometry plots and quantification of total myeloid cells, BMDM, MG, and lymphoid cells in tumors of *Ntv-a* (N=5) and *Ntv-a/Il1r1<sup>-/-</sup>* (N=6) mice bearing PDGFB-overexpressing glioblastoma. Two-tailed Student's t-test, ns=not significant, \*\*\* $P < 0.001$ , \*\*\*\* $P < 0.0001$ .

tumor-associated macrophages in tumors from *Ntv-a/Il1r1<sup>-/-</sup>* mice compared to tumors from *Ntv-a* mice. These results closely mimicked those seen following dexamethasone administration (**Figure 3.6C and D**).

To establish whether the reduction in IBA1-positivity could be attributed to BMDM, MG, or both cell types, I employed flow cytometry. My results indicated no significant reduction in total myeloid cells (CD45<sup>+</sup>CD11b<sup>+</sup>) in tumors from *Ntv-a/Il1r1<sup>-/-</sup>* mice (**Figure 3.11C**). Division of the total myeloid cells into BMDM (CD45<sup>high</sup>) and MG (CD45<sup>low</sup>) indicated a strong reduction in the influx of BMDM (**Figure 3.11C**). No decrease in the amount of total lymphoid cells (CD45<sup>+</sup>CD11b<sup>-</sup>) was apparent (**Figure 3.11C**). When assessing the circulating immune cell profiles of these mice, no differences were observed in the levels of circulating myeloid cells (CD45<sup>+</sup>CD11b<sup>+</sup>), lymphoid cells (CD45<sup>+</sup>CD11b<sup>-</sup>), inflammatory monocytes (CD45<sup>+</sup>CD11b<sup>+</sup>Ly6G<sup>low</sup>Ly6C<sup>high</sup>), or neutrophils (CD45<sup>+</sup>CD11b<sup>+</sup>Ly6G<sup>high</sup>Ly6C<sup>mid</sup>) (**Figure 3.12**).

The difference between dexamethasone treatment and IL-1 signaling ablation in this respect likely stems from slightly different mechanisms of action between the two modalities. In addition to the efficacy in decreasing chemokine expression that I have demonstrated, dexamethasone is also known to detach marginal myeloid cells from the wall of the blood vessel; thereby inhibiting their ability to initiate the process of extravasation<sup>317,318</sup>. Based on the lack of differences in circulating immune cell levels in *Ntv-a* and *Ntv-a/Il1r1<sup>-/-</sup>* mice, it is unlikely that IL-1 signaling ablation has a similar effect on marginal immune cells. Ablation of IL-1 ligands does induce a strong decrease in the tumor levels of the MCP family of chemokines (**Figure 3.13**). This effect is probably responsible for the reduction in BMDM infiltration seen in the tumors of *Ntv-a/Il1r1<sup>-/-</sup>* mice. The data presented here (**Figure 3.13**) confirm that IL-1 signaling ablation also has no effect on the tissue levels of VEGF, similar to what was observed following dexamethasone treatment.

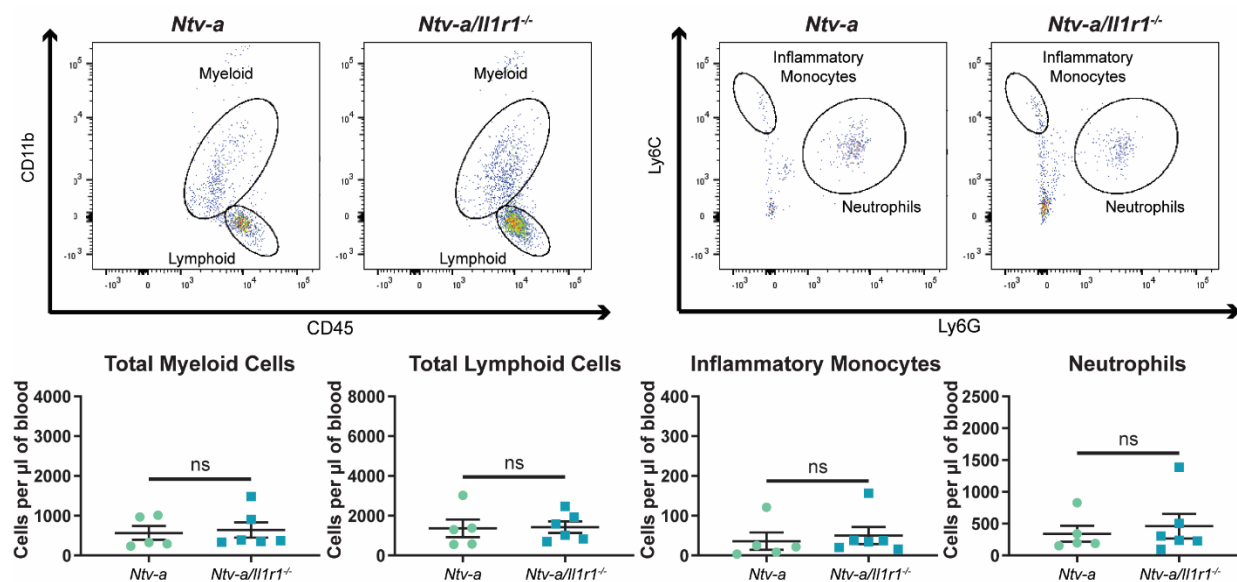


**Figure 3.12. Tumor-bearing *Ntv-a* and *Ntv-a/Il1r1<sup>-/-</sup>* mice display no differences in circulating immune cell profile.** Representative flow cytometry plots and quantification of myeloid cells, lymphoid cells, inflammatory monocytes, and neutrophils in the blood of tumor-bearing *Ntv-a* (N=5) and *Ntv-a/Il1r1<sup>-/-</sup>* (N=6) mice at endpoint. Two-tailed Student's t-test, ns=not significant.

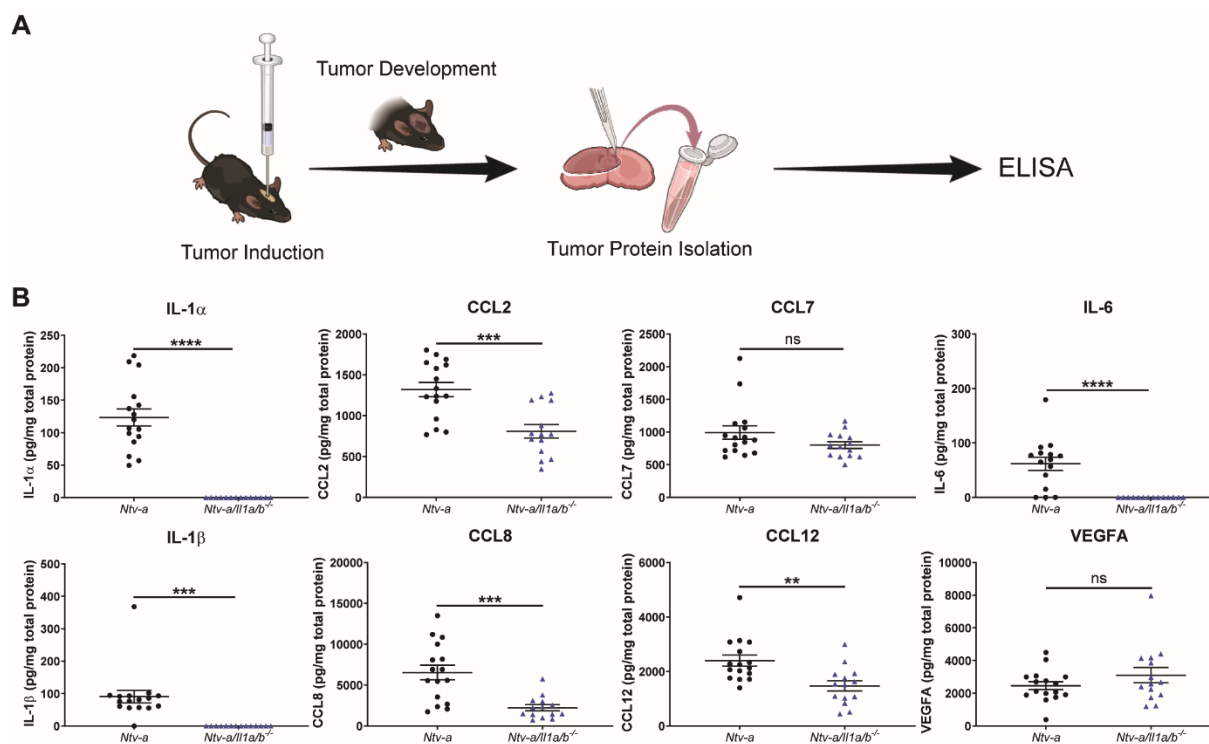


**Figure 3.13. Interleukin-1 ligand-ablated mice display a reduction in tumor tissue levels of MCP-family cytokines.** (A) An experimental protocol illustrating the workflow for tumor-induction, tissue isolation, and preparation for ELISA. (B) Comparison of tumor tissue expression of IL-1 $\alpha$ , IL-1 $\beta$ , CCL2, CCL7, CCL8, CCL12, IL-6, and VEGFA with ELISA. Two-tailed student's t-test. ns = not significant, \*\* $P < 0.01$ , \*\*\* $P < 0.001$ , \*\*\*\* $P < 0.0001$ .

*IL-1R1 ablation reduces blood-brain barrier permeability in PDGFB-overexpressing tumors, but no significant synergism with VEGF neutralization is observed*

Considering the similarities between dexamethasone treatment and IL-1R1 ablation with respect to BMDM infiltration, I next evaluated the ability of IL-1R1 ablation to reduce BBB permeability in PDGFB-overexpressing tumors. Additionally, I assessed whether IL-1R1 ablation in conjunction with VEGF-neutralization would have a synergistic effect on BBB disruption. To do so, I modified a previously established Hoechst dye-based assay<sup>307</sup>. Tumors were generated in *Ntw-a* and *Ntw-a/Il1r1<sup>-/-</sup>* mice that were treated with vehicle or the VEGF-neutralizing antibody B20-4.1.1 every four days at a dose of 5mg/kg following tumor initiation and up to endpoint (**Figure 3.14A**). Comparison of percent Hoechst positivity in the tumors of *Ntw-a* and *Ntw-a/Il1r1<sup>-/-</sup>* mice treated with vehicle indicated a significant reduction in BBB permeability in *Ntw-a/Il1r1<sup>-/-</sup>* mice (**Figure 3.14B**). No significant difference was observed between the two genotypes when treated with the VEGF-neutralizing antibody B20-4.1.1 (**Figure 3.14C**). The leakage in both VEGF-neutralized groups was similar to IL-1R1 ablation alone. These results suggest that IL-1 signaling regulates BBB permeability.

*IL-1 ligand ablation reduces edema formation in tumor-bearing mice at endpoint*

Since my results with IL-1R1 ablation indicated a reduction in BBB permeability, and both IL-1 $\alpha$  and IL-1 $\beta$  signal through the same receptor, I next assessed whether depletion of IL-1 $\beta$ , or IL-1 $\alpha$  and IL-1 $\beta$ , would drive a reduction in the formation of cerebral edema. I chose to utilize a previously established MRI-based assessment of edema formation in mice based upon endpoint tumor volume determination, where an increase in endpoint tumor volume is attributed to a decrease in edema<sup>192</sup>. I confirmed the MRI results in this experiment with *ex vivo* tumor volume reconstruction and a wet/dry tissue weight assay.

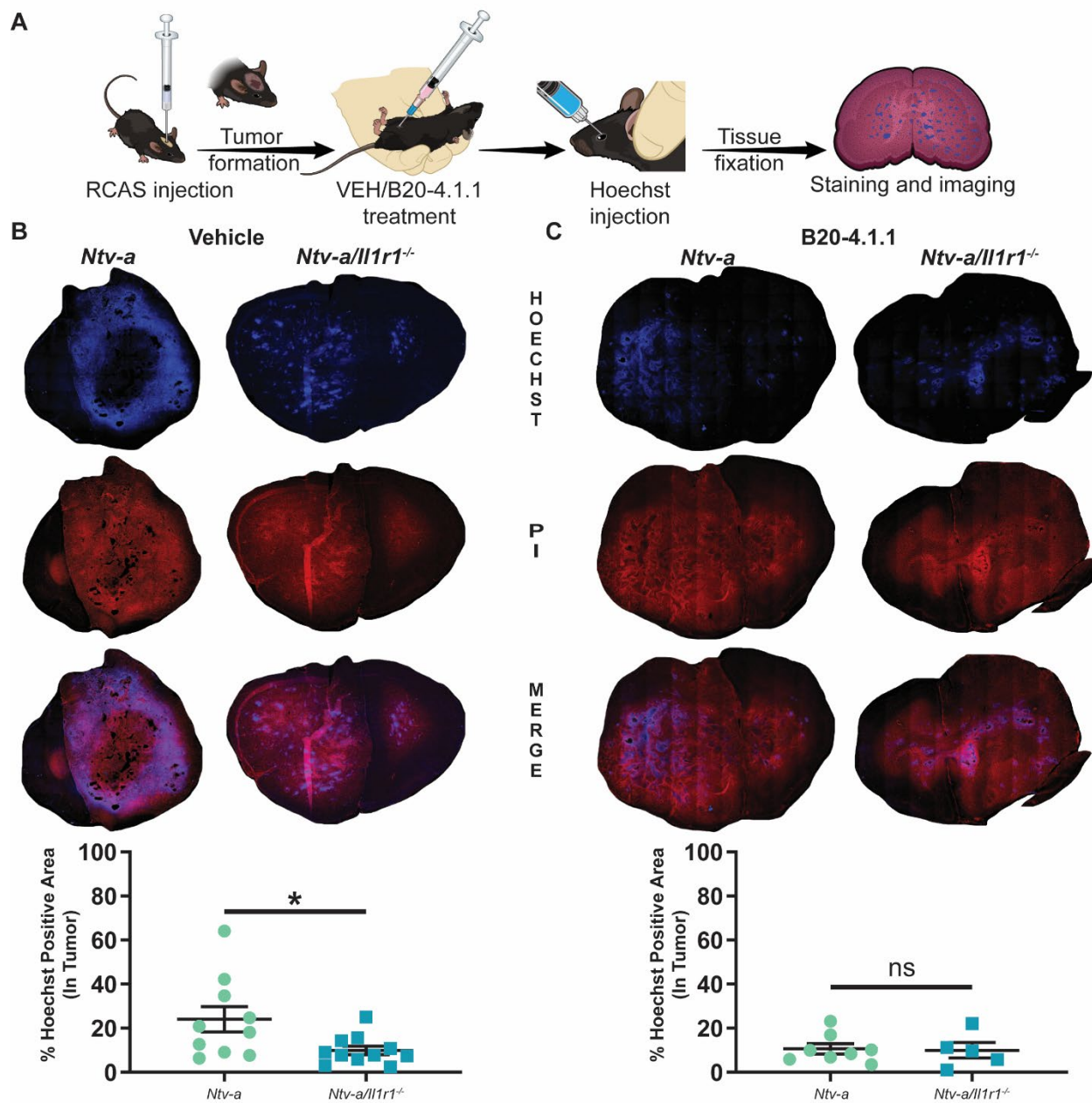


**Figure 3.14. Ablation of IL-1 signaling reduces blood-brain barrier permeability in mice bearing PDGFB-overexpressing tumors.** (A) A schematic outlining tumor generation, treatment, and tissue processing. (B) Comparison of Hoechst dye leakage in tumors from *Ntv-a* (N=10) and *Ntv-a/Il1r1<sup>-/-</sup>* (N=11) mice treated with vehicle solution. (C) Comparison of Hoechst dye leakage in tumors from *Ntv-a* (N=8) and *Ntv-a/Il1r1<sup>-/-</sup>* (N=5) mice treated with the VEGF-neutralizing antibody B20-4.1.1. Two-tailed Student's t-test, ns=not significant, \* $P < 0.05$ .

The schematic of this experiment employed tumor induction in *Ntw-a*, *Ntw-a/Il1b<sup>-/-</sup>*, and *Ntw-a/Il1a/b<sup>-/-</sup>* mice and submitted them to T2-weighted MRI at endpoint to determine tumor volume (**Figure 3.15A**). Tumors were then extracted and serially sectioned prior to H&E staining and *ex vivo* tumor volume reconstruction to confirm the MRI results. This experiment indicated a significant increase in endpoint tumor volume in the *Ntw-a/Il1b<sup>-/-</sup>* and *Ntw-a/Il1a/b<sup>-/-</sup>* mice relative to the *Ntw-a* mice with T2-weighted MRI (**Figure 3.15B**). No significant increase in endpoint tumor volume in the *Ntw-a/Il1b<sup>-/-</sup>* group and a significant increase in the *Ntw-a/Il1a/b<sup>-/-</sup>* group relative to the *Ntw-a* group were observed with serial histology (**Figure 3.15C**). Utilizing a wet/dry tissue weight-based measurement of edema (**Figure 3.15D**) I first validated the assay and the efficacy of dexamethasone in reducing edema (**Figure 3.16**). I then performed the assay in *Ntw-a* and *Ntw-a/Il1a/b<sup>-/-</sup>* mice and confirmed the results obtained with MRI and serial histology (**Figure 3.15E**). These data suggest a decrease in edema following IL-1 signaling ablation and imply that the effect may be IL-1 $\beta$ -driven.

*Genetic and pharmacological inhibition of IL-1 signaling does not compromise radiotherapy efficacy in a murine glioblastoma model in vivo*

The interference of dexamethasone treatment with the response to radiation in mice and humans has been previously documented<sup>192</sup>. I next evaluated whether IL-1 inhibition either by genetic or pharmacological approaches compromises the efficacy of radiation therapy in tumor-bearing mice. I first chose to assess the response to radiation in *Ntw-a* and *Ntw-a/Il1a/b<sup>-/-</sup>* tumor-bearing mice (**Figure 3.17A**) and demonstrated no reduction in median survival time following radiation in *Ntw-a/Il1a/b<sup>-/-</sup>* compared to *Ntw-a* mice. I then validated the ability of gallium nitrate to inhibit IL-1 release in bone marrow-derived macrophages (**Figure 3.18**) and assessed its impacts on the efficacy of radiation therapy. I utilized the same treatment schedule as dexamethasone in



**Figure 3.15. IL-1 ligand ablation reduces edema formation in tumor-bearing mice.** (A) A schematic illustration of the MRI and serial histology experimental workflow. (B) Comparison of endpoint tumor volumes between *Ntw-a* (N=8), *Ntw-a/Il1b<sup>-/-</sup>* (N=8), and *Ntw-a/Il1a/b<sup>-/-</sup>* (N=6) mice with T2-weighted MRI. (C) Comparison of endpoint tumor volumes between *Ntw-a* (N=7), *Ntw-a/Il1b<sup>-/-</sup>* (N=9), and *Ntw-a/Il1a/b<sup>-/-</sup>* (N=7) mice with serial sectioning followed by hematoxylin and eosin staining. (D) A schematic illustration of the wet/dry assay for edema measurement. (E) Comparison of percent brain water in naïve *Ntw-a* (N=5), naïve *Ntw-a/Il1a/b<sup>-/-</sup>* (N=5), tumor-bearing *Ntw-a* (N=7), and tumor-bearing *Ntw-a/Il1a/b<sup>-/-</sup>* (N=8) mice. One-way ANOVA, ns=not significant, \* $P < 0.05$ , \*\* $P < 0.01$ , \*\*\* $P < 0.001$ , \*\*\*\* $P < 0.0001$ .

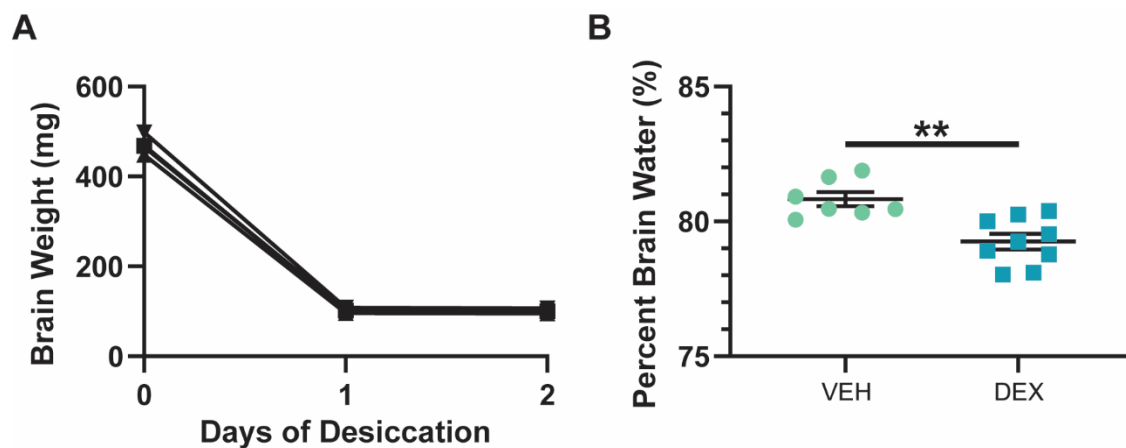


**Figure 3.16. Dexamethasone reduces edema formation as assessed by a wet/dry tissue weight assay.** (A) Brain weight of naïve C57BL/6 mice (N=5) after 24- and 48-hours of desiccation. (B) Comparison of percent brain water between vehicle- (N=7) and dexamethasone-treated (N=9) tumor-bearing *Ntv-a/Cdkn2a*<sup>-/-</sup> mice. Two-tailed student's t-test. \*\* $P < 0.01$ .

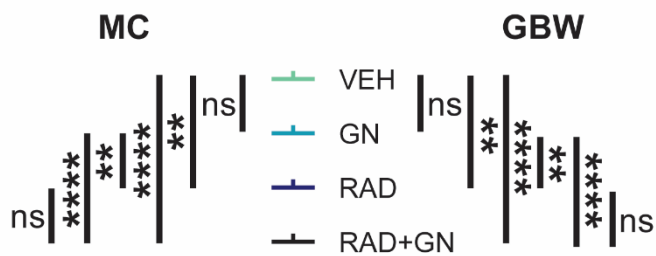
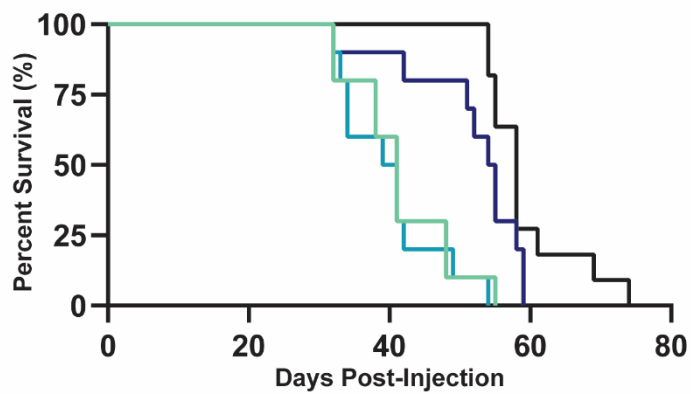
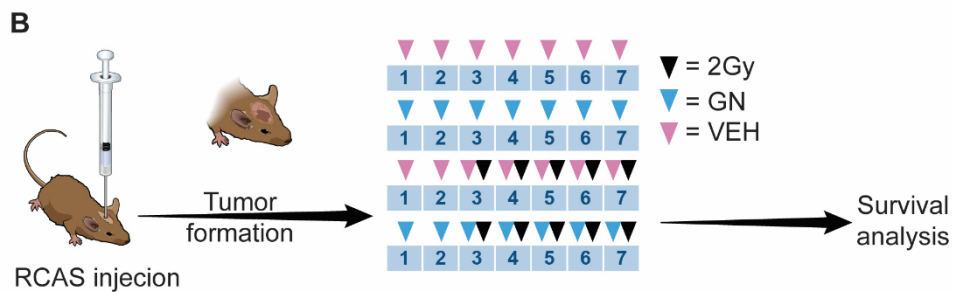
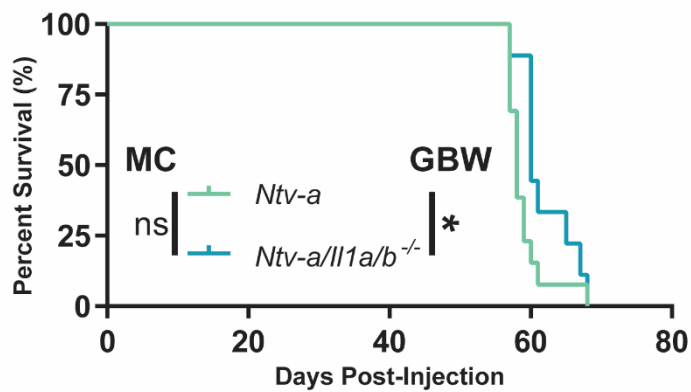
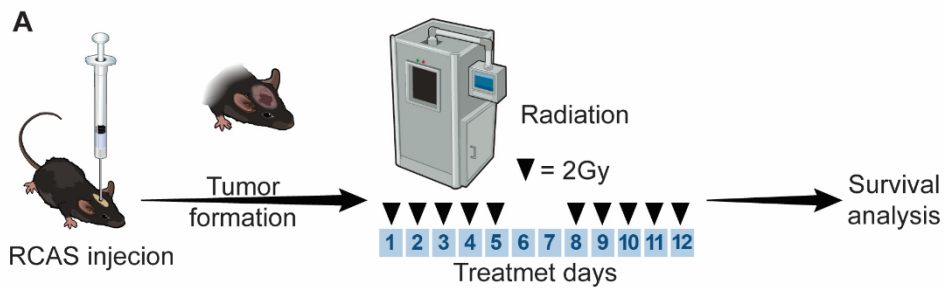


**Figure 3.17. Genetic and pharmacological inhibition of IL-1 signaling have no impact on****radiotherapy efficacy.** (A) A schematic illustration of the irradiation of tumor-bearing *Ntw-a*(N=13) and *Ntw-a/Il1a/b<sup>-/-</sup>* (N=9) mice with the associated survival curves. (B) A schematic

illustration of the treatment of tumor-bearing mice with vehicle (N=10), gallium nitrate (N=10),

vehicle plus radiation (N=10), or gallium nitrate plus radiation (N=11) with the associated survival

curves. MC and GBW tests, ns=not significant, \* $P<0.05$ , \*\* $P<0.01$ , \*\*\*\* $P<0.0001$ .

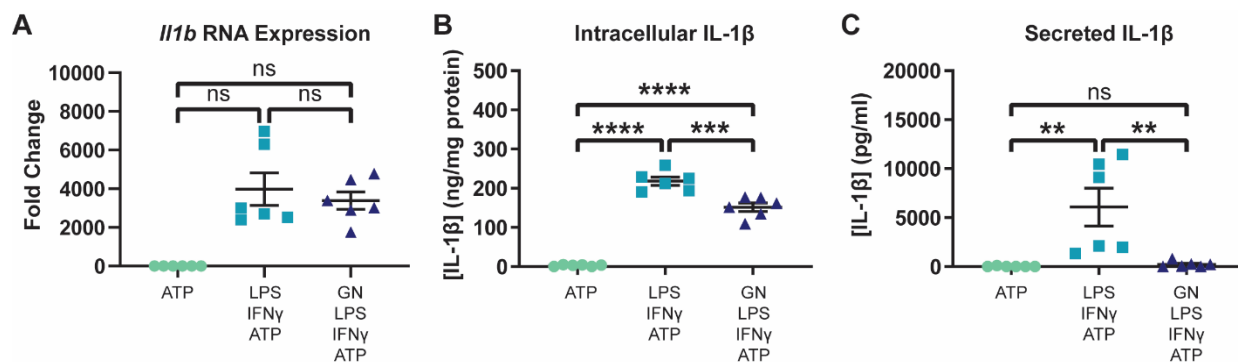


**Figure 3.18. Gallium nitrate inhibits the synthesis and secretion of IL-1 $\beta$  protein from primary BMDM.** (A) Quantitative-PCR for *Il1b*, (B) ELISA for intracellular IL-1 $\beta$ , and (C) ELISA for secreted IL-1 $\beta$  in BMDM stimulated with LPS and IFN $\gamma$  with or without gallium nitrate pretreatment. One-way ANOVA, ns=not significant, \*\* $P$ <0.01. \*\*\* $P$ <0.001, \*\*\*\* $P$ <0.0001.

the experiment demonstrating its interference with radiation<sup>192</sup>. Similar to dexamethasone, gallium nitrate alone had no impact on the survival of tumor-bearing mice when compared to the vehicle treated group. In contrast to dexamethasone, there was no significant difference between gallium nitrate plus radiotherapy-treated animals compared to radiotherapy alone, demonstrating that gallium nitrate treatment does not interfere with radiotherapy efficacy (**Figure 3.17B**).

### 3.4 Discussion

Following its introduction for the purpose, dexamethasone has long been recognized as the gold-standard for the management of glioblastoma-associated cerebral edema<sup>36,277</sup>. Recent attention has highlighted the need to find an alternative to dexamethasone for the long-term management of glioblastoma-associated cerebral edema due to the complications associated with prolonged dexamethasone therapy, as well as the interference of dexamethasone with anti-neoplastic therapies employed to combat the tumor<sup>192,276,280,319</sup>. Considering this sentiment, I initiated the investigations presented here with an intention to extract a beneficial anti-edema component from dexamethasone, while reducing off target effects that drive side-effects and impair the response to anti-neoplastic therapy.

Here, I utilized a murine model of glioblastoma where BMDM comprise the majority of the tumor-associated macrophage population. RNA-sequencing on these cells suggested previously that they upregulate the inflammatory mediator *Il1b* significantly compared to naïve BMDM or tumor-associated MG<sup>99</sup>. *In vitro*, I demonstrated that BMDM and MG both upregulate IL-1 family cytokines when stimulated with either LPS and IFN $\gamma$  or IL-1; effects that were significantly inhibited by dexamethasone treatment. My *ex vivo* experiments demonstrated that BMDM upregulate *Il1a* and *Il1b* when exposed to organotypic tumor slices, and that this effect can be abrogated by dexamethasone treatment. MG were surprisingly shown to downregulated IL-1 cytokines when co-

cultured with tumor slices. *In vivo*, I demonstrated a decrease in total tumor *Il1a* and *Il1b* levels following dexamethasone treatment.

My *in vivo* results further illustrated no effect on the expression levels of *Vegfa*, or vessel parameters in the tumors of dexamethasone-treated mice. These results differ from previous work that demonstrated a significant reduction in *Vegfa* produced by glioblastoma tumor cells in response to dexamethasone treatment<sup>292</sup>. This difference in results can be attributed in part to the genetic make-up of the tumors in these studies and the identity of the cells utilized in previous analyses. As discussed in Chapter 2, U87 cells – that were used in the referenced study – no longer recapitulate the phenotype of primary human tumors or patient derived cells. The murine tumors generated in this study are much closer approximations of their human counterparts. My data are consistent with results illustrating no effect of dexamethasone therapy on VEGF expression in human glioma samples<sup>293</sup>. In total, this suggests that dexamethasone likely does not significantly impact VEGF or angiogenesis in glioblastoma.

Therefore, the conclusion from this work is that dexamethasone impacts the permeability of the BBB in an angiogenesis-independent fashion. Experiments in naïve mice, with no cerebral injury or aberrant angiogenesis, have demonstrated that dexamethasone reduces the permeability of the BBB to macromolecules<sup>320</sup>. Moreover, following cerebral injury, dexamethasone treatment has been shown to upregulate tight junction molecules, such as Tight junction protein-1, in endothelial cells within the BBB<sup>275,321</sup>. Although cerebral injury and brain tumors are distinct entities, it is plausible that the mechanism of action of drugs used to treat edema induced by each trauma may be similar.

Although I was unable to establish a link between angiogenesis and dexamethasone treatment, I was able to demonstrate a significant reduction in the number of tumor-associated macrophages with immunohistochemistry following administration of dexamethasone. Further

analysis with flow cytometry elucidated that this effect was attributable to a reduction in the influx of BMDM from the circulation. Previous work in cancer and other inflammatory conditions has demonstrated impaired monocyte chemotaxis following treatment with dexamethasone<sup>322,323</sup>. The precise mechanism of this effect has not been determined; however, dexamethasone has been shown to suppress circulating cytokine levels in humans<sup>317,324</sup>. It has been suggested that dexamethasone does so through global suppression of nuclear factor-kappa B, which is a known mediator of IL-1 signaling<sup>325</sup>. Since macrophage chemotaxis is primarily controlled by the expression of MCP family chemokines, it is plausible that the effects of dexamethasone on macrophage chemotaxis are mediated by its effects on chemokine levels<sup>326,327</sup>. This hypothesis is strengthened by my data showing that tumors induced in *Ntv-a/Il1r1<sup>-/-</sup>* mice have reduced BMDM infiltration compared to those induced in *Ntv-a* mice as well as reduced. My evidence in *Ntv-a/Il1a/b<sup>-/-</sup>* mice also suggests that IL-1 acts as a regulator of MCP family chemokine expression specifically in the tumor microenvironment, but the precise mechanism has not been extensively examined in the context of glioblastoma. My *ex vivo* data clearly illustrated the ability of dexamethasone to reduce MCP chemokine levels in organotypic tumor slices co-cultured with BMDM or MG, lending further support to the hypothesis that this effect is in part chemokine-dependent.

In addition to the differences observed in myeloid cell infiltration, mice treated with dexamethasone displayed a significant reduction in the influx of lymphoid cells to their tumors. These results are in line with previous studies that demonstrated that dexamethasone decreases circulating lymphocyte levels in patients with brain tumors<sup>328</sup>. Direct studies on the effects of dexamethasone on circulating T lymphocytes in a bovine model established that dexamethasone is capable of reducing circulating CD3+ cell levels to 30% of normal, on par with the reduction I observed in mice<sup>329</sup>. The effects of dexamethasone on lymphoid cells may not be responsible for its ability to manage edema; however, they are almost certain to alter the efficacy of T cell-based

immunotherapies in glioblastoma. Previous work on ipilimumab in melanoma brain metastases demonstrated that dexamethasone may interfere with its efficacy<sup>330</sup>. Additionally, recent work in glioblastoma investigated mechanisms of dexamethasone-induced immunosuppression and their effects on brain tumor immunotherapy<sup>331</sup>. These investigations must continue if dexamethasone and immunotherapy are to co-exist in the therapeutic repertoire of clinicians in neuro-oncology. Furthermore, if IL-1 inhibition is to be considered as an alternative to dexamethasone for the management of edema, its precise effects on the action of the immune microenvironment in glioblastoma must be established.

To assess the effects of IL-1 loss on BBB permeability, I utilized a Hoechst dye-based assay and compared the response to pharmacological inhibition of VEGF signaling, a technique that has been shown to reduce BBB permeability in the past<sup>192</sup>. The results of this experiment demonstrated comparable restoration of BBB integrity between the two groups, but no synergism when IL-1R1 ablation and VEGF inhibition were combined. Overall, this suggests that IL-1 inhibition may offer similar anti-edema effects to those afforded by inhibition of VEGF signaling.

To expound on the BBB restoration observed in IL-1R1 ablated mice, I next strove to demonstrate a reduction in edema in IL-1 ablated mice and used complimentary MRI, serial histology, and wet/dry measurement of brain tissue weight at endpoint. Each of these techniques showed a reduction in edema formation in *Ntw-a/Il1a/b<sup>-/-</sup>* mice when compared to *Ntw-a* mice. The effects were similar in *Ntw-a/Il1b<sup>-/-</sup>* mice suggesting that IL-1 $\beta$  may be the driver of this effect. This result implicates BMDM directly to the development of cerebral edema in glioblastoma since they are the primary producers of IL-1 $\beta$  in the tumor microenvironment. Considering the collection of clinically approved drugs for specific IL-1 signaling inhibition, and the demonstration that IL-1 $\beta$  inhibition reduces edema formation in traumatic brain injury, IL-1 signaling inhibition warrants

additional investigation in the context of management of glioblastoma-associated cerebral edema<sup>298,303</sup>.

Once I was able to demonstrate that IL-1 signaling inhibition reduces edema formation in tumor-bearing mice, I was next interested if IL-1 inhibition would result in the decrease in response to radiotherapy observed following dexamethasone administration<sup>192</sup>. I assessed both genetic ablation of IL-1 ligands as well as pharmacological inhibition of IL-1 with gallium nitrate in combination with radiotherapy. These experiments demonstrated that both approaches do not reduce the efficacy of radiotherapy. In fact, the inhibition of IL-1 signaling lead to near significant increases in median survival compared to control groups when combined with radiation. These effects suggest that inhibition of tumor-associated macrophage activity through suppression of IL-1 signaling not only causes a reduction in edema but may also reduce the treatment resistance provided by tumor-associated macrophages in glioblastoma.

## **Chapter 4: Conclusions and Future Directions**

## 4.1 Conclusions

Glioblastoma is perhaps the most uncompromising cancer and limited therapeutic improvements have been made over the past fifty years<sup>31</sup>. A significant contributor to this lack of progress is the heterogeneity with respect to the molecular drivers of glioblastoma development, the cellular heterogeneity, and the necessity and complexity of the organ in which these tumors occur<sup>6,7,55</sup>. The model systems that have been widely employed for preclinical investigation of glioblastoma over the past few decades neglect facets of this complexity and likely have contributed to the lack of progress in improving patient outcomes. To this end, the overarching goal of this project was to develop improved mouse models of glioblastoma and to use these models to answer human disease-relevant questions. I strove to design and validate subtype-specific and immunocompetent murine models of glioblastoma and to use these models to dissect the role that tumor-associated macrophages play in the development of cerebral edema. My hope was that the improved murine models would allow me to identify an alternative therapeutic avenue to dexamethasone for the management of glioblastoma-associated cerebral edema.

Chapter 2 outlines my progress towards designing and validating novel and immunocompetent subtype-specific mouse models of glioblastoma. In total, I was able to establish three models in this chapter, each of which with a specific and unique driver mutation: a model of human Proneural glioblastoma driven by PDGFB-overexpression, a model of human Mesenchymal glioblastoma driven by NF1-silencing, and a model of human Classical glioblastoma driven by expression of the constitutively active EGFRvIII receptor (**Figure 4.1**). Profiling of these murine tumors on the molecular level with quantitative-PCR and immunohistochemistry established that they were similar to their human counterparts. Moreover, this analysis demonstrated that the murine tumors displayed differences in tumor-associated macrophage presence that are seen between

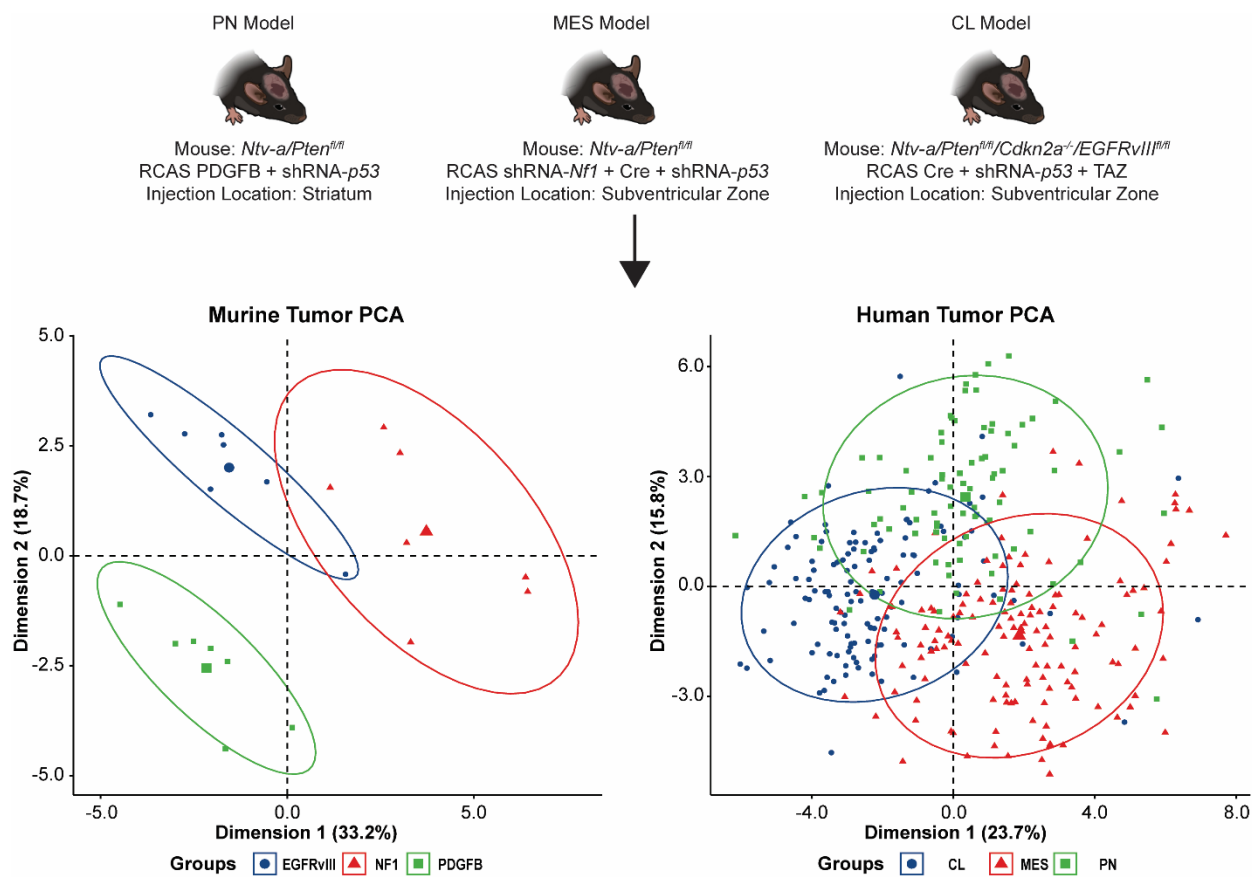


**Figure 4.1.** An illustrative summary of the results obtained in Chapter 2. Mouse models of human Proneural, Mesenchymal, and Classical glioblastoma were generated by introducing oncogenic alterations in PDGFB, NF1, or EGFR respectively. Clustering of murine tumors and their corresponding human counterpart with principle component analysis illustrated that the models recapitulate the expression profile of the human tumors they are meant to emulate.

subtypes in human tumors<sup>263</sup>. Assessment of response to the current standard of care TMZ and radiotherapy indicated that there may be differences in response to TMZ between subtypes; a result that should be considered clinically. Finally, I chose to test the efficacy of the burgeoning immunotherapeutic strategy of PD-L1 inhibition in PDGFB-overexpressing and NF1-silenced tumors and obtained results that are similar to what has been seen so far in clinical analyses. These results in total indicate that these murine models offer excellent tools for preclinical studies in glioblastoma; particularly those that are interested in subtype-specific differences or those that are interested in immune-related phenomena.

Chapter 3 discusses the results I obtained in my effort to discover an alternative to dexamethasone for the management of glioblastoma-associated cerebral edema. In this section, I chose to use the PDGFB-overexpressing mouse model that I had demonstrated in Chapter 2 to have impaired BBB integrity. Since this is a hallmark of edema development, I thought this tool would be well suited for *in vivo* investigations of the mechanism of edema development in glioblastoma. In this section, I first established a direct connection between dexamethasone and IL-1 signaling with *in vitro*, *ex vivo*, and *in vivo* model systems. Once established, I probed the ability of specific IL-1 inhibition to phenocopy dexamethasone treatment with respect to restoration of BBB integrity and reduction of edema development. These experiments illustrated that IL-1 inhibition is nearly as efficacious as dexamethasone for this purpose.

In this section, I additionally demonstrated that dexamethasone treatment impairs the ability of peripherally-derived immune cells to infiltrate into PDGFB-overexpressing tumors. IL-1 signaling inhibition was similarly efficacious in reducing the infiltration of myeloid cells, but with less impairment of lymphoid cell chemotaxis. These results will be important to consider as T cell-based immunotherapies become more prevalent for the management of glioblastoma. The mechanisms of

dexamethasone and IL-1 inhibition in reducing immune cell chemotaxis were shown to be overlapping, but unique. Both modalities were shown to alter chemokine production by the tumor; however, dexamethasone treatment is likely to also impact the association of circulating immune cells with the wall of the blood vessel and thus inhibit the initiation of extravasation.

The final experiments of this section investigated the impact of IL-1 signaling inhibition either genetically or pharmacologically on the efficacy of radiotherapy. Previous results indicated that dexamethasone impairs response to radiotherapy and prompted my interest in finding an alternative therapy for edema management<sup>192</sup>. I showed that inhibition of IL-1 via either mechanism does not impair response to radiation and may enhance its efficacy. These results merit further investigation.

Overall, Chapter 3 provided evidence supporting a novel connection between IL-1, BMDM, and edema development in glioblastoma (**Figure 4.2**). Furthermore, the establishment of IL-1 as a downstream effector of dexamethasone had not been previously reported. The effectiveness of IL-1 neutralization in managing edema coupled with its lack of impairment of radiotherapy efficacy establishes it as a prime candidate as the replacement of dexamethasone for this purpose. Moreover, this work suggests that specific anti-inflammatory modulators offer attractive therapeutic alternatives to steroids and will allow for the development of precision therapies for a wide array of inflammatory conditions.

## 4.2 Future Directions

Science is like the hydra of Greek mythology. Each experiment is a head of the hydra. As the results come in, it is as if the head of the hydra is severed and two more sprout in its place. The beauty of this process is that well performed experiments will always drive the formation of new questions and lead to exciting further avenues of research. This project represents the completion of a handful of experiments and puts forward suitable conclusions that can be drawn from the

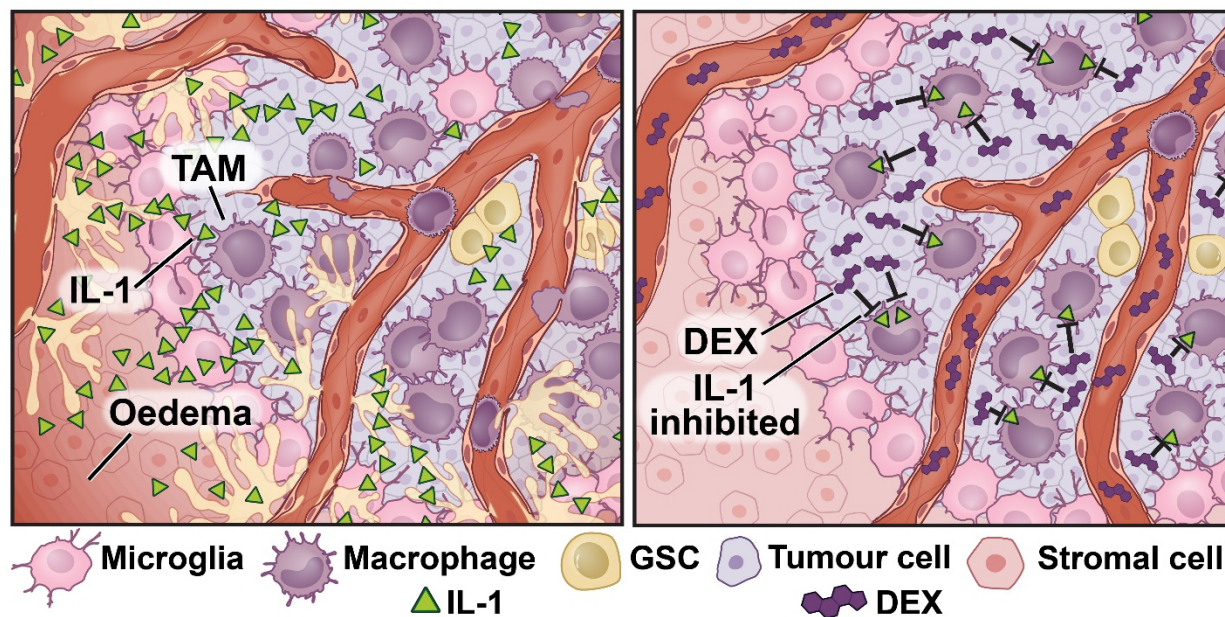


Figure 4.2. A graphical summary of the results presented in Chapter 3. This illustration depicts the production of interleukin-1 by bone marrow-derived macrophages in the glioblastoma tumor microenvironment and the promotion of edema by this cytokine. Dexamethasone is shown to block interleukin-1 production and thereby reduced the development of edema.

results. Many questions remain and this section will discuss routes of investigation that should stem from this work.

In the immediate future, further development and improvement of the murine models developed in this project will allow for more productive, accurate, and specific modeling of the human disease. The RCAS system allows for the combination of numerous genetic lesions to generate tumors. Expansion of the repertoire of RCAS viruses available for injection will allow for the modeling of more types of glioblastoma. For example, I have shown data here regarding the similarity between the PDGFB-overexpressing murine tumors and human Proneural tumors. In the human Proneural subtype, there are also frequently mutations in the enzyme IDH1<sup>332</sup>. Addition of an IDH1 mutant RCAS plasmid has allowed for the assessment of a more specific subclass of Proneural-like tumors<sup>333,334</sup>. An immediate comparison of the immune microenvironment and response to therapy in IDH1 wildtype and mutant PDGFB-overexpressing murine tumors would be a logical next step in model development. Furthermore, these models will allow for the preclinical assessment of precision therapies targeting IDH1 mutant tumors.

In addition to IDH1 mutations, there are a slew of additional genomic alterations present in human glioblastoma. More significant alterations will likely be uncovered through analysis of a larger dataset of human tumors as well. With the RCAS system, it is possible to rapidly synthesize and validate plasmids to model these alterations in mice. A logical next step towards the expansion and improvement of the RCAS system presented in this work will be to identify and model additional genetic lesions present in human tumors as well as determine the effects of these mutations on response to therapy as well as the composition of the immune microenvironment. Expansion of the RCAS repertoire will allow for interrogation of more specific subclasses of glioblastoma than have

already been established and will provide an excellent pathway towards development of precision therapeutics.

Another immediate goal of this research will be further optimization of the EGFRvIII model presented in Chapter 2. Although I have presented data here indicating the similarities between these murine tumors and their human counterparts, the utility of this model is still lacking due to the length of time necessary for tumor development following injection. In many cases tumors do not develop until over 100 days following injection and mice injected on the same day will develop tumors over a span of weeks. This limits the ability to test therapeutic regimens in these mice. To expedite and narrow the window of tumor development, I have developed and begun to validate an RCAS plasmid for overexpression of EGF, the ligand to EGFR. As demonstrated with the PDGFB-overexpressing model, ligand overexpression in mice can recapitulate the phenotype observed following receptor amplification or activation in human tumors. Perhaps EGF-overexpression will similarly emulate constitutive EGFR activation in human EGFRvIII tumors.

In the longer term, attractive future directions in analysis of these murine mouse models will employ high dimensional techniques like cytometry by time of flight (CyTOF) and single-cell RNA-sequencing to describe the subtype differences in immune microenvironment in higher resolution. CyTOF allows for analysis of upwards of thirty cellular markers simultaneously compared to the four markers used in the flow cytometry experiments in this work. Analysis of the subtype-specific mouse models with CyTOF will demonstrate more specific subpopulations of immune cells within each tumor subtype. It will allow for the assessment of differences in immune cell profile generated by different driver mutations and will validate if the models presented here show similar changes to what is observed between different human subtypes<sup>12</sup>. I hypothesize that there are further subsets of myeloid and lymphoid cells beyond what I have studied in this work and what has been shown with

traditional flow cytometry that will display correlations with positive and negative prognosis. These subsets could possibly be targeted or leveraged therapeutically. CyTOF provides the best technique to identify these subsets and will lay the groundwork for their analysis with other techniques.

The only drawback of CyTOF is that it only allows for sorting of cells into different populations and falls short of identifying the expression profiles of these cellular subsets. Single-cell RNA-sequencing will allow for changes in expression profile to be demonstrated. Combining single-cell RNA-sequencing with subtype-specific CyTOF analysis will allow for the expression profile of the cellular populations within the tumor to be identified and overlaid. This analysis should elucidate not just which specific populations are prevalent within each subtype, but also what alterations they demonstrate relative to baseline cells and which pathways relevant to these subsets are the most attractive to target therapeutically. In theory, this combined analysis should allow for direct modulation of the tumor microenvironment with pharmacological interventions. Populations of cells shown to be positive prognostic factors can be enhanced while populations shown to have significant detrimental effects can be eliminated. The main challenge with this methodology will be merging and making sense of the incredibly large datasets generated with these two techniques.

In Chapter 3, I was able to interrogate IL-1 as a therapeutic target for the management of glioblastoma-associated cerebral edema. Furthermore, I established for the first time a connection between macrophages and cerebral edema in glioblastoma. This work stopped short of defining a precise mechanism of this relationship and additionally was unable to provide an attractive pharmacological modality for targeting IL-1 to relieve edema. The future directions of this project should address these shortcomings.

I chose to investigate edema in the PDGFB-overexpressing model due to its previous utilization for the purpose as well as my work that indicated impaired BBB integrity in mice bearing

these tumors<sup>192,307</sup>. In human patients, all subtypes of glioblastoma display edema development and in all cases, it is managed by dexamethasone. The subtype-specific mouse models offer an excellent tool to interrogate differences in edema development and management between the subtypes. First, I would assess the propensity for edema development in each of the subtype-specific mouse models described in Chapter 3. If all subtypes displayed edema development, I would next characterize the response to dexamethasone in each. Since the proportion of BMDM and MG is different between the subtypes, this analysis will provide evidence if the effects of dexamethasone are BMDM-dependent as suggested by my work in PDGFB-overexpressing tumors. Since the impairment of radiotherapy efficacy by dexamethasone has only been established in PDGFB-overexpressing murine tumors, I would also immediately assess if this phenomenon is present in all the subtypes.

Ablation of IL-1 signaling and assessment of edema in each of these model systems according to the protocols outlined in this work will establish whether specific inhibition of IL-1 signaling is only efficacious in PDGFB-overexpressing tumors, or if the effects are broadly applicable to all subtypes. Furthermore, due to the different immune cell compositions between the tumor subtypes, this analysis will illustrate if IL-1 ablation is dependent upon BMDM comprising the majority of the tumor-associated macrophage population as suggested by the data in Chapter 3. Preliminary data also indicates that IL-1 signaling is differentially involved between human and murine subtypes of glioblastoma. Assessment of IL-1 genetic ablation in each of the murine subtypes will assess in which subtype it is likely to be the most efficacious or if the effects translate across subtypes.

In addition to these genetic experiments, I would work on optimizing pharmacological inhibition of IL-1 in each of the mouse models. Gallium nitrate was shown to have similar results to genetic ablation of IL-1; however, pharmacokinetics and pharmacodynamics of the drug *in vivo* have

yet to be established. Furthermore, the penetrance of gallium nitrate into the brain has not been evaluated. If it is to be considered as therapeutically relevant for the management of cerebral edema, its ability to get into the brain must be established. I also have yet to analyze the efficacy of the slew of other IL-1 inhibitors that are utilized clinically<sup>298</sup>. Although the majority of these are recombinant proteins and may display limited BBB penetrance, their efficacies should still be assessed.

Considering the nature of currently established pharmacological inhibitors of IL-1 signaling and their likely limited penetrance of the BBB, the development of novel, small molecule-based inhibitors would be attractive for the management of IL-1-based neuroinflammation. As a longer-term goal of this project, high throughput screening for small molecule lead compounds that inhibit IL-1 should be performed. Any leads could then be screened and optimized for potency, metabolic profile, toxicity, and BBB penetrance. A potent, small molecule-based IL-1 inhibitor is likely to have commercial relevance outside of edema management since IL-1 inhibition has already been established as therapeutically relevant in other diseases<sup>298</sup>. Therefore, identification of compound with these characteristics using high throughput screening will generate intellectual property with significant value.

As another longer-term goal, the precise mechanism underlying the promotion of edema development by macrophages should be elucidated. It is clear from my results that both dexamethasone treatment and IL-1 ablation inhibit the chemotaxis of BMDM into PDGFB-overexpressing tumors. In both cases, a reduction in BBB permeability and edema formation is observed. This implies that there may be a direct connection between BMDM infiltration and edema development in glioblastoma; however, I did not directly establish this connection. To conclusively derive this connection in future experiments, strategies to deplete circulating monocytes could be employed. A genetic approach for this would involve expressing the diphtheria toxin receptor

(DTR) only in circulating monocytes, perhaps under control of the CCR2 promoter, and administering diphtheria toxin (DT) to specifically ablate the cells. If performed following tumor development, this strategy would allow for the inhibition of BMDM chemotaxis to the tumor through ablation of their precursor cells. Depletion of the cells could be confirmed with flow cytometry-based analysis of circulating immune cells as well as whole tumor analysis as performed in this work. Immunohistochemistry for IBA1 could be employed as a complimentary approach. The formation of edema in mice administered DT could be compared to mice administered vehicle with the wet/dry assay or MRI. If mice administered DT had a reduction in edema, compared to vehicle-treated mice, a direct connection between BMDM infiltration and edema development would be established. Pharmacological depletion of circulating monocytes with clodronate would allow for assessment of this phenomenon with an alternative method.

It is also possible that modulation of the expression profile of BMDMs in glioblastoma is responsible for the anti-edema effect afforded by IL-1 ablation and not inhibition of chemotaxis. To address this hypothesis, flow cytometry could be employed to isolate pure populations of tumor-associated BMDM from wildtype and IL-1-ablated mice. RNA-sequencing on these cells could illustrate what genes are differentially regulated in the cells between the two groups. Macrophages are known to produce vasoactive factors that influence vessel permeability<sup>335</sup>. This experiment would elucidate whether these factors are differentially regulated when IL-1 signaling is ablated.

Another approach to this experiment would be investigating the anti-edema efficacy of other pathways known to modulate the behavior of macrophages. PD-L1 inhibition has not been demonstrated to alter BMDM chemotaxis in glioblastoma; however, it has been shown to alter the activation of tumor-associated macrophages in other cancers<sup>336</sup>. Direct assessment of the development of edema in PD-L1 wildtype and knockout tumor-bearing mice using the

methodologies presented here would illuminate what effect macrophage activation has on the development of edema. Furthermore, if PD-L1 neutralization were shown to effect edema development, comparison of the pathways altered between IL-1-ablated and PD-L1-neutralized mice would provide candidate pathways responsible for macrophage-associated edema development.

Overall, this work outlines improved preclinical models for glioblastoma research and establishes that these models are attractive for the development of immunomodulatory therapies. I emphasize that adoption of these mouse models will improve the translatability of compounds assessed in preclinical studies. Future work will further hone these models to address more specific questions and molecular alterations. My results illustrating IL-1 as a mediator of glioblastoma-associated cerebral edema provide rationale for targeting this pathway in lieu of administering dexamethasone. Additional work must be performed to establish the precise mechanism through which IL-1-ablation reduces edema. These results will guide further development of therapies that target this pathway and will establish their suitability for human trials. Regardless, the rationale is strong to move IL-1-targeted therapies forward in the treatment of glioblastoma.

## References:

- 1 Scherer, H. J. A Critical Review: The Pathology of Cerebral Gliomas. *J Neurol Psychiatry* **3**, 147-177 (1940).
- 2 Brown, T. M. & Fee, E. Rudolf Carl Virchow: medical scientist, social reformer, role model. *Am J Public Health* **96**, 2104-2105, doi:10.2105/AJPH.2005.078436 (2006).
- 3 A Classification of the Tumors of the Glioma Group on a Histogenetic Basis with a Correlated Study of Prognosis. *Archives of Neurology & Psychiatry* **17**, 570-570, doi:10.1001/archneurpsyc.1927.02200340146015 (1927).
- 4 Folkman, J. Tumor angiogenesis: therapeutic implications. *N Engl J Med* **285**, 1182-1186, doi:10.1056/NEJM197111182852108 (1971).
- 5 Scherer, H. J. The forms of growth in gliomas and their practical significance. *Brain* **63**, 35 (1940).
- 6 Brennan, C. W. *et al.* The somatic genomic landscape of glioblastoma. *Cell* **155**, 462-477, doi:10.1016/j.cell.2013.09.034 (2013).
- 7 Verhaak, R. G. *et al.* Integrated genomic analysis identifies clinically relevant subtypes of glioblastoma characterized by abnormalities in PDGFRA, IDH1, EGFR, and NF1. *Cancer Cell* **17**, 98-110, doi:10.1016/j.ccr.2009.12.020 (2010).
- 8 Louis, D. N. *et al.* The 2016 World Health Organization Classification of Tumors of the Central Nervous System: a summary. *Acta Neuropathol* **131**, 803-820, doi:10.1007/s00401-016-1545-1 (2016).
- 9 Quail, D. F. & Joyce, J. A. The Microenvironmental Landscape of Brain Tumors. *Cancer Cell* **31**, 326-341, doi:10.1016/j.ccell.2017.02.009 (2017).
- 10 Hambardzumyan, D., Gutmann, D. H. & Kettenmann, H. The role of microglia and macrophages in glioma maintenance and progression. *Nat Neurosci* **19**, 20-27, doi:10.1038/nn.4185 (2016).
- 11 Chen, Z. & Hambardzumyan, D. Immune Microenvironment in Glioblastoma Subtypes. *Front Immunol* **9**, 1004, doi:10.3389/fimmu.2018.01004 (2018).
- 12 Wang, Q. *et al.* Tumor Evolution of Glioma-Intrinsic Gene Expression Subtypes Associates with Immunological Changes in the Microenvironment. *Cancer Cell* **32**, 42-56 e46, doi:10.1016/j.ccell.2017.06.003 (2017).
- 13 Grier, J. T. & Batchelor, T. Low-grade gliomas in adults. *Oncologist* **11**, 681-693, doi:10.1634/theoncologist.11-6-681 (2006).
- 14 Kettenmann, H., Kettenmann, H. & Ransom, B. R. *Neuroglia*. 3rd edn, (Oxford University Press, 2013).
- 15 Omuro, A. & DeAngelis, L. M. Glioblastoma and other malignant gliomas: a clinical review. *JAMA* **310**, 1842-1850, doi:10.1001/jama.2013.280319 (2013).
- 16 Ostrom, Q. T. *et al.* CBTRUS Statistical Report: Primary Brain and Other Central Nervous System Tumors Diagnosed in the United States in 2011-2015. *Neuro Oncol* **20**, iv1-iv86, doi:10.1093/neuonc/noy131 (2018).
- 17 Ostrom, Q. T. *et al.* CBTRUS Statistical Report: Primary brain and other central nervous system tumors diagnosed in the United States in 2010-2014. *Neuro Oncol* **19**, v1-v88, doi:10.1093/neuonc/nox158 (2017).
- 18 Ellor, S. V., Pagano-Young, T. A. & Avgeropoulos, N. G. Glioblastoma: background, standard treatment paradigms, and supportive care considerations. *J Law Med Ethics* **42**, 171-182, doi:10.1111/jlme.12133 (2014).

- 19 Thakkar, J. P. *et al.* Epidemiologic and molecular prognostic review of glioblastoma. *Cancer Epidemiol Biomarkers Prev* **23**, 1985-1996, doi:10.1158/1055-9965.EPI-14-0275 (2014).
- 20 Curran, W. J., Jr. *et al.* Recursive partitioning analysis of prognostic factors in three Radiation Therapy Oncology Group malignant glioma trials. *J Natl Cancer Inst* **85**, 704-710, doi:10.1093/jnci/85.9.704 (1993).
- 21 Rice, T. *et al.* Understanding inherited genetic risk of adult glioma - a review. *Neurooncol Pract* **3**, 10-16, doi:10.1093/nop/npv026 (2016).
- 22 Larjavaara, S. *et al.* Incidence of gliomas by anatomic location. *Neuro Oncol* **9**, 319-325, doi:10.1215/15228517-2007-016 (2007).
- 23 Jones, C. *et al.* Pediatric high-grade glioma: biologically and clinically in need of new thinking. *Neuro Oncol* **19**, 153-161, doi:10.1093/neuonc/now101 (2017).
- 24 Claes, A., Idema, A. J. & Wesseling, P. Diffuse glioma growth: a guerilla war. *Acta Neuropathol* **114**, 443-458, doi:10.1007/s00401-007-0293-7 (2007).
- 25 Giese, A. & Westphal, M. Glioma invasion in the central nervous system. *Neurosurgery* **39**, 235-250; discussion 250-232, doi:10.1097/00006123-199608000-00001 (1996).
- 26 Lacroix, M. *et al.* A multivariate analysis of 416 patients with glioblastoma multiforme: prognosis, extent of resection, and survival. *J Neurosurg* **95**, 190-198, doi:10.3171/jns.2001.95.2.0190 (2001).
- 27 Sanai, N., Polley, M. Y., McDermott, M. W., Parsa, A. T. & Berger, M. S. An extent of resection threshold for newly diagnosed glioblastomas. *J Neurosurg* **115**, 3-8, doi:10.3171/2011.2.JNS10998 (2011).
- 10.3171/2011.7.JNS10998 (2011).
- 28 Pardridge, W. M. Drug transport across the blood-brain barrier. *J Cereb Blood Flow Metab* **32**, 1959-1972, doi:10.1038/jcbfm.2012.126 (2012).
- 29 Safari, M. & Khoshnevisan, A. Cancer Stem Cells and Chemoresistance in Glioblastoma Multiform: A Review Article. *J Stem Cells* **10**, 271-285, doi:jsc.2015.10.4.271 (2015).
- 30 Hegi, M. E. *et al.* MGMT gene silencing and benefit from temozolomide in glioblastoma. *N Engl J Med* **352**, 997-1003, doi:10.1056/NEJMoa043331 (2005).
- 31 Weller, M. *et al.* Glioma. *Nat Rev Dis Primers* **1**, 15017, doi:10.1038/nrdp.2015.17 (2015).
- 32 Vecht, C. J., Kerkhof, M. & Duran-Pena, A. Seizure prognosis in brain tumors: new insights and evidence-based management. *Oncologist* **19**, 751-759, doi:10.1634/theoncologist.2014-0060 (2014).
- 33 Wick, W. *et al.* Pharmacotherapy of epileptic seizures in glioma patients: who, when, why and how long? *Onkologie* **28**, 391-396, doi:10.1159/000086375 (2005).
- 34 van Breemen, M. S. *et al.* Efficacy of anti-epileptic drugs in patients with gliomas and seizures. *J Neurol* **256**, 1519-1526, doi:10.1007/s00415-009-5156-9 (2009).
- 35 Kerkhof, M. *et al.* Effect of valproic acid on seizure control and on survival in patients with glioblastoma multiforme. *Neuro Oncol* **15**, 961-967, doi:10.1093/neuonc/not057 (2013).
- 36 Galicich, J. H., French, L. A. & Melby, J. C. Use of dexamethasone in treatment of cerebral edema associated with brain tumors. *J Lancet* **81**, 46-53 (1961).
- 37 Shukla, G. *et al.* Advanced magnetic resonance imaging in glioblastoma: a review. *Chin Clin Oncol* **6**, 40, doi:10.21037/cco.2017.06.28 (2017).

- 38 Upadhyay, N. & Waldman, A. D. Conventional MRI evaluation of gliomas. *Br J Radiol* **84 Spec No 2**, S107-111, doi:10.1259/bjr/65711810 (2011).
- 39 Grossman, R. *et al.* Dynamics of FLAIR Volume Changes in Glioblastoma and Prediction of Survival. *Ann Surg Oncol* **24**, 794-800, doi:10.1245/s10434-016-5635-z (2017).
- 40 Li, W. B. *et al.* MRI manifestations correlate with survival of glioblastoma multiforme patients. *Cancer Biol Med* **9**, 120-123, doi:10.3969/j.issn.2095-3941.2012.02.007 (2012).
- 41 Omuro, A. M., Leite, C. C., Mokhtari, K. & Delattre, J. Y. Pitfalls in the diagnosis of brain tumours. *Lancet Neurol* **5**, 937-948, doi:10.1016/S1474-4422(06)70597-X (2006).
- 42 Perry, A. & Wesseling, P. Histologic classification of gliomas. *Handb Clin Neurol* **134**, 71-95, doi:10.1016/B978-0-12-802997-8.00005-0 (2016).
- 43 Plate, K. H., Breier, G., Weich, H. A. & Risau, W. Vascular endothelial growth factor is a potential tumour angiogenesis factor in human gliomas in vivo. *Nature* **359**, 845-848, doi:10.1038/359845a0 (1992).
- 44 Myung, J. K. *et al.* Prognosis of Glioblastoma With Oligodendroglioma Component is Associated With the IDH1 Mutation and MGMT Methylation Status. *Transl Oncol* **7**, 712-719, doi:10.1016/j.tranon.2014.10.002 (2014).
- 45 Gladson, C. L., Prayson, R. A. & Liu, W. M. The pathobiology of glioma tumors. *Annu Rev Pathol* **5**, 33-50, doi:10.1146/annurev-pathol-121808-102109 (2010).
- 46 Beroukhim, R. *et al.* Assessing the significance of chromosomal aberrations in cancer: methodology and application to glioma. *Proc Natl Acad Sci U S A* **104**, 20007-20012, doi:10.1073/pnas.0710052104 (2007).
- 47 Ruano, Y. *et al.* Identification of novel candidate target genes in amplicons of Glioblastoma multiforme tumors detected by expression and CGH microarray profiling. *Mol Cancer* **5**, 39, doi:10.1186/1476-4598-5-39 (2006).
- 48 Freije, W. A. *et al.* Gene expression profiling of gliomas strongly predicts survival. *Cancer Res* **64**, 6503-6510, doi:10.1158/0008-5472.CAN-04-0452 (2004).
- 49 Madhavan, S. *et al.* Rembrandt: helping personalized medicine become a reality through integrative translational research. *Mol Cancer Res* **7**, 157-167, doi:10.1158/1541-7786.MCR-08-0435 (2009).
- 50 Li, J., Di, C., Mattox, A. K., Wu, L. & Adamson, D. C. The future role of personalized medicine in the treatment of glioblastoma multiforme. *Pharmgenomics Pers Med* **3**, 111-127, doi:10.2147/PGPM.S6852 (2010).
- 51 Cancer Genome Atlas Research, N. Comprehensive genomic characterization defines human glioblastoma genes and core pathways. *Nature* **455**, 1061-1068, doi:10.1038/nature07385 (2008).
- 52 Phillips, H. S. *et al.* Molecular subclasses of high-grade glioma predict prognosis, delineate a pattern of disease progression, and resemble stages in neurogenesis. *Cancer Cell* **9**, 157-173, doi:10.1016/j.ccr.2006.02.019 (2006).
- 53 Huse, J. T., Phillips, H. S. & Brennan, C. W. Molecular subclassification of diffuse gliomas: seeing order in the chaos. *Glia* **59**, 1190-1199, doi:10.1002/glia.21165 (2011).
- 54 Cancer Genome Atlas Research, N. *et al.* The Cancer Genome Atlas Pan-Cancer analysis project. *Nat Genet* **45**, 1113-1120, doi:10.1038/ng.2764 (2013).
- 55 Patel, A. P. *et al.* Single-cell RNA-seq highlights intratumoral heterogeneity in primary glioblastoma. *Science* **344**, 1396-1401, doi:10.1126/science.1254257 (2014).

- 56 Meyer, M. *et al.* Single cell-derived clonal analysis of human glioblastoma links functional and genomic heterogeneity. *Proc Natl Acad Sci U S A* **112**, 851-856, doi:10.1073/pnas.1320611111 (2015).
- 57 Sottoriva, A. *et al.* Intratumor heterogeneity in human glioblastoma reflects cancer evolutionary dynamics. *Proc Natl Acad Sci U S A* **110**, 4009-4014, doi:10.1073/pnas.1219747110 (2013).
- 58 Quail, D. F. & Joyce, J. A. Microenvironmental regulation of tumor progression and metastasis. *Nat Med* **19**, 1423-1437, doi:10.1038/nm.3394 (2013).
- 59 Balkwill, F. & Mantovani, A. Inflammation and cancer: back to Virchow? *Lancet* **357**, 539-545, doi:10.1016/S0140-6736(00)04046-0 (2001).
- 60 Alcantara Llaguno, S. R. & Parada, L. F. Cell of origin of glioma: biological and clinical implications. *Br J Cancer* **115**, 1445-1450, doi:10.1038/bjc.2016.354 (2016).
- 61 Hambarzumyan, D., Cheng, Y. K., Haeno, H., Holland, E. C. & Michor, F. The probable cell of origin of NF1- and PDGF-driven glioblastomas. *PLoS One* **6**, e24454, doi:10.1371/journal.pone.0024454 (2011).
- 62 Conover, J. C. & Notti, R. Q. The neural stem cell niche. *Cell Tissue Res* **331**, 211-224, doi:10.1007/s00441-007-0503-6 (2008).
- 63 Shen, Q. *et al.* Adult SVZ stem cells lie in a vascular niche: a quantitative analysis of niche cell-cell interactions. *Cell Stem Cell* **3**, 289-300, doi:10.1016/j.stem.2008.07.026 (2008).
- 64 Shackleton, M., Quintana, E., Fearon, E. R. & Morrison, S. J. Heterogeneity in cancer: cancer stem cells versus clonal evolution. *Cell* **138**, 822-829, doi:10.1016/j.cell.2009.08.017 (2009).
- 65 Dirks, P. B. Brain tumor stem cells: the cancer stem cell hypothesis writ large. *Mol Oncol* **4**, 420-430, doi:10.1016/j.molonc.2010.08.001 (2010).
- 66 Lathia, J. D., Mack, S. C., Mulkearns-Hubert, E. E., Valentim, C. L. & Rich, J. N. Cancer stem cells in glioblastoma. *Genes Dev* **29**, 1203-1217, doi:10.1101/gad.261982.115 (2015).
- 67 Ignatova, T. N. *et al.* Human cortical glial tumors contain neural stem-like cells expressing astroglial and neuronal markers in vitro. *Glia* **39**, 193-206, doi:10.1002/glia.10094 (2002).
- 68 Hemmati, H. D. *et al.* Cancerous stem cells can arise from pediatric brain tumors. *Proc Natl Acad Sci U S A* **100**, 15178-15183, doi:10.1073/pnas.2036535100 (2003).
- 69 Singh, S. K. *et al.* Identification of a cancer stem cell in human brain tumors. *Cancer Res* **63**, 5821-5828 (2003).
- 70 Vescovi, A. L., Galli, R. & Reynolds, B. A. Brain tumour stem cells. *Nat Rev Cancer* **6**, 425-436, doi:10.1038/nrc1889 (2006).
- 71 Cheng, L. *et al.* Glioblastoma stem cells generate vascular pericytes to support vessel function and tumor growth. *Cell* **153**, 139-152, doi:10.1016/j.cell.2013.02.021 (2013).
- 72 Ben-Porath, I. *et al.* An embryonic stem cell-like gene expression signature in poorly differentiated aggressive human tumors. *Nat Genet* **40**, 499-507, doi:10.1038/ng.127 (2008).
- 73 Ligon, K. L. *et al.* Olig2-regulated lineage-restricted pathway controls replication competence in neural stem cells and malignant glioma. *Neuron* **53**, 503-517, doi:10.1016/j.neuron.2007.01.009 (2007).

- 74 Tunici, P. *et al.* Genetic alterations and in vivo tumorigenicity of neurospheres derived from an adult glioblastoma. *Mol Cancer* **3**, 25, doi:10.1186/1476-4598-3-25 (2004).
- 75 Kondo, T., Setoguchi, T. & Taga, T. Persistence of a small subpopulation of cancer stem-like cells in the C6 glioma cell line. *Proc Natl Acad Sci U S A* **101**, 781-786, doi:10.1073/pnas.0307618100 (2004).
- 76 Visvader, J. E. & Lindeman, G. J. Cancer stem cells in solid tumours: accumulating evidence and unresolved questions. *Nat Rev Cancer* **8**, 755-768, doi:10.1038/nrc2499 (2008).
- 77 Greaves, M. & Maley, C. C. Clonal evolution in cancer. *Nature* **481**, 306-313, doi:10.1038/nature10762 (2012).
- 78 Yao, Y. & Dai, W. Genomic Instability and Cancer. *J Carcinog Mutagen* **5**, doi:10.4172/2157-2518.1000165 (2014).
- 79 Nowell, P. C. Mechanisms of tumor progression. *Cancer Res* **46**, 2203-2207 (1986).
- 80 Stratton, M. R., Campbell, P. J. & Futreal, P. A. The cancer genome. *Nature* **458**, 719-724, doi:10.1038/nature07943 (2009).
- 81 Xie, Q., Mittal, S. & Berens, M. E. Targeting adaptive glioblastoma: an overview of proliferation and invasion. *Neuro Oncol* **16**, 1575-1584, doi:10.1093/neuonc/nou147 (2014).
- 82 Lun, M., Lok, E., Gautam, S., Wu, E. & Wong, E. T. The natural history of extracranial metastasis from glioblastoma multiforme. *J Neurooncol* **105**, 261-273, doi:10.1007/s11060-011-0575-8 (2011).
- 83 Watkins, S. *et al.* Disruption of astrocyte-vascular coupling and the blood-brain barrier by invading glioma cells. *Nat Commun* **5**, 4196, doi:10.1038/ncomms5196 (2014).
- 84 Noch, E. & Khalili, K. Molecular mechanisms of necrosis in glioblastoma: the role of glutamate excitotoxicity. *Cancer Biol Ther* **8**, 1791-1797, doi:10.4161/cbt.8.19.9762 (2009).
- 85 Raza, S. M. *et al.* Necrosis and glioblastoma: a friend or a foe? A review and a hypothesis. *Neurosurgery* **51**, 2-12; discussion 12-13, doi:10.1097/00006123-200207000-00002 (2002).
- 86 Gatenby, R. A., Gawlinski, E. T., Gmitro, A. F., Kaylor, B. & Gillies, R. J. Acid-mediated tumor invasion: a multidisciplinary study. *Cancer Res* **66**, 5216-5223, doi:10.1158/0008-5472.CAN-05-4193 (2006).
- 87 Gatenby, R. A. & Gillies, R. J. Why do cancers have high aerobic glycolysis? *Nat Rev Cancer* **4**, 891-899, doi:10.1038/nrc1478 (2004).
- 88 Hendriksen, E. M. *et al.* Angiogenesis, hypoxia and VEGF expression during tumour growth in a human xenograft tumour model. *Microvasc Res* **77**, 96-103, doi:10.1016/j.mvr.2008.11.002 (2009).
- 89 Shweiki, D., Itin, A., Soffer, D. & Keshet, E. Vascular endothelial growth factor induced by hypoxia may mediate hypoxia-initiated angiogenesis. *Nature* **359**, 843-845, doi:10.1038/359843a0 (1992).
- 90 Das, S. & Marsden, P. A. Angiogenesis in glioblastoma. *N Engl J Med* **369**, 1561-1563, doi:10.1056/NEJMcibr1309402 (2013).
- 91 Wang, R. *et al.* Glioblastoma stem-like cells give rise to tumour endothelium. *Nature* **468**, 829-833, doi:10.1038/nature09624 (2010).
- 92 Soda, Y. *et al.* Transdifferentiation of glioblastoma cells into vascular endothelial cells. *Proc Natl Acad Sci U S A* **108**, 4274-4280, doi:10.1073/pnas.1016030108 (2011).

- 93 Cantanhede, I. G. & de Oliveira, J. R. M. PDGF Family Expression in Glioblastoma Multiforme: Data Compilation from Ivy Glioblastoma Atlas Project Database. *Sci Rep* **7**, 15271, doi:10.1038/s41598-017-15045-w (2017).
- 94 Wolburg, H., Noell, S., Fallier-Becker, P., Mack, A. F. & Wolburg-Buchholz, K. The disturbed blood-brain barrier in human glioblastoma. *Mol Aspects Med* **33**, 579-589, doi:10.1016/j.mam.2012.02.003 (2012).
- 95 Sarkaria, J. N. *et al.* Is the blood-brain barrier really disrupted in all glioblastomas? A critical assessment of existing clinical data. *Neuro Oncol* **20**, 184-191, doi:10.1093/neuonc/nox175 (2018).
- 96 Armulik, A. *et al.* Pericytes regulate the blood-brain barrier. *Nature* **468**, 557-561, doi:10.1038/nature09522 (2010).
- 97 Caspani, E. M., Crossley, P. H., Redondo-Garcia, C. & Martinez, S. Glioblastoma: a pathogenic crosstalk between tumor cells and pericytes. *PLoS One* **9**, e101402, doi:10.1371/journal.pone.0101402 (2014).
- 98 Sena, I. F. G. *et al.* Glioblastoma-activated pericytes support tumor growth via immunosuppression. *Cancer Med* **7**, 1232-1239, doi:10.1002/cam4.1375 (2018).
- 99 Chen, Z. *et al.* Cellular and Molecular Identity of Tumor-Associated Macrophages in Glioblastoma. *Cancer Res* **77**, 2266-2278, doi:10.1158/0008-5472.CAN-16-2310 (2017).
- 100 Simmons, G. W. *et al.* Neurofibromatosis-1 heterozygosity increases microglia in a spatially and temporally restricted pattern relevant to mouse optic glioma formation and growth. *J Neuropathol Exp Neurol* **70**, 51-62, doi:10.1097/NEN.0b013e3182032d37 (2011).
- 101 Ginhoux, F., Lim, S., Hoeffel, G., Low, D. & Huber, T. Origin and differentiation of microglia. *Front Cell Neurosci* **7**, 45, doi:10.3389/fncel.2013.00045 (2013).
- 102 Ginhoux, F. *et al.* Fate mapping analysis reveals that adult microglia derive from primitive macrophages. *Science* **330**, 841-845, doi:10.1126/science.1194637 (2010).
- 103 Sierra, A. *et al.* The "Big-Bang" for modern glial biology: Translation and comments on Pio del Rio-Hortega 1919 series of papers on microglia. *Glia* **64**, 1801-1840, doi:10.1002/glia.23046 (2016).
- 104 Streit, W. J., Mrak, R. E. & Griffin, W. S. Microglia and neuroinflammation: a pathological perspective. *J Neuroinflammation* **1**, 14, doi:10.1186/1742-2094-1-14 (2004).
- 105 Nimmerjahn, A., Kirchhoff, F. & Helmchen, F. Resting microglial cells are highly dynamic surveillants of brain parenchyma in vivo. *Science* **308**, 1314-1318, doi:10.1126/science.1110647 (2005).
- 106 Bayerl, S. H. *et al.* Time lapse in vivo microscopy reveals distinct dynamics of microglia-tumor environment interactions-a new role for the tumor perivascular space as highway for trafficking microglia. *Glia* **64**, 1210-1226, doi:10.1002/glia.22994 (2016).
- 107 Colton, C. & Wilcock, D. M. Assessing activation states in microglia. *CNS Neurol Disord Drug Targets* **9**, 174-191 (2010).
- 108 Shaked, I., Porat, Z., Gersner, R., Kipnis, J. & Schwartz, M. Early activation of microglia as antigen-presenting cells correlates with T cell-mediated protection and repair of the injured central nervous system. *J Neuroimmunol* **146**, 84-93 (2004).
- 109 Boche, D., Perry, V. H. & Nicoll, J. A. Review: activation patterns of microglia and their identification in the human brain. *Neuropathol Appl Neurobiol* **39**, 3-18, doi:10.1111/nan.12011 (2013).

- 110 Orihuela, R., McPherson, C. A. & Harry, G. J. Microglial M1/M2 polarization and metabolic states. *Br J Pharmacol* **173**, 649-665, doi:10.1111/bph.13139 (2016).
- 111 Mantovani, A. *et al.* The chemokine system in diverse forms of macrophage activation and polarization. *Trends Immunol* **25**, 677-686, doi:10.1016/j.it.2004.09.015 (2004).
- 112 Mantovani, A., Ponzetta, A., Inforzato, A. & Jaillon, S. Innate immunity, inflammation and tumour progression: double-edged swords. *J Intern Med* **285**, 524-532, doi:10.1111/joim.12886 (2019).
- 113 Nagarsheth, N., Wicha, M. S. & Zou, W. Chemokines in the cancer microenvironment and their relevance in cancer immunotherapy. *Nat Rev Immunol* **17**, 559-572, doi:10.1038/nri.2017.49 (2017).
- 114 Penfield, W. A Method of Staining Oligodendroglia and Microglia (Combined Method). *Am J Pathol* **4**, 153-157 (1928).
- 115 Charles, N. A., Holland, E. C., Gilbertson, R., Glass, R. & Kettenmann, H. The brain tumor microenvironment. *Glia* **60**, 502-514 (2012).
- 116 Badie, B., Bartley, B. & Schartner, J. Differential expression of MHC class II and B7 costimulatory molecules by microglia in rodent gliomas. *J Neuroimmunol* **133**, 39-45 (2002).
- 117 Shi, C. & Pamer, E. G. Monocyte recruitment during infection and inflammation. *Nat Rev Immunol* **11**, 762-774, doi:10.1038/nri3070 (2011).
- 118 Geissmann, F., Jung, S. & Littman, D. R. Blood monocytes consist of two principal subsets with distinct migratory properties. *Immunity* **19**, 71-82 (2003).
- 119 Deshmane, S. L., Kremlev, S., Amini, S. & Sawaya, B. E. Monocyte chemoattractant protein-1 (MCP-1): an overview. *J Interferon Cytokine Res* **29**, 313-326, doi:10.1089/jir.2008.0027 (2009).
- 120 Yona, S. *et al.* Fate mapping reveals origins and dynamics of monocytes and tissue macrophages under homeostasis. *Immunity* **38**, 79-91, doi:10.1016/j.immuni.2012.12.001 (2013).
- 121 Davies, L. C. *et al.* Distinct bone marrow-derived and tissue-resident macrophage lineages proliferate at key stages during inflammation. *Nat Commun* **4**, 1886, doi:10.1038/ncomms2877 (2013).
- 122 Gabrusiewicz, K. *et al.* Characteristics of the alternative phenotype of microglia/macrophages and its modulation in experimental gliomas. *PLoS One* **6**, e23902, doi:10.1371/journal.pone.0023902 (2011).
- 123 Li, W. & Graeber, M. B. The molecular profile of microglia under the influence of glioma. *Neuro Oncol* **14**, 958-978, doi:10.1093/neuonc/nos116 (2012).
- 124 Umemura, N. *et al.* Tumor-infiltrating myeloid-derived suppressor cells are pleiotropic-inflamed monocytes/macrophages that bear M1- and M2-type characteristics. *J Leukoc Biol* **83**, 1136-1144, doi:10.1189/jlb.0907611 (2008).
- 125 Szulzewsky, F. *et al.* Glioma-associated microglia/macrophages display an expression profile different from M1 and M2 polarization and highly express Gpnmb and Spp1. *PLoS One* **10**, e0116644, doi:10.1371/journal.pone.0116644 (2015).
- 126 Muller, S. *et al.* Single-cell profiling of human gliomas reveals macrophage ontogeny as a basis for regional differences in macrophage activation in the tumor microenvironment. *Genome Biol* **18**, 234, doi:10.1186/s13059-017-1362-4 (2017).

- 127 Chen, Z., Ross, J. L. & Hambardzumyan, D. Intravital 2-photon imaging reveals distinct morphology and infiltrative properties of glioblastoma-associated macrophages. *Proc Natl Acad Sci U S A* **116**, 14254-14259, doi:10.1073/pnas.1902366116 (2019).
- 128 Han, S. *et al.* Rescuing defective tumor-infiltrating T-cell proliferation in glioblastoma patients. *Oncol Lett* **12**, 2924-2929, doi:10.3892/ol.2016.4944 (2016).
- 129 Bluestone, J. A., Mackay, C. R., O'Shea, J. J. & Stockinger, B. The functional plasticity of T cell subsets. *Nat Rev Immunol* **9**, 811-816, doi:10.1038/nri2654 (2009).
- 130 Curiel, T. J. Regulatory T cells and treatment of cancer. *Curr Opin Immunol* **20**, 241-246, doi:10.1016/j.coi.2008.04.008 (2008).
- 131 Heiland, D. H. *et al.* Comprehensive analysis of PD-L1 expression in glioblastoma multiforme. *Oncotarget* **8**, 42214-42225, doi:10.18632/oncotarget.15031 (2017).
- 132 Ishida, Y., Agata, Y., Shibahara, K. & Honjo, T. Induced expression of PD-1, a novel member of the immunoglobulin gene superfamily, upon programmed cell death. *EMBO J* **11**, 3887-3895 (1992).
- 133 Jin, H. T., Ahmed, R. & Okazaki, T. Role of PD-1 in regulating T-cell immunity. *Curr Top Microbiol Immunol* **350**, 17-37, doi:10.1007/82\_2010\_116 (2011).
- 134 Loke, P. & Allison, J. P. PD-L1 and PD-L2 are differentially regulated by Th1 and Th2 cells. *Proc Natl Acad Sci U S A* **100**, 5336-5341, doi:10.1073/pnas.0931259100 (2003).
- 135 Chen, R. Q., Liu, F., Qiu, X. Y. & Chen, X. Q. The Prognostic and Therapeutic Value of PD-L1 in Glioma. *Front Pharmacol* **9**, 1503, doi:10.3389/fphar.2018.01503 (2018).
- 136 DANDY, W. E. REMOVAL OF RIGHT CEREBRAL HEMISPHERE FOR CERTAIN TUMORS WITH HEMIPLEGIA: PRELIMINARY REPORT. *JAMA* **90**, 823-825, doi:10.1001/jama.1928.02690380007003 (1928).
- 137 Coley, W. B. The treatment of malignant tumors by repeated inoculations of erysipelas. With a report of ten original cases. 1893. *Clin Orthop Relat Res*, 3-11 (1991).
- 138 Kelly, K. A., Kirkwood, J. M. & Kapp, D. S. Glioblastoma multiforme: pathology, natural history and treatment. *Cancer Treat Rev* **11**, 1-26 (1984).
- 139 Kreth, F. W., Warnke, P. C., Scheremet, R. & Ostertag, C. B. Surgical resection and radiation therapy versus biopsy and radiation therapy in the treatment of glioblastoma multiforme. *J Neurosurg* **78**, 762-766, doi:10.3171/jns.1993.78.5.0762 (1993).
- 140 Stupp, R. *et al.* Radiotherapy plus concomitant and adjuvant temozolomide for glioblastoma. *N Engl J Med* **352**, 987-996, doi:10.1056/NEJMoa043330 (2005).
- 141 Manrique-Guzman, S., Herrada-Pineda, T. & Revilla-Pacheco, F. in *Glioblastoma* (ed S. De Vleeschouwer) (2017).
- 142 Vogelbaum, M. A. The benefit of surgical resection in recurrent glioblastoma. *Neuro Oncol* **18**, 462-463, doi:10.1093/neuonc/now004 (2016).
- 143 Keles, G. E. *et al.* Volumetric extent of resection and residual contrast enhancement on initial surgery as predictors of outcome in adult patients with hemispheric anaplastic astrocytoma. *J Neurosurg* **105**, 34-40, doi:10.3171/jns.2006.105.1.34 (2006).
- 144 Curran, W. J., Jr. *et al.* Does extent of surgery influence outcome for astrocytoma with atypical or anaplastic foci (AAF)? A report from three Radiation Therapy Oncology Group (RTOG) trials. *J Neurooncol* **12**, 219-227 (1992).
- 145 Paw, I., Carpenter, R. C., Watabe, K., Debinski, W. & Lo, H. W. Mechanisms regulating glioma invasion. *Cancer Lett* **362**, 1-7, doi:10.1016/j.canlet.2015.03.015 (2015).
- 146 Hadjipanayis, C. G. & Stummer, W. 5-ALA and FDA approval for glioma surgery. *J Neurooncol* **141**, 479-486, doi:10.1007/s11060-019-03098-y (2019).

- 147 Senft, C. *et al.* Intraoperative MRI guidance and extent of resection in glioma surgery: a randomised, controlled trial. *Lancet Oncol* **12**, 997-1003, doi:10.1016/S1470-2045(11)70196-6 (2011).
- 148 Suchorska, B. *et al.* Complete resection of contrast-enhancing tumor volume is associated with improved survival in recurrent glioblastoma-results from the DIRECTOR trial. *Neuro Oncol* **18**, 549-556, doi:10.1093/neuonc/nov326 (2016).
- 149 Young, R. M., Jamshidi, A., Davis, G. & Sherman, J. H. Current trends in the surgical management and treatment of adult glioblastoma. *Ann Transl Med* **3**, 121, doi:10.3978/j.issn.2305-5839.2015.05.10 (2015).
- 150 Zinn, P. O., Colen, R. R., Kasper, E. M. & Burkhardt, J. K. Extent of resection and radiotherapy in GBM: A 1973 to 2007 surveillance, epidemiology and end results analysis of 21,783 patients. *Int J Oncol* **42**, 929-934, doi:10.3892/ijo.2013.1770 (2013).
- 151 Walker, M. D. *et al.* Evaluation of BCNU and/or radiotherapy in the treatment of anaplastic gliomas. A cooperative clinical trial. *J Neurosurg* **49**, 333-343, doi:10.3171/jns.1978.49.3.0333 (1978).
- 152 Chargari, C. *et al.* Optimize and refine therapeutic index in radiation therapy: Overview of a century. *Cancer Treat Rev* **45**, 58-67, doi:10.1016/j.ctrv.2016.03.001 (2016).
- 153 Hochberg, F. H. & Pruitt, A. Assumptions in the radiotherapy of glioblastoma. *Neurology* **30**, 907-911, doi:10.1212/wnl.30.9.907 (1980).
- 154 Barani, I. J. & Larson, D. A. Radiation therapy of glioblastoma. *Cancer Treat Res* **163**, 49-73, doi:10.1007/978-3-319-12048-5\_4 (2015).
- 155 Babu, R. *et al.* Glioblastoma in the elderly: the effect of aggressive and modern therapies on survival. *J Neurosurg* **124**, 998-1007, doi:10.3171/2015.4.JNS142200 (2016).
- 156 Mann, J., Ramakrishna, R., Magge, R. & Wernicke, A. G. Advances in Radiotherapy for Glioblastoma. *Front Neurol* **8**, 748, doi:10.3389/fneur.2017.00748 (2017).
- 157 Warwick, G. P. The Mechanism of Action of Alkylating Agents. *Cancer Res* **23**, 1315-1333 (1963).
- 158 Reithmeier, T. *et al.* BCNU for recurrent glioblastoma multiforme: efficacy, toxicity and prognostic factors. *BMC Cancer* **10**, 30, doi:10.1186/1471-2407-10-30 (2010).
- 159 Silvani, A. *et al.* Cisplatinium and BCNU chemotherapy in primary glioblastoma patients. *J Neurooncol* **94**, 57-62, doi:10.1007/s11060-009-9800-0 (2009).
- 160 Baer, J. C. *et al.* Depletion of O6-alkylguanine-DNA alkyltransferase correlates with potentiation of temozolomide and CCNU toxicity in human tumour cells. *Br J Cancer* **67**, 1299-1302, doi:10.1038/bjc.1993.241 (1993).
- 161 Minniti, G., Muni, R., Lanzetta, G., Marchetti, P. & Enrici, R. M. Chemotherapy for glioblastoma: current treatment and future perspectives for cytotoxic and targeted agents. *Anticancer Res* **29**, 5171-5184 (2009).
- 162 Heimberger, A. B. *et al.* Prognostic effect of epidermal growth factor receptor and EGFRvIII in glioblastoma multiforme patients. *Clin Cancer Res* **11**, 1462-1466, doi:10.1158/1078-0432.CCR-04-1737 (2005).
- 163 Frederick, L., Wang, X. Y., Eley, G. & James, C. D. Diversity and frequency of epidermal growth factor receptor mutations in human glioblastomas. *Cancer Res* **60**, 1383-1387 (2000).
- 164 Prados, M. D. *et al.* Phase II study of erlotinib plus temozolomide during and after radiation therapy in patients with newly diagnosed glioblastoma multiforme or gliosarcoma. *J Clin Oncol* **27**, 579-584, doi:10.1200/JCO.2008.18.9639 (2009).

- 165 Raizer, J. J. *et al.* A phase II trial of erlotinib in patients with recurrent malignant gliomas and nonprogressive glioblastoma multiforme postradiation therapy. *Neuro Oncol* **12**, 95-103, doi:10.1093/neuonc/nop015 (2010).
- 166 Stea, B. *et al.* Time and dose-dependent radiosensitization of the glioblastoma multiforme U251 cells by the EGF receptor tyrosine kinase inhibitor ZD1839 ('Iressa'). *Cancer Lett* **202**, 43-51, doi:10.1016/j.canlet.2003.07.006 (2003).
- 167 Uhm, J. H. *et al.* Phase II evaluation of gefitinib in patients with newly diagnosed Grade 4 astrocytoma: Mayo/North Central Cancer Treatment Group Study N0074. *Int J Radiat Oncol Biol Phys* **80**, 347-353, doi:10.1016/j.ijrobp.2010.01.070 (2011).
- 168 Nazarenko, I. *et al.* PDGF and PDGF receptors in glioma. *Ups J Med Sci* **117**, 99-112, doi:10.3109/03009734.2012.665097 (2012).
- 169 McMahan, G. VEGF receptor signaling in tumor angiogenesis. *Oncologist* **5 Suppl 1**, 3-10, doi:10.1634/theoncologist.5-suppl\_1-3 (2000).
- 170 Abounader, R. & Laterra, J. Scatter factor/hepatocyte growth factor in brain tumor growth and angiogenesis. *Neuro Oncol* **7**, 436-451, doi:10.1215/S1152851705000050 (2005).
- 171 Morrison, R. S. *et al.* Fibroblast growth factor receptor gene expression and immunoreactivity are elevated in human glioblastoma multiforme. *Cancer Res* **54**, 2794-2799 (1994).
- 172 Hainsworth, J. D. *et al.* Concurrent radiotherapy and temozolomide followed by temozolomide and sorafenib in the first-line treatment of patients with glioblastoma multiforme. *Cancer* **116**, 3663-3669, doi:10.1002/cncr.25275 (2010).
- 173 Kalpathy-Cramer, J. *et al.* Phase II study of tivozanib, an oral VEGFR inhibitor, in patients with recurrent glioblastoma. *J Neurooncol* **131**, 603-610, doi:10.1007/s11060-016-2332-5 (2017).
- 174 Batchelor, T. T. *et al.* Phase III randomized trial comparing the efficacy of cediranib as monotherapy, and in combination with lomustine, versus lomustine alone in patients with recurrent glioblastoma. *J Clin Oncol* **31**, 3212-3218, doi:10.1200/JCO.2012.47.2464 (2013).
- 175 Kamoun, W. S. *et al.* Edema control by cediranib, a vascular endothelial growth factor receptor-targeted kinase inhibitor, prolongs survival despite persistent brain tumor growth in mice. *J Clin Oncol* **27**, 2542-2552, doi:10.1200/JCO.2008.19.9356 (2009).
- 176 Pearson, J. R. D. & Regad, T. Targeting cellular pathways in glioblastoma multiforme. *Signal Transduct Target Ther* **2**, 17040, doi:10.1038/sigtrans.2017.40 (2017).
- 177 Reardon, D. A. *et al.* Phase I study of AEE788, a novel multitarget inhibitor of ErbB- and VEGF-receptor-family tyrosine kinases, in recurrent glioblastoma patients. *Cancer Chemother Pharmacol* **69**, 1507-1518, doi:10.1007/s00280-012-1854-6 (2012).
- 178 Kilic, T. *et al.* Intracranial inhibition of platelet-derived growth factor-mediated glioblastoma cell growth by an orally active kinase inhibitor of the 2-phenylaminopyrimidine class. *Cancer Res* **60**, 5143-5150 (2000).
- 179 Wen, P. Y. *et al.* Phase I/II study of imatinib mesylate for recurrent malignant gliomas: North American Brain Tumor Consortium Study 99-08. *Clin Cancer Res* **12**, 4899-4907, doi:10.1158/1078-0432.CCR-06-0773 (2006).
- 180 Yu, Y. J. & Watts, R. J. Developing therapeutic antibodies for neurodegenerative disease. *Neurotherapeutics* **10**, 459-472, doi:10.1007/s13311-013-0187-4 (2013).

- 181 Daneman, R. & Prat, A. The blood-brain barrier. *Cold Spring Harb Perspect Biol* **7**, a020412, doi:10.1101/cshperspect.a020412 (2015).
- 182 Van Itallie, C. M. & Anderson, J. M. Claudins and epithelial paracellular transport. *Annu Rev Physiol* **68**, 403-429, doi:10.1146/annurev.physiol.68.040104.131404 (2006).
- 183 Van Itallie, C. M. *et al.* The density of small tight junction pores varies among cell types and is increased by expression of claudin-2. *J Cell Sci* **121**, 298-305, doi:10.1242/jcs.021485 (2008).
- 184 Noack, A. *et al.* Drug-induced trafficking of p-glycoprotein in human brain capillary endothelial cells as demonstrated by exposure to mitomycin C. *PLoS One* **9**, e88154, doi:10.1371/journal.pone.0088154 (2014).
- 185 Hagenbuch, B., Gao, B. & Meier, P. J. Transport of xenobiotics across the blood-brain barrier. *News Physiol Sci* **17**, 231-234 (2002).
- 186 Cox, D. S., Scott, K. R., Gao, H., Raje, S. & Eddington, N. D. Influence of multidrug resistance (MDR) proteins at the blood-brain barrier on the transport and brain distribution of enaminone anticonvulsants. *J Pharm Sci* **90**, 1540-1552, doi:10.1002/jps.1104 (2001).
- 187 Belda-Iniesta, C. *et al.* Long term responses with cetuximab therapy in glioblastoma multiforme. *Cancer Biol Ther* **5**, 912-914, doi:10.4161/cbt.5.8.3118 (2006).
- 188 Neyns, B. *et al.* Stratified phase II trial of cetuximab in patients with recurrent high-grade glioma. *Ann Oncol* **20**, 1596-1603, doi:10.1093/annonc/mdp032 (2009).
- 189 Shih, T. & Lindley, C. Bevacizumab: an angiogenesis inhibitor for the treatment of solid malignancies. *Clin Ther* **28**, 1779-1802, doi:10.1016/j.clinthera.2006.11.015 (2006).
- 190 Gilbert, M. R. *et al.* A randomized trial of bevacizumab for newly diagnosed glioblastoma. *N Engl J Med* **370**, 699-708, doi:10.1056/NEJMoa1308573 (2014).
- 191 Chinot, O. L. *et al.* Bevacizumab plus radiotherapy-temozolomide for newly diagnosed glioblastoma. *N Engl J Med* **370**, 709-722, doi:10.1056/NEJMoa1308345 (2014).
- 192 Pitter, K. L. *et al.* Corticosteroids compromise survival in glioblastoma. *Brain* **139**, 1458-1471, doi:10.1093/brain/aww046 (2016).
- 193 Sandmann, T. *et al.* Patients With Proneural Glioblastoma May Derive Overall Survival Benefit From the Addition of Bevacizumab to First-Line Radiotherapy and Temozolomide: Retrospective Analysis of the AVAglio Trial. *J Clin Oncol* **33**, 2735-2744, doi:10.1200/JCO.2015.61.5005 (2015).
- 194 De Vleeschouwer, S. & Bergers, G. in *Glioblastoma* (ed S. De Vleeschouwer) (2017).
- 195 Pyonteck, S. M. *et al.* CSF-1R inhibition alters macrophage polarization and blocks glioma progression. *Nat Med* **19**, 1264-1272, doi:10.1038/nm.3337 (2013).
- 196 Butowski, N. *et al.* Orally administered colony stimulating factor 1 receptor inhibitor PLX3397 in recurrent glioblastoma: an Ivy Foundation Early Phase Clinical Trials Consortium phase II study. *Neuro Oncol* **18**, 557-564, doi:10.1093/neuonc/nov245 (2016).
- 197 Papadopoulos, K. P. *et al.* First-in-Human Study of AMG 820, a Monoclonal Anti-Colony-Stimulating Factor 1 Receptor Antibody, in Patients with Advanced Solid Tumors. *Clin Cancer Res* **23**, 5703-5710, doi:10.1158/1078-0432.CCR-16-3261 (2017).
- 198 Sarkar, S. *et al.* Therapeutic activation of macrophages and microglia to suppress brain tumor-initiating cells. *Nat Neurosci* **17**, 46-55, doi:10.1038/nn.3597 (2014).
- 199 Kees, T. *et al.* Microglia isolated from patients with glioma gain antitumor activities on poly (I:C) stimulation. *Neuro Oncol* **14**, 64-78, doi:10.1093/neuonc/nor182 (2012).

- 200 Rosenfeld, M. R. *et al.* A multi-institution phase II study of poly-ICLC and radiotherapy with concurrent and adjuvant temozolomide in adults with newly diagnosed glioblastoma. *Neuro Oncol* **12**, 1071-1077, doi:10.1093/neuonc/noq071 (2010).
- 201 Priceman, S. J. *et al.* Targeting distinct tumor-infiltrating myeloid cells by inhibiting CSF-1 receptor: combating tumor evasion of antiangiogenic therapy. *Blood* **115**, 1461-1471, doi:10.1182/blood-2009-08-237412 (2010).
- 202 Yang, I., Han, S. J., Kaur, G., Crane, C. & Parsa, A. T. The role of microglia in central nervous system immunity and glioma immunology. *J Clin Neurosci* **17**, 6-10, doi:10.1016/j.jocn.2009.05.006 (2010).
- 203 Falk, W. & Leonard, E. J. Human monocyte chemotaxis: migrating cells are a subpopulation with multiple chemotaxin specificities on each cell. *Infect Immun* **29**, 953-959 (1980).
- 204 Vakilian, A., Khorramdelazad, H., Heidari, P., Sheikh Rezaei, Z. & Hassanshahi, G. CCL2/CCR2 signaling pathway in glioblastoma multiforme. *Neurochem Int* **103**, 1-7, doi:10.1016/j.neuint.2016.12.013 (2017).
- 205 Richardson, P. J. CXCR4 and Glioblastoma. *Anticancer Agents Med Chem* **16**, 59-74 (2016).
- 206 Gravina, G. L. *et al.* The brain-penetrating CXCR4 antagonist, PRX177561, increases the antitumor effects of bevacizumab and sunitinib in preclinical models of human glioblastoma. *J Hematol Oncol* **10**, 5, doi:10.1186/s13045-016-0377-8 (2017).
- 207 Wolchok, J. D. *et al.* Overall Survival with Combined Nivolumab and Ipilimumab in Advanced Melanoma. *N Engl J Med* **377**, 1345-1356, doi:10.1056/NEJMoa1709684 (2017).
- 208 Long, G. V. *et al.* Combination nivolumab and ipilimumab or nivolumab alone in melanoma brain metastases: a multicentre randomised phase 2 study. *Lancet Oncol* **19**, 672-681, doi:10.1016/S1470-2045(18)30139-6 (2018).
- 209 Berghoff, A. S. *et al.* Programmed death ligand 1 expression and tumor-infiltrating lymphocytes in glioblastoma. *Neuro Oncol* **17**, 1064-1075, doi:10.1093/neuonc/nou307 (2015).
- 210 Antonios, J. P. *et al.* Immunosuppressive tumor-infiltrating myeloid cells mediate adaptive immune resistance via a PD-1/PD-L1 mechanism in glioblastoma. *Neuro Oncol* **19**, 796-807, doi:10.1093/neuonc/nou287 (2017).
- 211 Mirghorbani, M., Van Gool, S. & Rezaei, N. Myeloid-derived suppressor cells in glioma. *Expert Rev Neurother* **13**, 1395-1406, doi:10.1586/14737175.2013.857603 (2013).
- 212 Lukas, R. V. *et al.* Clinical activity and safety of atezolizumab in patients with recurrent glioblastoma. *J Neurooncol* **140**, 317-328, doi:10.1007/s11060-018-2955-9 (2018).
- 213 Collins, J. M. & Gulley, J. L. Product review: avelumab, an anti-PD-L1 antibody. *Hum Vaccin Immunother* **15**, 891-908, doi:10.1080/21645515.2018.1551671 (2019).
- 214 Schalper, K. A. *et al.* Neoadjuvant nivolumab modifies the tumor immune microenvironment in resectable glioblastoma. *Nat Med* **25**, 470-476, doi:10.1038/s41591-018-0339-5 (2019).
- 215 Cloughesy, T. F. *et al.* Neoadjuvant anti-PD-1 immunotherapy promotes a survival benefit with intratumoral and systemic immune responses in recurrent glioblastoma. *Nat Med* **25**, 477-486, doi:10.1038/s41591-018-0337-7 (2019).
- 216 George E. P. Box, J. S. H., William G. Hunter. *Statistics for Experimenters: Design, Innovation, and Discovery, 2nd Edition*. 2nd Edition edn, (Wiley, 2005).

- 217 Ponten, J. & Macintyre, E. H. Long term culture of normal and neoplastic human glia. *Acta Pathol Microbiol Scand* **74**, 465-486 (1968).
- 218 Xie, Y. *et al.* The Human Glioblastoma Cell Culture Resource: Validated Cell Models Representing All Molecular Subtypes. *EBioMedicine* **2**, 1351-1363, doi:10.1016/j.ebiom.2015.08.026 (2015).
- 219 Fogh, J., Wright, W. C. & Loveless, J. D. Absence of HeLa cell contamination in 169 cell lines derived from human tumors. *J Natl Cancer Inst* **58**, 209-214, doi:10.1093/jnci/58.2.209 (1977).
- 220 Allen, M., Bjerke, M., Edlund, H., Nelander, S. & Westermark, B. Origin of the U87MG glioma cell line: Good news and bad news. *Sci Transl Med* **8**, 354re353, doi:10.1126/scitranslmed.aaf6853 (2016).
- 221 Kijima, N. & Kanemura, Y. in *Glioblastoma* (ed S. De Vleeschouwer) (2017).
- 222 Huszthy, P. C. *et al.* In vivo models of primary brain tumors: pitfalls and perspectives. *Neuro Oncol* **14**, 979-993, doi:10.1093/neuonc/nos135 (2012).
- 223 Mahesparan, R. *et al.* Expression of extracellular matrix components in a highly infiltrative in vivo glioma model. *Acta Neuropathol* **105**, 49-57, doi:10.1007/s00401-002-0610-0 (2003).
- 224 Kijima, N. *et al.* Wilms' tumor 1 is involved in tumorigenicity of glioblastoma by regulating cell proliferation and apoptosis. *Anticancer Res* **34**, 61-67 (2014).
- 225 Richmond, A. & Su, Y. Mouse xenograft models vs GEM models for human cancer therapeutics. *Dis Model Mech* **1**, 78-82, doi:10.1242/dmm.000976 (2008).
- 226 Bjerkvig, R., Tonnesen, A., Laerum, O. D. & Backlund, E. O. Multicellular tumor spheroids from human gliomas maintained in organ culture. *J Neurosurg* **72**, 463-475, doi:10.3171/jns.1990.72.3.0463 (1990).
- 227 Fei, X. F. *et al.* Development of clinically relevant orthotopic xenograft mouse model of metastatic lung cancer and glioblastoma through surgical tumor tissues injection with trocar. *J Exp Clin Cancer Res* **29**, 84, doi:10.1186/1756-9966-29-84 (2010).
- 228 Patrizii, M., Bartucci, M., Pine, S. R. & Sabaawy, H. E. Utility of Glioblastoma Patient-Derived Orthotopic Xenografts in Drug Discovery and Personalized Therapy. *Front Oncol* **8**, 23, doi:10.3389/fonc.2018.00023 (2018).
- 229 Oh, T. *et al.* Immunocompetent murine models for the study of glioblastoma immunotherapy. *J Transl Med* **12**, 107, doi:10.1186/1479-5876-12-107 (2014).
- 230 Sampson, J. H. *et al.* Characterization of a spontaneous murine astrocytoma and abrogation of its tumorigenicity by cytokine secretion. *Neurosurgery* **41**, 1365-1372; discussion 1372-1363, doi:10.1097/00006123-199712000-00024 (1997).
- 231 Martinez-Murillo, R. & Martinez, A. Standardization of an orthotopic mouse brain tumor model following transplantation of CT-2A astrocytoma cells. *Histol Histopathol* **22**, 1309-1326, doi:10.14670/HH-22.1309 (2007).
- 232 Ausman, J. I., Shapiro, W. R. & Rall, D. P. Studies on the chemotherapy of experimental brain tumors: development of an experimental model. *Cancer Res* **30**, 2394-2400 (1970).
- 233 Brinster, R. L. *et al.* Transgenic mice harboring SV40 T-antigen genes develop characteristic brain tumors. *Cell* **37**, 367-379, doi:10.1016/0092-8674(84)90367-2 (1984).
- 234 Macleod, K. F. & Jacks, T. Insights into cancer from transgenic mouse models. *J Pathol* **187**, 43-60, doi:10.1002/(SICI)1096-9896(199901)187:1<43::AID-PATH246>3.0.CO;2-P (1999).

- 235 Young, J. A., Bates, P. & Varmus, H. E. Isolation of a chicken gene that confers susceptibility to infection by subgroup A avian leukosis and sarcoma viruses. *Journal of Virology* **67**, 1811-1816 (1993).
- 236 Federspiel, M. J., Bates, P., Young, J. A., Varmus, H. E. & Hughes, S. H. A system for tissue-specific gene targeting: transgenic mice susceptible to subgroup A avian leukosis virus-based retroviral vectors. *Proc Natl Acad Sci U S A* **91**, 11241-11245, doi:10.1073/pnas.91.23.11241 (1994).
- 237 Holland, E. C., Hively, W. P., DePinho, R. A. & Varmus, H. E. A constitutively active epidermal growth factor receptor cooperates with disruption of G1 cell-cycle arrest pathways to induce glioma-like lesions in mice. *Genes Dev* **12**, 3675-3685 (1998).
- 238 Holland, E. C. *et al.* Combined activation of Ras and Akt in neural progenitors induces glioblastoma formation in mice. *Nat Genet* **25**, 55-57, doi:10.1038/75596 (2000).
- 239 Uhrbom, L., Kastemar, M., Johansson, F. K., Westermark, B. & Holland, E. C. Cell type-specific tumor suppression by Ink4a and Arf in Kras-induced mouse gliomagenesis. *Cancer Res* **65**, 2065-2069, doi:10.1158/0008-5472.CAN-04-3588 (2005).
- 240 Dai, C. *et al.* PDGF autocrine stimulation dedifferentiates cultured astrocytes and induces oligodendrogliomas and oligoastrocytomas from neural progenitors and astrocytes in vivo. *Genes Dev* **15**, 1913-1925, doi:10.1101/gad.903001 (2001).
- 241 Hambarzumyan, D., Amankulor, N. M., Helmy, K. Y., Becher, O. J. & Holland, E. C. Modeling Adult Gliomas Using RCAS/t-va Technology. *Transl Oncol* **2**, 89-95 (2009).
- 242 Hu, X. *et al.* mTOR promotes survival and astrocytic characteristics induced by Pten/AKT signaling in glioblastoma. *Neoplasia* **7**, 356-368 (2005).
- 243 Franklin, K. B. J. & Paxinos, G. *The mouse brain in stereotaxic coordinates*. (Academic Press, 1997).
- 244 Koutcher, J. A. *et al.* MRI of mouse models for gliomas shows similarities to humans and can be used to identify mice for preclinical trials. *Neoplasia* **4**, 480-485, doi:10.1038/sj.neo.7900269 (2002).
- 245 Schindelin, J. *et al.* Fiji: an open-source platform for biological-image analysis. *Nat Methods* **9**, 676-682, doi:10.1038/nmeth.2019 (2012).
- 246 Aranda, P. S., LaJoie, D. M. & Jorcyk, C. L. Bleach gel: a simple agarose gel for analyzing RNA quality. *Electrophoresis* **33**, 366-369, doi:10.1002/elps.201100335 (2012).
- 247 Cerami, E. *et al.* The cBio cancer genomics portal: an open platform for exploring multidimensional cancer genomics data. *Cancer Discov* **2**, 401-404, doi:10.1158/2159-8290.CD-12-0095 (2012).
- 248 Gao, J. *et al.* Integrative analysis of complex cancer genomics and clinical profiles using the cBioPortal. *Sci Signal* **6**, p11, doi:10.1126/scisignal.2004088 (2013).
- 249 Hambarzumyan, D. *et al.* PI3K pathway regulates survival of cancer stem cells residing in the perivascular niche following radiation in medulloblastoma in vivo. *Genes Dev* **22**, 436-448, doi:10.1101/gad.1627008 (2008).
- 250 Halliday, J. *et al.* In vivo radiation response of proneural glioma characterized by protective p53 transcriptional program and proneural-mesenchymal shift. *Proc Natl Acad Sci U S A* **111**, 5248-5253, doi:10.1073/pnas.1321014111 (2014).
- 251 Lei, L. *et al.* Glioblastoma models reveal the connection between adult glial progenitors and the proneural phenotype. *PLoS One* **6**, e20041, doi:10.1371/journal.pone.0020041 (2011).

- 252 Liu, C. *et al.* Mosaic analysis with double markers reveals tumor cell of origin in glioma. *Cell* **146**, 209-221, doi:10.1016/j.cell.2011.06.014 (2011).
- 253 Lim, D. A. & Alvarez-Buylla, A. Interaction between astrocytes and adult subventricular zone precursors stimulates neurogenesis. *Proc Natl Acad Sci U S A* **96**, 7526-7531, doi:10.1073/pnas.96.13.7526 (1999).
- 254 Ozawa, T. *et al.* Most human non-GCIMP glioblastoma subtypes evolve from a common proneural-like precursor glioma. *Cancer Cell* **26**, 288-300, doi:10.1016/j.ccr.2014.06.005 (2014).
- 255 Brennan, C. *et al.* Glioblastoma subclasses can be defined by activity among signal transduction pathways and associated genomic alterations. *PLoS One* **4**, e7752, doi:10.1371/journal.pone.0007752 (2009).
- 256 Bhat, K. P. L. *et al.* Mesenchymal differentiation mediated by NF-kappaB promotes radiation resistance in glioblastoma. *Cancer Cell* **24**, 331-346, doi:10.1016/j.ccr.2013.08.001 (2013).
- 257 Ji, H. *et al.* Epidermal growth factor receptor variant III mutations in lung tumorigenesis and sensitivity to tyrosine kinase inhibitors. *Proc Natl Acad Sci U S A* **103**, 7817-7822, doi:10.1073/pnas.0510284103 (2006).
- 258 Research, N. C. I. C. f. C. *The RCAS System*, <<https://home.ncifcrf.gov/hivdrp/RCAS/overview.html>> (
- 259 Zhu, H. *et al.* Oncogenic EGFR signaling cooperates with loss of tumor suppressor gene functions in gliomagenesis. *Proc Natl Acad Sci U S A* **106**, 2712-2716, doi:10.1073/pnas.0813314106 (2009).
- 260 Hambardzumyan, D. & Bergers, G. Glioblastoma: Defining Tumor Niches. *Trends Cancer* **1**, 252-265, doi:10.1016/j.trecan.2015.10.009 (2015).
- 261 Imai, Y., Ibata, I., Ito, D., Ohsawa, K. & Kohsaka, S. A novel gene *iba1* in the major histocompatibility complex class III region encoding an EF hand protein expressed in a monocytic lineage. *Biochem Biophys Res Commun* **224**, 855-862, doi:10.1006/bbrc.1996.1112 (1996).
- 262 Engler, J. R. *et al.* Increased microglia/macrophage gene expression in a subset of adult and pediatric astrocytomas. *PLoS One* **7**, e43339, doi:10.1371/journal.pone.0043339 (2012).
- 263 Kaffes, I. *et al.* Human Mesenchymal glioblastomas are characterized by an increased immune cell presence compared to Proneural and Classical tumors. *OncImmunology*, 1-11, doi:10.1080/2162402X.2019.1655360 (2019).
- 264 Fedele, M., Cerchia, L., Pegoraro, S., Sgarra, R. & Manfioletti, G. Proneural-Mesenchymal Transition: Phenotypic Plasticity to Acquire Multitherapy Resistance in Glioblastoma. *Int J Mol Sci* **20**, doi:10.3390/ijms20112746 (2019).
- 265 Lu, K. V. *et al.* VEGF inhibits tumor cell invasion and mesenchymal transition through a MET/VEGFR2 complex. *Cancer Cell* **22**, 21-35, doi:10.1016/j.ccr.2012.05.037 (2012).
- 266 Doetsch, F., Caille, I., Lim, D. A., Garcia-Verdugo, J. M. & Alvarez-Buylla, A. Subventricular zone astrocytes are neural stem cells in the adult mammalian brain. *Cell* **97**, 703-716, doi:10.1016/s0092-8674(00)80783-7 (1999).
- 267 Yamashita, T. *et al.* Subventricular zone-derived neuroblasts migrate and differentiate into mature neurons in the post-stroke adult striatum. *J Neurosci* **26**, 6627-6636, doi:10.1523/JNEUROSCI.0149-06.2006 (2006).

- 268 Tamagno, I. & Schiffer, D. Nestin expression in reactive astrocytes of human pathology. *J Neurooncol* **80**, 227-233, doi:10.1007/s11060-006-9181-6 (2006).
- 269 Jiang, Y. *et al.* Glioblastoma Cell Malignancy and Drug Sensitivity Are Affected by the Cell of Origin. *Cell Rep* **18**, 977-990, doi:10.1016/j.celrep.2017.01.003 (2017).
- 270 Kitange, G. J. *et al.* Induction of MGMT expression is associated with temozolomide resistance in glioblastoma xenografts. *Neuro Oncol* **11**, 281-291, doi:10.1215/15228517-2008-090 (2009).
- 271 Bleau, A. M. *et al.* PTEN/PI3K/Akt pathway regulates the side population phenotype and ABCG2 activity in glioma tumor stem-like cells. *Cell Stem Cell* **4**, 226-235, doi:10.1016/j.stem.2009.01.007 (2009).
- 272 Nguyen, S. A. *et al.* Novel MSH6 mutations in treatment-naive glioblastoma and anaplastic oligodendroglioma contribute to temozolomide resistance independently of MGMT promoter methylation. *Clin Cancer Res* **20**, 4894-4903, doi:10.1158/1078-0432.CCR-13-1856 (2014).
- 273 Agarwala, S. S. & Kirkwood, J. M. Temozolomide, a novel alkylating agent with activity in the central nervous system, may improve the treatment of advanced metastatic melanoma. *Oncologist* **5**, 144-151, doi:10.1634/theoncologist.5-2-144 (2000).
- 274 Schmid, R. S. *et al.* Core pathway mutations induce de-differentiation of murine astrocytes into glioblastoma stem cells that are sensitive to radiation but resistant to temozolomide. *Neuro Oncol* **18**, 962-973, doi:10.1093/neuonc/nov321 (2016).
- 275 Raslan, A. & Bhardwaj, A. Medical management of cerebral edema. *Neurosurg Focus* **22**, E12 (2007).
- 276 Kostaras, X., Cusano, F., Kline, G. A., Roa, W. & Easaw, J. Use of dexamethasone in patients with high-grade glioma: a clinical practice guideline. *Curr Oncol* **21**, e493-503, doi:10.3747/co.21.1769 (2014).
- 277 McClelland, S., 3rd & Long, D. M. Genesis of the use of corticosteroids in the treatment and prevention of brain edema. *Neurosurgery* **62**, 965-967; discussion 967-968, doi:10.1227/01.neu.0000318183.25783.77 (2008).
- 278 Kofman, S., Garvin, J. S., Nagamani, D. & Taylor, S. G., 3rd. Treatment of cerebral metastases from breast carcinoma with prednisolone. *J Am Med Assoc* **163**, 1473-1476 (1957).
- 279 French, L. A. The use of steroids in the treatment of cerebral edema. *Bull N Y Acad Med* **42**, 301-311 (1966).
- 280 Lim-Fat, M. J. *et al.* Letter: When Less is More: Dexamethasone Dosing for Brain Tumors. *Neurosurgery* **85**, E607-E608, doi:10.1093/neuros/nyz186 (2019).
- 281 Luedi, M. M. *et al.* A Dexamethasone-regulated Gene Signature Is Prognostic for Poor Survival in Glioblastoma Patients. *J Neurosurg Anesthesiol* **29**, 46-58, doi:10.1097/ANA.0000000000000368 (2017).
- 282 Wong, E. T., Lok, E., Gautam, S. & Swanson, K. D. Dexamethasone exerts profound immunologic interference on treatment efficacy for recurrent glioblastoma. *Br J Cancer* **113**, 1642, doi:10.1038/bjc.2015.404 (2015).
- 283 Coutinho, A. E. & Chapman, K. E. The anti-inflammatory and immunosuppressive effects of glucocorticoids, recent developments and mechanistic insights. *Mol Cell Endocrinol* **335**, 2-13, doi:10.1016/j.mce.2010.04.005 (2011).
- 284 Cheyne, J. *An Essay on Hydrocephalus Acutus*. (Finley, 1814).
- 285 Whytt, R. *Observations on the Dropsy in the Brain*. (Balfour, 1768).

- 286 Spatz, H. Die bedeutung der 'symptomatischen hirnschwellung' fur die hirntumoren und fur andere raumbeengende prozesse in der schadelgrube *Archives of Psychiatry* **88**, 790-794 (1929).
- 287 Rovit, R. L. & Hagan, R. Steroids and cerebral edema: the effects of glucocorticoids on abnormal capillary permeability following cerebral injury in cats. *J Neuropathol Exp Neurol* **27**, 277-299 (1968).
- 288 Kotsarini, C., Griffiths, P. D., Wilkinson, I. D. & Hoggard, N. A systematic review of the literature on the effects of dexamethasone on the brain from in vivo human-based studies: implications for physiological brain imaging of patients with intracranial tumors. *Neurosurgery* **67**, 1799-1815; discussion 1815, doi:10.1227/NEU.0b013e3181fa775b (2010).
- 289 Ostergaard, L. *et al.* Early changes measured by magnetic resonance imaging in cerebral blood flow, blood volume, and blood-brain barrier permeability following dexamethasone treatment in patients with brain tumors. *J Neurosurg* **90**, 300-305, doi:10.3171/jns.1999.90.2.0300 (1999).
- 290 Stokum, J. A., Gerzanich, V. & Simard, J. M. Molecular pathophysiology of cerebral edema. *J Cereb Blood Flow Metab* **36**, 513-538, doi:10.1177/0271678X15617172 (2016).
- 291 Michinaga, S. & Koyama, Y. Pathogenesis of brain edema and investigation into anti-edema drugs. *Int J Mol Sci* **16**, 9949-9975, doi:10.3390/ijms16059949 (2015).
- 292 Heiss, J. D. *et al.* Mechanism of dexamethasone suppression of brain tumor-associated vascular permeability in rats. Involvement of the glucocorticoid receptor and vascular permeability factor. *J Clin Invest* **98**, 1400-1408, doi:10.1172/JCI118927 (1996).
- 293 Carlson, M. R. *et al.* Relationship between survival and edema in malignant gliomas: role of vascular endothelial growth factor and neuronal pentraxin 2. *Clin Cancer Res* **13**, 2592-2598, doi:10.1158/1078-0432.CCR-06-2772 (2007).
- 294 Dinarello, C. A. Interleukin-1 and its biologically related cytokines. *Adv Immunol* **44**, 153-205 (1989).
- 295 March, C. J. *et al.* Cloning, sequence and expression of two distinct human interleukin-1 complementary DNAs. *Nature* **315**, 641-647 (1985).
- 296 Gabay, C., Lamacchia, C. & Palmer, G. IL-1 pathways in inflammation and human diseases. *Nat Rev Rheumatol* **6**, 232-241, doi:10.1038/nrrheum.2010.4 (2010).
- 297 Barksby, H. E., Lea, S. R., Preshaw, P. M. & Taylor, J. J. The expanding family of interleukin-1 cytokines and their role in destructive inflammatory disorders. *Clin Exp Immunol* **149**, 217-225, doi:10.1111/j.1365-2249.2007.03441.x (2007).
- 298 Dinarello, C. A., Simon, A. & van der Meer, J. W. Treating inflammation by blocking interleukin-1 in a broad spectrum of diseases. *Nat Rev Drug Discov* **11**, 633-652, doi:10.1038/nrd3800 (2012).
- 299 Guarda, G. *et al.* Differential expression of NLRP3 among hematopoietic cells. *J Immunol* **186**, 2529-2534, doi:10.4049/jimmunol.1002720 (2011).
- 300 Gottschall, P. E., Tatsuno, I. & Arimura, A. Increased sensitivity of glioblastoma cells to interleukin 1 after long-term incubation with dexamethasone. *Mol Cell Neurosci* **3**, 49-55 (1992).
- 301 Argaw, A. T. *et al.* IL-1beta regulates blood-brain barrier permeability via reactivation of the hypoxia-angiogenesis program. *J Immunol* **177**, 5574-5584 (2006).

- 302 Wang, Y. *et al.* Interleukin-1beta induces blood-brain barrier disruption by  
downregulating Sonic hedgehog in astrocytes. *PLoS One* **9**, e110024,  
doi:10.1371/journal.pone.0110024 (2014).
- 303 Clausen, F. *et al.* Neutralization of interleukin-1beta reduces cerebral edema and tissue  
loss and improves late cognitive outcome following traumatic brain injury in mice. *Eur J*  
*Neurosci* **34**, 110-123, doi:10.1111/j.1460-9568.2011.07723.x (2011).
- 304 Weischenfeldt, J. & Porse, B. Bone Marrow-Derived Macrophages (BMM): Isolation and  
Applications. *CSH Protoc* **2008**, pdb prot5080, doi:10.1101/pdb.prot5080 (2008).
- 305 Roy, J. Primary microglia isolation from mixed cell cultures of neonatal mouse brain  
tissue. *Brain Res* **1689**, 21-29, doi:10.1016/j.brainres.2018.03.018 (2018).
- 306 Wewers, M. D. & Sarkar, A. P2X(7) receptor and macrophage function. *Purinergic*  
*Signal* **5**, 189-195, doi:10.1007/s11302-009-9131-9 (2009).
- 307 Herting, C. J. *et al.* Genetic driver mutations define the expression signature and  
microenvironmental composition of high-grade gliomas. *Glia* **65**, 1914-1926,  
doi:10.1002/glia.23203 (2017).
- 308 Glaccum, M. B. *et al.* Phenotypic and functional characterization of mice that lack the  
type I receptor for IL-1. *J Immunol* **159**, 3364-3371 (1997).
- 309 Horai, R. *et al.* Production of mice deficient in genes for interleukin (IL)-1alpha, IL-  
1beta, IL-1alpha/beta, and IL-1 receptor antagonist shows that IL-1beta is crucial in  
turpentine-induced fever development and glucocorticoid secretion. *J Exp Med* **187**,  
1463-1475 (1998).
- 310 Preibisch, S., Saalfeld, S. & Tomancak, P. Globally optimal stitching of tiled 3D  
microscopic image acquisitions. *Bioinformatics* **25**, 1463-1465,  
doi:10.1093/bioinformatics/btp184 (2009).
- 311 Tait, M. J., Saadoun, S., Bell, B. A., Verkman, A. S. & Papadopoulos, M. C. Increased  
brain edema in aqp4-null mice in an experimental model of subarachnoid hemorrhage.  
*Neuroscience* **167**, 60-67, doi:10.1016/j.neuroscience.2010.01.053 (2010).
- 312 Beuscher, H. U., Gunther, C. & Rollinghoff, M. IL-1 beta is secreted by activated murine  
macrophages as biologically inactive precursor. *J Immunol* **144**, 2179-2183 (1990).
- 313 Dinarello, C. A. *et al.* Interleukin 1 induces interleukin 1. I. Induction of circulating  
interleukin 1 in rabbits in vivo and in human mononuclear cells in vitro. *J Immunol* **139**,  
1902-1910 (1987).
- 314 Warner, S. J., Auger, K. R. & Libby, P. Interleukin 1 induces interleukin 1. II.  
Recombinant human interleukin 1 induces interleukin 1 production by adult human  
vascular endothelial cells. *J Immunol* **139**, 1911-1917 (1987).
- 315 Warner, S. J., Auger, K. R. & Libby, P. Human interleukin 1 induces interleukin 1 gene  
expression in human vascular smooth muscle cells. *J Exp Med* **165**, 1316-1331 (1987).
- 316 van Mourik, J. A., Leeksa, O. C., Reinders, J. H., de Groot, P. G. & Zandbergen-  
Spaargaren, J. Vascular endothelial cells synthesize a plasma membrane protein  
indistinguishable from the platelet membrane glycoprotein IIa. *J Biol Chem* **260**, 11300-  
11306 (1985).
- 317 Schuld, A. *et al.* Effects of dexamethasone on cytokine plasma levels and white blood  
cell counts in depressed patients. *Psychoneuroendocrinology* **26**, 65-76 (2001).
- 318 Nakagawa, M. *et al.* Glucocorticoid-induced granulocytosis: contribution of marrow  
release and demargination of intravascular granulocytes. *Circulation* **98**, 2307-2313  
(1998).

- 319 Wong, E. T. & Swanson, K. D. Dexamethasone-Friend or Foe for Patients With Glioblastoma? *JAMA Neurol*, doi:10.1001/jamaneurol.2018.4530 (2019).
- 320 Hedley-Whyte, E. T. & Hsu, D. W. Effect of dexamethasone on blood-brain barrier in the normal mouse. *Ann Neurol* **19**, 373-377, doi:10.1002/ana.410190411 (1986).
- 321 Hue, C. D. *et al.* Dexamethasone potentiates in vitro blood-brain barrier recovery after primary blast injury by glucocorticoid receptor-mediated upregulation of ZO-1 tight junction protein. *J Cereb Blood Flow Metab* **35**, 1191-1198, doi:10.1038/jcbfm.2015.38 (2015).
- 322 Badie, B. *et al.* Dexamethasone-induced abolition of the inflammatory response in an experimental glioma model: a flow cytometry study. *J Neurosurg* **93**, 634-639, doi:10.3171/jns.2000.93.4.0634 (2000).
- 323 Kim, B. Y. *et al.* Dexamethasone inhibits activation of monocytes/macrophages in a milieu rich in 27-oxygenated cholesterol. *PLoS One* **12**, e0189643, doi:10.1371/journal.pone.0189643 (2017).
- 324 Remmelts, H. H. *et al.* Dexamethasone downregulates the systemic cytokine response in patients with community-acquired pneumonia. *Clin Vaccine Immunol* **19**, 1532-1538, doi:10.1128/CVI.00423-12 (2012).
- 325 Auphan, N., DiDonato, J. A., Rosette, C., Helmberg, A. & Karin, M. Immunosuppression by glucocorticoids: inhibition of NF-kappa B activity through induction of I kappa B synthesis. *Science* **270**, 286-290 (1995).
- 326 Jones, G. E. Cellular signaling in macrophage migration and chemotaxis. *J Leukoc Biol* **68**, 593-602 (2000).
- 327 Xuan, W., Qu, Q., Zheng, B., Xiong, S. & Fan, G. H. The chemotaxis of M1 and M2 macrophages is regulated by different chemokines. *J Leukoc Biol* **97**, 61-69, doi:10.1189/jlb.1A0314-170R (2015).
- 328 Hughes, M. A., Parisi, M., Grossman, S. & Kleinberg, L. Primary brain tumors treated with steroids and radiotherapy: low CD4 counts and risk of infection. *Int J Radiat Oncol Biol Phys* **62**, 1423-1426, doi:10.1016/j.ijrobp.2004.12.085 (2005).
- 329 Burton, J. L. & Kehrli, M. E., Jr. Effects of dexamethasone on bovine circulating T lymphocyte populations. *J Leukoc Biol* **59**, 90-99 (1996).
- 330 Margolin, K. *et al.* Ipilimumab in patients with melanoma and brain metastases: an open-label, phase 2 trial. *Lancet Oncol* **13**, 459-465, doi:10.1016/S1470-2045(12)70090-6 (2012).
- 331 Giles, A. J. *et al.* Dexamethasone-induced immunosuppression: mechanisms and implications for immunotherapy. *J Immunother Cancer* **6**, 51, doi:10.1186/s40425-018-0371-5 (2018).
- 332 Yan, H. *et al.* IDH1 and IDH2 mutations in gliomas. *N Engl J Med* **360**, 765-773, doi:10.1056/NEJMoa0808710 (2009).
- 333 Amankulor, N. M. *et al.* Mutant IDH1 regulates the tumor-associated immune system in gliomas. *Genes Dev* **31**, 774-786, doi:10.1101/gad.294991.116 (2017).
- 334 Nunez, F. J. *et al.* IDH1-R132H acts as a tumor suppressor in glioma via epigenetic up-regulation of the DNA damage response. *Sci Transl Med* **11**, doi:10.1126/scitranslmed.aaq1427 (2019).
- 335 He, H. *et al.* Perivascular Macrophages Limit Permeability. *Arterioscler Thromb Vasc Biol* **36**, 2203-2212, doi:10.1161/ATVBAHA.116.307592 (2016).

- 336 Hartley, G. P., Chow, L., Ammons, D. T., Wheat, W. H. & Dow, S. W. Programmed Cell Death Ligand 1 (PD-L1) Signaling Regulates Macrophage Proliferation and Activation. *Cancer Immunol Res* **6**, 1260-1273, doi:10.1158/2326-6066.CIR-17-0537 (2018).